UNIVERSITAT POLITÈCNICA DE CATALUNYA BARCELONATECH

Advanced wind farm control strategies for enhancing grid support

Sara Siniscalchi Minna

UNIVERSITAT POLITÈCNICA DE CATALUNYA

Doctoral Program:

AUTOMATIC CONTROL, ROBOTICS AND COMPUTER VISION

Doctoral Thesis

ADVANCED WIND FARM CONTROL STRATEGIES FOR ENHANCING GRID SUPPORT

Sara Siniscalchi Minna

Advisors:
Carlos Ocampo Martínez, PhD
Mikel De Prada Gil, PhD

November 2019

Universitat Politècnica de Catalunya (UPC)

Departament d'Enginyeria de Sistemes, Automàtica i Informàtica Industrial
Doctoral Program:
Automatic Control, Robotics and Computer Vision

This PhD thesis was completed at:

Institut de Robòtica i Informàtica Industrial, (CSIC-UPC), and Catalonia Institute for Energy Research, (IREC)

Advisors:
Carlos Ocampo-Martínez, PhD[1]
Mikel De-Prada-Gil, PhD[2]

Co-advisors:
Fernando D. Bianchi, PhD[3]
Jose-Luis Dominguez Garcia, PhD[4]

External Reviewers:
Ricardo S. Sánchez-Peña, PhD (Buenos Aires Institute of Technology (& CONICET))
Olimpo Anaya-Lara, PhD (University of Strathclyde, Glasgow)

PhD Thesis Committee:
Ramon Costa Castellò, PhD (Universitat Politècnica de Catalunya)
Ricardo S. Sánchez-Peña, PhD (Buenos Aires Institute of Technology (& CONICET))
Olimpo Anaya-Lara, PhD (University of Strathclyde, Glasgow)

Acknowledgment:
This work has received funding from the European Union's Horizon 2020 research and innovation programme under the Marie Skłodowska-Curie grant agreement No 675318 (INCITE).

[1]Advisor at Universitat Politècnica de Catalunya
[2]Advisor at General Electric
[3]Advisor at Buenos Aires Institute of Technology (& CONICET))
[4]Advisor at Catalonia Institute for Energy Research

To my sister,
my anchor in the storm..

Acknowledgements

When I sent my application letter for this PhD position I wrote: "For me doing a PhD means satisfying my desire of curiosity, self-development and research experience". Today, I can definitely confirm these words and I would add that a PhD means doing a journey that changes you into a more responsible and self-confident person.

This is why, I do want to express my gratitude to my former supervisor Prof. Fernando Bianchi and my supervisor Prof. Carlos Ocampo-Martinez, who believed in me since the beginning giving me the possibility to pursue this intense and challenging doctoral experience. They have been a significant support during my thesis. Being constantly available for academic discussions, they have urged me to learn by following my ideas, making mistakes, asking questions. Thanks to this constant support, I acquired knowledge and skills for quality research, which ended up with novel and interesting research ideas.

I would like to thank also Dr. Mikel De-Prada-Gil and Dr. Jose-Luis Garcia-Dominguez, my supervisors at IREC, for investing time entering into details in academic discussions, and for suggesting formal alternatives to address new research challenges.

As PhD Fellow of the INCITE Doctoral Program, I had the possibilities to interact with many people, with whom I shared both an enriching professional and human experience. In particular, I would like to acknowledge Prof. Bart De-Schutter and Prof. Jan-Willem Van-Wingerden from TU-Delft for receiving me as a visitor researcher and the opportunity to collaborate with the other researchers in their groups. Their valuable work inspired me throughout my research work. I also want to thank Dr. Vahan Gevorgian (NREL) for giving me a place to work within his research group where I learned on reactive power control for wind farms. I sincerely thank all the researchers I have collaborated with during these secondments, and I believe that our fruitful scientific dialogues are starting points for a durable professional network.

I would also like to convey my thanks to Prof. Ricardo Sanchez-Peña at Buenos Aires Institute of Technology (ITBA) and Olimpo Anaya-Lara (University of Strathclyde, Glasgow) for having accepted to review this thesis, and Prof. Ramon Costa Castellò from UPC for joining my thesis committee.

Last but not least, my special thanks go to my mother, my father, my sister without whom this doctoral journey would not have been possible. Thanks to remember me day by day what it is really important in the life, what I am and what I can do. Also many thanks to all my friends, in particular Thibeault and Arianna, who always made me smile in stressful moments, and have provided a lot of happiness into my days with their friendship. Finally, thanks to Filippo.

And now, let's follow the wind.

Abstract

Nowadays, there is rising concern among Transmission System Operators (TSOs) about the declining of system inertia due to the increasing penetration of wind energy, and other renewable energy systems (RES), and the retirements of conventional power plants. On the other hand, by properly operating wind farms, wind generation may be capable of enhancing grid stability and ensuring continued security of power supply. In this doctoral thesis, new control approaches for designing wind farm optimization-based control strategies are proposed to improve the participation of wind farms in grid support, specially in primary frequency support.

Firstly, an overview about the classical approaches for controlling wind farms and wind turbines discusses how the existing control concepts can be exploited to provide the new challenges expected from wind farms. Therefore, the classical concept of controlling wind farms through two-level hierarchical control structure is adopted and improved to optimally regulate the active power for both the wind farm and the wind turbine levels. In this regards, this dissertation assigns special interest on how the overall objective function can be formulated such that the power demanded by the grid is continuously tracked. On the other hand, as long as the power demand is below the wind farm available power, there is some extra power, known as *power reserve*, that can be used to enhance frequency support. One of the main challenges of this dissertation is to maximize this power reserve, while also ensuring the tracking of the power reference. However, the impact of the wake generated by an upstream turbine on the wind faced by the downstream turbines needs to be minimized in order to improve the power reserve. Therefore, throughout this thesis centralized wind farm control strategies are proposed to optimally dispatch the power among the turbines so that the negative impact of the wake effect on the overall power reserve is reduced.

Basically, two control techniques are discussed to provide the aforementioned control objectives. Firstly, it is proposed an optimal control algorithm to find the best power distribution among the turbines while solving an iterative linear-programming problem. This approach provides a significant improvement in terms of power reserve, while keeping the computational burden to find the optimal solution low enough for ensuring on-line control. Secondarily, the model predictive control technique is used to solve a multi-objective control problem that could also include, along with the maximization of power reserve, other control objectives. For instance, the minimization of the electrical cable losses in the inter-array collection grid. Furthermore, a dedicated investigation is carried out in order to highlight the capability of the proposed control strategies to provide higher value of power reserve with respect the more common concepts of distributing the overall wind farm power reference.

The main idea behind the design of a wind farm control strategy in order to provide grid support should be to guarantee an optimal solution within relatively low computational

burden. In fact, the power reference, and/or frequency or voltage references, sent by the TSO must be provided by the wind farm controller within almost 1 second (or even lower time when a frequency-voltage event affects the grid stability). Although the proposed centralized controllers reacts quickly to the changes in the input reference, some issues may occur when considering large-scale wind farms.

Large wind farms can include more than hundred turbines, in this circumstance the power production of each turbine is highly coupled by the wake propagation to the operating conditions of the other turbines. Thus, centralized control approaches may demand large information sharing between turbines and the central controller. Complex communications and large information exchange result difficult to process over times suitable to satisfy the current power generation requirements and the high communication dependency make the system exposed to failures. In order to deal with these issues, this thesis proposes a non-centralized wind farm control scheme based on a partitioning approach to divide the wind farm in independent subsets of turbines. With the proposed control approach the computation time is consistently reduced compared to the centralized control strategy meanwhile the performance on optimal power distribution is slightly affected.

The performance of all the proposed control strategies are tested using a wind farm simulator that models the dynamic behavior of the wake effect by using the common dynamic wake meandering model and, for a more realistic analysis, some tests are performed with advanced software based on Large Eddy simulations.

Keywords: wind farm control, centralized control, model predictive control, non-centralized control, partitioning algorithms, frequency control, wind farm power regulation, de-loading operation, power reserve maximization, wake effect

Resumen

Hoy en día, existe una creciente preocupación entre los Operadores de Sistemas de Transmisión (TSO) sobre la cresciente penetración de le energía eólica y de otros sistemas de energía renovable (RES) y la tendiente eliminación de las centrales eléctricas convencionales que implica la disminuciónde la inercia del sistema eléctrico. Por otro lado, operando adecuadamente los parques eólicos, la generación eólica puede mejorar la estabilidad de la red eléctrica y garantizar la seguridad y un continuo suministro de energía. Esta tesis doctoral propone nuevas estrategias para diseñar controladores basados en optimización dinámica para parques eólicos y mejorar la participación de los parques eólicos en el soporte de la red eléctrica, especialmente pensados para maximizar la provisión de soporte de frecuencia primaria.

En primer lugar, esta tesis doctoral presenta los enfoques clásicos para el control de parques y turbinas eólicas y cómo los conceptos de control existentes pueden ser explotados para hacer frente a los nuevos desafíos que se esperan de los parques eólicos. Por lo tanto, los conceptos clásicos de controlar los parques eólicos a través de una estructura de control jerárquico de dos niveles se adoptan y mejoran para regular de manera óptima la potencia activa de las turbinas eólicas para cumplir con lor requerimientos de los TSOs. En este sentido, esta tesis doctoral asigna un interés especial a cómo formular la función objetivo de que la potencia demandada por la red sea continuamente regulada a los valores deseados considerando el impacto de los efectos estela. Por otro lado, en caso de que la potencia demandada estuviera debajo de la energía disponible del parque eólico, hay una parte de energía potencial sobrante, definida como *power reserve*, que se puede usar para ayudar a la red eléctrica por ejemplo, el soporte de frecuencia, en caso de necesidad. Uno de los principales desafíos de esta tesis es maximizar esta reserva de potencia, y al mismo tiempo seguir la potencia de referencia.

Sin embargo, el impacto de la estela de viento generada por una turbina sobre otras turbinas necesita ser minimizado para mejorar la reserva de potencia. Por lo tanto, a lo largo de esta tesis se proponen estrategias de control centralizado para parques eólicos enfocadas en distribuir óptimamente la energía entre las turbinas para que el impacto negativo de la estela en la reserva de potencia total se reduzca.

Se discuten dos técnicas de control para proporcionar los objetivos de control mencionados anteriormente. En primer lugar, se propone un algoritmo de control óptimo para encontrar la mejor distribución de potencia entre las turbinas en el parque mientras se resuelve un problema iterativo de programación lineal.

Este enfoque proporciona una mejoría significativa en términos de reserva de potencia, mientras que mantiene la carga computacional para encontrar la solución óptima lo suficientemente baja para garantizar control on-line.

En segundo lugar, la técnica de control predictivo basada en modelo se utiliza para

resolver un problema de control multi-objetivo que también podría incluir, junto con la maximización de reserva de potencia, otros objetivos de control, tales como la minimización de las perdidas eléctricas en los cables de la red de interconexión entre turbinas y un controlador/supervisor. Además, la investigación realizada resalta la capacidad de las estrategias de control propuestas en esta tesis para proporcionar mayor reserva de potencia respecto a los conceptos comúnmente usados para distribuir la potencia total del parque eólico.

La idea principal detrás del diseño de una estrategia de control de parques eólico es de encontrar una solución óptima dentro de un cálculo computacional relativamente bajo. De hecho, las consignas requeridas para proveer soporte a la frecuencia son de tiempos muy cortos en el orden de segundos para la provisión del servicio. Aunque los controladores centralizados propuestos en esta tesis reaccionan rápidamente a los cambios en la potencia de referencia enviada desde el controlador, algunos problemas pueden ocurrir cuando se consideran parques eólicos de gran escala debido a los retrasos existentes por el viento entre turbinas.

Los grandes parques eólicos pueden incluir más de cien turbinas. Bajo estas circunstancias, la producción de energía de cada turbina está altamente acoplada con la propagación de la estela y, por ende, con las condiciones de funcionamiento de las otras turbinas. Por lo tanto, los enfoques de control centralizado pueden exigir un gran intercambio de información entre las turbinas y el controlador central. Sistemas de comunicaciones complejos y el gran intercambio de información resultan difíciles de gestionar a lo largo del tiempo adecuado para satisfacer los requisitos actuales de generación de energía. Adicionalmente, la alta dependencia en la comunicación entre turbinas y la necesidad de sincornización entre el control y las turbinas hace que el sistema pueda estar expuesto a fallos. Para hacer frente a estos problemas, esta tesis doctoral propone un esquema de control de parques eólicos no centralizados basado en una estrategia de partición para dividir el parque eólico en sub-conjuntos independientes de turbinas. Con la estrategia de control propuesta, el tiempo de cálculo se reduce adecuadamente en comparación con la estrategia de control centralizado mientras que el rendimiento en la distribución óptima de potencia es ligeramente afectado.

El rendimiento de todas las estrategias de control propuestas en esta tesis se prueba con un simulador de parque eólico que modela el comportamiento dinámico del efecto de estela mediante el uso de un conocido y consolidado modelo dinámico de estela y, para un análisis más realista, algunas simulaciones se realizan con software avanzado basado en la técnica de Large Eddy Simulation.

Contents

List of Figures

List of Tables

Notation

Symbol	Description
$\{\cdots\}$	set
$i \in \mathcal{X}$	i is an element of the set $\mathcal{X}$
$\mathbb{R}$	set of real numbers
$\mathbb{R}_{>c}$	$\mathbb{R}_{>c} \triangleq \{x \in \mathbb{R} : x > c\}$ for some $c \in \mathbb{R}$
$\mathbb{R}_{\geq c}$	$\mathbb{R}_{\geq c} \triangleq \{x \in \mathbb{R} : x \geq c\}$ for some $c \in \mathbb{R}$
$\mathbb{R}^n$	space of n-dimensional (column) vectors with real entries
$\mathbb{R}^{n \times m}$	space of n by m matrices with real entries
$\mathbb{Z}$	set of integers
$\mathbb{Z}_{>c}$	$\mathbb{Z}_{>c} \triangleq \{x \in \mathbb{Z} : x > c\}$ for some $c \in \mathbb{Z}$
$\mathbb{Z}_{\geq c}$	$\mathbb{Z}_{\geq c} \triangleq \{x \in \mathbb{Z} : x \geq c\}$ for some $c \in \mathbb{Z}$
$\mathbf{x}^\top$ ($\mathbf{X}^\top$)	transpose of a vector $\mathbf{x} \in \mathbb{R}^n$ (matrix $\mathbf{X} \in \mathbb{R}^{n \times m}$)
x_i	i-th element of the vector $\mathbf{x} \in \mathbb{R}^n$
$[a_{ij}]$	element in the i-th row and j-th column of the matrix $\mathbf{A} \in \mathbb{R}^{n \times m}$
$\operatorname{diag}(\cdots)$	operator that builds a diagonal matrix with the elements of its argument, i.e.,

$$\operatorname{diag}(A_1, \ldots, A_k) = \begin{bmatrix} A_1 & 0 & \cdots & 0 \\ 0 & A_2 & \ddots & \vdots \\ \vdots & \ddots & \ddots & 0 \\ 0 & \cdots & 0 & A_k \end{bmatrix}$$

$\lvert\cdot\rvert$	$\lvert x \rvert \geq 0$ with $x \in \mathbb{R}$ returns the absolute value of the scalar x
$\lVert\cdot\rVert$	2-norm (Euclidian norm) of a vector, i.e., $\lVert\mathbf{x}\rVert \triangleq \sqrt{\sum_{i=1}^n x_i^2}$, where $\mathbf{x} \in \mathbb{R}^n$
$\mathbf{I}_n$	identity matrix of dimension $n \times n$, where $n \in \mathbb{Z}_{\geq 1}$
$\mathbf{1}_n$	vector with $n \in \mathbb{Z}_{\geq 1}$ unitary entries, i.e., $\mathbb{1}_n = [1 \quad \ldots \quad 1]^\top \in \mathbb{R}^n$

$\mathbf{0}_{m\times n}$	zero matrix of dimension $m \times n$, where $m, n \in \mathbb{Z}_{\geq 1}$
$(\cdot)^\star$	The super index $\star$ denotes optimality, e.g., $\mathcal{P}^\star$ denotes the optimal partition
$\dot{x}$	derivative of $x(t)$ with respect to the continuous time, i.e., $\dot{x} = \frac{d}{dt}x(t)$. Moreover, arguments in continuous time are expressed in parenthesis, e.g., $x(t)$, $\mathbf{A}(t)$, and the argument corresponding to the continuous time is mostly omitted throughout this thesis in order to simplify notation
$\mathbf{x}(k)$	the sub-index k indicates the discrete time
$\mathbf{x}(k+j\|k)$	prediction of $\mathbf{x}$ made at time instant k for the time instant $k+j$, where $k, j \in \mathbb{Z}_{\geq 0}$. In the argument $k+j\|k$, the first element $k+j$ indicates discrete time prediction, whereas the second element k indicates the actual discrete time

Acronyms

Acronym	Description
APC	Active Power Control
AGC	Automatic Generation Control
CC	Central Controller
CMPC	Centralized Model Predictive Control
CPU	Central Processing Unit
DFIG	Double-fed induction generator
DMPC	Decentralized Model Predictive Control
LES	Large-Eddy-Simulation
MIMO	Multi-Input multi-output
MPC	Model Predictive Control
PCC	Point of Common Coupling
PID	Proportional-Integral-Derivative Control
PLC	Partitioning Local Controller
QP	Quadratic Programming
RES	Renewable Energy Sources
RMS	Root-Mean-Square
SISO	Single Input Single Output Systems

TSO	Trasmission System Operator
WECS	Wind Energy Conversion Systems
WF	Wind Farm
WPP	Wind Power Plant
WT	Wind Turbine

Nomenclature

ρ	air density
R	rotor radius
r_{ij}	wake radius
d_{ij}	turbines distance
A_0	rotor area
A_s	shadowed area
z_0	roughness coefficient
v_∞	freestream wind speed
v_i	incoming effective wind speed
ϕ	freestream wind direction
ϵ_{ij}	wake strength of turbine j affecting the turbine i
β	pitch angle
τ_g	generator torque
ω_r	angular speed
λ	tip speed ratio
a	induction factor
C_p	power coefficient
C_T	thrust coefficient
P_g	power generated wind turbine
P_dem	power demand
P_N	wind turbine rated power
P_res	wind farm power reserve
P^loss	electrical power losses
P_av	available power
P_r	reference power

P_{greedy}	maximum power for greedy control
P_{w}	power generated by the turbine in the partition
P_{max}^{ss}	steady-state available power
P_{g}^{ss}	steady-state generated power
T_i	i-th turbine
n_t	number of turbines in the farm
T_s	sample time
H_p	prediction horizon
η	time constant wind turbine model
γ	weight related to the objective function
f	frequency, sub-script s and over-script * indicate respectively
	frequency of the grid and standard frequency (50 Hz in Europe)
$\mathcal{P}_l$	Partition set l-th partition
$\bar{\mathcal{V}}_{\text{so}}$	Set of source elements
$\bar{\mathcal{V}}_{\text{si}}$	Set of sink elements
$\bar{\mathcal{V}}_{\text{ac}}$	Set of actuator elements
τ_i	Network resource-feeding indices, $\tau^* = \max(\tau_i)$
σ	sink co-relation index
α	resource feeding co-relation index
μ	exponential dynamical weight term

Part I

Preliminaries

Chapter 1

Introduction

1.1 Motivations

Since the early 2000s, renewable power has been the driver of a global energy transformation largely due to the commitment of industrialized countries to both endorse global environmental concern on pollution and greenhouse gases emission and lessen the nation's dependence on fossil fuels. A third of global power capacity is now based on renewable energy sources (RES) with an installed capacity of 2351 GW at the end of 2018. Starting from less than 20 GW of annual growth in 2001, in the last four years the installed capacity witnessed unprecedented growth of about 160 GW per year, which enabled the renewable generation capacity to improve from 22% to 63% of the worldwide power capacity, see Figure 1.1. The 20-20-20 target set by the European Commission has drove the European countries to install even more RES by retiring or converting the conventional power plants to fulfill the expectation of covering more than 40% of the worldwide electrical consumption in 2040 [2]. Specifically, solar and wind power are the fastest growing sources of electricity and, up to 2016, have counted of more than 11% and $16,7\%$ of the shared installed capacity, see Figure 1.2. As Europe, also North America and Oceania have experienced a significant replacement of conventional generation, while in Asia and Middle East the increasing of RES installation has been almost of the same amount as the conventional one.

Among the RES, hydropower accounts for the largest share with an installed capacity of 1172 GW, i.e., around half of the total. Wind and solar energy account for most of the remainder with capacities of 564 GW and 480 GW, respectively. Meanwhile, the

other RES include 121 GW of bio-energy, 13 GW of geothermal energy and 500 MW of marine energy according to IRENA's data [82].

Wind energy represents today one of the leading energy generation thanks to the advanced wind turbine technologies, commercially available. Wind turbine capacity has reached more than 8 MW, and to the recently fall of the manufacturing and maintenance costs. Nevertheless, in Europe, the installation of large wind power plants (WPPs) with nominal capacities close to the one of fossil-fuel plants has overtaken coal-based energy generation, making wind energy the second largest power source for installed capacity. Moreover, in 2018 wind energy was the largest investment opportunity in the power sector in Europe; several investors have purchased wind power plants in operation or under construction for doubled in value respect to 2017 [164]. The low interest rates were beneficial especially for the offshore market, which has seen financed more than double of the offshore projects with respect to 2016, with a consistent growth of offshore wind generation especially in Germany, Belgium and Denmark, see Figure 1.3. Such an increasing trend has characterized also the global offshore market grew by 0.5% in 2018, reaching an installation of 23 GW, making China the first country for annual installation of both offshore and onshore WPPs (see Figure 1.3).

The massive penetration of wind generation in the energy market shall be supported by a wider and innovative research work to push forward the deployment of wind systems for reducing the costs of installation and production as well as for providing the grid services typically relied on conventional power systems. For instance, these objectives can be achieved by

- Improving the turbine's lifetime by investigating innovative structural designs.
- Increasing the turbine's energy extraction by properly designing turbine's controllers.
- Placing the turbines close each other, i.e., in a wind farm, to reduce the maintenance costs and electrical interconnection.
- Regulating the wind farm generation taking into account power system stability issues.

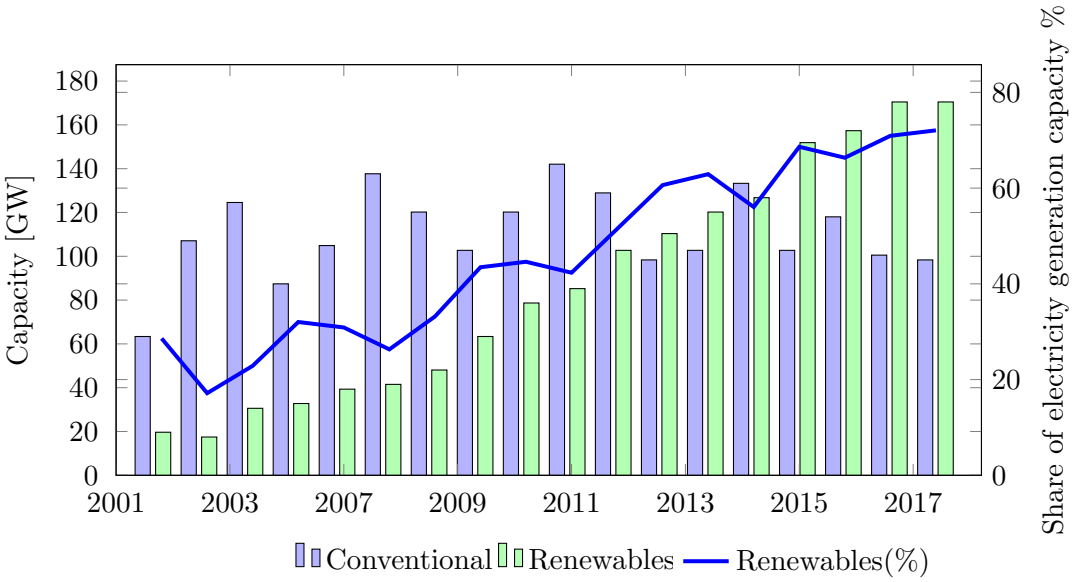

Figure 1.1: Capacity of renewable and conventional generations and contribution of RES to the global energy transition. Source: [82].

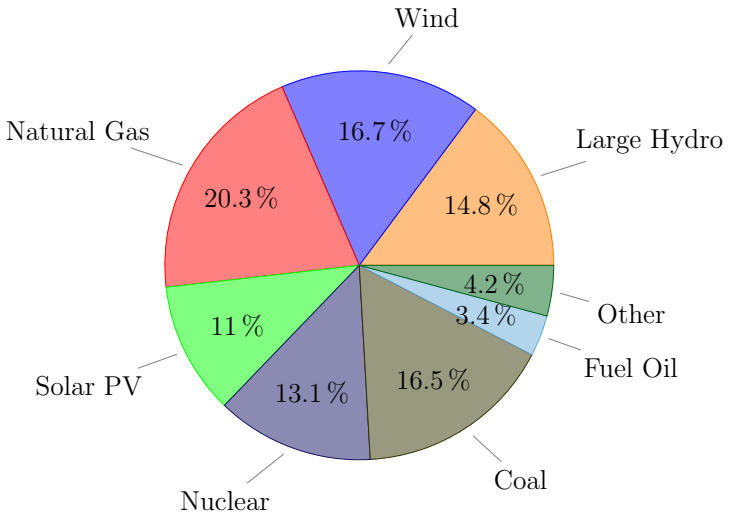

Figure 1.2: Shared installed power capacity in Europe in 2016. Source: WindEurope [163].

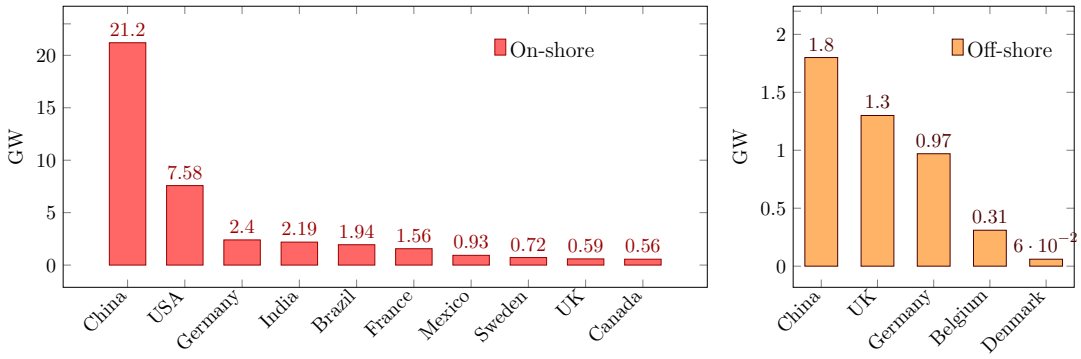

Figure 1.3: The top on-shore and off-shore markets in 2018 according to GWEC's findings, [73].

If in the past years, the wind farms were basically operated to deliver into the grid the maximum power available from the wind conditions, nowadays the high penetration of wind energy is affecting the role of WPPs in providing power system stability issues. Nevertheless, one crucial downside of the massive presence of wind power generators (and other RES) in the electrical networks is the reduction of the system inertia to maintain nominal operating conditions under disturbances, which affect the system stability (e.g., load changes, fault events, etc.).

Unlike conventional power plants, based on synchronous generation, modern wind turbines (type 3 and 4) are decoupled from the grid frequency through power electronics, hence they are unable to automatically restore the nominal frequency of the grid after that a change in active power demand or production generates a frequency excursion, and/or to keep the voltage within acceptable limits. Therefore, nowadays, different grid codes established by the Transmission System Operators (TSOs) require WPPs to be able to provide *frequency and voltage controls, and fault ride-through capabilities* [35]. To do this, WPPs need to be controlled through active and reactive power controls, which aim to control the active power output and the injected/absorbed reactive power of a wind farm in order to assess (among with conventional plants) the stability of the grid. Some studies also show that there is an economical potential benefits for WPPs operators to participate in the ancillary services market [89], which may encourage the WPPs owners to provide grid requirements. Especially, significant steps forward to the integration of new grid codes for WPPs have been made in those countries where the wind generation covers a high part of the electrical consumption, such as Germany, Den-

mark, China and the state of California, among others. Specifications are imposed at the large wind farms (i.e., with a capacity close to the one of conventional systems) in order to: 1) provide tolerance for the rate of frequency change, 2) follow common operation modes for frequency response and automatic voltage control. However, although significant harmonization of national grid codes has been made, a general guideline for power systems to make full harmonization among the countries is still missing [115].

The new grid codes are pushing researchers and industries for providing innovative operating strategies for WPPs. Over the last years, advanced control strategies have been proposed to achieve active power control to allow wind turbines to help in frequency support. Changes in power supply or demand lead to a temporary imbalance of the system frequency and affect operating conditions of power plants as well as consumers. Large drops in frequency can trigger a cascade tripping of power stations and generate a complete shutdown of electricity supply. Hence, the maintenance of frequency involves additional active power that should be delivered into the grid by WPPs to smooth the frequency droop.

Four power reserve levels can be defined according to the timescale necessary to deliver these powers, see Figure 1.4. *Inertia and primary reserves*, which act on time scale between $0.01 - 1$ s to stop the initial frequency drop, *secondary and tertiary reserves* that draw back the frequency at the nominal value and replace the secondary reserves, to manage some constraints in the transmission lines. Wind turbines can participate in inertial control emulating the inertia response of the conventional plants by designing an artificial control loop to inject into the grid kinetic energy, through control of the wind turbine rotor speed, [102]. Furthermore, also primary control can be ensured to provide both upward and downward frequency regulations. While the former is always possible by limiting the power injected from the wind farm, the latter requires additional power reserve. Therefore, if WPPs are required to participate in frequency control they should operate in deloaded mode by keeping a certain capacity reserve. There are several approaches for doing so, and the investigation of new approaches based on a better understanding of the wind and wind turbine dynamics is acquiring relevance as a major-focus research topic among the wind energy researchers.

Since frequency support is and will be of central interest in the next years, especially

with the occurrence of new grid codes, this doctoral thesis presents new concepts on both model development and control design for wind farms. Novel control strategies are addressed with the aim to improve the wind energy participation in the power generation market and in the electrical balancing market. Wind farm generation is optimized by designing closed-loop control strategies able to account of the fast dynamics characterizing the wind turbine operation, as well as, of the slower dynamics of the wind flowing through the wind farm. Surrogate low-fidelity models for describing these dynamics are used to design wind farm controllers based on the receding horizon idea, i.e., predictive controllers, stated to solve multi-objective optimization problems able to optimally regulate the wind turbines power set-points. Reliability and performance are the main drivers for designing proper control strategies that ensure accurate enough prediction behaviour and, at the same time, low computational costs to provide real-time control. In fact, the computational time should be kept small enough to guarantee fast response in order to ensure grid support, which usually should be provided within second scale. Furthermore, with the aim to guarantee the aforementioned objectives, also when large WPPs are considered, both *centralized* and *non-centralized* control architectures are proposed. On the other hand, with the growing number of turbines in the wind farm, the large communication links required for a centralized control approach might have associated high computational burden, especially when some optimization is solved in the control algorithms, and low resiliency in case of the failure of one sensor. Furthermore, the proposed methodologies are tested in MATLAB-Simulink wind farm toolbox, which is able to simulate the slow dynamics of the wind flow field, to assess the closed-loop performance and the effectiveness of the control strategies by making comparisons with results obtained from the different proposed approaches and among the centralized and non-centralized control techniques.

1.2 Research Questions

This dissertation is devoted to the design of wind farm optimization-based controllers. The main research goal of this thesis is motivated by the following key research questions:

Q1 Which kind of wind farm controllers can be designed to provide grid support?

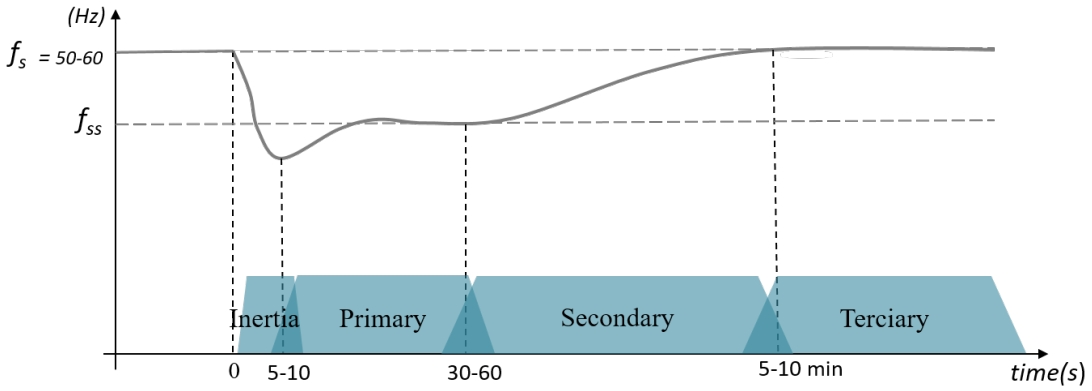

Figure 1.4: Frequency response after a droop from the nominal value f_s and deployment of power reserve.

Q2 How the operation of a wind turbine can influence the power delivered by a wind farm?

Q3 Which wind farm dynamics are needed to be considered when designing a wind farm model such that a control strategy can be used in an online closed-loop framework?

Q4 Which control objective should be stated in an optimization-based control for wind farm to provide frequency support?

Q5 How the computational burden can be reduced while ensuring the reliability of the controller when the number of turbines in the wind farm becomes larger?

Q6 How can optimally distributed the wind controllers? Is a centralized approach the best solution?

Q7 How the non-centralized control topology influences the overall closed-loop performance when controlling a wind farm with respect the centralized counterpart?

Detailed answers to the aforementioned questions will be given throughout this dissertation. Questions Q1 and Q2 allow to provide an overview of the wind farm models and control approaches already present in the literature. On the other hand, they identify possible research opportunities in which this thesis provides its contribution. Questions Q3-Q5 are the hearth of this thesis, proposing the design of novel optimization-based both model-free and model-based control strategies to optimize the participation of wind

farm in frequency support while satisfying other constraints imposed by the electrical grid and wind turbine characteristics. Finally, questions Q6-Q7 are devoted to solve the problem of controlling large-scale wind farms in a clever way, considering the aerodynamic couplings among the turbines and additional constraints imposed by the electrical grid.

1.3 Thesis Outline

This thesis is divided into the following parts:

I Preliminaries,

II Centralized control approaches for power reserve maximization,

III Non-centralized wind farm control strategies for optimizing wind farm power generation,

IV Concluding remarks.

In Figure 1.5, it is shown a road map for helping the reader to summarize the structure and the main connections about the topics covered in this thesis.

Chapter 2: Literature Review and Background

This chapter is devoted to present an overview of the main topics covered in this thesis. Firstly, a brief description about the most common wind turbines, together with their mechanical and electrical characteristics, are discussed. Then, the main issues when controlling wind turbines located in a wind farm are presented with a general review about the principal objectives that want to be optimized when controlling the wind farm operation. In addition, the background and preliminary concepts associated to model predictive control and partitioning approaches are also presented.

Chapter 3: A wind farm control strategy for power reserve maximization

This chapter presents a new wind farm control strategy to optimally distribute the power set-points among the turbines inside a wind farm such that the tracking of the power

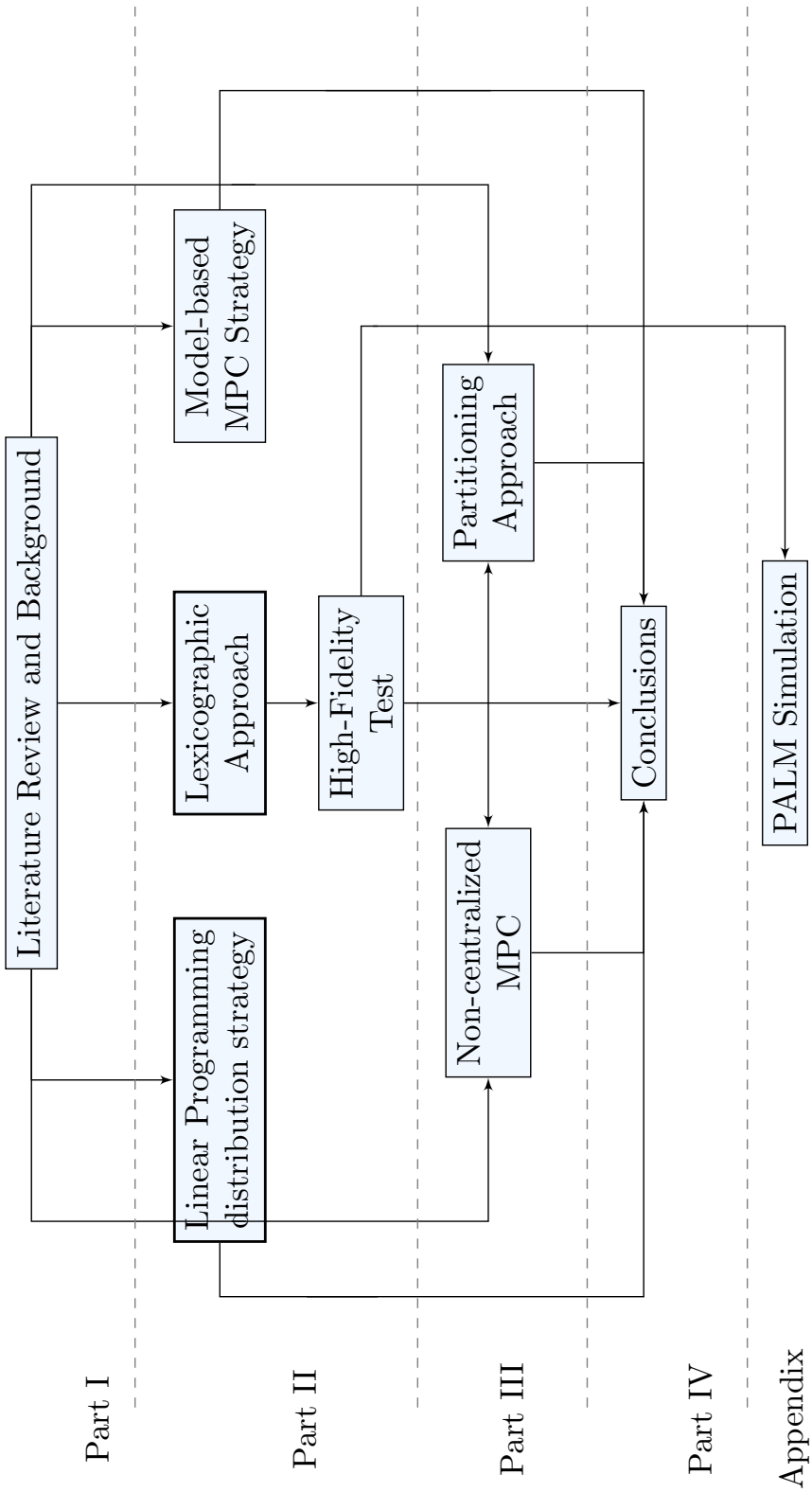

Figure 1.5: Road map of the thesis.

demanded by the grid is ensured. Moreover, a linear programming problem is stated to improve the extra power that the wind farm can provide in case of deloading operations, such that the capacity reserve of the wind farm is improved. The test of the proposed strategy is made under different wind conditions and power generations to ensure the reliability and performance of the proposed methodology for each operation conditions. This chapter is mainly based on the following publication:

- Siniscalchi-Minna, S., Bianchi, F. D., De-Prada-Gil, M., Ocampo-Martinez, C. (2019). A wind farm control strategy for power reserve maximization. *Renewable energy*, 131, 37-44.

Chapter 4: Predictive Control based on Lexicographic Minimizers

This chapter copes with the non-convexity nature of the cost functions of a multi-objective optimization-based problem stated to minimize the tracking error, for providing automatic generation control, and to maximize the power reserve, for enhancing the participation of the wind farm in primary frequency support. The lexicographic solution method is applied to ensure the priority among the different objectives and avoids the min-max non-convexity problem. The receding horizon technique is used to design the predictive wind farm central controller, here the dynamics of the turbines are described with simplified linear models that allow to keep low computational burden such that the controller can be used for on-line optimization. Simulations are shown in high-fidelity wind farm simulator able to reproduce the highly dynamic nature of the wind and to test the wind turbine operation under a turbulent flow-field considering. This chapter is mainly based on the following publication:

- Siniscalchi-Minna, S., Bianchi, F. D., Ocampo-Martinez, C. (2018, June). Predictive control of wind farms based on lexicographic minimizers for power reserve maximization. In *2018 Annual American Control Conference (ACC)* (pp. 701-706). IEEE.

Chapter 5: A multi-objective predictive wind farm controller for enhancing primary frequency support

This chapter states a multi-objective predictive control strategy where the power distribution among the turbines is optimally regulated by a predictive central controller. In light of the results obtained from the two previous chapters, in this control strategy the active power distribution is ensured by properly setting specific weighting parameters that guarantee the minimization of the power losses due to the wake propagation throughout the farm. Furthermore, along with the aerodynamics interactions also the minimization of the power losses within the inter-array collection grid is considered. Therefore, specific simulations will show how the minimization of electrical and aerodynamics interaction can be treated for several wind speed directions, since the minimization of aerodynamic interactions for certain wind directions may result from the opposite regulation to reduce the electrical cable losses. In order to highlights the improvements of using the proposed control approach with respect to the common power distribution approaches in terms of power reserve, a comparative study is presented. Moreover, the wind farm contribution to restore the frequency of the grid after a droop is also investigated for the investigated different distribution approaches. This chapter is mainly based on the following publication:

- Siniscalchi-Minna, S., De-Prada-Gil, M., Bianchi, F. D., Ocampo-Martínez, C., De Schutter, B. (2018, June). A multi-objective predictive control strategy for enhancing primary frequency support with wind farms. In *Journal of Physics: Conference Series* (Vol. 1037, No. 3, p. 032034). IOP Publishing.

Chapter 6: A non-centralized predictive control strategy for wind farm active power control: a wake-based partitioning approach

This chapter is devoted to present a non-centralized control strategy for controlling large-scale wind farms. Firstly, a new partitioning approach is proposed to cluster the turbines in the farm according to the aerodynamic coupling due to the wake effects. Then, each subset is controlled independently by a central control unit based on the receding horizon idea. Each subset can be considered to behave as an equivalent wind turbine, hence an aggregated first-order model is used to describe its dynamic. At the partition

level, the centralized approach presented in Chapter 5 is used to control the single wind turbine. Simulations show the improvements in terms of reduction of computational burden and the negative impact on the overall performance for maximizing the wind farm power reserve, when the proposed model is used. Furthermore, a sensitivity analysis on the overall wind farm control performance is shown for different number of partitions. This chapter answers the research question Q6-Q7 and it is based on the following publications:

- Siniscalchi-Minna, S., Bianchi, F. D., Ocampo-Martinez, C., Dominguez-Garcia, J.L., De-Schutter, B. A non-centralized predictive control strategy for wind farm active power control: a wake-based partitioning approach. Submitted to *Renewable Energy Journal*. Elsevier.
- Siniscalchi-Minna, S., Ocampo-Martinez, C., Bianchi, F. D., De-Prada-Gil, M., De-Schutter, B. (2018, December). Partitioning approach for large wind farms: Active power control for optimizing power reserve. In *2018 IEEE Conference on Decision and Control (CDC) (pp. 3183-3188)*. IEEE.

Chapter 7: Contributions and Concluding Remarks

This chapter draws the concluding remarks of this dissertation and proposes some open research questions as future work. The key research questions presented are also addressed in this chapter.

Other Publications and Awards

- Boersma, S., Doekemeijer, B. M., Siniscalchi-Minna, S., van Wingerden, J. W. (2019). A constrained wind farm controller providing secondary frequency regulation: An LES study. *Renewable energy*, 134, 639-652.
- Best poster award at Wind Europe 2017.

Chapter 2

Background and Literature Review

This chapter presents a literature review related to the main topics treated in this doctoral thesis. First, some relevant notions of wind energy and wind turbine aerodynamics are described to derive the expressions for power and forces developed on the wind turbines. Afterwards, a literature overview of wind farm control strategies is made focusing on active power control. Firstly, some relevant works related to centralized and non-centralized wind farm controller designs are discussed. Secondly, the model predictive control strategy is presented, highlighting its versatility in the design of optimization-based wind farm controllers. Thirdly, the partitioning of large-scale systems applied to wind energy systems is briefly revised, being used throughout the thesis.

2.1 Wind Turbine Overview

This section is devoted to provide an overview about the main mechanical and electrical characteristics of a wind turbine and to derive the mathematical formulations of the torque, forces and power developed on a wind turbine.

The wind turbines are basically classified according to the way the turbine spins into *horizontal* and *vertical* axis. Wind turbines that rotate around a horizontal axis are more common, while the use of vertical axis wind turbines has considerably been reduced during the last years due to the less energy intercepted by the rotor. Two sub-groups of horizontal axis wind turbines can be identified, i.e., *fixed-speed* and *variable-speed* wind

turbines. The former, known also as Type 1, has the advantage of being simple and reliable to control. However, the direct connection to the grid imposes the generator to rotate at synchronous speed avoiding the possibility to optimize the power extraction. Meanwhile, the idea behind variable speed wind turbines is to keep the generator torque constant while the wind variations are absorbed by changes in the generator speed. From the electrical point of view three different types of variable-speed wind turbines have been proposed over the years. Limited variable-speed wind turbine (or Type 2), such that the speed operation range change from 0% to 10% above the synchronous speed, but the problems of the fixed-speed concept are not totally solved. In order to cope with this issue, two other types have been proposed, i.e., variable speed with partial-scale converter and variable speed with full-scale converter, which will be thoroughly discussed in Chapter 2.1.3.

Therefore, in this dissertation only the variable-speed variable-pitch horizontal axis wind turbines are considered, as nowadays they represent the most employed wind technology [79]. However, the interested reader can find a more complete and detailed description about wind turbines development and innovation in [8, 23, 54, 80].

Typically, the main components of a wind turbine are:

- *Rotor*, which is the assembly of the blades, typically three or two, connected to a central hub.
- *Nacelle*, which hosts the gearbox, generator, and all the other components enabling mechanical transmission, such as heat exchangers, coolers and heaters.
- *Tower*, which holds up the nacelle. Recently, the yaw system is located between the wind turbine nacelle and tower in order to ensure that the rotor is facing into the wind as the wind direction changes.

The components along with the main control variables are shown in Figure 2.1, the latter are: 1) *pitch angle* (β) that can be set to properly rotate the blades in order to regulate the power extracted by the turbine for high wind speed conditions; 2) *generator torque* (τ_g), it is controlled to ensure specific turbine operations when the incoming wind speed is low and the pitch is not activated; 3) *yaw angle* (γ), by setting a yaw angle different from 0 degrees the orientation of the rotor turbine changes with respect to the incoming

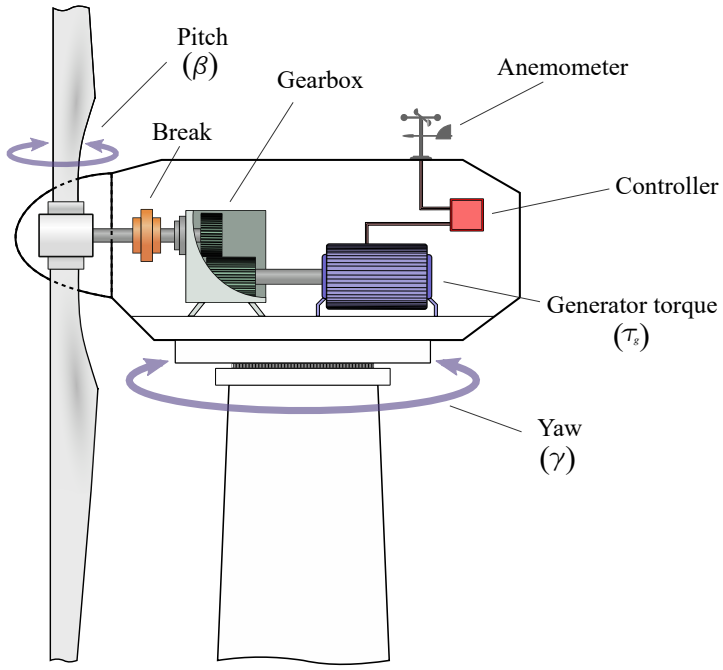

Figure 2.1: Main components of a wind turbine.

wind direction. All these control variables can be optimized to improve the performance of the wind turbine operation.

2.1.1 Aerodynamics

The wind turbine converts the kinetic energy contained into the moving air into mechanical energy. The rotor turbine turning at an angular speed ω_r exerts a force on the wind flowing through the rotor F_t while a torque T_r acts on the rotor. The most common approach to derive the aerodynamic model of a wind turbine is the actuator disc theory, also known as disc theory [23, 83], which is based on the assumptions that the wind turbine behaves as an actuator disc (represented as a dark shadowed area in Figure 2.2), the wind flows in a tube where the external pressure is the same as undisturbed field (i.e., the flow is incompressible), and the mass flow rate remains the same throughout the flow. Therefore, applying the conservation of axial momentum and the equilibrium of forces law on the rotor area, the following formulation for the mechanical torque is obtained:

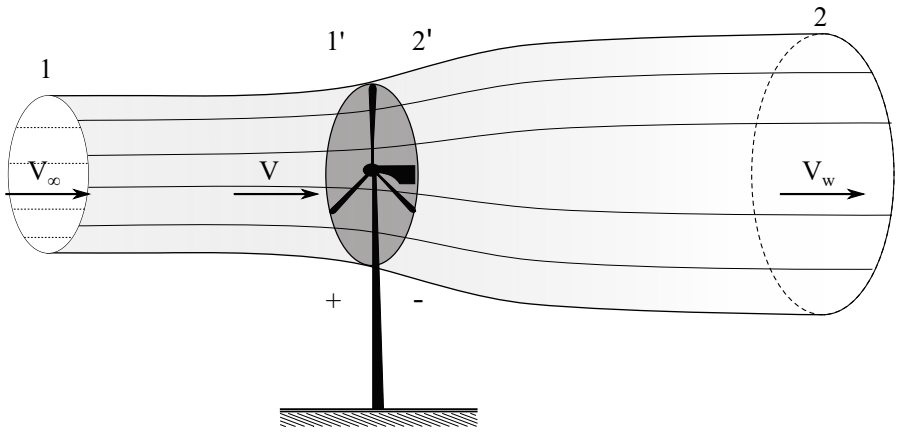

Figure 2.2: Cone development based on the disc theory.

$$\begin{aligned} T_r &= \rho A_r v_{\mathrm{r}}(v_\infty - v_{\mathrm{w}}), \\ T_r &= A_{\mathrm{r}}(p^+ - p^-), \end{aligned} \tag{2.1}$$

where $A_{\mathrm{r}} = \pi R^2$ indicates the rotor area, being R the rotor radius, ρ the air density, v_{r} the wind speed faced by the rotor, v_∞ and v_{w} respectively the wind speeds at the tube inlet and outlet. Finally, p^+, p^- indicate the air pressures immediately before and after the rotor, see Figure 2.2. Applying the Bernoulli's equation for the section $1 - 1'$ and $2 - 2'$, the pressure drop can be written as

$$(p^+ - p^-) = \frac{1}{2}\rho(v_\infty^2 - v_{\mathrm{w}}^2). \tag{2.2}$$

Replacing (2.2) into (2.1) the expression of the outlet wind speed is

$$v_{\mathrm{w}} = (1 - 2a)v, \tag{2.3}$$

where a indicates the *induction factor*, which gives information about the interference between the wind speed and the rotor turbine. Finally, the thrust force can be expressed as

$$F_{\mathrm{t}} = 2\rho A_r v_\infty^2 a(1 - a), \tag{2.4}$$

and the power extracted by the wind as

$$P_{\mathrm{g}} = 2\rho A_r v_\infty^3 a(1 - a)^2. \tag{2.5}$$

It is clear that, for a given freestream wind speed, those equations depend on the generation conditions of the wind turbines counted by the induction factor. Therefore, the

wind turbine capability of capturing the energy from the wind flow field can be indicated by the power and trust coefficients, defined as

$$\begin{aligned} C_{\mathrm{T}} &= 4a(1-a) \\ C_{\mathrm{P}} &= 4a(1-a)^2. \end{aligned} \tag{2.6}$$

In normal operation of the wind turbine, the induction factor a can be assumed taking values between 0 and 1/3. Therefore, the coefficients in (2.6) are increasing functions of a_i and the maximum theoretical value of $C_{\mathrm{p,max}}$ is obtained at $a = 1/3$. This is a theoretical upper bound for limiting the wind turbine operation. Typically, for the commercialized wind turbines the maximum value of C_{P} is lower than the theoretical limits, being almost equal to 0.45 [23]. The manufacturer provides the C_{P} and C_{T} tables as function of the pitch angle β and the tip speed ratio λ, defined as

$$\lambda = \frac{\omega_r R}{v_\infty}, \tag{2.7}$$

where ω_r is the angular speed. Notice that the equations of C_{P} and C_{T} as function of the blade pitch and tip speed ratio can be obtained by modeling the wind turbine aerodynamics following the blade element theory [23]. Therefore, the power generated by a wind turbine facing a freestream wind speed v_∞ is

$$P_{\mathrm{g}} = \frac{1}{2}\rho A_r C_P(\beta, \lambda) v_\infty^3. \tag{2.8}$$

In this thesis, the power and thrust coefficient curves of the benchmark NREL-5MW wind turbine shown in Figure 2.3 are used.

2.1.2 Mechanics

Conceptually, the mechanical components of a wind turbine can be treated as rigid bodies linked by flexible joints, in number equal to the degrees of freedom of the structure. Although simple models may not represent the complex dynamics of wind turbines, they are quite helpful for controller design, where the complex dynamics can be treated as uncertainties. Usually, the variable-speed fixed-pitch wind turbines are well designed considering one or two degrees of freedom. Therefore, the most common mechanical models of the wind turbine, derived using Multi-body System approach, consist of two or one mass model. Because of its huge dimension with respect to the other components,

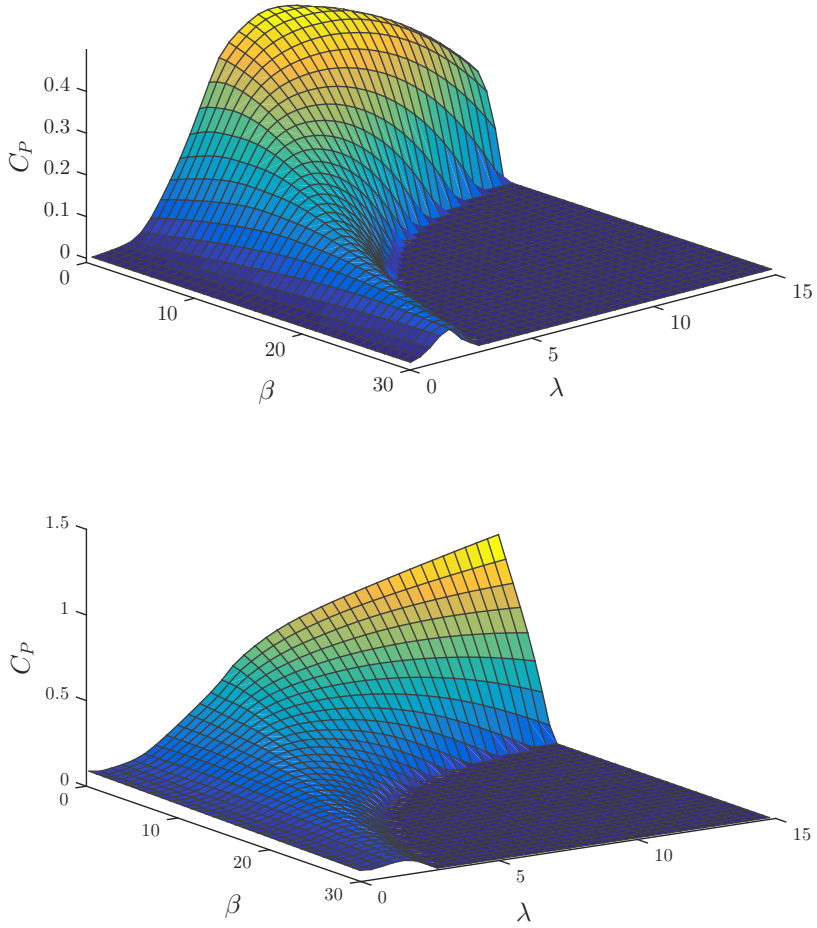

Figure 2.3: Power coefficient curve (top plot) and thrust coefficient curve (bottom plot) of the benchmark NREL-5MW wind turbine.

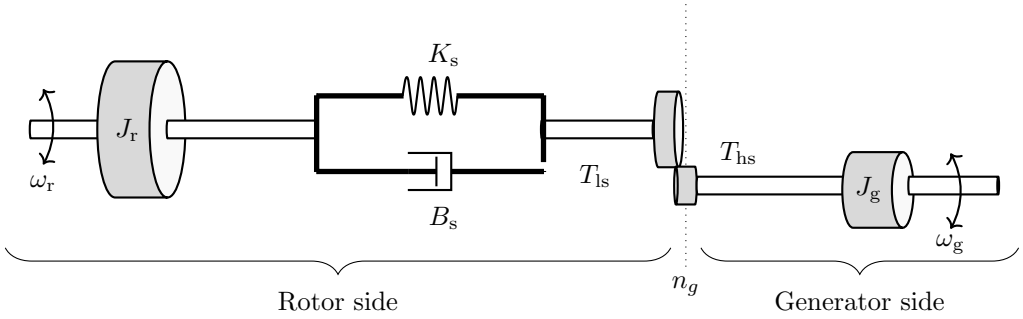

Figure 2.4: Two mass wind turbine model.

the rotor can be modeled as one mass. The drive train turns the slow rotor speed ω_r into high speed on the generator side, ω_g. Those two different speeds characterize the *two-mass model*; rotor, gear box and the slow speed shaft inertia are integrated in J_r, while the high speed shaft inertia is integrated in J_g, and the slow and high-speed parts are connected by a flexible shaft see Figure 2.4. The twisting of the rotor, gear-box, and low wind speed shaft are integrated in the torsional spring K_s and in the damping coefficient is D_s, while the two masses frictions are indicated as K_r, K_g. Hence, the rotor dynamics at the rotor side can be represented by the equation of motion

$$J_r\dot{\omega}_r = T_r - T_{ls} - K_r\omega_r, \tag{2.9}$$

being T_{ls} the torque of the low speed shaft equal to

$$T_{ls} = K_s\sigma + D_s\dot{\sigma}, \tag{2.10}$$

where $\sigma \triangleq \theta_r - \theta_g/n_g$ is the torsion angular displacement between the rotor and generator angular positions θ_r, θ_g. Similarly, at the generator side,

$$J_g\dot{\omega}_g = T_{hs} - K_g\omega_g - T_g, \tag{2.11}$$

being $T_{ls} = T_{hs}/n_g$.

Table 2.1: NREL 5MW wind turbine parameters.

Symbol	Value	Units
R	63	m
n_g	97	-
K_s	$867 \cdot 10^1 0^6$	Nm/rad
D_s	$6215 \cdot 10^3$	Nm/rad/s
J_g	534.116	kg·m^2
J_r	$387 \cdot 10^5$	kg·m^2
ω_r, N	1.26	rad/s
T_g	43093	kN·m
P_n	5	MW

Therefore, the wind turbine dynamics are described by the following system of equations:

$$\begin{aligned} J_r\dot{\omega}_r &= T_r - D_s\left(\omega_r - \frac{\omega_g}{n_g}\right) - K_r\omega_r - K_s\sigma \\ J_g\dot{\omega}_g &= \frac{D_s}{n_g}\left(\omega_r - \frac{\omega_g}{n_g}\right) - K_g\omega_g + \frac{\sigma K_s}{n_g} - T_g \\ \sigma &= \omega_r - \frac{\omega_g}{n_g} \\ P_g &= T_g\omega_g. \end{aligned} \tag{2.12}$$

Hence, the wind turbine is a multi-input multi-output (MIMO) system governed (2.12), which can be used to control the operation while acting on the generator torque T_g and the pitch angle β. Table 2.1 lists the parameters for the wind turbine NREL 5-MW used in this dissertation [85].

2.1.3 Electric

The aim of this subsection is to provide a brief description of the electrical power conversion of a wind turbine, the interested reader can find a detailed overview in [23, 166]. This work is focused on two electrical wind turbine topologies from all the different existing configurations in the wind industry: the Doubly Fed Induction Generator (DFIG - also called Type 3 wind turbine) and the fully-rated power converter (known as Type 4 wind turbine), see Figure 2.5.. These electrical topologies have been chosen due to their higher regulation capacity of rotor speed and they are explained in detail below.

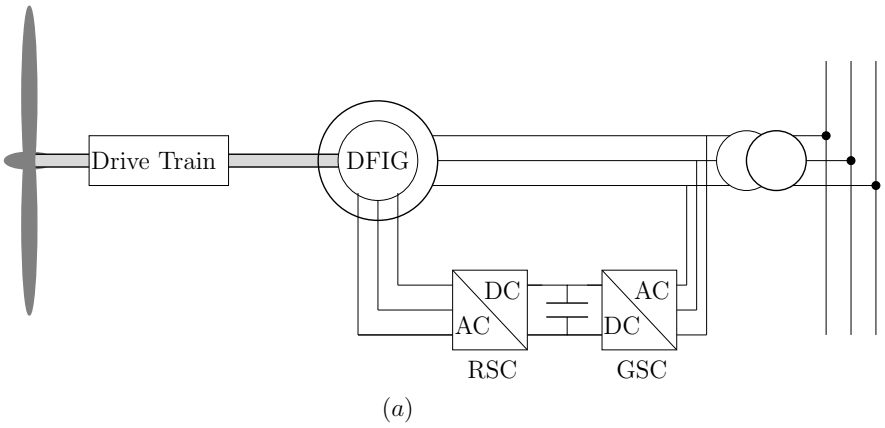

(*a*)

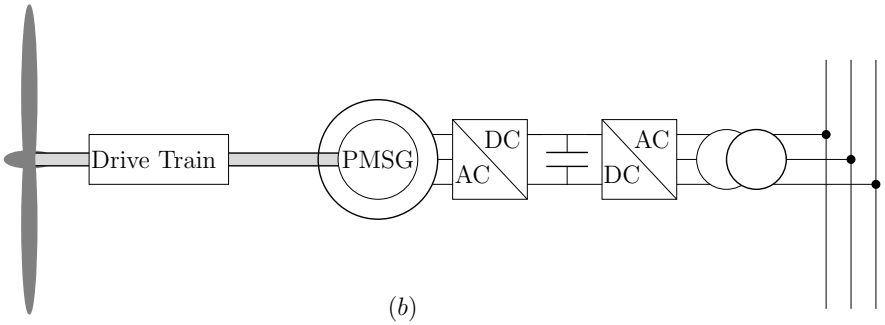

(*b*)

Figure 2.5: Figure(a): simplified structure of a DFIG. Figure(b): full-power converter (*b*).

Doubly-fed Induction Generators

Due to the improvements in power electronics and their high reliability, so far the DFIG is the most used electrical configuration for wind power applications. One of the main reasons of the massive employment of DFIG is that the power electronics devices have to manage just a fraction (almost $30-40\%$) of the power captured reducing the converter size and losses compared to a full power converter solutions [122]. In fact, the connection to the grid occurs by two different ways, see Figure 2.5a. The stator windings are connected directly to the AC grid, i.e., three-phase, constant-frequency (f_s) connection, while the rotor windings are connected to the grid through a static converter that includes a *rotor-side* converter (RSC) and a *grid-side* converter (GSC). Conventionally, the RSC controls the rotor currents in magnitude and phase to regulate the active and reactive power, while the GSC controls the DC-link voltage to ensure DC voltage stability. By regulating the generator behavior through the GSC controller, the rotation speed is allowed to operate over a range directly related to the converter rating, typically the range is limited from $-40\% to + 30\%$. The ability to change the generator rotor speed over a wide range enables the improvement of the power production by:

- Optimization of power output, the variable rotor speed increases the energy capture, especially in case of low wind speed conditions, load alleviations and more power quality
- Exploitation of the kinetic energy used to alleviate the variation of power transferred to the grid or to provide grid support.
- Possibilities of reactive power control without using the capacitors.

Furthermore, the reactive and active powers are controlled separately by transformation of the electromagnetic variables into the dq-reference frame. The reactive power depends on the quadrature rotor current (q-axis), while the active power can be influenced by controlling the d-axis components.

Full Power Converter

Figure 2.5b shows the scheme of the Type 4 wind turbine. This turbine is fully connected though a frequency converter to the AC grid that uncouples the turbine generator to

the grid frequency. The generator can be of either synchronous or induction nature, even if the wound-rotor synchronous generators have had a larger employment. The RSC ensures the rotational speed adjustment within a large range, since the converter must effort all the energy supplied to the utility. Meanwhile, the GSC transfers the active power to the grid and attempts to cancel the reactive power consumption. In the past, the large converter capacity was the main drawback of this topology, in fact the converter should be rated up 120% of the nominal generator power resulting in higher cost of this configuration respect the DFIG. However, the advances in power electronics achieved over the last years have provided converters with the capability of handing large amounts of power at accessible prices [78]. Nowadays, a large number of new wind farm installations include this wind turbine topology that ensures major performance for controlling the power and voltage as well as to guarantee ancillary services.

In this thesis, the active and reactive powers are assumed to be controlled separately by two uncoupled inner loops. Furthermore, for performing the active power, it is assumed that its effect on the reactive power is not included. Being interested in the active power control, and being the dynamics of electric machines as well as power electronics faster than the mechanical dominant modes, a steady-state first order system is used to model the generator power. Therefore, the following model of electromagnetic torque T_g is implemented

$$\dot{T}_{\mathrm{g}} = \frac{T_{\mathrm{g}} - T_{\mathrm{g,r}}}{\tau_T}, \tag{2.13}$$

being $T_{\mathrm{g,r}}$ the reference generator torque and τ_T the time constant used to describe the generator dynamics.

2.1.4 Operation

This section is devoted to present the *mode of operation* of a variable-speed variable-pitch wind turbine. The operation of a wind turbine depends on the control objectives to be achieved given the atmospheric conditions, i.e., under a certain freestream wind speed. Figure 2.6 shows the ideal power curve of a wind turbine, where the power generation is obtained from (2.8) for the wind speed range between v_{min} and v_{N}. The latter indicates the rated wind speed; while the former, also known as cut-in wind speed value, indicates the limit above which the wind turbine starts to operate. In fact, at lower wind speeds the power generated is too low to compensate the operational costs. On the other hand,

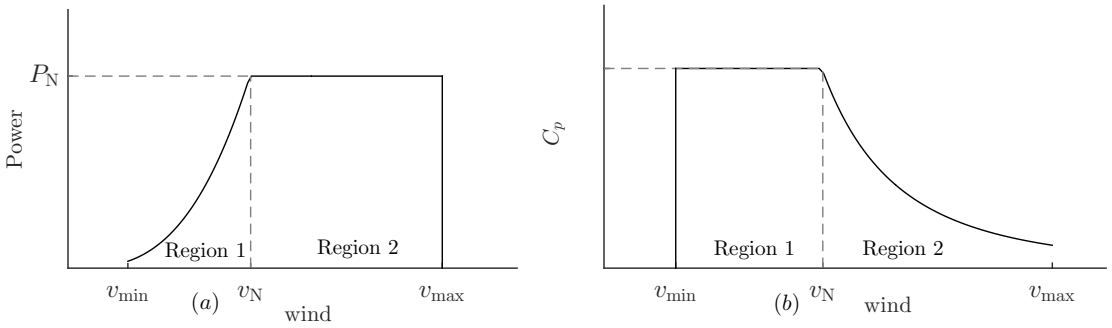

Figure 2.6: Figure (a): $P-v$ characteristic curve. Figure(b): $Cp-v$ characteristic curve

the wind speed has also an upper limit, limit of cut-out $v_{\max}$, which avoids structural overload for high wind speed conditions. Mechanical stresses and loads are also reasons of keeping the power constant to the rated value, indicated as P_{N}, from v_{N} to $v_{\max}$. This rated value is a compromise between the energy captured by the turbine and the economical aspects, e.g., the maintenance and manufacturing costs.

Classical Operation Mode

Typically, the wind turbine operation can be divided in two regions, as shown in Figure 2.6. In Region 1, called partial load operation mode and being the wind speed low ($v \leq v_{\mathrm{N}}$), the goal is to extract all the available power, i.e., the maximum generation capacity for the incoming wind conditions v. The available power is obtained using the power equation in (2.8) but computed for the maximum theoretical power coefficient $C_{p,\max}$ in (2.6), that is

$$P_{\mathrm{av}}(v) = \frac{1}{2}\rho\pi R^2 C_{p_{\max}} v^3. \tag{2.14}$$

In order to operate along the maximum power coefficient, the most common approach is based on the generator torque control while keeping the pitch angle at the constant value, typically equal to $\beta^o = 0$ degrees. Under this circumstance, the power coefficient is only function of the tip speed ratio in (2.7), i.e., $C_p(\lambda, \beta^o)$. Being the wind speed v a uncontrollable variable, the only parameter to change for providing the maximum power coefficient is the rotor angular speed ω_{r}. Figure 2.9 shows some curves of the power profile as function of the rotor speed for different values of the incoming wind speed. It can be noted that connecting the points corresponding to $C_{p_{\max}}$ the curve of optimal power P_{r} is obtained, red line in Figure 2.9. Therefore, the aforementioned

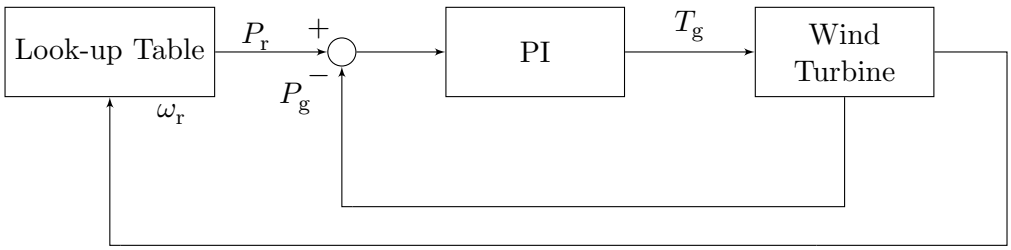

Figure 2.7: Block scheme of power control for operation mode in Region 1.

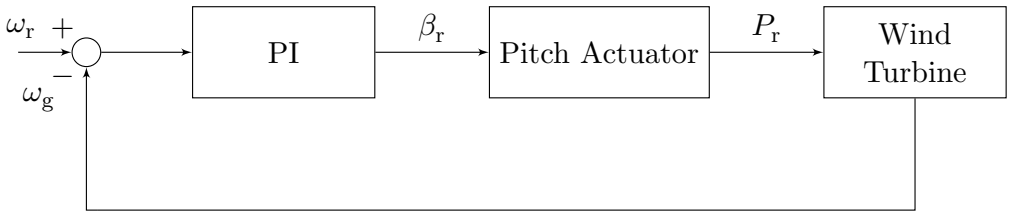

Figure 2.8: Block scheme of power control for operation mode in Region 2.

characteristics curves can be used as look-up table to provide the optimal power set-point at the turbines. This control technique is know as *Power Signal Feedback Control*, a simplified block scheme is shown in Figure 2.7. Here, a PI-based controller is used to reduce the power error by acting on the system input T_g.

At high wind speeds, the available power cannot be tracked, being higher than the power rated. Therefore, in order to achieve the ideal curve in Figure 2.6, the common operation mode in Region 2 is to limit the power generation by regulating the pitch angle with a PI-based control strategy, as shown in Figure 2.8. While for low wind speed the pitch control is only used to keep the pitch at the optimal value β^o, at $v < v_N$ it is activated to manage the transient response around the transition region, i.e., close to the rated point (P_N, v_N). In this circumstance, the aerodynamic power is quickly set at the rated value by the speed controller but, the high wind conditions increase the kinetic energy stored in the rotor inertia then transmitted to the grid, generating transient loads. Using, the pitch control this effect can be smoothed [110] with the drawback of loosing some energy capture [23].

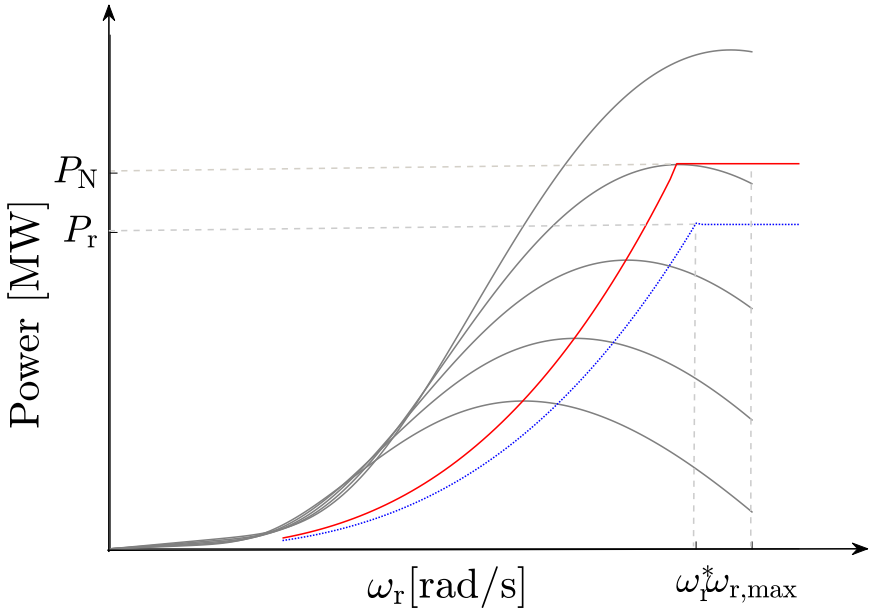

Figure 2.9: P-v and $C_P - v$ characteristics curves in MMPT mode (black line) and deloading mode (red line).

2.1.5 Operation for Grid Support

As mentioned in Chapter 1, wind farms can be demanded to meet grid code specifications. Typically, wind turbines do not automatically provide these requirements, thus it is expected to optimally regulate the power generation of the wind turbines to meet such requirements. Basically, two main modes of operation can be set at the wind turbines in a wind farm to provide the grid requirements: 1) MPPT (maximum power point tracking) operation; 2) De-loaded operation. The latter is basically provided when the grid requires to track a power demand profile lower than the available power of the wind farm, thus some wind turbines must be curtailed. Meanwhile, the former is set to provide the maximum power for all the wind range, that is

$$P_{\max} = \min\left(\frac{1}{2}\rho\pi R^2 C_{p_{\max}} v^3, P_N\right). \tag{2.15}$$

When this operation mode is used to regulate the wind turbine operation, the kinetic energy stored in the blades can be used to provide inertia frequency support, when it is required. It is worth to anticipate that when power maximization concerns a wind farm

whose wind turbines are aerodynamically coupled, the optimal power production is no longer obtained by setting the MPPT operation to all the turbines in the farm [36].

Frequency Support

Because most wind turbines provide asynchronously generated power which cannot contribute to system inertia because their spinning masses are decoupled electronically from the grid. Therefore, high penetration of wind generation reduces the system inertia causing increased rates of change of frequency immediately following a disturbance. This concern has pushed both academia and industry to provide advanced control strategies to comprehensively address the issues related to frequency response. In this regards, three main approaches can be identified for providing system frequency support:

1. Use the rotating kinetic energy stored in the turbine blades through proper designed emulated inertia control [36, 102].
2. Regulate the pitch and the rotor speed to keep a certain wind turbine capacity reserve [160, 168].
3. DC-link voltage and pitch angle are controlled for smoothing wind turbine output power [59, 150]. Since the voltage control is out of the scope of this thesis, this operation mode is not further discussed.

For the former case, the idea is to emulate the system inertia by means of artificial control. There are several control schemes to draw the frequency support approaches [46, 151]. One common approach consists in adding a PI-based extra control loop sensitive to the network frequency [167]. For a variation of the frequency from f_s to f^*, where the latter indicates the system frequency in normal operation, the controller sets an input reference ΔP_r to be added to the input reference in the control loop, shown in Figure 2.10, which is computed by

$$\Delta P_\mathrm{r} = -K_I \frac{(f_s - f^*)}{t} - K_P(f_s - f^*), \tag{2.16}$$

being $K_I, K_P \in \mathbb{R}_{\geq 0}$ constants properly tuned.

A quite similar concept to facilitate an inertial response is presented in [109]. Here, a *droop-loop* controller is activated only when the grid frequency exceeds some limits

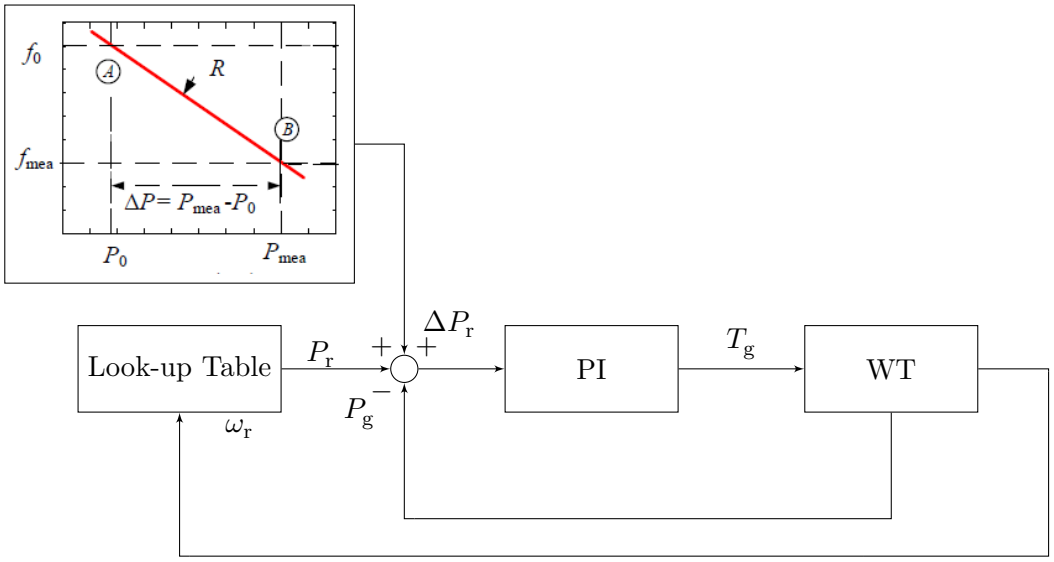

Figure 2.10: Simplified block schemes of wind turbine operation mode, including frequency support.

in order to provides an active power change proportionally to the frequency deviation, see Figure 2.10. Droop controller has not high impact on the initial rate of change of frequency but it largely influences the frequency in the most critical condition of the transient. The main limitations of those approaches appears at high wind speed, since the wind turbine produces the rated power additional power cannot be provided by the turbine; in this circumstance only downward regulation is guaranteed to balance under-frequency deviation.

At low wind speed, the control loop for frequency response can be designed to inject into the grid extra active power obtained by releasing the amount of kinetic energy stored in the rotor mass within short term (about of milliseconds scale), that is

$$\Delta E_k = E_k^* \left(1 - \left(\frac{\omega_s}{\omega^*}\right)^2\right), \tag{2.17}$$

$$E_k^* = \frac{1}{2} J_r \omega^{*2}, \tag{2.18}$$

where E_k^* indicates the kinetic energy at frequency f^*, and the rotor speed is $\omega^* = 2\pi f^*$. Hence, the set-point $\Delta\omega_r = \omega^* - \omega_s$ should be added as additional input to the rotor speed control in Figure 2.7, so that the active power to be injected into the grid should be increased after a frequency droop or decreased after an over-frequency event.

So far, the main drawback of providing primary frequency support with wind turbines is the undesirable stall conditions due to the over-decreasing in rotational speed of wind turbines after the kinetic energy is released along with the increasing of mechanical stresses. Moreover, the *recovery process* results in decreased wind turbine power production.

Deloaded Mode of Operation

When a wind turbine works in de-loaded operation, the power generated by a wind turbine is

$$P_{\text{min}} \leq P_{\text{g}} \leq \min(P_{\text{r}}, P_{\text{max}}), \tag{2.19}$$

being P_{min} an arbitrary minimum value of power, typically set different from zero to avoid the shut-down of the turbine, and P_{r} the power reference set by the controller. In case of derating operation, the latter (indicated by the blue line in Figure 2.14) is lower than the maximum power (red line). Thus, according to (2.8), for a given P_{g}^* the choice of (β^*, λ^*) that provide P_{g}^* is not unique. This degree-of-freedom on deloading the wind turbine can be used to reach different goals, such as mechanical loads reduction and/or frequency support.

By deloading a wind turbine there exists an extra amount of active power that can still be delivered into the grid to provide primary frequency support. This power is commonly called *power reserve* or *capacity reserve* and is given by

$$P_{\text{res}} = P_{\text{max}} - P_{\text{g}}. \tag{2.20}$$

In the literature, deloading control strategies are based on pitch control and speed control. Usually, in the case of high wind speed operation, the pitch is controlled to maintain the power generated to a value lower than the rated one for all the wind range $v > v^*$, while the rotor is typically kept to its optimal MPPT value (red line in Figure 2.14), i.e., for $v \leq v^*$, the maximum power is generated. The characteristic power curve for this case is represented with the dotted blue line in Figure 2.14. More general deloaded control strategies consist in the choice of rotor speed ω_{r}^*, see blue line in Figure 2.14, and pitch angle λ_{r}^* such that the power reserve is guaranteed for any values of wind speed in order to optimize the amount of kinetic energy stored in the rotor masses [36, 169]. With this approach, primary frequency support can be guaranteed for the entire wind range, i.e., for both downward and upward frequency regulations.

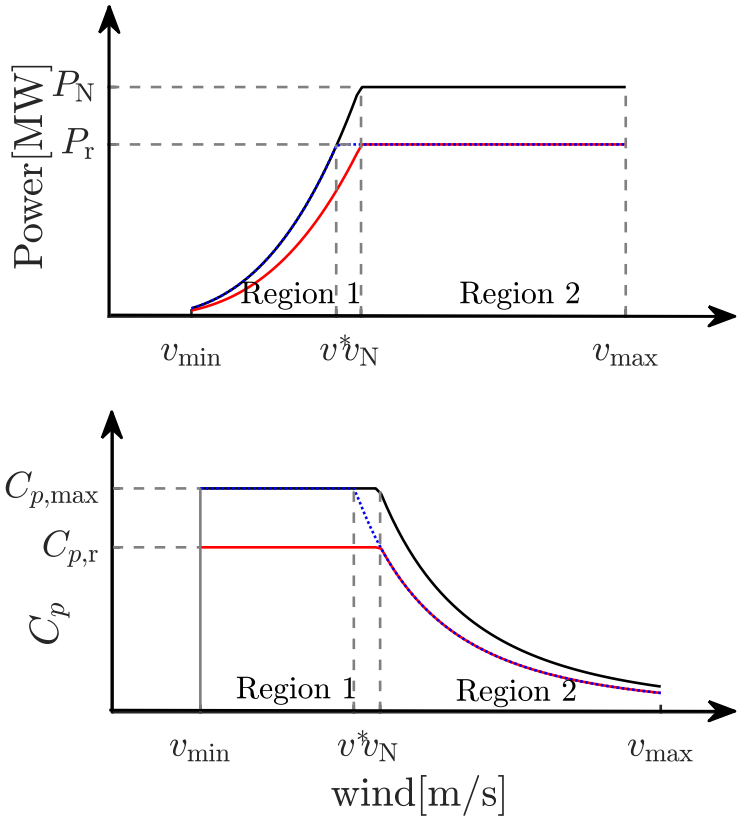

Figure 2.11: P-v and Cp-v characteristics curves in MMPT mode (black line) and deloading mode (red line).

2.2 Wind Farms

Nowadays, the displacement of conventional power plants with renewable energy systems, such as wind energy systems, is one of the major challenges attracting worldwide attention. In order to achieve this goal along with economies of scale to reduce the cost of installation, maintenance, and transmission line construction, wind turbines are arranged in even more larger clusters laid out in a grid-like pattern, commonly known to as *wind farms* or *wind power plants*. The mature technology level of variable-speed variable-pitch wind turbines together with the developments in the field of optimization and control allow wind farms to optimize the power quality generation for a wide range of wind conditions. One central feature affecting the power generated and the performance of the wind turbines is related with the aerodynamic phenomena involved in a wind farm, which make the difference between the control strategies typically used to provide optimal control of a single wind turbine with respect to those necessary for controlling a wind turbine within a wind farm.

2.2.1 Wind and Wake effect

The kinetic energy in the wind flow field is harvested by the rotor turbine and transformed into mechanical power, computed as (2.8). However, in a large wind farm, the wind speed $v = v_i$ faced by a generic wind turbine i depends on the wind turbine position and the generation power conditions of the other turbines in the wind farm. Indeed, when extracting kinetic energy from the wind, a wind turbine causes a reduction of the wind speed in the downstream wake. As a result, the wake moves downstream and interacts with other turbines standing in the wake modifying the mean velocity intensity and the turbulence in the out-flow field, such that the available power of the downstream turbines experiences a reduction. Therefore, to take into account those couplings among the turbines when optimizing wind farm production, several wake models estimating the *wake effect* on the incoming wind speed have been proposed in the literature [136]. However, modeling the highly dynamic behaviour of the aerodynamic interactions among the wind turbines with high-fidelity degree is not a trivial task.

An initial categorization of the wake models is based on the *model's fidelity*. High-fidelity models involve numerical solutions to systems of 3-D Navier-Stokes partial dif-

ferential equations, which require computational fluid dynamics (CFD)[1] simulation to be employed. Among the most popular high-fidelity wind farm 3-D models based on large-eddy simulations, it is worth to mention the NREL's Simulator fOr Wind Farm Applications (SOWFA) [30], the UTDWF [100] and SP-Wind [105]. Whilst the expensive computational costs (days on parallel computation) make those models not affordable for real-time estimations, they should be used to test the reliability and accuracy of less sophisticated wake models [44]. Nevertheless, for the sake of engineering applications, such as the real time control of a wind farm, for which fast algorithms should be employed, simplified low-fidelity wake models should be considered to estimate the wake within reasonable time. Commonly, such models are the 2-D parametric models in which only the main elements of the wake are considered.

Even though in the literature there exist many wake model representations, they basically are variants of the pioneer wake models presented in [84], also known as *Jensen's model*. This as first proposed the formulation of the wind speed deficit among an upstream and the downstream turbine due to the wake effect. In [86], an extension of this model was proposed by accounting for multiple wind turbine interactions. These relatively simple formulations give reasonable results for the wake effect estimations, however they present some limitations. For instance, the influence of the yaw angle is not considered, in this regards the authors in [50, 62] proposed parametric wake model considering the yaw effect to be tuned with SOWFA or real wind farm data. A recent simulation tool, FLORIS (FLOw Redirection In Steady-state), based on this parametric model and including also Gaussian velocity profile [20] and vorticity effects [100] has been shown to match the wind farm power predictions with small errors (almost lower than 5.3%).

Due to the fact that these models contain a number of tuning parameters, it is difficult to generalize the obtained results but some additional strategies have been provided to update online the parameters according to real measurements [26]. Furthermore, the aforementioned engineering wake models are based on steady-state assumptions, i.e., given the operating conditions, and the free upstream wind value, the wind distribution is computed by a static wake model. By neglecting the wake dynamics allows the discussed

[1] Computational Fluid Dynamics (CFD) is a branch of fluid mechanics that solves fluid flows governed by the three-dimensional (3-D) Navier-Stokes (N-S) equations. The most accurate simulation direct numerical simulation (DNS) uses a very dense grid to capture all eddy scales, however the computational costs are high thus large-eddy simulations (LES) and Reynolds-averaged N-S (RANS) models can reduce them reducing accuracy.

models to be suitable for solving real-time optimization-based problems, e.g., layout optimization and power maximization. Hence, the dynamics of the wakes moving across the wind farm are neglected. In fact, depending on the free-stream wind speed the travel time of wakes from one row to another is approximately 1-3 min [31]. The authors in [93] propose the dynamic wake meandering model (DWM) based on 2-D Navier-Stokes equations, where at the steady-state wake model aforementioned is added a stochastic (meandering) wake model directly solved by LES in order to consider the effect of the changes in turbulence intensity during the wake propagation. In [144], it is presented a first attempt to consider the dynamics of the wind within a wind farm, while allowing the use of efficient control algorithms that are not based on CFD simulation. In this model, a state space wake representation is obtained from a system of partial differential equations via finite volume method, and this allows the employment of control theory results rather than static optimization ones. Moreover, a dynamical version of the Jensen's model is used in [137], which represents each wind turbine wake as one-dimension partial differential equation and includes the dynamic effect of thrust modulation through wake advection and the variable nature of the wake is considered using the Kalman filter. Despite these dynamic models are more sophisticated of the steady-state ones, they still present the issue of the computational time, especially if the wind farm is expected to provide some specific requirements, such as grid support.

Summarizing, in the literature, there is not yet a wake model based on unsteady Navier-Stokes equations that can be used for on-line control. However, on-line re-calibration of the tuning parameters used for simplified wake models is becoming increasingly popular in the literature being a suitable trade-off between computational burden and model fidelity [44]. It is worth to mention that only a very brief overview about wake models has been treated in this section. For the interested reader, a more complete overview about wake models can be found in [88].

2.2.2 Control Objectives and Strategies

The need for control wind farms with optimization-based control strategies is directly linked with the presence of the couplings among the turbines due to the wake effect. Furthermore, as wind farms improves in size and power capacity, control specifications become more and more demanding. Starting from merely extract all the maximum power

by operate the turbines at their MPPT, nowadays wind farms controllers are typically designed to

- maximize the power generation,
- reduce the mechanical loads,
- guarantee specific requirements, for instance to grid support purpose.

These control objectives, sometimes conflicting, are closely related and should not be achieved separately.

Intuitively as the number of wind turbines of a wind farm increases, the wake effect becomes more important, so that maximization of power production of wind farms should be provided to optimally coordinate the control settings of the individual wind turbines to prove potential gain with respect to classic individual turbine MPPT operating mode. In general, to do so two common approaches can be adopted: *induction control* and *wake steering control*. The former is based on de-rating strategy to optimally regulate the induction factors a presented in (2.3) in order to reduce the wind speed deficit behind the rotor of an upstream turbine. It has been shown that the reduction of the power production of upstream turbines can increase the kinetic energy of wind reaching downstream turbines [11, 140]. Wind tunnel tests have shown that this approach is extremely sensitive to the fast changes in wind speed and direction. In fact, a slow reaction of the controller would imply operating in suboptimal conditions, which might be outperformed by the power maximization at the level of each wind turbine [29].

Being the axial induction control the main approach used to design the novel control strategies presented in this dissertation, additional literature review on this topic will be further discussed in Part II. The idea behind the wake steering control is to purposely introduce a misalignment between the rotor axis and the incoming wind flow by regulating the control settings, i.e., the tilt angle δ, pitch angle β and yaw angle γ, in order to deflect the wake downstream to minimize the overlap of rotor area with the area of the wake downstream. Notice that the tilt angle refers to the angle between the horizontal axis and rotor shaft, the benefits on regulating this angle are presented in [11, 52]. In general, wake redirection has been demonstrated successfully in a number of situations in the literature, with an improvement in power production of more than 4%

[90]. Among others, [62, 112] have demonstrated the concept in high-fidelity simulation. Furthermore, [20, 29] tested in wind tunnel experiments the concept of wake redirection control, and [51] even tested the concept in full-scale field experiments. Despite of the promising results reached with wake redirecting, the increasing of fatigue loads on the downstream turbines is still an important drawback that should be considered to properly set the control actions. Finally, some recent works proposed to optimize both the axial induction factor and the yaw control by using adapted formulation of the Jensen's wake model to include the yaw angle as additional control parameter [21, 64, 113].

Closed-loop Wind Farm Control

As discussed in Section 2.1.4, some wind turbines work in de-loaded operation mode to sustain the grid by providing some ancillary services, e.g. for frequency and/or voltage purposes or curtailment constraints. Under this circumstance, the wind turbine should track a certain control reference that can be optimally regulated by a higher control level, which ensures that the wind farm provides the expected grid requirements. Due to the complicated dynamics at a range of spatial and temporal scales inside the wind farm, accurate control cannot be achieved without feedback [44]. Hence, a *closed-loop framework* is preferred. Figure 2.12 shows a summary block scheme of a common closed-loop wind farm control strategy. Here, a supervisory high-level controller determines a collective control action by solving an optimization-based control problem using measurements and/or simplified surrogate models. The latter can be calibrated by an observer in real-time using noisy-measurements from wind farms to improve the control performance by considering the wind farms and wind field dynamics. Hence, the optimal control inputs are sent to the individual wind turbine controllers, typically PI-based nature. The closed-loop control can be designed as two different communication architectures, i.e., *centralized* or *distributed* control structures. A comparison of these architectures is shown in Figure 2.13. In the centralized control system, the wind farm controller receives measured wind velocity and control degree-of-freedom magnitudes from all wind turbines, and likewise transfers control set-points to all machines [77]. In a distributed wind farm control system instead, the set-points of individual wind turbines are regulated by their respective distributed control units [171], which are permitted to communicate with all the control units or just to those of the turbine's immediate neighbors.

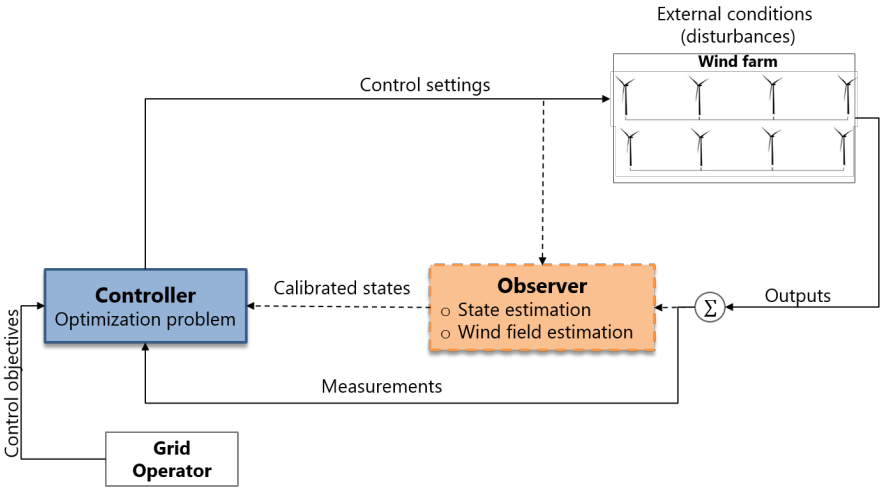

Figure 2.12: The closed-loop feedback block scheme of a general wind farm control system. The measurements, control settings and outputs include several signals used to state the optimization-based control problem.

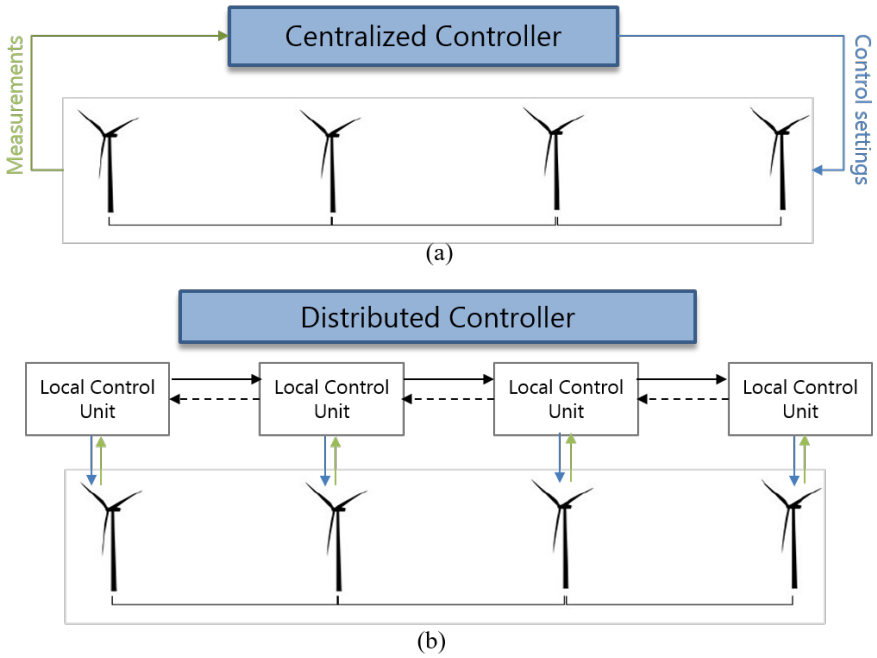

Figure 2.13: The closed-loop feedback block scheme of a general control system for wind farm. The measurements, control actions and outputs can include several signals.

A comprehensive overview on the design of the supervisory controller can be found in [88, 90]. Basically, two main approaches can be identified: *model-based controller*, and *model-free controller*. The former consists of an internal model which is used to estimate the wind farm performance. The latter, relies on simple control algorithms typically provided to ensure the tracking of a certain power reference profile required by the TSO. In [77], the regulation of the total power among the turbines is set proportionally to the available power. The authors in [139] provided an on-line optimization-based control algorithm to maximize the whole power reserve, i.e., the reserve at the wind farm level, when the wind farm works in deloading operation. Other model-free approaches find the optimal inputs for the wind turbines using *game theory*. The authors in [98] presented a centralized game-theoretic dynamic optimization for power derating conditions. Starting from baseline values of the induction factors for the turbines, at each time-step these values are perturbed. They are updated if the wind farm power output increases with respect the initial conditions, otherwise the baseline values of the induction factors are kept. This model, tested for the HornsRev wind farm, resulted in increasing the wind farm efficiency by 34% with respect to *greedy* conditions (i.e., the wind turbines produce the maximum power at any time), but the iterative process to converge was too much computationally expensive for real-time control (almost 10^3 iterations). In [16], the authors provide a data-driven distributed control scheme to reduce the communications among the turbines and speed-up the computational burden to maximize the energy captured and to reduce the computational burden, which increases the reliability of the wind farm operation. Moreover, distributed game-theoretic control algorithms have been presented in [61] and [174]. The latter work is based on the model presented in [98], however the information sharing is only limited at the neighbour turbines and the perturbed values of induction factors are based on some probability distribution function. The performance in power maximization is around 3.8% but the number of iteration is drastically reduced (almost 200). Despite the proper results obtained, those models have not been tested with high-fidelity wind farm simulators. Therefore, it is not clear whether they can be applied to real wind farms. The only exception is the model in [61], where a game theoretic algorithm is proposed for wake redirection and tested with the high-fidelity model SOWFA. Other model-free controllers are designed on the basis of the *extremum seeking control technique*, an optimization-based approach that works for non-linear, time-varying systems. In [31], this technique is coupled with

large-eddy simulations to find optimal torque gain settings for the wind turbines while considering the dynamic of the aerodynamic couplings among neighbour turbines. The model presented an improvement of 7.8% in the efficiency of wind farm power production. For both game-theory and extremum seeking control approaches, the computation time to converge to a unique solution remains a critical issue. Furthermore, the proposed models are basically provided to maximize the power generation but it has not yet further investigated if they can be used to provide ancillary services. Finally, to deal with the non-linearity of the model and dynamics of the system other wind farm control approaches defined as dynamic controllers can be designed using linear models as PID, $\mathcal{H}_2, \mathcal{H}_\infty$ based controllers. A distributed $\mathcal{H}_2$ optimal controller to mitigate the structural loads and track a power reference is proposed in [145], while wake steering redirection based on a robust $\mathcal{H}_\infty$ controller is designed in [128].

The second common approach to design a wind farm controller requires a surrogate model of the system to be controlled to estimate the future behavior of the system in response to any hypothetical control input. This approach, also known as *model predictive control* (MPC) strategy, enables to solve optimization problems subjected to several objective functions and constraints. Being this strategy largely used in this thesis, it will be discussed in the dedicated Section 2.3.

It is worth to mention that, another distinction between closed-loop control schemes can be made with respect the measurements used to find the optimal control actions. In the case of closed-loop state-feedback, all the states to be controlled are assumed measured. However, this assumption can be impractical especially when the wind farm counts of hundreds of turbines. In this case, only a certain number of measurements is used, while the states are estimated using some observers. Typically, the observer is used to estimate the flow velocity by using surrogate models that are based on parameters that need to be adjusted according to the real-time operation. For this purpose, the authors in [66] propose a control strategy where the wind speed is estimated re-calibrating the DWM model. However, such an estimation is restricted for off-shore wind turbines operating in de-loading strategy. Some works estimate the variable nature of the wake using the Ensemble Kalman filter as proposed in [138],[43]. The dynamic wake model represents each wind turbine wake as a one-dimension partial differential equation and includes the dynamic effect of thrust modulation through wake advection. The work in [138] presents

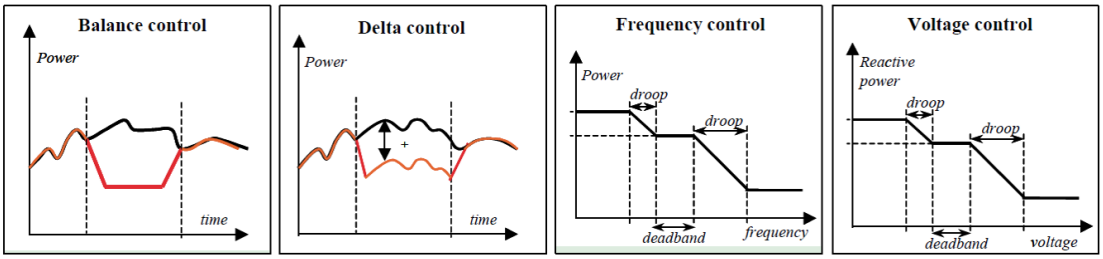

Figure 2.14: Frequency and Voltage control approaches for wind farm control. Figure adapted form [77].

the observer combined with an MPC controller to track a power reference; although the simulation time is still high (around 30 s), this model seems promising for track the real-time grid set-points. Despite of the scarce number of control strategies that use an observer, future wind farm control research should incorporate such estimation technique to provide more reliable controllers.

Active and Reactive Power Control

Nowadays, one of the major research challenge for wind farm is related to comply with the grid requirements while ensuring wind turbine safe operation and quality of the wind farm power generation. Therefore, in order to fulfill these requirements wind farms need to be controlled with dedicated control strategies that enable optimal active (or frequency) and reactive power (or voltage) control. The active power control functions required by the system operators are:

- Balance Control, wind farm is downward or upward regulated in steps of constant level.
- Delta Control, the wind farm operates in de-rating mode by keeping a certain amount of power reserve for ensuring frequency support.
- Power gradient limiter, the power delivered by the wind farm for supplying frequency imbalances is regulated according to the rate of change of frequency. In this case, the balance between wind farms and conventional power plants is guaranteed.
- Automatic frequency control, the frequency measured at the Point of Common Coupling (PCC) is controlled to automatically produce more or less power.

In the literature, different strategies to provide frequency support can be found while tracking the power profile demanded by the grid. Among others, some works reported control approaches to optimally regulate the power set-points among the turbines, in order to control the rotor speed set-points of each turbine such that the kinetic energy at the wind farm level is maximized, [3, 4, 37, 38, 130, 169]. For instance, in [37] an heuristic control strategy is proposed to maximize the kinetic energy released by the turbines inside wind farm. The heuristic approach is based on a scheduling of the generated power solution of the optimization problem, in which the constraints on the generated power are not considered. Hence, the optimal power profiles are used as set-point for rotor speed controller in order to reduce the losses of kinetic energy during the normal operation mode. The authors provide also this strategy for the energy recovery problem, a downside of the inertial control that can cause the wind turbine to produce less power after the inertial response, which could adversely affect grid frequency. In [4], the maximization of kinetic energy is proposed for wind turbine operating in de-loaded mode. In [169], the stored kinetic energy is maximized by reducing the power generated by some wind turbines without reducing the total power delivered into the grid. The authors in [38] propose to use the stored kinetic energy to smooth the variability on the generated power, which is given by the self-induced turbulence levels. Here, Pareto frontiers were constructed to optimize the amount of kinetic energy stored and the maximization of power extraction.

Likewise, in case of de-rating operation the power set-points can be coordinated among the turbines such that the power reserve is maximized [141]. Moreover, other control strategies provide frequency support by equipping wind farms with energy storage systems to compensate the mismatch between the power demand by the grid and the power generated by the farm.

On the other hand, the grid requires wind farms to control reactive power power so that the voltage at the PCC is regulated within the admissible limits. The reactive power flows and voltage profile within the offshore grid are influenced by the electrical components in the system as well as their operating points and actively controllable by the WT converters, on-load tap changers (OLTC) of transformers and other controllable reactive power compensators. Typically, a transformer has a discrete number of tap setting positions to be adjusted. Thus, the inclusion of this variable into the system leads to deal

with mix integer optimization problems. The reactive power injection could be carried out by capacitor banks, synchronous condensers, or parallel FACTS like Static Var Compensators (SVC) or Static Compensators (STATCOM). The reactive power output of SVC, STATCOM and synchronous condensers can be continually adjusted, while the capacitor banks have discrete steps that are usually connected through switches. Using such devices, the service of the wind turbines during grid faults is guaranteed avoiding the disconnection of wind turbines to prevent a risk of voltage oscillations [127]. The reactive power flows are strictly affected by the electrical connection between wind farms and electrical grid. The most common is the alternating current (AC) connection, however the distance from the cost for offshore wind farms motivates the use of high voltage direct current (HVDC) system. In this case, the onshore AC-grid is interfaced with voltage source converter (VSC), which fulfills the grid requirements and the reactive power stability, whereas the offshore VSC-HVDC provides the voltage reference to offshore grid. Recently, the project PROMOTioN [104] proposes offshore AC grid control of wind farms connected through Diode-Based HVDC systems to deal with the voltage stability. In the novel Diode-based HVDC links the wind turbines are responsible of ensuring stability of the offshore AC grid (i.e., frequency and voltage), which modifies completely the conventional control schemes of wind farms and wind turbines.

Nowadays, the optimization of active and reactive powers as unique problem able to track the grid requirements and minimize the power losses is a pretty new on-going research topic. A significant impact is getting the control of voltage adjusting both active and reactive power references [173]. Here, the combined scheme can efficiently coordinate the power regulation devices towards guaranteeing the stability of the wind farm.

2.3 Model Predictive Control

Model Predictive Control (MPC) is an advanced control technique that has had a large impact on industrial control engineering. The main reason of this is the ability of the predictive controller to handle either one or even more than one constraint in order to ensure quality and safety of the process. Typically, the MPC strategy is an optimization-based technique that computes an optimal control sequence that minimizes a cost function subject to a number of physical and/or operational constraints over a receding time

horizon. A predictive controller has an internal model to generate prediction of the plant behaviour over a future *prediction horizon*. Usually, the models used are of black-box linear input-output nature obtained from simple tests of the plant or by system identification using data taken from the plant [95]. However, non-linear models are also used for understanding the physical aspects of some complex engineering systems, e.g. those characterized by high dynamics as chemical transformations or flow computations. In the rest of this thesis the internal model is assumed linear; this makes the calculation relatively straightforward.

2.3.1 MPC Strategy

Usually, the MPC controllers are designed in discrete time and by using a state-space model of the plant to be controlled [95, 116, 131]. Suppose that the dynamic behaviour of the plant is governed by the state-space discrete-time non-linear model of the general form

$$\mathbf{x}(k+1) = g(\mathbf{x}(k), \mathbf{u}(k), \mathbf{d}(k)), \tag{2.21}$$

where $k \in \mathbb{Z}_{\geq 0}$ denotes the discrete time. The vector $\mathbf{x} \in \mathcal{X} \subseteq \mathbb{R}^{n_x}$ is an n_x-dimensional state vector, $\mathbf{u} \in \mathcal{U} \subseteq \mathbb{R}^{n_u}$ is an n_u-dimensional vector of control inputs, $\mathbf{d} \in \mathbb{R}^{n_d}$ corresponds to the vector of disturbance affecting the system that may be obtained using forecasting algorithms [45, 171], $\mathbf{y} \in \mathcal{Y} \subseteq \mathbb{R}^{n_y}$ is the n_y-dimensional output vector. Furthermore, the sets $\mathcal{X}$, and $\mathcal{U}$ indicate the feasible sets according to physical and/or operational constraints for the system states and control inputs, respectively. These constraints are defined in a polytopic fashion as

$$\mathcal{X} = \{\mathbf{x} \in \mathbb{R}^{n_x} \,|\, \mathbf{x}(k) \in [\underline{\mathbf{x}}, \overline{\mathbf{x}}], \forall\, k\}, \tag{2.22a}$$

$$\mathcal{U} = \{\mathbf{u} \in \mathbb{R}^{n_u} \,|\, \mathbf{u}(k) \in [\underline{\mathbf{u}}, \overline{\mathbf{u}}], \forall\, k\}, \tag{2.22b}$$

where $\underline{\mathbf{x}} \in \mathcal{X}$ and $\overline{\mathbf{x}} \in \mathcal{X}$ denote the vectors of minimum and maximum admissible values of system states, respectively, while $\underline{\mathbf{u}} \in \mathcal{U}$ and $\overline{\mathbf{u}} \in \mathcal{U}$ denote the vectors of minimum and maximum admissible values of manipulated variables, respectively.

The predictive behavior of the system (2.21), that is the state vector sequence

$$\hat{\mathbf{x}}(k) \triangleq (\mathbf{x}(k+1|k), \mathbf{x}(k+2|k), \ldots, \mathbf{x}(k+H_p|k)) \tag{2.23}$$

at $\mathbf{x}(k+i), i = (1, \ldots, H_p - 1)$ depends on the assumed feasible control input sequence

$$\hat{\mathbf{u}}(k) \triangleq (\mathbf{u}(k|k), \mathbf{u}(k+1|k), \ldots, \mathbf{u}(k+H_p-1|k)), \tag{2.24}$$

which is to be applied over a fixed-time prediction horizon denoted by $H_p \in \mathbb{Z}_{\geq 0}$. The notation $\hat{\mathbf{u}}$ rather than $\mathbf{u}$ here indicates that at time k there is only a prediction of what the input at time $k+i, i = 0, \ldots, H_p - 1$ will be. Hence, the actual input at that time $\mathbf{u}(k+i)$ will probably be different from $\hat{\mathbf{u}}(k+i)$. Once the control input is computed, according to the receding horizon philosophy [95], only the first element of the trajectory in (2.26) is applied as the input signal to the plant in (2.21), that is $\mathbf{u}^*(k) = \mathbf{u}^*(k|k)$. Typically, the optimal control input sequence is obtained by stating the predictive control approach to solve an open-loop optimization problem with the following general formulation:

$$\underset{\hat{\mathbf{u}}(k)\in\mathbb{U}}{\text{minimize}} \; J(\mathbf{x}(k), \mathbf{u}(k)) \triangleq J^m(\mathbf{x}(k+H_p|k)) + \sum_{i=0}^{H_p-1} J^l(\mathbf{x}(k+i|k), \mathbf{u}(k+i|k)) \tag{2.25a}$$

subject to

$$\mathbf{x}(k+i+1|k) = g(\mathbf{x}(k+i|k), \mathbf{u}(k+i|k), \mathbf{d}(k+i|k)), \forall i \in [0, H_p - 1], \tag{2.25b}$$

$$\mathbf{u}(k+i|k) \in \mathbb{U}, \forall i \in [0, H_p - 1], \tag{2.25c}$$

$$\mathbf{x}(k+i|k) \in \mathbb{X}, \forall i \in [1, H_p]. \tag{2.25d}$$

In this case, the function $J^m : \mathbb{R}^{n_x} \to \mathbb{R}$ represents the terminal cost, meanwhile $J^l : \mathbb{R}^{n_x} \times \mathbb{R}^{n_u} \to \mathbb{R}$ represents the cost over the prediction horizon. Assuming that the optimal problem in (2.25) is feasible, the optimal control input sequence throughout the prediction horizon is given by

$$\hat{\mathbf{u}}^*(k) \triangleq (\mathbf{u}^*(k|k), \mathbf{u}^*(k+1|k), \ldots, \mathbf{u}^*(k+H_p+1|k)), \tag{2.26}$$

where the first optimal control input corresponds to the decision variable to be applied to the system (2.25b). The procedure is applied iteratively, computing a new optimal control sequence for each simulation step. Algorithm 1 summarizes the entire MPC procedure.

Algorithm 1 Model Predictive Control Formulation

1: $N_s \leftarrow$ simulation length
2: $H_p \leftarrow$ prediction horizon
3: $k \leftarrow$ initial time
4: $x(k) = x_0 \in \mathcal{X} \leftarrow$ initialization of state vector
5: **for** $k = 1$ to H_p **do**
6: $\quad \hat{\mathbf{u}}^*(k) \leftarrow$ solve the optimization problem in (2.25)
7: $\quad \mathbf{x}(k+1) = g(\mathbf{x}(k), \mathbf{u}^*(k|k), \mathbf{d}(k))$
8: $\quad k = k + 1$
9: **end for**

2.3.2 MPC Tuning

Multiple objectives are usually implemented by solving a sequence of optimisation problems. The cost function is composed from different objectives having different priority; hence, the cost function of the problem in (2.25a) is composed of n objectives, i.e., the objective function in (2.25a) is replaced by the following expression:

$$\underset{\hat{\mathbf{u}}(k)\in\mathbb{U}}{\text{minimize}} \;\; J(\mathbf{x}(k), \mathbf{u}(k)) \triangleq J^m(\mathbf{x}(k+H_p|k)) + \sum_{j=0}^{n} \sum_{i=0}^{H_p-1} \gamma_j J_j^l(\mathbf{x}(k+i|k), \mathbf{u}(k+i|k)), \tag{2.27a}$$

where $\gamma_i \in \mathbb{R}$ with $i = \{1, \ldots, n\}$ indicates the weight prioritizing the $i-th$ objective. There are many parameters that can be adjusted for obtaining the desired effects from the controller. This requires to set several design parameters as

- Weights γ_i
- Prediction horizon H_p
- Value of the terminal cost function J^m in Algorithm 1
- Reference trajectory

In many cases, the tuning process is solved intuitively on the basis of the real-world requirements and applications or selecting the weights by a trial-and-error procedure. Otherwise, efficient setting of these tunable parameters often requires a systematic tuning guideline for MPC, an extensive review about the explicit and implicit tuning approaches for MPC is presented in [57]. Basically, the tuning procedures are based on a trade-off

between performance and robustness. For example, off-line tuning procedures propose to tune the prediction horizon such that the closed-loop stability of the control system is ensured, the common approach is to set the prediction horizon so large such that further increase has no effect on the control system performance [165]. Moreover, a detailed theorem to ensure closed-loop stability based on the prediction horizon value has been proposed in [56]. Afterwards, an extension of this approach has been reported in [101] and [155].

Another tuning parameter is the choice of reference trajectories for each controlled variable, the idea is to find the appropriate tuning by matching the MPC performance with the performance of a pre-established controller that provides the mentioned references [41]. Furthermore, the stability of the closed loop can also be improved by using disturbance models and observer dynamics: for instance, in [162] an automatic tuning approach consisting of a controller and a state observer is presented. In [1], developed frequency domain tuning techniques based on the $\mathcal{H}_\infty$-norm of a mixed sensitivity function for disturbance rejection scenarios are provided for single-input-single-output (SISO) structured controllers. One of the advancements in this area is the application of concepts like neural networks, fuzzy logic, and genetic algorithms to tackle the difficulties associated with the tuning of MPC. For instance, in order to save computational time in [156] the authors have used genetic algorithms and multi-objective fuzzy decision makers to establish the tuning of MPC controller considering the errors between outputs and reference trajectories. Finally, the weights γ_i can be tuned without the use of a reference model. Focusing on the characterization of the set of feasible optimum solutions for multi-objective optimization problems, that is computing several points along the Pareto front associated with a given objective function [132].Then, a pre-established management point allows to determine the desired value within the Pareto front from which the appropriate tuning weights are determined. However, a large number of objectives lead to complex non-convex Pareto curves and the optimization problem needed to be solved using an evolutionary algorithm [154]. On-line dynamical tuning based on evolutionary game theory is proposed in [15] to set the appropriate prioritization weights according to a desired region of the Pareto front. Further methods have been explored to consider the priority in solving multi-objective problems by ranking the objective functions instead of solving a single objective [108].

2.3.3 Non-centralized MPC for Large-Scale Systems

Over the years, more and more large-scale engineering systems have been developed to cope with new environmental and technical concerns. For instance, the ever-growing integration of RES into the electrical network has caught the interest of many researcher groups for providing reliable and highly performance controllers to achieve different requirements, for instance to optimize the electrical power generation [6, 159], to provide voltage and frequency regulation [40, 107], traffic control [19], water network distribution [71, 117] and many others requirements. For large-scale systems, the high number of elements characterizing the system to be controlled has associated an high number of decision variables and constraints makes the centralized control approach not suitable to provide a reliable control due to the high computational complexity. Therefore, one can solve the control problem by decomposing the overall system into smaller subsystems, such that the original problem is divided into computationally lighter sub-problems to be solved separately. This approach is known as *partitioning control approach* and the control of the overall system is ensured by a non-centralized design. In this case when each sub-system corresponds to a specific partition controlled by local controllers; each controller may be treated as an independent unit exchanging information with only the elements within the partition or it may partially communicate also with some elements in other partitions. Despite there are several classifications within the non-centralized MPC controllers depending on how the controllers share information between each other [134], in this dissertation only the two main architectures for MPC controllers are identified: *decentralized* control scheme and *distributed* control scheme. If the latter control approach allows dynamical couplings among the sub-systems (dotted line in Figure 2.15), the former approach assumes that the dynamical couplings are weak and the sub-systems are independent units. There are several ways to solve non-centralized control problems, however going through them is out of the scope of this thesis. For a deep understanding, the reader could find an extensive review about decentralized approaches in [134] and in [96] for distributed control designs.

2.3.4 Partitioning Problems

Besides the benefits of reducing the number of variables to be controlled in order to provide a certain control performance, dividing the systems in several partitions could

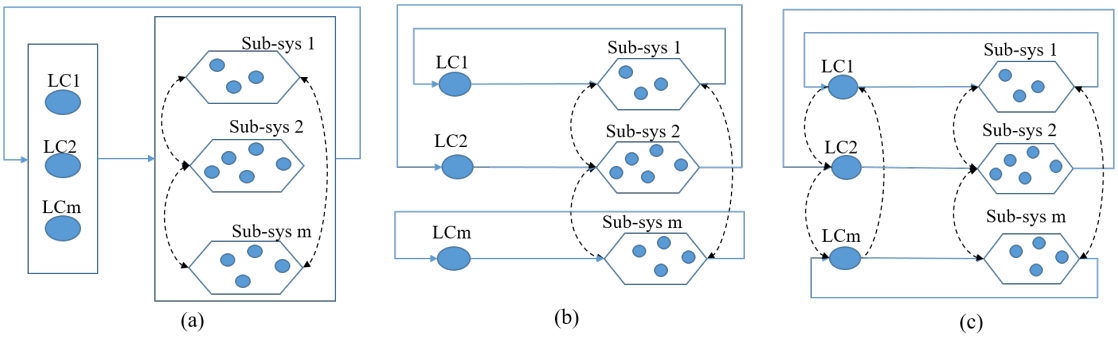

Figure 2.15: Different non-centralized architectures for MPC controllers: (a) general design for non-centralized architectures, (b) decentralized design, (c) distributed (sequential) design. Dashed arrows connecting different sub-systems represent that the dynamical coupling might exist or not. LC: Local Controller. Sub-sys: sub-system.

reduce the communication issues and economic costs due to long distance connections to transport measurements and control signals. The partitioning strategy allows the identification of multiple sub-systems such that the controller can be performed in a distributed or decentralized fashion. The system decomposition problem is typically recommended during the system modeling process through cleaver identification of sub-systems on the basis of physical insight, intuition or experience. However, for a large-scale complex system this approach is not suitable, thus the main challenge is to design systematic partitioning methods to automatically decompose a given large-scale system. Since the partitioning approaches are strictly based on specific dynamics of the couplings among the elements within the systems, or on detailed control performance, such as on existing coupled constraints that are imposed to guarantee some warranties and specifications, determining a general partitioning problem is quite challenging. Mainly, two general cases can be identified for partitioning large-scale systems [15]: 1) determining a partitioning based on the dynamical coupling of the whole system; 2) taking into account not only the dynamical representation of the system, but also considering all the coupled constraints involved in the control design. The former case can be applied when a given sub-system $i \in \mathcal{S}$ with $\mathcal{S} = \{1, \ldots, m\}$ and m the total number of sub-systems, has only interaction with neighborhood sub-systems. Meanwhile, the latter case is required to provide partitions also if there are not dynamical couplings among the sub-systems, which instead are coupled by constrains to be included in the optimization problem in (2.27).

Since most of networking systems can be represented by using a graph, for performing certain partitioning procedures a graph-theoretical strategy can be used [135]. In this case, the elements of the system coincide with the nodes of the graph while the couplings among the elements represent the arcs. Typically, the main objective for partitioning the system consists in minimize the couplings among the elements in different sub-systems such that the controller can be performed in a non-centralized fashion [74]. How the information should be shared among the sub-systems and the appropriate manner to implement the partitioning approach to provide online control for any decentralized, distributed and hierarchical approaches are presented in [114]. A quite general optimal partitioning problem independent from the control strategy used is presented in [118], where it has been applied to define decentralized predictive controllers. Another general partitioning problem is presented in [17], this work sought to partition the graph with a trade-off among minimization of sub-system sizes, interconnections, pairwise distances while considering information relevance. Other partitioning approaches applied to control power systems networks are presented in [13, 92] where, respectively, voltage control and reactive power control are provided.

2.3.5 MPC for Wind Farms Control

As wind provides more and more of the energy the world consumes, there is a growing interest in active power control (APC), in which the wind farm manages its power output in accordance with the electrical grid requirements. The generation conditions of the wind turbines may be optimized in order to achieve several objectives while respecting some constraints to ensure technical and/or operational limits. In the past decade, control techniques such PID control [158] and $\mathcal{H}_\infty$ have been prevalent in the literature [128, 129, 145]. However, these controller designs cannot incorporate the system and input constraints in a systematic fashion, additionally violating constraints will cause the undesired shutdown of wind turbine [91]. Therefore, MPC in wind energy applications has become popular in academic community due to its intrinsic capacity for dealing with multi-variable systems and constraints. Furthermore, its accessible design formulation handles more complex issues and guarantees proper performance and robustness [27, 34]. For those reasons, the predictive controllers represent a good alternative to classical control designs since they solve multi-objective optimization-based control problems to

regulate the wind farm generation during deloaded mode of functioning by optimally regulate the operation balance between the strictness of the wind turbine power reference following and the reduction of the wind turbine structural loading [25, 147, 172] or the minimization of the wake-induced power losses [10, 21, 138, 153].

A pioneering work is presented in [147], where the idea to exploit the freedom in power distribution to reduce fatigue loads was first presented in the context of disturbance rejection. There, the problem is divided into two parts. First, optimal power set points are computed explicitly off-line for each turbine using a receding horizon strategy. These set points are based on other auxiliary power variables that are then used for online coordination of the turbines in order to meet the total power demand. In [25], an optimal constrained centralized predictive control strategy is proposed to minimize the fatigue loads affecting the turbines by controlling the induction factors and the yaw settings. Distributed control design for reduction of loads is presented in [172], the control scheme is based on the fast gradient method via dual decomposition implemented using the clustering-based piecewise affine wind turbine model. The proposed strategy shows fast control to coordinate the wind power generation with energy storage systems linked to the wind farms. In [173], the authors use the same approach for optimally dispatching the active and reactive power set-points among the turbines such that frequency and voltage supports can be provided by the wind farms.

Adjoint-model predictive control has been proposed in [153], where Lagrange multipliers were used to remove constraints for the optimization problem, while WFSim was used to simulate wake aerodynamics. The authors keep measurements of the entire wind field that can become cumbersome as the size of wind farms grow. Recent works [67, 68, 111] used the receding horizon technique for designing centralized controllers that consider the wake dynamics estimated with a full high fidelity LES model of the wind farm to compute the optimal control commands. Despite the large wind farm efficiency gained of up to 21.2%, the computational costs of running LES makes these controllers unpractical for on-line optimization. To enable real-time operations, the authors in [138] propose a method that utilizes a time-varying one dimensional wake model in which rows of turbines are considered to behave similarly. This assumption greatly speeds the computation but neglects differences in the incoming wind profiles and requires turbines to be fully waked, which eliminates the possibility of wake steering control.

In order to cope with the computational costs, in [10] an efficient model to estimate the wind speed changes using SCADA data is proposed and the estimations used to optimally dispatch the power set-points among the turbines. The distributed consensus-based predictive control strategy proposed in [21] is used, including time-varying axial induction factors, yaw misalignment, and wake characteristics, is described and used to determine optimal axial induction and yaw control actions. However, the use of linear model for the wake estimation limits the use of this strategy for advanced purposes as loads or power optimization. Finally, [65] examined the available power gain due to the wake reduction controlling the induction factors when using a wake model with MPC to represent the interactions between turbines.

Part II

Centralized Wind Farm Control:

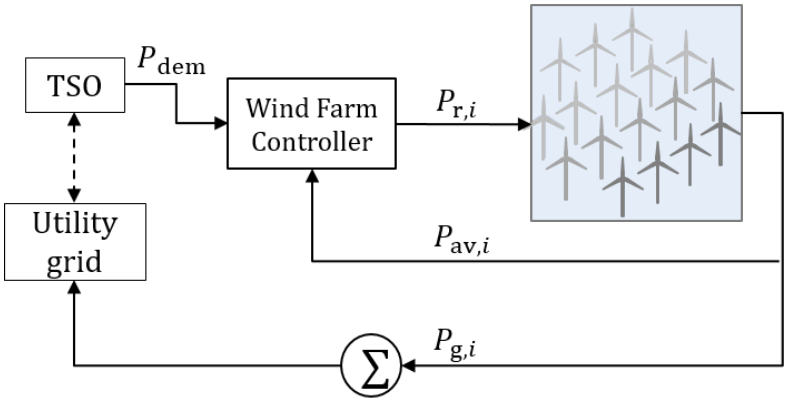

Figure 2.16: WPP control scheme under study.

Overview

The objective of wind farm control is to reduce the levelized cost of wind energy by intelligently operating the turbines inside the farm. When the wind conditions and the power demanded by the TSO permit, so that the latter is lower than the available power at the farm level, there is a degree-of-freedom in tracking the power demand. Therefore, besides tracking, the regulation of the power among the turbines can be optimized to reach different subgoals; for instance, the decrease of mechanical loads acting on the wind turbine and/or the increase of available power and the reduction of electrical cable losses. For doing so, a closed-loop central controller should be properly designed to solve a multi-objective optimization problem. As part of this dissertation, three novel wind farm control strategies are presented and tested by simulations in MATLAB/SIMULINK. Finally, for the sake of completeness, the proposed methodologies are compared for different wind speed conditions and directions values. fig. 2.16 shows a schematic illustration of the centralized closed-loop control scheme of the optimization-based control approaches proposed. The gray block contains the main components of the controller, which is required to regulate the power reference among the turbines P_{r} according to some constraints and measurement information, such that the total power generated by the wind farm, indicated as $P_{\text{g,tot}}$, meets the power demanded by the grid P_{dem}.

Chapter 3

A wind farm control strategy for power reserve maximization

Nowadays, in many countries wind energy is responsible for a significant part of the electricity generation. For this reason, TSOs are now demanding the WPPs to contribute with ancillary services such as frequency support. To this end, WPPs must be able to temporally increase the active power delivered into the grid to compensate consume and demand imbalances. This implies that WPPs now work below their maximum capacity to keep some power reserve to be able to inject extra power into the grid when needed. This reserve depends on the available wind power, which is directly connected with the wind speed faced by each turbine within the WPP.

Within a wind farm, the wind conditions are imposed by the wakes produced by the upstream turbines [53] that make the control of the turbines in the farm challenging. One approach for dealing with these aerodynamic interactions is to develop wake models for use in the optimal control problem formulation [21],[64]. However, the highly dynamic behaviour of the wind makes the estimation of the wake incredibly challenging, in particular if this goal wants to be achieved by first-order models. As mentioned in the extensive literature review about wake control presented in Section 2.2, several strategies have been proposed to minimize the wake effect in order to maximize the total power generation and minimize the power losses caused by the wakes. Some of them are based on redirecting the wakes around the downstream turbines by yawing [62, 121] or tilting [12, 152] the wind turbines, whereas others seek to redistribute the power contribution of each turbine [137]. Among others, an alternative approach in line with the goal of the

control strategy proposed in this chapter is to develop an online control algorithm where a centralized controller adjusts the axial induction factors of the turbines according to wind turbine performance information, local wind conditions and grid requirements. In particular, this chapter is devoted to present the wind farm control strategy as published in [139]. Here, a centralized wind farm controller solves an optimal control algorithm that seeks to determine the power set-points for every turbine considering that commonly wind farms operate in waked conditions. With the goal of maximizing the power reserve, the proposed wind farm control strategy distributes the power contribution of each turbine in order to maximize the available power (i.e., the power reserve) at the wind farm level.

The proposed approach has tested for a wind farm model of 12 wind turbines using a simulator that models the dynamic behavior of the wake effect by using the common dynamic wake meandering model [93].

3.1 Wind Turbine and Wind Farm Models

The power reserve for a wind farm of N turbines is computed by

$$P_{\text{res,tot}} = \sum_{i=1}^{N} P_{\text{res},i} = \sum_{i=1}^{N} (P_{\text{av,tot}} - P_{\text{dem}}) \tag{3.1}$$

where

$$P_{\text{av,tot}} = \sum_{i=1}^{N} P_{\text{av},i}(v_i), \tag{3.2}$$

and v_i the wind speed experienced by the turbine. In circumstances with high wind energy conditions, wind farms are able to meet the total power demanded by the TSO by de-loading some wind turbines, i.e., by keeping a certain amount of power reserve $P_{\text{res},i}$ as defined in (2.20). For wind turbines with this capability, the generated power can be expressed as

$$P_{\text{g},i} = \kappa_1 C_{\text{p}}(a_i) v_i^3 = \min(\kappa_1 C_{\text{p,max}} v_i^3, P_{\text{r},i}), \tag{3.3}$$

where $\kappa_1 = (\pi \rho R^2/2)$ and C_{p} is the power coefficient that can be written as a function of the induction factor a_i [97], see (2.3). In normal operation, according to the Betz's theory, the induction factor a_i can be assumed taking values between 0 and 1/3. Therefore, C_{p}

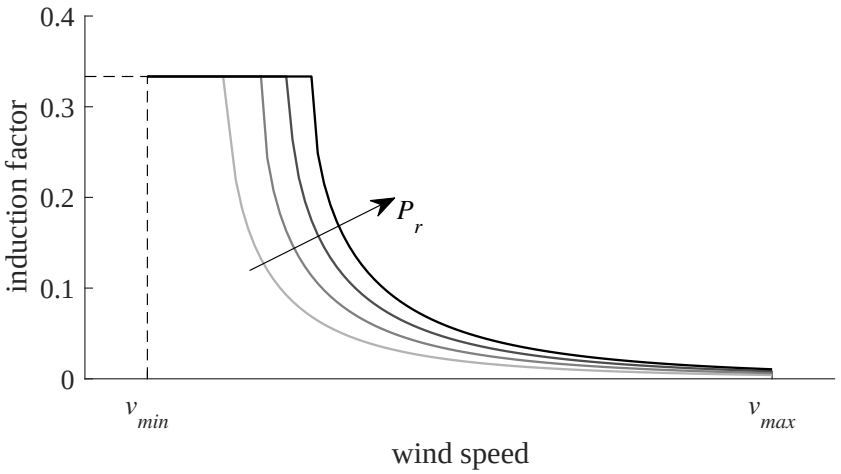

Figure 3.1: Induction factor a – wind speed v characteristic for several power set-points P_r. The black line corresponds to the nominal case ($P_r = P_{\text{rated}}$).

is an increasing function of a_i and the maximum value $C_{\text{p,max}}$ is obtained at $a_i = 1/3$. It is worth to recall, that the induction factor is only a control parameter that is empirically related with pitch and torque regulation. In fact, de-loading operations can be achieved by acting, individually [81] or in simultaneously [169], on both pitch and torque control actions to ensure sub-optimal operational conditions. According to (3.3), the generated power can be set to a given value $P_{\text{r},i}$ if wind conditions allow. This expression also indicates that, for a given v_i, there exists a unique $0 \leq a_i \leq 1/3$ producing $P_{\text{g},i} = P_{\text{r},i}$. The relationship among $P_{\text{g},i}$, v_i and a_i is shown in Figure 3.1.

The available power at each wind turbine, i.e., the maximum generation capacity for the wind conditions v_i, is a monotonically increasing function of the wind speed until to reach the rated value P_N in *Region*2, as shown in Figure 2.6. Therefore, for a given power reference $P_{\text{r},i}$ each turbine within a farm has different capacity reserve as wind conditions depend strongly on the geographical distribution of the wind turbines, variations of wind direction, surface roughness, turbulence and the air flow disturbances caused by the wake effects induced by up-stream turbines [18]. Despite of the complexity of the aerodynamic interactions between turbines, suitable estimations can be achieved by modeling the wind speed deficit as a function of the geographical positions of the wind turbines, the atmospheric wind conditions, and the control actions required for the turbines, which affect the induction factor a_i. Assuming the velocity deficit behind the upstream turbine modeled as a quasi-steady state model with a linear relation between

the induction factor and the downstream inlet velocity, [24, 84], the incoming wind speed for the downstream turbine is given by

$$v_j = v_i(1 - \delta v(x_{ji}, s_i, a_i)), \tag{3.4}$$

where $i \in \{1, \dots, N-1\}$, $j = i+1$, s_i is the spanwise distance behind the i-th turbine while the velocity deficit is

$$\delta v(x_{ji}, \mathrm{s}_i, a_i) = \begin{cases} 2a_i c_{ji} & \text{if } s_i \leq \frac{2R+2\kappa_r c_{i,j}}{2} \\ 0 & \text{otherwise,} \end{cases}$$

with the coupling parameter $c_{ji} = (2R/(2R + 2\kappa_r(x_i - x_j)))^2$ including the information about the wind turbine distance, being x_i and x_j the positions of the upstream and downstream turbines respectively, and the roughness coefficient κ_r that defines the wake expansion when passing through a turbine.

In light of the previous expressions, the wake effect may be modified by properly acting on the induction factors a_i with the aim of attenuating the wind deficits and thus for instance maximizing the power reserve and the wind farm capability for providing frequency support.

3.2 Wind Farm Controller

The primary objective of the wind farm controller is to track a power demand profile set by the TSO. This goal can be achieved with different power contributions of each turbine. This leaves an additional degree of freedom that can be used to satisfy other requirements. In the literature, several dispatch functions have been proposed to ensure different goals. For example, a simple approach distributes the total power proportionally to the available power of each turbine [77], while other distributions minimize the structural loads with the aim of ensuring a long turbine lifetime [50, 171]. Here, a model-free control strategy that uses this degree of freedom to maximize the power reserve is proposed.

Assuming that the power P_{dem} demanded by the TSO is lower than the total available power $P_{\text{av,tot}}$, the objectives are to regulate the total generated power at P_{dem} and maximize the total power reserve P_{res}. Being the power demand P_{dem} a parameter set

by the TSO, the maximization of power reserve implies maximizing the total available power $P_{\text{av,tot}}$.

The available power at each turbine $P_{\text{av},i}$ depends on an increasing function of the wind speed faced by the rotor v_i (see Figure 3.1). Therefore, the maximization of the total available power can be seen as maximizing

$$J = \sum_{i=2}^{N} v_i(\mathbf{P_r}), \tag{3.5}$$

where $\mathbf{P_r} = [P_{r,1}, \ldots, P_{r,N}]^T$, and $P_{\text{r},i}$ is the power generation set-point at i-th turbine imposed by the wind farm control.

Due to the propagation of the wake effect, the generation conditions of the upstream turbines will affect the wind speed experienced by downstream turbines only after a certain time interval T_{s}, being this the time needed by the air flow to travel from one turbine to another. Notice that T_{s} can be approximated as

$$T_s = s_i/(v'_\infty), \tag{3.6}$$

where $v'_\infty = 0.7v_\infty$ indicates the variation of the convection velocity from the bottom to the top of the rotor disk and s_i the distance between turbines [31].

Assume the wind turbines are evenly spaced and the set of turbine indexes

$$\mathcal{N} = \{i : 1 \leq i \leq N \text{ and } v_i \geq v_j, \text{ for } i < j\}$$

is sorted according to the farm layout and dominant free-stream wind speed direction. That is, $i = 1$ corresponds to the turbine facing the free-stream speed (v_∞) and $i = N$ the last one, facing the wind speed after passing through the entire farm. Hence, the value of the coupling parameter $c_{j,i}$ in (3.4) can be replaced by the constant κ_2. Therefore, defining $t = kT_{\text{s}}$ with $k \in \mathbb{Z}_{\geq 0}$, or simply k, the wind speeds faced by each turbine can be modelled as

$$\begin{aligned}
v_1(k+1) &= v_\infty \\
v_2(k+1) &= v_1(k)(1 - \kappa_2 a_1(k)), \\
v_3(k+1) &= v_2(k)(1 - \kappa_2 a_2(k)), \\
&\vdots \\
v_N(k+1) &= v_{N-1}(k)(1 - \kappa_2 a_{N-1}(k)),
\end{aligned} \tag{3.7}$$

with

$$v_\infty(k) = v_1(k) \geq v_2(k) \geq v_3(k) \geq \cdots \geq v_N(k). \tag{3.8}$$

The induction factor a_i is given by $P_{\mathrm{r},i}$ according to (5.3). It can be seen from 5.3 that for a given v_i an increase in $P_{\mathrm{r},i}$ leads to an increase in a_i. From 3.7, this results in a higher wind speed deficit. Therefore, a heuristic approach to maximize 3.5 may be to minimize the power contributions of first wind turbines and maximize the contributions of the last ones (sorted according to $\mathcal{N}$). Keeping this idea in mind, in this chapter it is proposed to compute the power set-point $P_{\mathrm{r},i}$ for each wind turbine by solving the following linear programming problem:

$$\underset{P_{\mathrm{r},i}}{\text{minimize}} \quad w^T \epsilon \tag{3.9a}$$

$$\text{subject to} \quad P_{\mathrm{dem}} = \sum_{i=1}^{N} P_{\mathrm{r},i}, \tag{3.9b}$$

$$|P_{\mathrm{dem}} - \sum_{j=i}^{N} P_{\mathrm{r},j}| \leq \epsilon_i, \quad i \in \mathcal{N}, \tag{3.9c}$$

$$P_{\mathrm{min},i} \leq P_{\mathrm{r},i} \leq P_{\mathrm{av},i}, \quad i \in \mathcal{N}, \tag{3.9d}$$

where $\epsilon = [\epsilon_1, \ldots, \epsilon_N]^T$, $w = [w_1, \ldots, w_N]^T$ are weights such that $w_1 < w_2 < \ldots < w_N$, and $P_{\mathrm{min},i}$ is the minimum power contribution.

Notice that constraint (3.9b) can be satisfied with multiple linear combinations of $P_{\mathrm{r},i}$. The optimization problem (3.9) seeks to find the combination with higher power contribution from the last group of turbines. In particular, with the selection of weights w and the constraint (3.9c), the optimization problem can be seen as

Algorithm 2 Linear Programming Optimization Problem

try first $P_{\mathrm{r},N} = P_{\mathrm{dem}}$,

if $P_{\mathrm{r},N} > P_{\mathrm{av},N}$ then try $P_{\mathrm{r},N-1} = P_{\mathrm{dem}} - P_{\mathrm{r},N}$,

if $P_{\mathrm{r},N-1} > P_{\mathrm{av},N-1}$ then try $P_{\mathrm{r},N-2} = P_{\mathrm{dem}} - P_{\mathrm{r},N} - P_{\mathrm{r},N-1}$,

and so on, until ((3.9)b) is satisfied.

In fact, if the lower limit $P_{\min}$ is removed, the problem can be solve algorithmically. Nevertheless, the lower limit is useful to prevent the shutdown of some turbines in high wind conditions.

The optimization problem (3.9) is solved at every time $T < T_s$ to produce a set of power references $P_{\mathrm{r},i}$, $i \in \mathcal{N}$. The application of these references alters the induction factors and thus the wake effect. As the proposed control strategy reduces the power contribution from the first set of turbines, the wind speeds faced by the last turbines increase resulting in higher available powers. As will be shown in the case study, after a few iterations this control strategy is able to increase the available power in the last turbines and then in the total power reserve.

3.3 Case Study

Case description

The proposed control strategy has been evaluated by simulation in the case of a wind farm with 12 benchmark NREL 5MW wind turbines with radius of 63 m (a diameter $D = 126$ m). The wind turbines are evenly spaced along x- and y-directions by 630 m ($5D$). Simulations were performed with the AEOLUS SimWindFarm (SWF) Simulink toolbox [72], which uses the dynamic wake meandering model to estimate the wake effects according with the wind turbine layout and the ambient turbulence intensity. The wind field size was 2500×2500 m^2 and the 2d (x,y) grid was spaced 15 m. Simulations were performed with laminar flow conditions, while the turbulence intensity was set equal to 0 to have a clearer view of the wind speed changes produced by the proposed strategy. Different wind directions were simulated by rotating the wind farm layout. Figure 3.3 shows the wind fields $v_\infty = 11$ m/s with directions of 0 and 30 degrees in steady-state conditions. Although wind farms layout are designed such that the occurrence of highly waked conditions are minimized, e.g., when the wind direction is 0 degrees, it remains an interesting case study to investigate the wind farm conditions in the worst case scenario [50].

With the aim of evaluating the improvement in the power reserve, the proposed control algorithm was compared with the commonly used power distribution [72, 81] established

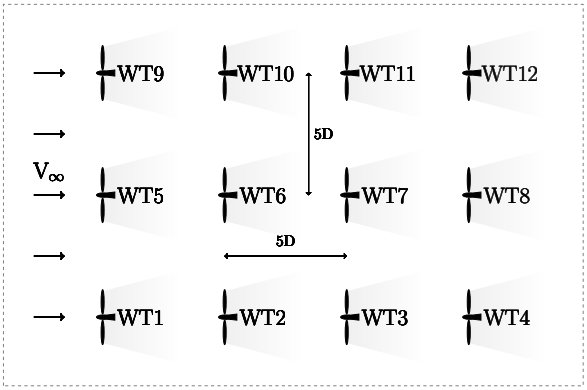

Figure 3.2: Wind farm layout corresponding to the case study. The turbines are considered oriented to the free-stream wind speed direction.

as

$$P_{\mathrm{r},i} = \min\left(\frac{P_{\mathrm{dem}}}{P_{\mathrm{av,tot}}} P_{\mathrm{av},i}, P_{\mathrm{av},i}\right), \quad i = 1, \ldots N. \tag{3.10}$$

Simulation Results

Scenario 1: low power demand and zero degrees wind speed direction

First, it is analyzed the system response when the power required by the TSO is set at 20 MW and the free-stream wind speed is 11 m/s with a direction of 0 degrees. Figure 3.4 shows the total values of the available power $P_{\mathrm{av,tot}}$ (red line), the power demand P_{dem} (dashed line), the power generated P_{g} (blue line), and the power reserve P_{res} (black line). Initially, for $t < 200$ s (shadow area), the wind farm controller sets the power set-points of each turbine according to the baseline power distribution (3.10). After $t = 200$ s, the controller starts computing the power set-points with the proposed control strategy (3.9). It can be observed in Figure 3.4 that such strategy ensures the regulation of P_{g} around the constant set-point $P_{\mathrm{dem}} = 20$ MW during the whole simulation. On the other hand, it can also be seen that when the proposed control strategy is applied ($t \geq 200$ s), the available power $P_{\mathrm{av,tot}}$ increases from 48 to 51 MW after a few steps. This represents an increase in the power reserve P_{res} from 28 to 31 MW. The new steady-state value is reached after 200 s.

Figure 3.5 shows the power available $P_{\mathrm{av},i}$ (red line), the power set-points $P_{\mathrm{r},i}$ (dashed

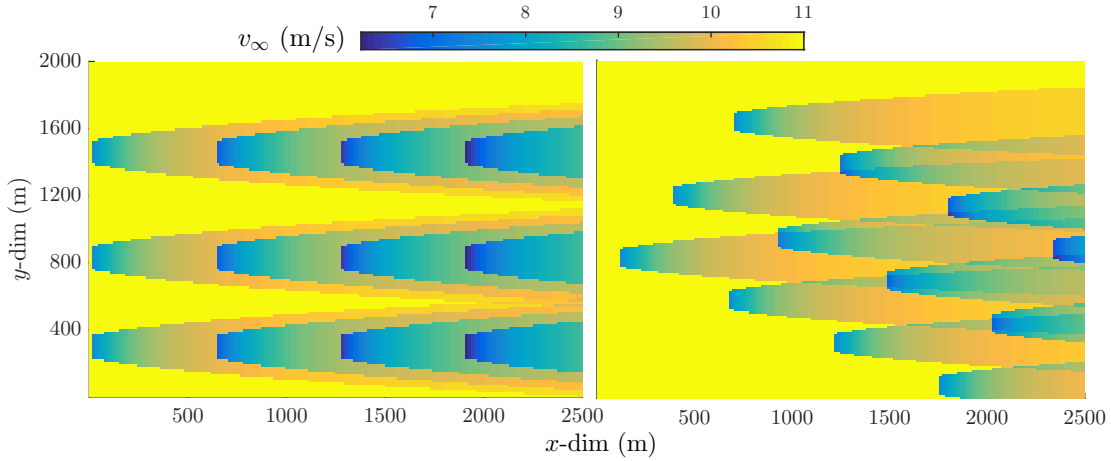

Figure 3.3: Wind fields simulated with SWF for a wind farm of 12 turbines facing a $v_\infty = 11$ m/s. Left plot: wind field for a direction of 0 degrees. Right plot: wind field for a direction of 30 degrees.

line) and the power generated $P_{g,i}$ (blue line) for each wind turbine. The wind speed experienced by each turbine is shown in Figure 3.6. The shadow areas in both figures correspond to the use of the baseline power distribution (3.10) ($t < 200$ s), in the analyzed scenario $P_{\text{dem}}/P_{\text{av,tot}} = 0.47$. In Figure 3.6, it can be observed the wind speed deficit caused by the wake effect. With the baseline distribution, each turbine must contribute with 47% of its available power. The turbines in the first column are facing the free-stream speed 11 m/s, whereas the ones in the last column are experienced 10.23 m/s. As a result, the available power $P_{\text{av,i}}$ decreases from 5 MW in the first column (WT1, WT5, WT9) up to 3.71 MW in the last column (WT4, WT8, WT12).

When the proposed control strategy is applied at $t = 200$ s, the power set-points of the turbines in last column are set at the their available power. As a consequence of the larger contribution from these turbines, the remaining turbines reduce the power generation until the minimum value $P_{\text{min},i} = 1$ MW. As explained in Section 3.2, this reduction of the power generation in the turbines of the first columns implies a decrease of their induction factors and of the wind speed deficit in downstream turbines. These changes take about $T_s = 60$ s to reach the last column ($t_1 \simeq 260$ s) for the current case. This is the time needed by the wakes to travel through the columns. At $t = t_1$, the reduction in $P_{g,i}$ only affects the wind speeds faced by the turbines in the adjacent downstream column. The wind speed v_i in Figure 3.6 increases with respect to the

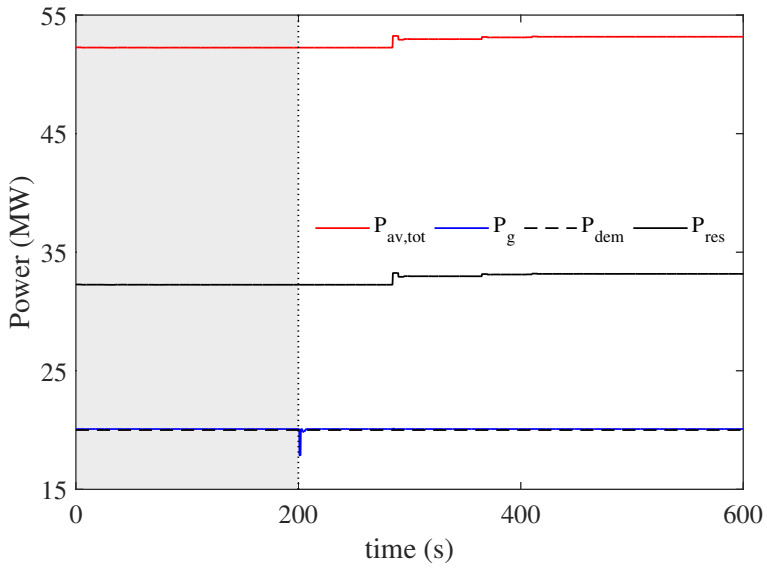

Figure 3.4: Scenario 1: Power evolution for $v_\infty = 11$ m/s with a direction of 0 degrees.

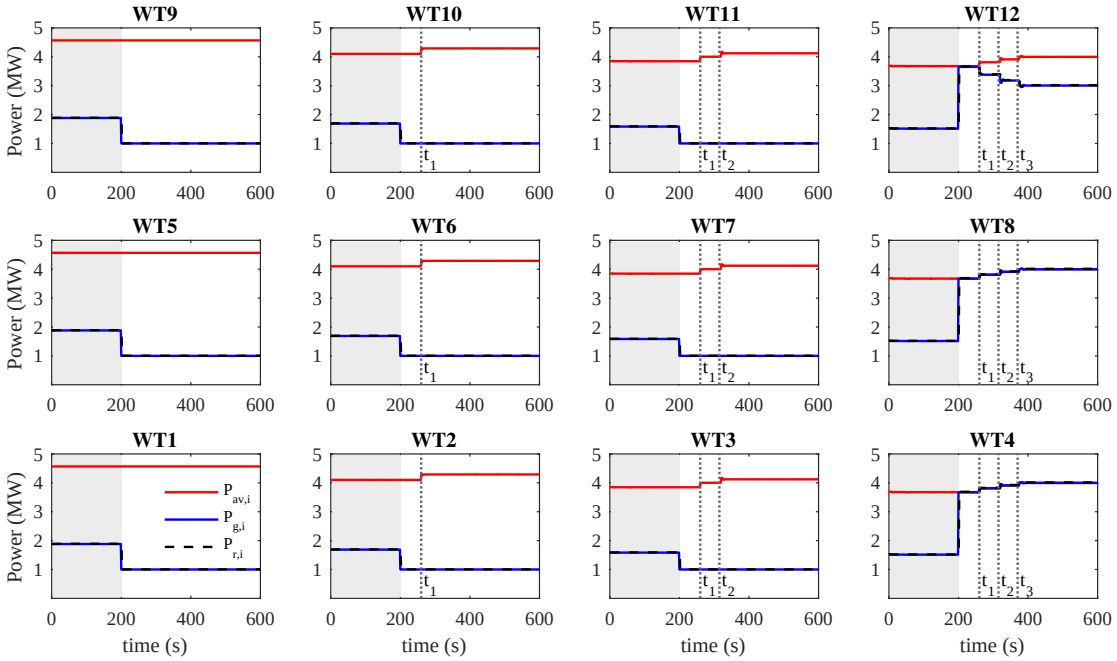

Figure 3.5: Scenario 1: generated ($P_{\mathrm{g,i}}$), available ($P_{\mathrm{av,i}}$) and set-point ($P_{\mathrm{r,i}}$) powers for each wind turbine. Shadow area: baseline power distribution function. White area: proposed distribution algorithm.

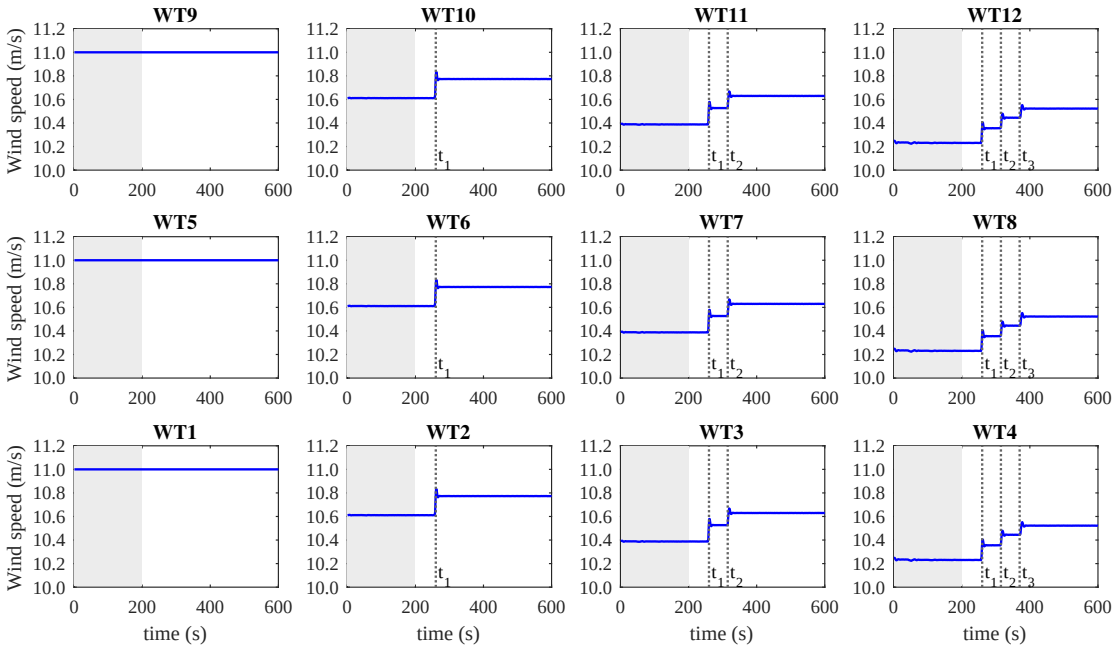

Figure 3.6: Scenario 1: wind speeds faced by each turbine. Shadow area: baseline power distribution function. White area: proposed distribution algorithm.

initial conditions ($t < 200$ s) in 1.5% for turbines WT2, WT6, WT10, in 1.3% for WT3, WT7, WT11 and 1.2% for the last column. The increase in the wind speed faced by the downstream turbines causes an additional increase of the available power in the last column. As a result, the control strategy imposes a higher set-point to WT8 and WT4. The contribution of WT12 is now lower because the total available power is enough to reach the power demand. This new distribution causes a new increase in the wind speed and thus in the available power until an equilibrium is reached after three steps, i.e., at $t_3 = 200 + 3T_s$ s.

Figure 3.4,3.5,3.6 show that the proposed algorithm is able to reduce the wake effects and thus improves both the overall available power and the total power reserve.

Scenario 2: low power demand and different wind directions

For a more complete evaluation of the proposed strategy towards power reserve maximization, the control system was simulated under low power demand $P_{\text{dem}} = 20$ MW for different wind speed directions. Figure 3.7 shows the power reserve for a free-stream

wind speed $v_\infty = 11$ m/s with directions of 0, 20, 40, 60, 80, 90 degrees. As in the previous case, the baseline control is used for $t < 200$ s, then the new power distribution algorithm is applied. In Figure 3.7, it can be seen that the proposed strategy increases the power reserve for all wind directions compared with the baseline case. As mentioned in Section 3.2, the proposed algorithm needs several steps before reaching the equilibrium and these step times are affected by the time required from the wakes to travel through the wind farm columns. This propagation time is different for each direction because the distance the air flow must travel depends on the wind speed direction. Notice that higher improvements in P_{res} are obtained when the wind turbines are totally in the wakes of the upstream turbines (see Figures 3.2 and 3.3). As a result, the higher improvement occurs for both 0 and 90 degrees, namely when the wind direction is perpendicular to x- or y- directions. Under these circumstances, P_{res} increases from 28 MW for $t < 200$ s to 30.5 MW for $t > 500$ s when the direction of the wind is 0 degrees and from 30 MW to 31.8 MW when the direction is 90 degrees. If the turbines are only partially affected by the wakes, as the cases for 20, 40, 60 and 80 degrees, the additional power reserve obtained with the proposed control strategy is low but the approach is still advantageous. For example, the difference between P_{res} for $t < 200$ s and $t > 500$ s is about 0.4 MW at 20 and 60 degrees, 0.92 MW and 1.4 MW for both 40 and 80 degrees, respectively.

Figure 3.8 presents the power reserve increments obtained with the proposed control strategy compared with the baseline expression, i.e., $\Delta P_{\text{res}} = P_{\text{res,new}} - P_{\text{res,base}}$, where $P_{\text{res,new}}$ is the reserve at $t > 500$ and $P_{\text{res,base}}$ is the power at $t = 0$. In this figure, three free-stream speeds, 11, 13, 15 m/s, were considered for several wind directions. Clearly, the proposed control achieves the highest improvement for $v_\infty = 11$ m/s. Under these circumstances, the total available power in the farm is close to the power demand and a clever distribution of the power contribution from each turbine makes a significant impact over the power reserve. In this case, the maximum ΔP_{res} is 2.36 MW at 0 degrees, while lower differences are obtained for high wind speed conditions. Comparing different wind speed directions, it can be observed that the proposed control strategy produces higher improvements in the reserve for those cases with higher air flow disturbances caused by the wakes. In particular, the lower reserve increment for the case of 90 degrees compared with the 0 degrees case can be understood as a consequence of the wind farm layout. When the wind speed reaches the farm with 90 degrees, there are less turbines

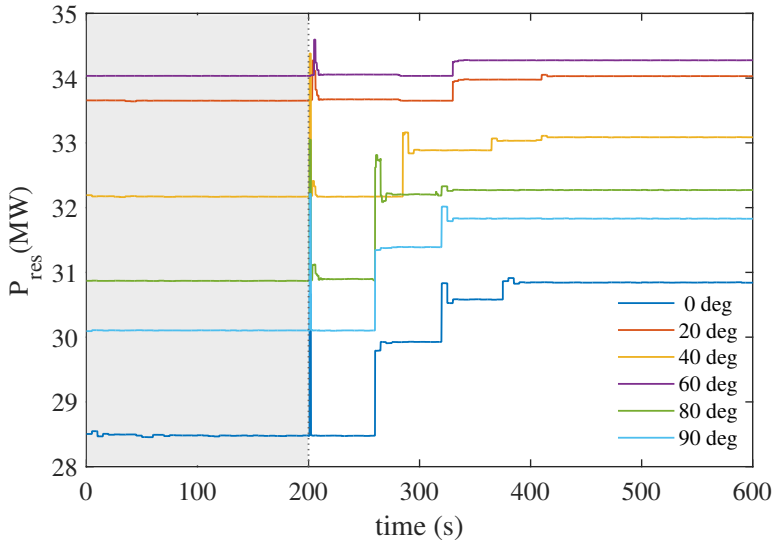

Figure 3.7: Scenario 2: power reserve for several wind directions, $P_{\text{dem}} = 20$ MW, $v_\infty = 11$ m/s.

downstream and thus a lower wake effect. For the higher free-stream wind speed (13 and 15 m/s), the increase in the power reserve is lower because the available power is higher and the ratio $P_{\text{dem}}/P_{\text{av,tot}}$ is lower. As a consequence, the power required to the first column of turbines is lower and the wake effect less marked.

Scenario 3: high power demand and different wind directions

In Figure 3.9, it can be observed the power reserve in case of a high power demand scenario. The power demand was $P_{\text{dem}} = 45$ MW and the free-stream wind speed $v_\infty = 11$ m/s, with directions of 0, 20, 40, 60, 80, 90 degrees. Under these wind conditions, the available power is not enough to ensure the power demand. As a result, the reserve is almost zero except for the cases of 20, 40 and 60 degrees, in which the wake effect has less impact on the available power. Nevertheless, the proposed approach is able to increase P_{res} with respect to the value obtained with the baseline power distribution in 1.05 MW for 20 degrees, in 1.6 MW for 60 degrees and in 0.8 MW for 40 degrees.

Figure 3.10 presents the corresponding reserve increments ΔP_{res} for three free-stream

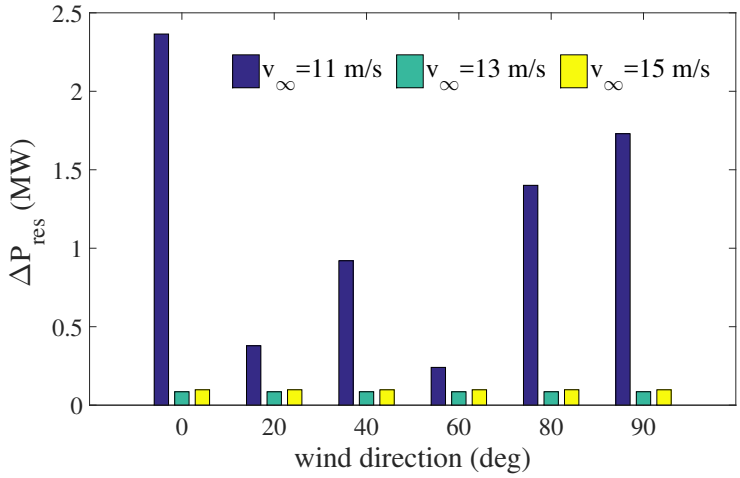

Figure 3.8: Scenario 2: Summary of power reserve levels obtained with the proposed algorithm for several free-stream wind speeds and directions.

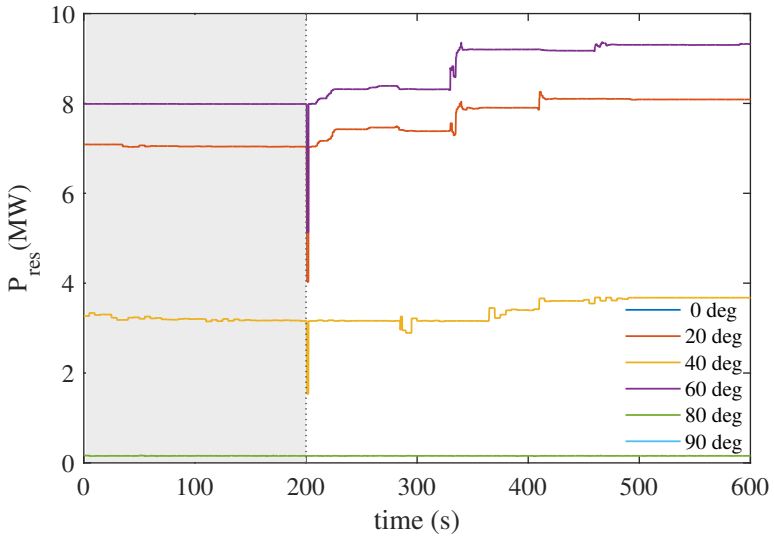

Figure 3.9: Scenario 3: power reserve for several wind directions, $P_{\text{dem}} = 45$ MW, $v_\infty = 11$ m/s.

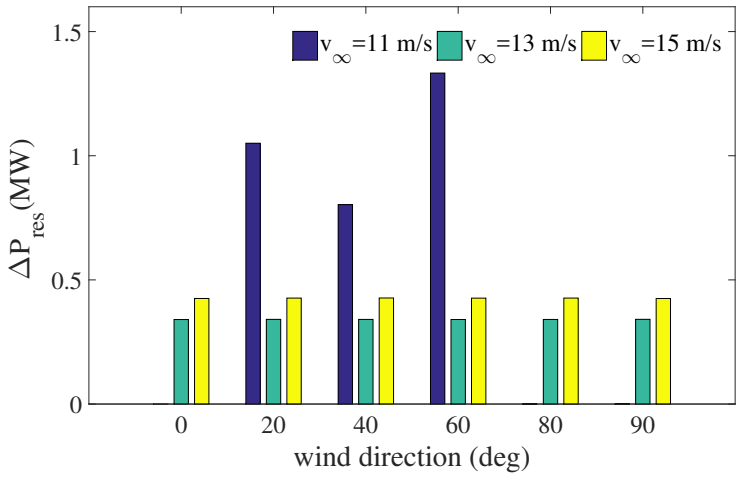

Figure 3.10: Scenario 3: Summary of power reserve levels obtained with the proposed algorithm for several free-stream wind speeds and directions.

wind speeds 11, 13, 15 m/s with the directions aforementioned. As the power demand is high and the available power is low in the case of 11 m/s, the improvement is only significant for the case in which the available power is higher than zero. On the other hand, when the wind speed is higher (13 and 15 m/s), the benefits of the proposed control strategy is more noticeable for all the wind directions as a result of higher wind power resources.

3.4 Summary

This chapter has proposed a new control strategy to maximize the power reserve in WPPs while the power demanded by the TSO is satisfied. The proposed approach seeks to distribute the power contribution of each turbine in order to reduce the wind speed deficits caused by wake effects. The idea is to prioritize the power contribution of the most downstream turbines and thus attenuating the wake disturbances. The proposed strategy was evaluated by simulation in the case of 12 turbine WPP under different scenarios, including low and high power demands and several wind speed conditions. The results show that the control strategy is capable of increasing the power reserve compared with the conventional power distribution where the power set-points of each wind turbine are proportional to its available power. The best performance is obtained when the

power demanded by the TSO is close to the total available power. In these cases, a clever distribution of the power contributions from each turbine reduces the negative effects of wakes and produces a significant increase in the power reserve compared to the conventional approach.

Chapter 4

Predictive Control based on Lexicographic Minimizers

This chapter presents a novel de-loading control strategy aimed to regulate the total power delivered from a wind farm at the PCC to provide the power set-point given by the TSO whereas the power reserve available for frequency support is maximized. The contributions presented in this chapter have been published in [141]. The control strategy consists of a wind farm MPC controller that uses the information about the generated and available powers by each turbine and solves a multi-objective optimization problem in order to coordinate the best power contribution for each wind turbine. The optimization problem is solved using the lexicographic formulation introduced in [106] in order to consider the hierarchy of the control objectives. Conventionally, a multi-objective optimization problem is solved by stating a global cost function, composed of a linearly weighted sum of cost functions associated with each objective. However, finding appropriate weights is not a trivial problem and specific tuning of the weights are necessary due to different numerical values of cost functions for different scenarios. Moreover, the common tuning methodologies require a reference controller or an observer, e.g., [42, 161], involving a lot of numerical simulations. As an alternative to automatic tuning, the lexicographic approach addresses the issue of prioritizing the objectives by setting *a priori* the prioritization among the competing objectives. How the lexicographic approach can be applied to MPC has been shown in [87], and some application to fault diagnosis and optimal aircraft trajectories are presented in [124**?**]. The application of lexicographic multi-objective optimization for controlling large-scale

systems is presented in [119], where an MPC is stated to optimally regulate a sewer network.

The lexicographic approach in the present work is used to guarantee that the MPC controller solves the optimal problem of regulating the power set-points among the turbines providing the highest priority to the power reference tracking and less priority to the power reserve maximization. Nevertheless, due to the opposite nature of the two cost-functions the lexicographic approach avoids the problem of stating a non-convex cost-function by solving the two objectives separately. In order to illustrate the enhancement over the performance of the MPC controller, the proposed control strategy is evaluated by simulations for the case of a wind farm with three turbines in a row taking into account the variation of wind speed faced by downstream turbines due to the wake effect.

4.1 Wind Farm and Wind Turbine Models

Since the MPC strategy is based on the receding horizon idea, in order to predict at each sample time the wind farm dynamics, a model of the wind farm is necessary. Moreover, since the control objectives must be ensured quickly (about seconds-scale) to follow the fast variation of the power demanded by the grid, the wind farm model must be simple and computationally efficient. When doing so, some critical issues are related to the modeling of the nonlinear wind turbine dynamics and aerodynamic couplings among the turbines, discussed in Chapter 2. Complex wind farm models are presented in [137]. However, when the main objective of the controller is to ensure the wind farm power tracking within small computational time, the flow dynamics can be neglected [158] and the wind farm can be modeled as a graph including n_{t} uncoupled subsystems, i.e., the wind turbines. Assuming that each wind turbine is equipped with a power controller that ensures the power curve in Figure 2.6, and so allows working in derated mode if necessary [23]; the dynamic behaviour of the i-th turbine from the power set-point to the generated power can be modeled as a first order system delivering a power

$$\dot{P}_{\mathrm{g},i} = -\frac{1}{\eta}(P_{\mathrm{g},i} - \min(P_{\mathrm{av},i}, P_{\mathrm{r},i})), \tag{4.1}$$

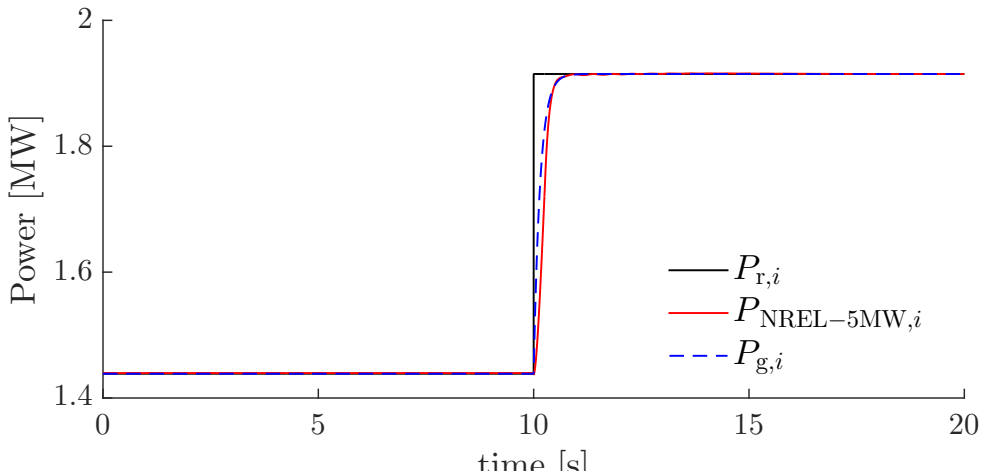

Figure 4.1: Wind turbine power response. Grey line: power reference $P_{\mathrm{r},i}$, red line: power generated $P_{\mathrm{NREL-5MW},i}$, and blue dashed-line: power generated $P_{\mathrm{g},i}$, obtained from (4.1).

where η is a time constant, $P_{\mathrm{r},i}$ is the power reference set by the wind controller and

$$P_{\mathrm{av},i} = \min\left(\frac{\rho\pi R^2}{2} C_{\mathrm{p,max}} v_i^3, P_N\right). \tag{4.2}$$

The reader is referred to (2.8) for the variables definitions. In order to check the validity of this approximation, Figure 4.1 shows the power response obtained by modeling the wind turbine as a first-order system for the value of time constant $\eta = 0.15$ s and the power response of the more detailed wind turbine model, that is the two-masses NREL-5MW wind turbine model used in [72]. Finally, from (4.1) follows that the wind farm power response is obtained as

$$P_{\mathrm{g,tot}} = \sum_{i=1}^{n_{\mathrm{t}}} P_{\mathrm{g},i}. \tag{4.3}$$

The presented simplified wind turbine model can be used to estimate the wind turbine response for the design of the MPC controller.

4.2 MPC Controller for Power Reserve Maximization

The proposed centralized wind farm control approach has the structure as shown in Figure 4.2. The MPC controller uses the $P_{\mathrm{g},i}$ and $P_{\mathrm{av},i}$ sent by each turbine and the total

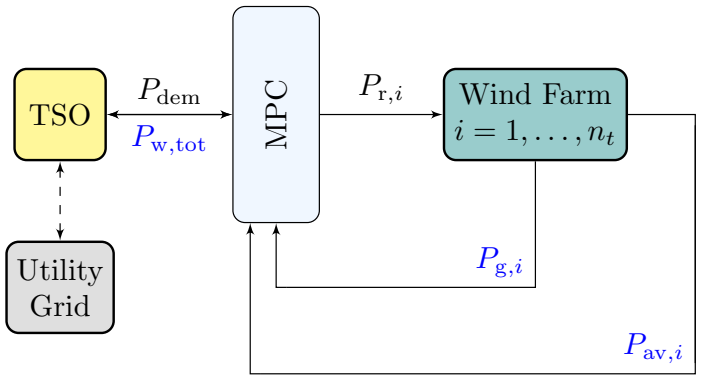

Figure 4.2: Scheme of the proposed wind farm centralized control strategy. The MPC shares information with the TSO (i.e., $P_{\text{dem}}, P_{\text{r,tot}}$) and sets the power reference ($P_{\text{r},i}$) among the wind turbines according to the information of the wind turbine operational conditions (i.e., $P_{\text{g},i}, P_{\text{av},i}$)

.

power demand P_{dem} to produce the power set-point $P_{\text{r},i}$ for each turbine. The control objectives to be considered for optimally distributing the power references among the turbines are the following:

Obj1: Ensure the tracking of a power demand profile P_{dem}.

Obj2: Maximize the total power reserve defined as (3.1).

The former objective is basically a reference-tracking problem. The latter implies to coordinate the power contribution from each turbine taking into account the interaction among the turbines caused by the wake effects in order to maximize the total power reserve.

According to the wind turbine response model in (4.1), the dynamics of the wind turbine power generation are represented by the following continuous-time state-space model

$$\dot{\mathbf{x}}(t) = \mathbf{A}\mathbf{x}(t) + \mathbf{B}_u\mathbf{u}(t) + \mathbf{B}_d\mathbf{d}(t), \tag{4.4}$$

where the vector $\mathbf{x} \in \mathbb{R}^{n_x}$ denotes the system states, $\mathbf{u} \in \mathbb{R}^{n_u}$ denotes the vector of manipulated variables, $\mathbf{d} \in \mathbb{R}^{n_d}$ is the vector of disturbance and $\mathbf{A}$ and $\mathbf{B}$ indicate the system matrices in the simplified wind turbine model (4.4) of specific dimensions.

Specifically,

$$\begin{aligned}
&\mathbf{x} = \begin{bmatrix} P_{\mathrm{g},1}, & \ldots, & P_{\mathrm{g},n_t}, & \xi \end{bmatrix}^T, && n_x = n_t + 1 \\
&\xi = (P_{\mathrm{dem}} - \sum_{i=1}^{n_t} P_{\mathrm{g},i}), && \\
&\mathbf{u} = \begin{bmatrix} P_{\mathrm{r},1}, & \ldots, & P_{\mathrm{r},n_t} \end{bmatrix}^T, && n_u = n_t \\
&\mathbf{d} = P_{\mathrm{dem}}, && n_d = 1
\end{aligned} \tag{4.5}$$

$$\mathbf{A} = \begin{bmatrix} -\frac{1}{\eta}\mathbf{I}_{n_t \times n_t} & 0 \\ -\mathbf{1}_{n_t \times n_t} & 0 \end{bmatrix}, \ \mathbf{B_u} = \begin{bmatrix} \frac{1}{\eta}\mathbf{I}_{n_t \times n_t} \end{bmatrix}, \ \mathbf{B_d} = \begin{bmatrix} \mathbf{0}_{n_t \times 1} \\ 1 \end{bmatrix}.$$

Notice that ξ is an integral action added to ensure null steady-state error.

In order to implement the MPC strategy as presented in Section 2.3 the system (4.4) is discretized for a sampling time T_s, resulting in the following state-space difference equations:

$$\mathbf{x}(k+1) = \mathbf{A}_d\mathbf{x}(k) + \mathbf{B}_{u,d}\mathbf{u}(k) + \mathbf{B}_{d,k}\mathbf{d}(k), \tag{4.6}$$

where $k \in \mathbb{Z}_{\geq 0}$ denotes the discrete-time instant and $\mathbf{A}_k$, $\mathbf{B}_{u,k}$ and $\mathbf{B}_{d,k}$ the discrete-time versions of matrices in (4.5).

System states and manipulated variables are constrained because of physical and/or desired operational limits. These constraints are defined in a polytopic fashion as

$$\mathcal{X} = \{\mathbf{x} \in \mathbb{R}^{n_x} \,|\, \mathbf{x}(k) \in [\underline{\mathbf{x}}, \overline{\mathbf{x}}], \forall\, k\}, \tag{4.7a}$$

$$\mathcal{U} = \{\mathbf{P}_{\mathrm{r}} \in \mathbb{R}^{n_u} \,|\, \mathbf{P}_{\mathrm{r}}(k) \in [\underline{\mathbf{P}}_{\mathrm{r}}, \overline{\mathbf{P}}_{\mathrm{r}}], \forall\, k\}, \tag{4.7b}$$

where $\underline{\mathbf{x}} \in \mathbb{R}^{n_x}$ and $\overline{\mathbf{x}} \in \mathbb{R}^{n_x}$ denote the vectors of minimum and maximum admissible values of system states, respectively, while $\underline{\mathbf{P}}_{\mathrm{r}} \in \mathbb{R}^{n_u}$ and $\overline{\mathbf{P}}_{\mathrm{r}} \in \mathbb{R}^{n_u}$ denote the vectors of minimum and maximum admissible values of manipulated variables, respectively.

In order to design the MPC strategy for the considered system, let $\hat{\mathbf{u}}(k)$ be a sequence of feasible control inputs (manipulated variables) within a pre-establish prediction horizon denoted by $H_p \in \mathbb{Z}_{>0}$. Similarly, let $\hat{\mathbf{x}}(k)$ be the sequence of feasible system states when

applying the control input sequence $\hat{\mathbf{u}}(k)$ to the system in . Finally, let $\hat{\mathbf{d}}(k)$ be the available forecasting of the power demands (disturbances). Hence,

$$\hat{\mathbf{u}}(k) \triangleq \{\mathbf{P}_{\mathrm{r}}(k|k), \ldots, \mathbf{P}_{\mathrm{r}}(k+H_p-1|k)\}, \tag{4.8a}$$

$$\hat{\mathbf{x}}(k) \triangleq \{\mathbf{x}(k+1|k), \ldots, \mathbf{x}(k+H_p|k)\}, \tag{4.8b}$$

$$\hat{\mathbf{d}}(k) \triangleq \{P_{\mathrm{dem}}(k|k), \ldots, P_{\mathrm{dem}}(k+H_p-1|k)\}. \tag{4.8c}$$

Thus, the MPC controller is designed by stating the following open-loop finite-horizon multi-objective optimization problem:

$$\underset{\hat{\mathbf{u}}(k) \in \mathcal{U}}{\text{minimize}} \quad J(\mathbf{x}(k), \hat{\mathbf{u}}(k), \mathbf{d}(k)) \triangleq \sum_{m=1}^{3} \sum_{i=0}^{H_p-1} J_m(\mathbf{x}(k+i), \hat{\mathbf{u}}(k+i), \mathbf{d}(k+i)), \tag{4.9a}$$

subject to

$$\mathbf{x}(k+j+1|k) = \begin{bmatrix} \mathbf{A}_d & \mathbf{B}_{u,k} & \mathbf{B}_{d,k} \end{bmatrix} \begin{bmatrix} \mathbf{x}(k+j|k) \\ \mathbf{P}_{\mathrm{r}}(k+j|k) \\ P_{\mathrm{dem}}(k+j|k) \end{bmatrix}, \quad j \in [0, H_p-1] \cap \mathbb{Z}_{\geq 0}, \tag{4.9b}$$

$$\mathbf{u}(k+j|k) \in \mathcal{U}, \qquad j \in [0, H_p-1] \cap \mathbb{Z}_{\geq 0}, \tag{4.9c}$$

$$\mathbf{x}(k+j|k) \in \mathcal{X}, \qquad j \in [1, H_p] \cap \mathbb{Z}_{\geq 0}, \tag{4.9d}$$

where $\mathbf{x}(k|k) \in \mathbb{R}^{n_x}$ is the current measured system state. Assuming that the optimization problem in (4.9) is feasible, its solution yields the optimal sequence

$$\hat{\mathbf{u}}^{\star}(k) \triangleq \{\mathbf{P}_{\mathrm{r}}^{\star}(k|k), \ldots, \mathbf{P}_{\mathrm{r}}^{\star}(k+H_p-1|k)\}.$$

Therefore, following the receding horizon control philosophy, the controller applies to the system in (4.6) the first control input from $\hat{\mathbf{u}}^{\star}(k)$, which corresponds with $\mathbf{P}_{\mathrm{r}}^{\star}(k|k)$. Then, a new state vector is measured from (4.6) and the procedure is repeated in order to determine the optimal control sequence from which the optimal control input for $\hat{\mathbf{u}}^{\star}(k+1)$ is obtained.

Notice that the multi-objective cost function in (4.9a) is defined according to the stated objectives **Obj1** and **Obj2** as follows. Objective **Obj1** is formulated as the minimization of the linear cost function

$$J_1(k) \triangleq \|Q\,\mathbf{x}(k)\|_1, \tag{4.10}$$

being $Q = q\left[\mathbf{0}_{1\times n_t},\ldots,1\right]^T, q \in \mathbb{R}$ a weighting matrix prioritizing the corresponding system state such as the minimization of the tracking error is achieved. Due to the cost convenience of wind power generation, this minimization has the highest priority in order to supply the TSO power demand in the best possible way.

On the other hand, it is also required the wind farm to contribute with ancillary services like primary frequency support. This feature can be achieved by releasing the power reserve into the grid when the available power is higher than the demand. Hence, maximizing the cost function

$$J_2(k) \triangleq -\|\mathbf{P}_{\text{av,tot}} - S\mathbf{x}(k)\|_1, \tag{4.11}$$

with $S = s\left[\mathbb{1}_{1\times n_t},\ldots,0\right]^T, s \in \mathbb{R}$ a weighting matrix prioritizing the sum of power generated by the turbines, i.e., the control strategy may ensure the capability of the system for increasing the power generation when needed.

As a complementary action, the cost function

$$J_3(k) \triangleq \|R\,\Delta\mathbf{P}_{\text{r}}(k)\|_1, \tag{4.12}$$

with $\Delta\mathbf{P}_{\text{r}}(k) \triangleq \mathbf{P}_{\text{r}}(k) - \mathbf{P}_{\text{r}}(k-1)$ and $R = r\left[\mathbf{I}_{n_t\times n_t}\right], r \in \mathbb{R}$ a weighting term of suitable dimensions, aims at smoothing the variation of the manipulated inputs and then avoiding undesired peaks in the output power signal.

A weighted sum of the aforementioned objectives leads to a non-convex objective function as a consequence of the opposite nature of the objective functions in (4.10) and (4.11). Hence, in order to guarantee the convexity of the problem (i.e., the termination of the optimization problem), the objectives are optimized separately in a sequential order starting from the minimization of the most important objective J_1.

Lexicographic Approach

Optimal control for a number of engineering systems deals with several objectives, e.g. safety process, economic considerations, production levels or product quality [87]. In order to guarantee the process requirements, the specific objectives are considered while stating the optimal control problem as either optimization objective or as constraints. In general, multiple objectives can be considered into a single cost function. In case the

objectives have a different priority, the most common approach is to set the cost function equal to a weighted sum of multiple objectives [108, 125], such that the highest weight is referred to the most important cost function. Typically, the weights are performed in a multiple trial-and-error manner, requiring many repetitive optimization until an acceptable solution is found [149]. However, specific tuning of the weights are necessary to adapt the controller if any change affects the system process; for example, in the case of wind farm control, some objectives are only relevant under specific circumstances (e.g., high wind conditions, high turbulence intensity, derated operations). The common approach for tuning the weights requires either to compute several points along the Pareto fronts in order to select an appropriate prioritization for the local objectives, which implies a high computational burden, [70]. Furthermore, most of the tuning techniques are static and performed off-line as part of a design procedure to find a trade-off between the many solutions that are optimal in terms of the Pareto optimality concept [15, 148]. As an alternative, the method used in this chapter considers the hierarchy among the objectives without the need of tuning the weights.

Let consider a general multi-objective optimization problem

$$\underset{\theta \in \Theta}{\text{minimize}} \quad f(\theta) = \left[f_1(\theta), f_2(\theta), \ldots, f_r(\theta)\right]^T, \tag{4.13a}$$

where $\Theta \subseteq \mathbb{R}^z$ is the admissible set of decision variables, and $f_i : \Theta \to \mathbb{R}$ with $i \in \{1, \ldots, r\}$ is the scalar-valued objective functions. A minimizer of problem (4.13) follows the Definition 4.1 below:

Definition 4.1. *A certain* θ^* *is a* Pareto optimal minimizer *and* $f(\theta^*)$ *is a* Pareto optimal minimum *of problem* (4.13) *if there does not exist a* $\theta \in \Theta$ *and an* i *such that* $f_i(\theta) \leq f_i(\theta^*)$.

Therefore, a minimizer is Pareto-optimal if and only if an objective f_i can be reduced only at the expense of increasing at least one of the other objectives. As a consequence, a minimizer and a minimum are guaranteed to exist but the solution may not be unique. However, if a priority exists between the objectives, a unique solution exists on the Pareto surface where this order is respected. Let the objective functions be arranged according to their priority from the most important to the least important,

Definition 4.2. *A certain* θ^* *is a* lexicographic minimizer *and* $f(\theta^*)$ *is a* lexicographic minima *of problem* (4.13) *if there does not exist a* $\theta \in \Theta$ *and an* i^* *such that* $f_{i^*}(\theta) \leq f_{i^*}(\theta^*)$ *and* $f_i(\theta) = f_i(\theta^*)$, $i = 1, \ldots, i^*$.

Hence, a lexicographic minima is a special type of Pareto-optimal solution and exists if and only if an objective f_i can be reduced only at the expense of increasing at least one of the higher-prioritized objectives $\{f_1, \ldots, f_{(i-1)}\}$. Therefore, the optimization problem can be stated as a set of optimization problems, such that in each problem one or more objectives are considered.

This approach is known as lexicographic programming [103]. The fundamental concept of such a strategy is to solve sequentially a set of minimization problems. After the objective functions are arranged according to their priority from the most to the least important, the slack variable associated with violating the first objective is minimized subject to the original constraints. If this problem has a unique solution, it is also the solution of the overall multi-objective problem. Otherwise, the second optimal problem is solved using the optimal value of the slack variable to impose additional constraints on the second optimization, and so on until the objectives are satisfied. At each step of the algorithm, all primary variables for higher priority objectives must be recalculated.

Hence, the way of solving (4.13) follows the procedure shown in Algorithm 3. Notice that functions f_i are arranged according to their priority from the most important f_1 up to the least important f_r.

Algorithm 3 Lexicographic multi-objective optimization

1: $f_1^* = \min_{\theta \in \Theta} f_1(\theta)$
2: **for** $l = 2$ to r **do**
3: $\quad f_l^* = \min\{f_l(\theta) | f_j(\theta) \leq f_j^* + \epsilon,\ j = 1, \ldots, l-1\}, \epsilon > 0$
4: **end for**
5: Determine the lexicographic minimizer set as:
$\theta^* \in \{\theta \in \Theta | f_j(\theta) \leq f_j^*,\ j = 1, \ldots, r\}$.

In Algorithm 3 $\epsilon > 0$ is a small tolerance used to relax the constraints in order to improve the numerical conditions. Given the structure of the problem in (4.9) and the nature of cost functions in (4.10), (4.11) and (4.12), this thesis uses the sequential solution method of lexicographic minimizers [106, 119] to solve the multi-objective optimization problem. Hence, regarding the combined problem of power reference tracking plus power reserve

maximization addressed in this chapter, the solution of (4.9) is obtained by considering a first optimization problem taking into account cost functions (4.10) and (4.12), that is, an optimization problem composed of two linear cost functions properly prioritized such as the reference tracking was more important than the smoothness of the control input (by means of Q and R in (4.10) and (4.12), respectively). This optimization problem is therefore stated as

$$\begin{aligned} \min_{\hat{\mathbf{u}}(k) \in \mathbb{U}} \quad & \sum_{i=0}^{H_p-1} J_1(k+i) + J_2(k+i) \\ \text{s.t.} \quad & (4.9b), (4.9c) \text{ and } (4.9d), \end{aligned} \tag{4.14}$$

from which an optimal sequence $\hat{\mathbf{u}}_1^\star(k) = \hat{\mathbf{u}}^\star(k)$ is obtained and used to define an extra constraint for a second optimization problem focused on the maximization of the power reserve, i.e.,

$$\begin{aligned} \max_{\hat{\mathbf{u}}(k) \in \mathbb{U}} \quad & \sum_{i=0}^{H_p-1} J_3(k+i) \\ \text{s.t.} \quad & (4.9b), (4.9c) \text{ and } (4.9d), \\ & \sum_{i=0}^{H_p-1} J_1(k+i) + J_2(k+i) \leq \hat{\mathbf{u}}_1^\star(k) + \alpha, \end{aligned} \tag{4.15}$$

where $\alpha > 0$ is a small tolerance in order to avoid numerical problems and the infeasibility of the optimization problem in (4.15). Finally, the resultant optimal sequence $\hat{\mathbf{u}}_2^\star(k)$ from the solution of (4.15) corresponds with the definitive sequence from which the first element $\hat{\mathbf{u}}_2^\star(k|k) = P_r^\star(k|k)$ will be taken and applied to the system.

4.3 Simulation Model

The proposed control strategy was evaluated in the case of a wind farm with three turbines in a row ($n_t = 3$). The simulation model used to test the MPC controller is programmed in MATLAB. The wind turbine aerodynamics and electrical properties are modeled as proposed in [85] for the NREL 5-MW baseline wind turbine. For the simulations, the wind turbines were described by a nonlinear two-mass model including also the pitch actuator and a power control as proposed in [72]. This model has been used

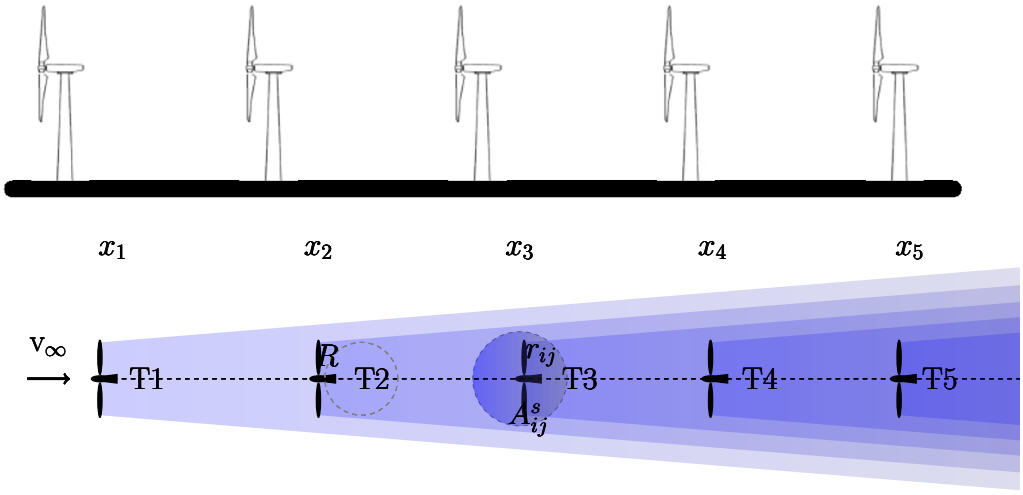

Figure 4.3: Wake expansion based on Jensen's model.

as a reference by research teams throughout the world to standardize baseline offshore wind turbine specifications and to quantify the benefits of advanced land- and sea-based wind energy technologies. The aerodynamics of the wind flowing through the wind farm along with the wake effect on the wind speed v_i are modeled by the common *Park's model* [86]. This model estimates the effect of multiple wake interactions assuming that wakes expand as a cone-like fashion with circular cross section for a given free-stream wind speed v_∞, and the wind speed profile has a top-hat shape in the crosswind direction. Under these assumptions, the wind speed faced by the i-th turbine T_i is computed as

$$v_i = v_\infty \left(1 - 2\sqrt{\sum_{j\in\mathcal{N}_i}\left(2(1-a_j)\frac{R}{r_{ij}(x_{ij})}\right)^2 \frac{A^s_{ij}(x_{ij})}{A_{0,i}}}\right), \tag{4.16}$$

where x_{ij} is the distance in the x-direction between turbines T_j and T_i, $r_{ij}(x_{ij}) = R + z_0\, x_{ij}$ is the radius of the wake generated by turbine T_j, z_0 the roughness coefficient and $\mathcal{N}_i$ is the set of indexes corresponding to the turbines upstream of T_i. The symbols $A_{0,i}$ and $A^s_{ij}(x_{ij})$ denote the rotor area and the shadowed area due to the upstream turbine, respectively (see Figure 4.3). If the wind turbines have the same radius R, then the shadowed area can be computed as

$$A^s_{ij}(x_{ij}) = r_{ij}(x_{ij})^2 \cos^{-1}\left(\frac{L_{ij}}{r_{ij}(x_{ij})}\right) + R\cos^{-1}\left(\frac{d_{ij}-L_{ij}}{r_{ij}(x_{ij})}\right) + d_{ij}z_{ij}, \tag{4.17}$$

with L_{ij} the distance between the centres of the wake area A_{ij}^x and the shadowed area A_{ij}^s, d_{ij} the distance between the centres of the wake area A_{ij}^x and the rotor area $A_{0,i}$, and z_{ij} the vertical distance between the intersection points of the previously mentioned areas (see Figure 4.3).

The wake impact on the wind speed faced by downstream turbines depends on the free-stream wind speed direction ϕ (defined as the angle between v_∞ and the farm layout and the turbine geographical disposition within the farm [18]. Hence, the wake effect faced by some turbines can be either partial or total. As stated before, the effect over downstream turbines also depends on the operational conditions of upstream turbines, which are taken into account with the induction factor a_i in (4.16). Therefore, the degree of coupling due to the wake effects between turbine T_i and T_j is basically a function of the wind speed direction, the shadowed areas, the induction factors, and the distance among the turbines. The latter affects the wake propagation delay, i.e., the time for the wake to travel through the rows of wind turbines in the farm, computed as the ratio between the turbine separation distance and the wake convection velocity [31].

4.4 Case Study

The turbines were considered aligned with the free-stream wind speed direction and the distance between turbines was 630 m (five rotor diameters). The freestream wind speed is assumed to be equal to 11 m/s with a constant main direction $\phi = 0^\circ$.

The MPC strategy was implemented with a sampling time $T_s = 0.08$ s and a prediction horizon $H_p = 10$, which have been set to be relatively small since the turbines are required to regulate power on milliseconds scale. The time constant η in the simplified model (4.4) was set at 0.15 s. The parameters of the weighting matrixes in the cost functions (4.10), (4.11) were set as $q = 5$, $r = 1$ and $s = 1$. Simulations have been run using YALMIP [94] and CPLEX under MATLAB in a PC with an Intel i7 processor and 8 Gb RAM. In order to evaluate how the controller coordinates the power contribution of each turbine, two scenarios were considered. The first scenario analyzes changes in the power demand set-point. The second evaluates the system response under a change of the free-stream wind speed. In both cases, the free-stream wind speed was set in order to

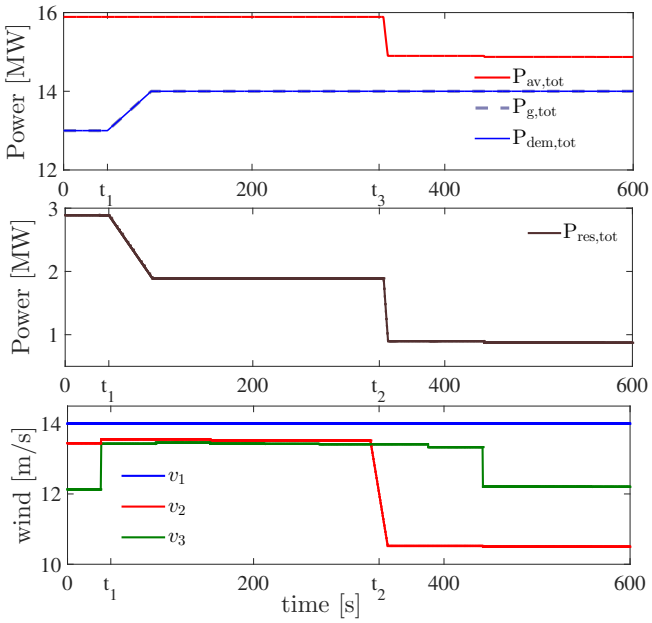

Figure 4.4: System response for scenario 1. Top plot: generated, available and demanded total power. Middle plot: total power reserve. Bottom plot: wind speed faced by each turbine.

ensure that the available power was higher than the one demanded by the TSO. Finally the last case study presents the system response when for five turbines in a row.

4.4.1 Scenario 1: Constant Power Demand Set-Point and Wind Speed

This scenario analyzes the system behavior when the power set-point P_{dem} increases from 13 to 14 MW (at $t_1 = 100$ s) and the wind speed v_2 falls to 10.5 m/s (at $t_2 = 360$ s). The initial free-stream wind speed was 12 m/s. The system response with the proposed control strategy is shown Figure 4.4. In the top plot, it can be observed the power demand set-point P_{dem} (blue line), the total generated power $P_{\text{g,tot}}$ (dashed line) and the total available power $P_{\text{av,tot}}$ (red line). The middle plot shows the total power reserve and the bottom plot the wind speeds v_1, v_2 and v_3 faced by each wind turbine, respectively. The generated and available powers for each wind turbine is displayed in Figure 4.5, with solid and dashed lines, respectively.

As shown in the top plot Figure 4.4, the control is able to achieve a proper tracking in spite of the disturbances, delivering to the grid the power demanded by the TSO. This

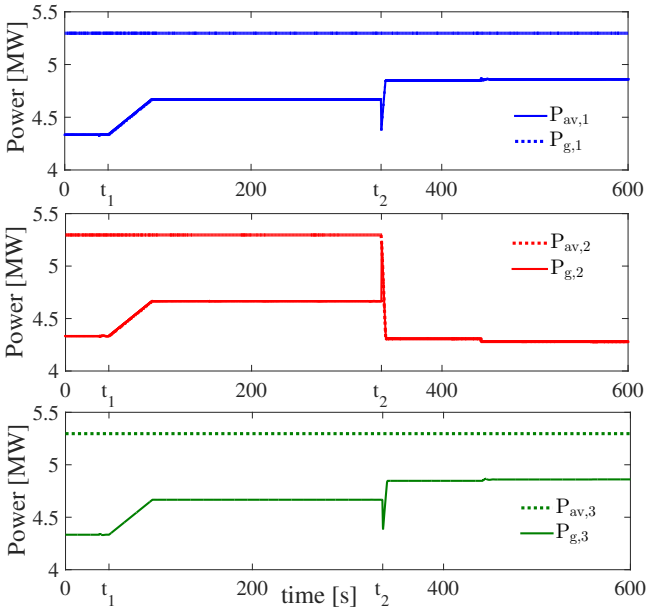

Figure 4.5: System response for scenario 1. Available and generated powers for each turbine.

tracking is achieved by increasing the power contribution of each turbine, which reduces the total power reserve and slightly affects the wind speed faced by Turbines 2 and 3 due to the wake effects. The subsequent reduction of the wind speed v_2 for $t < t_2$ causes a significant decrease in the available power in Turbine 2. After t_2, Turbine 2 is forced to work at maximum generation. As a consequence, the controller re-distributes the power contribution of the remaining turbines increasing $P_{\text{g},1}$ and $P_{\text{g},3}$. Nevertheless, the total power demanded at the PCC is still satisfied. In the bottom plot of Figure 4.4, it can be seen that v_3 decreases once the wake disturbance caused by the increase $P_{\text{g},1}$ finally arrived at Turbine 3. However, this does not affect $P_{\text{av},3}$ because the wind speed v_3 is still sufficient to operate at Region 2.

4.4.2 Scenario 2: Change in Free-stream Wind Speed and in v_2

The second scenario considers a change in the free-stream wind speed $v_\infty = v_1$ from 14 to 13 m/s at $t_3 = 150$ s followed by an additional reduction in v_2 at $t = 360$ s. These changes can be observed in the bottom plot of Figure 4.6. It can be also seen in top plot of Figure 4.6 that the control is able to manage this situation keeping the total power

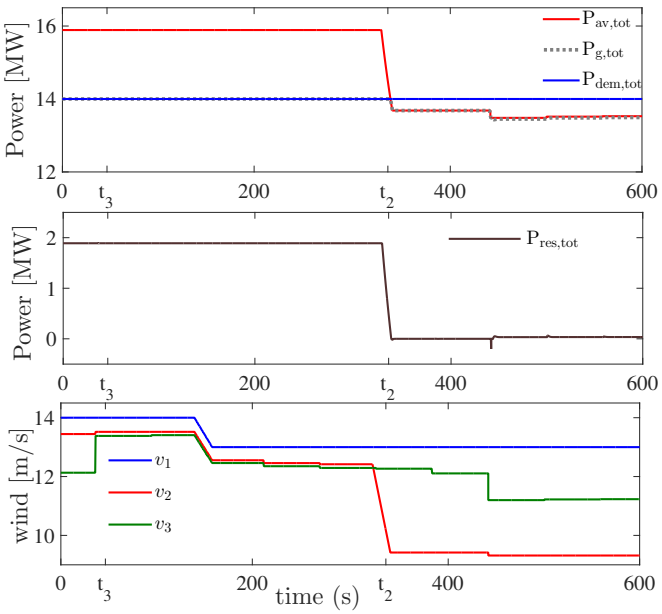

Figure 4.6: System response for scenario 1. Top plot: generated, available and demanded total power. Middle plot: total power reserve. Bottom plot: wind speed faced by each turbine.

delivered to the grid, but a significant reduction in the available power, and consequently in the reserve, occurs after $t = t_2$.

Figure 4.7 shows the generated and available powers corresponding to each turbine. The first change in the free-stream wind speed does not have a significant effect on generated and available powers as the wind speeds faced by each turbines ensure the operation in Region 2. On the other hand, the subsequent reduction of v_2 forces Turbine 2 to enter in Region 1 and delivered all its available power ($P_{\mathrm{g},2} = P_{\mathrm{av},2}$). The lower contribution from Turbine 2 must be compensated with increments in the power supplied for the remaining turbines. In Figure 4.7, it can be observed that once the increase in $P_{\mathrm{g},1}$ starts to affect the wind speed v_3, $P_{g,3}$ also reaches the available power $P_{\mathrm{av},3}$.

4.4.3 Scenario 3: Five Wind Turbines in a Row

This scenario is devoted to show how the proposed controller distributes the power among the turbines for different values of power demand. The number of turbines is increased to five and the turbines are considered totally waked as shown in Figure 4.3.

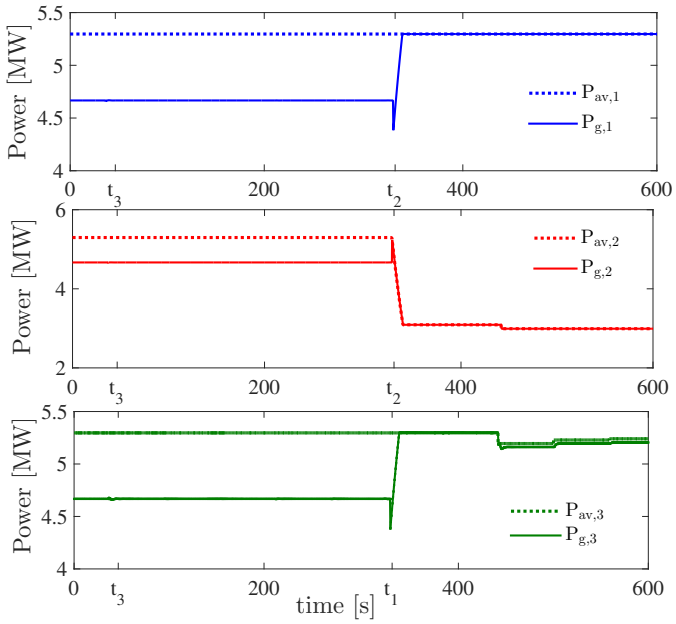

Figure 4.7: System response for scenario 1. Available and generated powers for each turbine.

In order to evaluate the effect of considering the maximization of power reserve, until time $t = 200$ s only the minimization of the tracking error is considered in the general cost function of problem (4.9a), then for $t > 200$ s the power distribution is optimized to maximize the power reserve. Top plot of Figure 4.8 shows the tracking response for different values of the power demand $P_{\text{dem}} = (65\%, 75\%, 85\%, 95\%)P_{\text{greedy}}$, P_{greedy} is the maximum power that can be delivered in steady-state condition if all the turbines operate at MPPT. It can be seen that the power demand is ensured for all the cases. Nevertheless, such a result is a consequence of using the lexicographic technique that ensures the priority of the tracking with respect the maximization of power reserve, hence the effect of including the latter cost function in the optimization problem has not effect on the tracking performance. Figure 4.9 left plot shows the power response at wind farm and wind turbine level when the power demand is $P_{\text{dem}} = 85\%P_{\text{greedy}}$. With the increasing of the number of turbines, in order to maximize the power reserve the controller sets the power reference among the turbines such as a backward distribution, see Figure 4.9 right plot. Initially, for $t < 170$ s, the usptream turbines T_1, T_2 and T_3 produce the maximum power while the turbines T_4 and T_5 are deloaded respectively to $P_{\text{g},4} = 0.76$ MW and $P_{\text{g},5} = 0.5$ MW. However, for maximizing the power reserve the

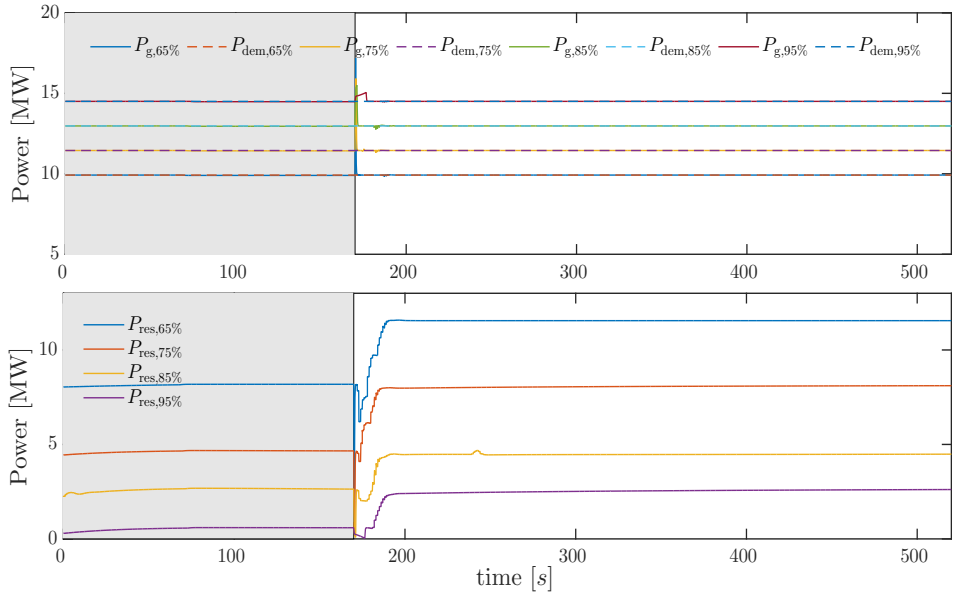

Figure 4.8: Power response for different deloading operations. Top plot: power generated total. Bottom plot: power reserve total.

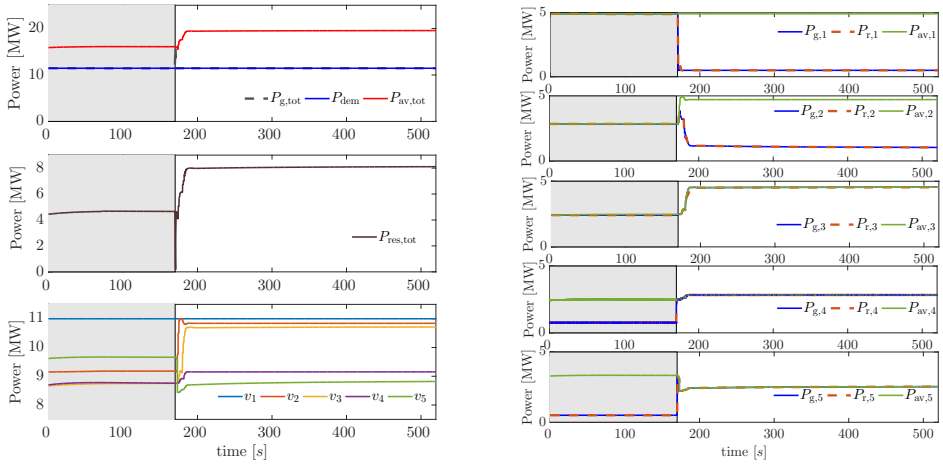

Figure 4.9: Left plot: Power response ate the wind farm level and wind speed faced by the turbines. Right plot: Power response at the wind turbine level.

controller changes the power set-points to require the maximum power at the turbines T_5, T_4, T_3 by deloading the first to $P_{g,1} = 0.5$ MW and the second to $P_{g,2} = 1$ MW. This affects the wind speeds faced by the turbines, as shown in the bottom plot of Figure 4.9. Especially, while at the beginning the wind speed faced by the last turbine is higher than the wind investigated by the turbine T_4 for the effect of the its lower generation, then the wind speed faced by the last turbine decreases of more than 1 m/s as a consequence of the higher generation of T_4. Meanwhile, the wind speeds crossing all the other upstream turbines increase, thus increasing the available power for these turbines.

4.5 PALM Simulation Results

In order to test the effectiveness of the proposed control strategy under more realistic wind flow conditions, this section shows the results obtained when the proposed MPC-based controller is evaluated with LES. For this end, the open-source PArallelized Large-eddy simulation Model (PALM) is used [99], it is a meteorological model for atmospheric and oceanic boundary-layer flows available in the public domain [75]; a more detailed presentation of PALM simulator is given in Appendix A. The wind turbine model used in PALM is based on the actuator disk model as presented in Section 2.1.1, as a consequence the control signal for the turbine is the disk-based thrust coefficient C'_T as presented in [105],[25]. Hence, the power generation dynamics of a wind turbine can be estimated by the first-order filtered response of C'_T, that is

$$\frac{\mathrm{d}C'_T}{\mathrm{dt}} = \frac{(C'_T - C'_{T,\mathrm{r}})}{\eta}, \tag{4.18}$$

being $C'_{T,\mathrm{r}}$ the reference value sent by the MPC controller and η the time constant of the first-order system. Hence, the power generated by the *i-th* turbine is computed as,

$$P_{\mathrm{r},i} = \frac{\pi R^2}{2} \left(v_i \cos[\gamma_i]\right)^3 C'_{T,i}, \tag{4.19}$$

where the yaw angle γ_i, that is the second parameter that can be controlled in PALM, is set equal to zero being yaw control out of the scope of this thesis. For the interested reader, in Appendix B it is presented an optimal control problem considering optimal yaw setting and loads minimization.

Table 4.1: PALM Simulation set-up

grid dimensions	$L_x \times L_y \times L_z$	$15.3 \times 3.8 \times 1.3$	[km^3]
grid spacing	$\Delta_x \times \Delta_y \times \Delta_z$	$15 \times 15 \times 10$	[m^3]
sample time	Δt	1	[s]
diameter, hub height	D, z_h	$120, 90$	[m]
turbine spacing	s_x, s_y	$5D \times 3D$	[m]
freestream wind	v_∞	8	[m/s]
turbulence intensity	TI_∞	6	%
prediction horizon	H_p	10	[s]
time constant	η	5	[s]
simulation lenght	T	800	[s]

Therefore, since the power is regulated indirectly by controlling the C'_T the state vector and the vector of control input in (4.8) should be replaced by

$$\hat{\mathbf{u}}(k) \triangleq \{\mathbf{C}'_{T,\mathrm{r}}(k|k), \ldots, \mathbf{C}'_{T,\mathrm{r}}(k+H_p-1|k)\} \in \mathbb{R}^{n_u} \qquad (n_u = n_t), \tag{4.20a}$$

$$\hat{\mathbf{x}}(k) \triangleq \{\mathbf{x}(k+1|k), \ldots, \mathbf{x}(k+H_p|k)\} \in \mathbb{R}^{n_x} \qquad (n_x = 2n_t + 1), \tag{4.20b}$$

$$\text{being, } \hat{\mathbf{x}} = \left[\mathbf{P}_\mathrm{g}, \mathbf{C}'_\mathbf{T}, \xi\right], \tag{4.20c}$$

$$\hat{\mathbf{d}}(k) \triangleq \{P_\mathrm{dem}(k|k), \ldots, P_\mathrm{dem}(k+H_p-1|k)\} \in \mathbb{R}. \tag{4.20d}$$

Therefore, the matrices of the state-space system in (4.4) become

$$\mathbf{A} = \begin{bmatrix} \mathbf{0}_{n_t \times n_t} & \pi \frac{R^2}{2} v_i^3 \mathbf{I}_{n_t \times n_t} & 0 \\ \mathbf{0}_{n_t \times n_t} & -\frac{1}{\eta}\mathbf{I}_{n_t \times n_t} & 0 \\ -\mathbf{1}_{1 \times n_t} & \mathbf{0}_{1 \times n_t} & 0 \end{bmatrix}, \ \mathbf{B_u} = \begin{bmatrix} \mathbf{0}_{n_t \times n_t} \\ \frac{1}{\eta}\mathbf{I}_{n_t \times n_t} \\ \mathbf{0}_{1 \times n_t} \end{bmatrix}, \ \mathbf{B_d} = \begin{bmatrix} \mathbf{0}_{2n_t \times 1} \\ 1 \end{bmatrix}.$$

It follows that also the weighting terms for the single objective functions in (4.9) should be replaced as $Q = q\left[\mathbf{0}_{1\times 2n_t}, \ldots, 1\right]^T, q \in \mathbb{R}$, $S = s\left[\mathbb{1}_{1\times n_t}, \ldots, \mathbf{0}_{1\times n_t+1}\right]^T, s \in \mathbb{R}$ and $R = r\mathbf{I}_{n_t \times n_t}$, $r \in \mathbb{R}$.

The PALM simulation results are obtained for a neutral boundary layer for the wind farm with 6 wind turbines as shown in Figure 4.10. In Table 4.1 the summary of the simulation set-up and turbine parameters are listed,

In order to test the performance of the proposed control strategy under more realistic scenarios the power demanded by the grid is defined as a profile changing during the simulation time, it is formulated as

$$P_\mathrm{dem}(t) = pP_\mathrm{greedy} + 0.2P_\mathrm{greedy}\delta P(t), \tag{4.21}$$

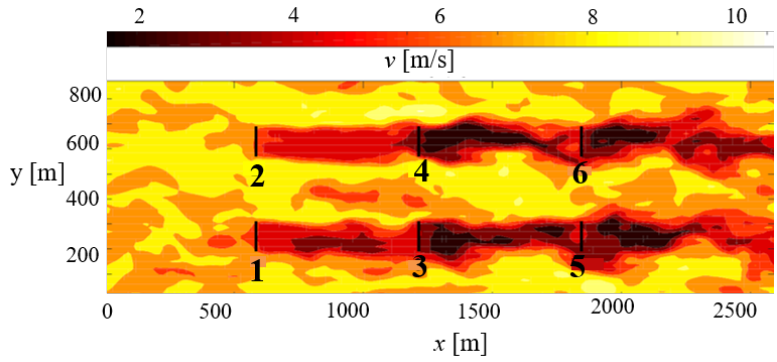

Figure 4.10: Wind field longitudinal direction flowing through a wind farm with 6 wind turbines placed in a matrix of 2. Figure adapted from [25]

.

being $p \in \mathbb{Z}_{\geq 0}$ a fraction of P_{greedy}, $\delta P(t)$ a normalized "RegD" type automatic generation control (AGC) signal [123] given by the TSO and $P_{\text{greedy}} = 7.5$ MW, therefore it is guaranteed that the wind farm operates in deloading operation during the simulation period. Figure 4.11 and Figure 4.12 show the power tracking response in the case of low and high power demand profiles, respectively obtained for $p = 0.7$ and $p = 0.9$ in (4.21). Furthermore, in order to evaluate the influence of considering power reserve maximization two different cases are shown: Baseline case (referred as *case 1*), when the optimal control problem is formulated only to minimize the tracking error, i.e., in (4.9a) $J(k) = J_1(k) + J_3(k)$. Meanwhile, for the second case (referred as *case 2*), the maximization of power reserve is included in the optimization problem formulation, hence $J_m(k) = \sum_{l=1}^{3} J_l(k)$. It can be observed that the power tracking is ensured for both the cases. However, in the circumstance of high power demand around $t = 450$-500 s the tracking decays for the *case*1. In fact, the available power within this period decreases going below power demand, thus the controller cannot guarantee a good tracking. Nevertheless, if the maximization of power reserve is considered by the MPC controller then the decay of the tracking can be recovered for an increasing of the overall power available. In order to estimate how good is the tracking achieved with the proposed control strategy, it can be considered as performance parameter the root-mean-square (RMS) of the tracking error computed as,

$$e = \sqrt{\frac{\sum_{t=1}^{T} (P_{\text{dem}}(t) - P_{\text{g,tot}}(t))^2}{T}}. \tag{4.22}$$

Notice that, only ideally the wind farm could provide a zero mean tracking error. However, it is clear that a low RMS would result in increased payments for the AGC services and improved grid reliability. In order to understand if the proposed MPC control strategy ensures good power tracking performance, the obtained results can be compared with the ones presented in [158], where a PI-based feedback control strategy is proposed for the same scope of minimizing the tracking error when following the power profile in (4.21). Here, two RMS errors were found for two different scenarios. The best scenario corresponding to an upward power distribution among the turbines, i.e., the first row of turbines produced more power than the downstream turbines. Meanwhile, the worst scenario resulted when the same amount of power was required at each turbine. In both the cases, the performance resulted good and able to guarantee the CAISO coefficient above 0.5. The latter is the California Independent System Operator performance score, which rates power tracking between 0 and 1, as described in [5] and it is used in the US power markets to partially determine the payments for providing total power of the wind farm with and without the AGC services. CAISO scores above 0.5 must be guaranteed by the wind farm owner to be qualified in providing ancillary services [28]. A summary of the comparison between the results obtained using the presented MPC control strategy and the PI-based strategy proposed in [158] is given in Table 4.2. In order to

Table 4.2: Performance results compared with the PI-based feedback control strategy presented in [158].

	MPC-Controller				PI-Controller	
	Low Demand		High Demand			
Case:	1	2	1	2	Upward	Equal
Error [W]	98330	99070	108200	108250	91554	107000
CAISO	0.938	0.938	0.927	0.927	0.94	0.93

Table 4.3: Variation in power reserve for each turbine; values given as percentage of the power reserve with respect *case*1.

	T1	T2	T3	T4	T5	T6	Total
ΔP_{res} [%]	20	14	24	-20	-6	-16	3.4

In Figure 4.13 is illustrated how the controller regulates the power among the turbines. Here, due to the variable and turbulence nature of the incoming wind speed, it can

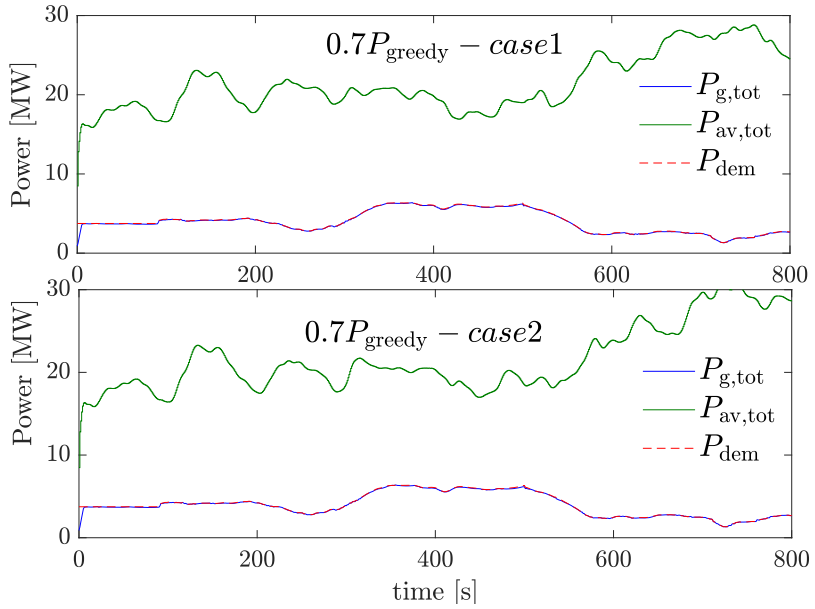

Figure 4.11: Total power response of the wind farm without ($case1$) and with ($case2$) power reserve maximization for low power demand.

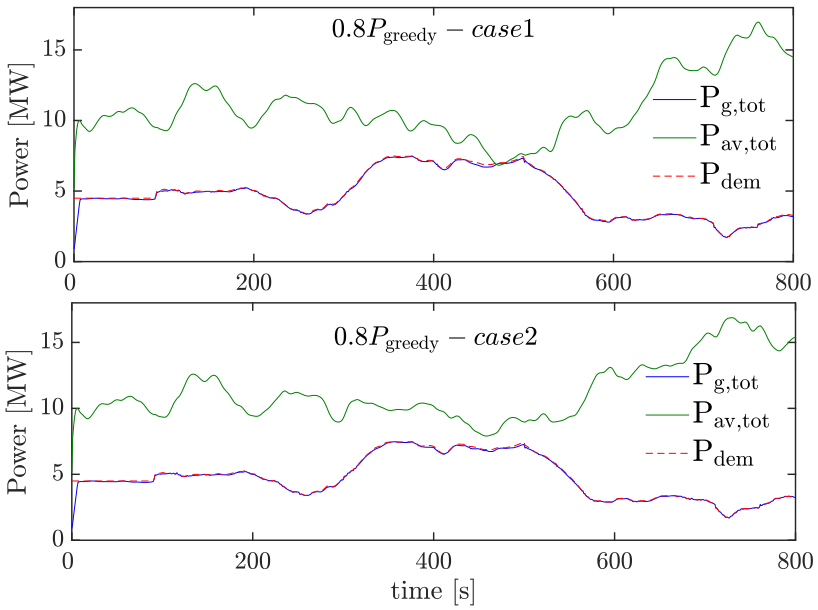

Figure 4.12: Total power response of the wind farm for high power demand without ($case1$) and with ($case2$) power reserve maximization for low power demand.

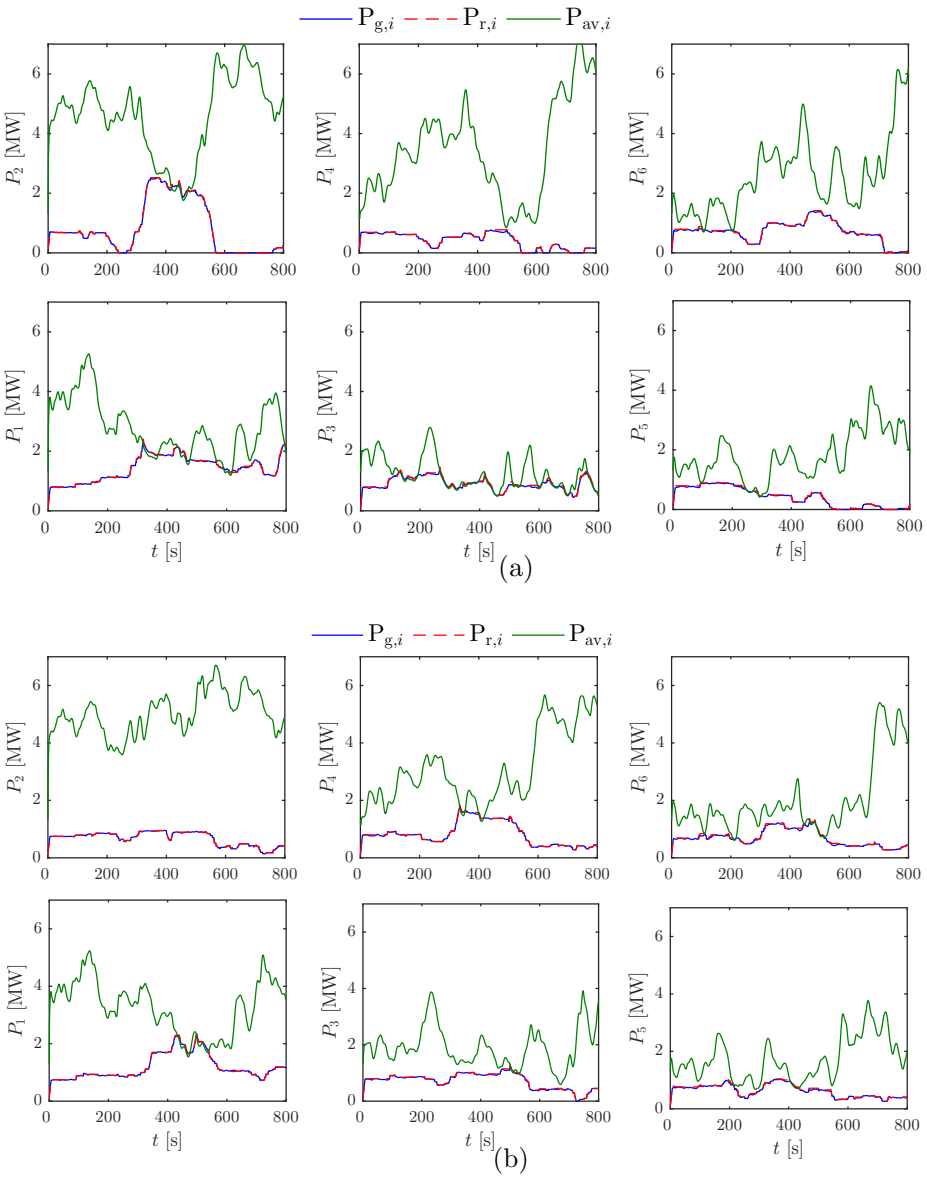

Figure 4.13: Power response of the wind turbines. Top plot: *case*1. Bottom plot: *case*2.

.

be seen that the available powers (green line) and so the power references (red dashed line) for the turbine change a lot during the simulation time. Moreover, the available power for each turbine is not only affected by the generation conditions of the upstream turbines, but also by its own generation. In fact, with LES, the effect of the convection vortexes at the rotor area generated by the rotating mass are considered, which have an additional negative impact on the measured wind speed at the rotor disk. For the $case1$, top plot, the upstream turbines produce globally more than the turbines downstream, affecting the available power of the downstream turbines for the wake generation and its own available power for the high rotor speed. Meanwhile, for $case2$ illustrated in bottom plot, with the aim of maximizing the available power, the controller seeks to regulate the power reference among the turbines by deloading more the upstream turbines. This causes an improvement in power available for the second and third rows of turbines and reduces the negative impact of the high generation in its own power available. In order to show the benefits of the proposed control strategy in terms of power reserve, Table 4.3 lists the values of the difference in power reserve between $case2$ and $case1$ given as percentage of the power reserve in $case1$ for each turbine and for the overall wind farm.

System response after wind turbine failure

Finally, the MPC control strategy is tested for the case of an unexpected event, represented as a shut-down of the third turbine $T3$. Until time $t = 99$ s, all the turbines produce power to contribute to the power tracking task, then the third turbine is shut-down generating a dip in the power reference profile, see Figure 4.14. However, it can be seen that the central controller is able to cope with this unexpected event by improving the control set-points for the remaining turbines, see Figure 4.15, and so restoring the proper tracking of P_{dem}.

Computational Effort

With the aim of regulating the power demanded by the grid the wind farm central controller needs to be fast enough to solve the optimal control problem. In this study the controller ensures an on-line optimal power dispatch by solving the problem in (4.9) every second, which is in line with the time variation of the power demand profile.

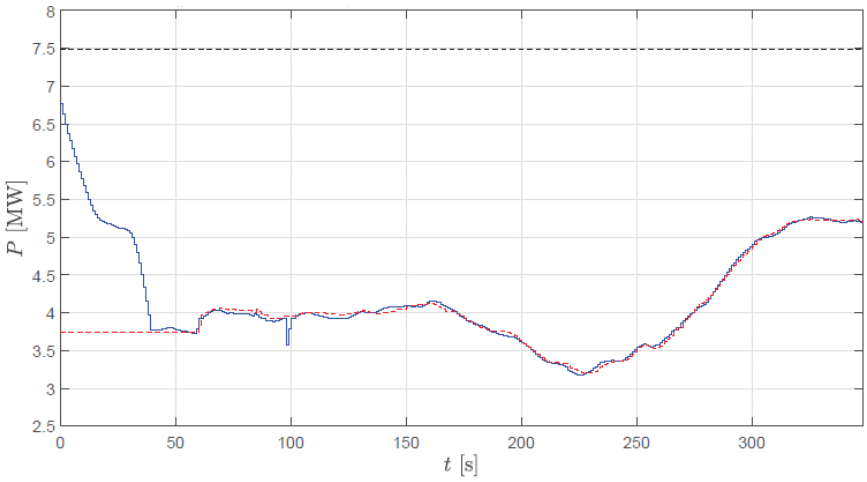

Figure 4.14: Power response of the wind farm for an unexpected event.

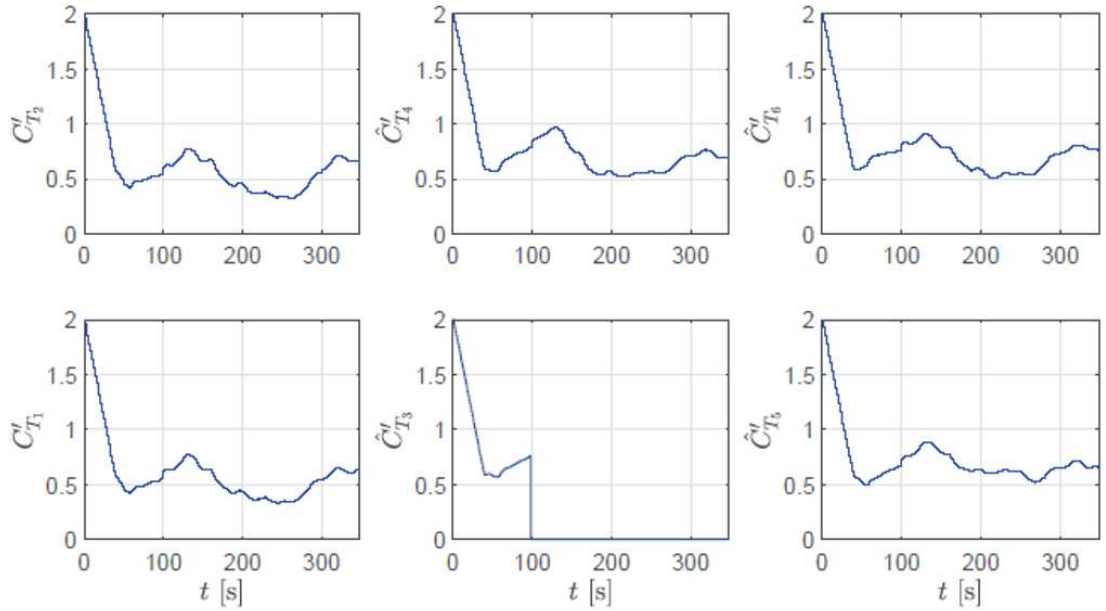

Figure 4.15: Control action C'_T profiles for each wind turbines in the case of an unexpected event.

However, the mean computation time is function of several factors, as: complexity of the system model used to predict the wind turbine power response, and number of states and control actions to be controlled. The latter increases proportionally to the number of turbines within the farm, making the system to control larger. Hence, the number of turbines represents a limit on the performance of the centralized control approaches proposed so far. A sensitivity analysis of the proposed control strategy with respect to the wind turbine number is given in Table 4.4, it can be concluded that up to 36 turbines the controller is able to ensure an online optimal control but already for 49 turbines the mean time is about 1.5 s. It could be interesting to investigate if the controller can still provide an online control by formulating the overall control problem as a bilevel problem, as presented in [146, 147]. In this circumstance, the tracking objective can be solved every second while the power set-points are updated according to the optimal solution found by a slow level control. This is however not further investigated in this dissertation.

Table 4.4: Effect of the number of turbines on the mean computation time per controller time step Δt_{CPU}.

n_t	3	9	15	20	25	36	42	49	64
Δt_{CPU}[s]	0.049	0.091	0.16	0.22	0.38	0.77	0.9	1.5	2.9

4.6 Summary

This chapter has proposed an MPC strategy for the regulation of the power generated by a wind farm. Currently, wind farms must contribute to the grid support as other conventional power sources. To this end, wind farms must keep some power reserve that allows them to increase the power generation and thus help, for instance, the primary frequency control. Unlike conventional power sources, to keep a certain power reserve in a wind farms requires the coordination of many small generators (turbines) that are exposed to different conditions (wind and generated power) coupled each others due to the wake effects. Here, we have proposed a multi-objective MPC scheme aimed to regulate the total power generated and coordinate the contribution of each turbine to maximize the power reserve. The control seeks to exploit the degree-of-freedom in the

distribution of the power contribution of each turbine to obtain the total demanded power and maximize the total power reserve. Firstly, this strategy has been evaluated in a simple array of three and five wind turbines showing promising results. Thus, in order to validate the proposed approach a layout of 3 by 2 wind turbines has been tested with the LES simulator, PALM. As future work, motivated by the fact that usually within a wind farm there are tens of turbines, it is proposed to test the MPC strategy for more complex wind farm layout.

Chapter 5

A multi-objective predictive wind farm controller for enhancing primary frequency support

In this chapter, it is proposed a model predictive control strategy stated to solve a multi-objective optimization problem to: 1) provide automatic generation control by following a certain power demand profile, 2) minimize the power losses within a wind farm, considering the wake interactions and the electrical cable interconnections within the farm. Part of the contributions proposed in this chapter have been presented in [142]. Furthermore, for completeness of the investigation, additional results are presented in this chapter in order to assess the improvements achieved with the proposed control strategy on frequency regulation by simulating a frequency droop in the interconnected system network. Moreover, different wind turbine regulations obtained by properly setting the weights of the multi-objective cost function are compared to evaluate the improvements in terms of power reserve.

Up to this point, only the power losses due to the wake effect have been considered when optimizing the wind farm operation. Even though the latter mainly affect the wind farm power production, for large-scale wind farms also the electrical losses within the cable connections are responsible for a significant part of the reduction of the wind farm annual energy production. Nevertheless, yearly electrical losses around 2%–3% of the energy generated occur in on-shore and even more in off-shore wind farms [32]. Furthermore, the design of ever-growing wind turbine rated power requires larger cable

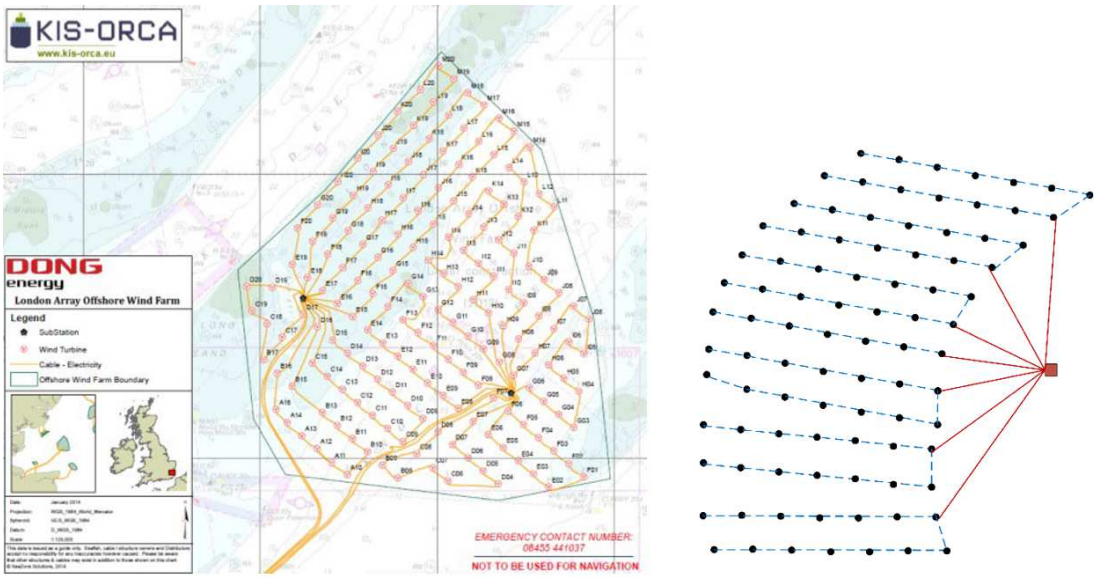

(a) (b)

Figure 5.1: Figure (a): London Array wind farm of 630 MW of power capacity made up of 175 wind turbines and two offshore substations [Figure adapted from [47]]. Figure (b): Horns Rev-2 wind farm with a capacity of 210 MW produced by 91 wind turbines located in the North Sea [figure adapted from [133]].

capacities, i.e., greater cable dimensions with higher costs, which makes even more important to consider the losses within the cables when maximizing the wind farm annual energy production. As first step for reducing the electrical losses, the cable connections should be properly designed considering also an installation cost perspective. In fact, the electrical infrastructures account for 15%-30% of the overall installation costs of an offshore wind farm [69]. Therefore, it is quite important when designing a wind farm: 1) to consider the site specifications, e.g., considering the existing electrical grid [126]; 2) to optimize the location of each turbine and the cable connections among turbines [49]. As an example, Figure 5.1 shows the electrical connections for two existing offshore wind farms, the left one presents a new concept of wind farm topology while the right one is a more common topology where a parallel cable connection is used. For this reason, the proposal of optimum electrical topologies able to minimize both electrical and aerodynamics losses continue to be an open issue for wind farm industry [157].

To the best of author knowledge, despite the high number of works concerning optimal active power dispatch presented in Section 2.2, in the current literature there exists a

gap related to the optimization of wind farm power generation when considering electrical cable losses. Perhaps, the main reason of this is that the electrical cable loss is a nonlinear function of the current flowing in the cable. Typically, complex models considering also the geographical properties (e.g., soil), converter (rectifier and inverter) and temperature correction factors are used to estimate the losses [120], hence such highly non-linear models are difficult to handle with real-time controllers. Therefore, to facilitate the integration of electrical losses computation within the optimization control strategies, a simplified estimation should be considered. In [173], the power loss in the collection cables is modeled as a first-order system by linearizing the voltage-current non-liner functions with sensitivity coefficients properly calculated through an updated Jacobian matrix. Moreover, simplified analytical models of cable losses are used in [133] to provide aggregated impedance and susceptance of wind farm collection system, thereby incorporating losses in the collection system in the wind farm reactive power capability calculation.

Given the existing gap in the literature, this chapter is devoted to present a wind farm control strategy to provide active power control while minimizing the wake effect as well as the power losses in the inter-arrays connecting the wind turbines within the wind farm collection grid. A constrained multi-objective optimization-based problem is solved by a predictive central controller, to facilitate the estimation of cable-losses within reasonable computational cost and without external simulation software several assumptions are made. Nevertheless, this rough approach allows to consider the effect of power losses for regulating the power set-points among the turbines. Finally, the proposed control strategy is also used to assess a comparative analysis among three possible approaches to distribute the power among the turbines such that the power reserve is improved. Furthermore, the benefit of providing such an improvement is shown by investigating the effect of wind energy generation on the frequency response of an electrical grid after a frequency droop.

5.1 Cable Losses Model

Losses in power cables occur due to heat dissipated from the interior of the cables towards the surroundings when the cables are energised and under load. Cable losses

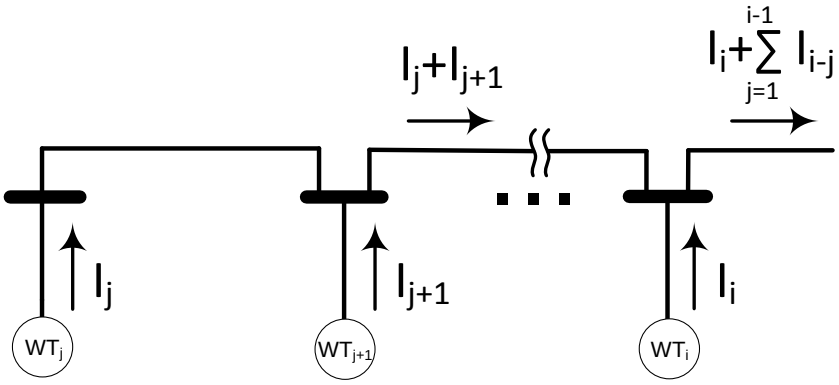

Figure 5.2: Electrical configuration of i turbines connected at the same feeder.

can be divided into conductor or ohmic losses due to the inner resistance of the cable, dielectric losses due to the charging current flowing through the capacitance created inside the isolation, and sheath and armour losses resulting from induced circulating currents within the conductor. For the sake of simplicity, this approach will only consider the ohmic losses, which are the main cause of losses in cables [48], specially in inter-array cables where the lengths of the cables inter-connecting wind turbines within the collection grid are relatively short.

Ohmic or resistive losses in a cable i of length L_i can be calculated as

$$P_i^{\text{loss}} = R_i I_i^2, \quad \text{with} \qquad R_i = r_i L_i, \tag{5.1}$$

where R_i, r_i are respectively the cable resistance and the resistance per unit of cable length and I_i is the current that flows through the cable.

For this study, it is assumed that reactive power flowing among wind turbines is small (i.e., the power factor is close to one) and the voltage magnitudes in each bus within the collection grid are quite close to the nominal value, so that voltage drops are negligible [7]. Thus, the current flowing for each inter-array cable i can be estimated as

$$I_i = \frac{P_i}{V_{\text{n}}}, \tag{5.2}$$

where $P_{\text{g},i}$ is the active power flowing through the cable i and V_n the voltage nominal value.

Assuming a radial electrical configuration within the wind farm (see Figure 5.2), and replacing expression (5.2) in (5.1), the power losses in a certain cable i belongs to a

feeder f connecting several turbines is

$$P_{f,i}^{\text{loss}} = \frac{R_{f,i}}{V_{\text{n}}^2}(P_{\text{g},i} + \sum_{j=1}^{i-1} P_{\text{g},j})^2, \qquad \forall i \geqslant 2, \tag{5.3}$$

where $P_{\text{g},i}$ is the power generated by turbine i connected to the cable i and $P_{\text{g},j}$ refers to the power generated by the turbine j located before the turbine i and connected at the same feeder f. Hence, the total power losses in a wind farm of n_t turbines with l feeders and N turbines for each feeder is denoted by

$$P_{\text{tot}}^{\text{loss}} = \frac{1}{V_{\text{n}}^2}\mathbf{R}\,(\mathbf{K}\,\mathbf{P_g^2}), \tag{5.4}$$

where

$$\mathbf{R} = \begin{bmatrix} R_{1,1} & \cdots & R_{1,N} \\ \vdots & \ddots & \vdots \\ R_{l,1} & \cdots & R_{l,N} \end{bmatrix} \in \mathbb{R}^{l\times N}, \qquad \mathbf{P}_g = [P_{g,1}, \ldots, P_{g,n_t}]^T \in \mathbb{R}^{n_t} \tag{5.5}$$

$$\mathbf{K} = diag[K_1, \ldots, K_l] \in \mathbb{R}^{(l\times N)\times n_t} \qquad K_i = \begin{bmatrix} 1 & & \\ \vdots & \ddots & \\ 1 & \cdots & 1 \end{bmatrix}. \tag{5.6}$$

Here, $\mathbf{R}$ denotes the resistance matrix, $\mathbf{P}_{\text{g}}$ the vector of generated powers, and $\mathbf{K}$ a block diagonal matrix, for which each element is equal to the matrix K_i.

5.2 Control Strategy

The wind farm controller acts as a single centralized unit, which has as inputs the power demanded by the TSO P_{dem}, the power generated $P_{\text{g},i}$, the power loss P_i^{loss} and available $P_{\text{av},i}$ from the wind turbines and inter-array connections, while as outputs the optimal power references for each turbine namely $P_{\text{r},i}^*$. The latter are sought by solving a multi-objective optimization problem stated to regulate the total power delivered by the wind farm at the PCC, such that the following objectives are minimized:

O1) *Tracking error*: minimize the difference between power demand required by the TSO and total mechanical power generated by the wind turbines. This objective

can be denoted as

$$J_1 = P_{\text{dem}} - \sum_{i=1}^{n_t} P_{\text{g},i}. \tag{5.7}$$

O2) *Peaks on power generation*: minimize the variation over the control inputs to avoid peaks in the power output, i.e., power generated, avoiding possible damage due to quick variations on the mechanical loads affecting the turbines. This objective is defined as

$$J_2 = \Delta \mathbf{P}_{\text{r}}. \tag{5.8}$$

O3) *Wake effect*: minimize the wind deficits, i.e., maximize the power available. In the previous chapters, it has been shown that properly optimizing the sequence of the power reference $\mathbf{P}_{\text{r}}$ has a direct impact on the wind speed faced by the downstream turbines, as there is a one-to-one relation between a_i and $P_{\text{r},i}$ as shown in Figure 3.1. Furthermore, with the aim of maximizing the power reserve it was shown that the backward power distribution was able to reduce the wind speed deficits, and so to improve the overall power available. Therefore, this third objective can be ensured by regulating the power generation to contribute more to the total power generated with the most downstream turbines. There are several proposals to do this, see for example Algorithm 2. Here, a simple weighted sum is used in order to simplify the entire optimization problem. The weights are selected according to the wind farm layout and predominant wind speed directions. That is,

$$J_3 = \sum_{i=1}^{n_t} \omega_i P_{\text{g},i}. \tag{5.9}$$

Assuming the set of turbine indices to be $\aleph = \{i : 1 \leq i \leq n_t \text{ with } v_i \geq v_j, \text{ for } i < j\}$, then the weights $\omega_i \in [0, 1]$ must satisfy $\omega_1 \geq \omega_2 \geq \cdots \geq \omega_{n_t}$. Notice that the set $\aleph$ is sorted to the dominant free-stream wind speed direction, such that $i = 1$ indicates the turbine facing the free-stream wind speed while $i = n_t$ is the turbine most affected by the wakes. Hence, the same weights correspond to the turbines facing the same wind conditions.

O4) *Power losses*: minimize the electrical power losses. Hence, according to 5.4 the objective is denoted by

$$J_4 = P_{\text{tot}}^{\text{loss}}. \tag{5.10}$$

The aforementioned objectives should be ensured by the central controller that needs to consider the different priority among each objective.

5.2.1 Multi-objective Predictive Controller

In this section, an MPC strategy is proposed to solve the multi-objective optimization problem. The wind turbine system has been shown to be properly modelled as a first-order system (4.4), hence the dynamical model to be controlled is given by

$$\mathbf{x}_{k+1} = \mathbf{A}_d \mathbf{x}_k + \mathbf{B}_{1d} \mathbf{u}_k + \mathbf{B}_{2d} P_{\text{dem}}, \tag{5.11}$$

where $k \in \mathbb{Z}_{\geq 0}$ denotes the discrete-time step, $\mathbf{x}_k = [\mathbf{P}_{\text{g},k}^T, \xi]^T \in \mathbb{R}^{n_x}$ is the vector of system states, $\mathbf{P}_{\text{g},k} \in \mathbb{R}^{n_t}$ is the vector of generated powers, ξ is an integral action to ensure a zero steady-state tracking error and $\mathbf{u}_k \in \mathbb{R}^{n_u}$ denotes the vector of control inputs corresponding to the vector of manipulated power references $\mathbf{u} = [P_{r,1}, \ldots, P_{r,n_t}] \in \mathbb{R}^u$. Moreover, the formulation of the discrete-time matrices $\mathbf{A}_d$, $\mathbf{B}_{1d}$ and $\mathbf{B}_{2d}$ depending on the time constant used to model the wind turbine system is elaborated in (4.5).

In order to design the MPC strategy for the considered system, let $\hat{\mathbf{u}}(k) \triangleq \{\mathbf{P}_r(k|k), \ldots, \mathbf{P}_r(k+H_p-1|k)\}$ be a set of feasible control inputs within a pre-established prediction horizon $H_p \in \mathbb{Z}_{>0}$ that is constrained to ensure desired operational limits. Consider that the system in (5.11) is controlled using the multi-objective optimization problem with $m = 4$ control objectives. Thus, the optimization problem behind the MPC controller is stated as follows:

$$\begin{aligned} &\underset{\hat{\mathbf{u}}(k)}{\text{minimize}} \quad \sum_{j=1}^{m} w_j J_j(\mathbf{x}_k, \hat{\mathbf{u}}_k) \\ &\text{subject to} \\ &\quad \mathbf{x}_{(k+j+1|k)} = \mathbf{A}_d \mathbf{x}_{(k+j|k)} + \mathbf{B}_d \mathbf{u}_{(k+j|k)} + \mathbf{B}_l P_{dem} \quad j \in [0, H_p - 1] \cap \mathbb{Z}_{\geq 0} \\ &\quad P_{\min} \leq \mathbf{u}_{(k+j|k)} \leq \mathbf{P}_{\text{av}}(k) \end{aligned} \tag{5.12}$$

being $P_{\min}$ and $\mathbf{P}_{\text{av}}$ respectively the minimum and maximum power limits. Note that the former is included to avoid the shutdown of the turbines. The solution of the optimization problem finds the sequence of the optimal power set-point $\mathbf{u}^* = [P_{r,1}^*, \ldots, P_{r,n_t}^*]$ such that the objectives aforementioned are minimized.

Taking into account the parameters used to define the dynamical wind turbine model, the cost functions from J_1 to J_4 should be rewritten as

O1) $J_1 = (Q\mathbf{x}_k)'(Q\mathbf{x}_k)$, with $Q = [0, \dots, 0, 1] \in \mathbf{R}^{n_x}$.

O2) $J_2 = (S\Delta\mathbf{u}_k)'(S\Delta\mathbf{u}_k)$, with $\Delta\mathbf{u}_k = \mathbf{u}_k - \mathbf{u}_{k-1}$ and $S = \mathbf{I}_{n_t}$.

O3) $J_3 = \mathbf{1}_{n_t}(\Omega\mathbf{x}_k)$, with $\Omega = diag[\omega_1, \dots, \omega_{n_t}] \in \mathbb{R}^{n_t}$.

O4) $J_4 = P_{tot,k}^{loss}$.

Notice that the overall power loss is neglected with respect to the total power generated in the evaluation of J_1, being at most four orders of magnitude lower than the power demand. Moreover, such an assumption allows to guarantees the cost function linear.

The weights w_j used to prioritized the objective functions J_j in (5.12) are properly tuned such that the highest priority is given at the tracking error minimization then at the second objective to guarantee the safety of the wind turbines, while a more detailed tuning process depending on the main freestream wind direction is required to properly balance the electrical and wake losses. Since the objectives have different order of magnitude, it is necessary to normalize the multi-objective cost function and then assign the appropriate weights for each control objectives, such that $\sum_{j=1}^{4} w_j = 1$, as proposed in [15]. The normalized cost function has the form

$$\tilde{J}_j(\mathbf{x}_k, \mathbf{u}) = \frac{J_j(\mathbf{x}_k, \mathbf{u})}{J_j(\mathbf{x}_k^{\mathrm{M}}, \mathbf{u}^{\mathrm{M}}) - J_j^{\mathrm{m}}(\mathbf{x}_k^{\mathrm{m}}, \mathbf{u}^{\mathrm{m}})}, \tag{5.13}$$

where M, m indicate the maximum and minimum values of the states and control inputs of the controlled system.

For the sake of clarity, the aforementioned objectives could be reached on the basis of the lexicographic programming approach presented in Chapter 4. However, there is not a fixed hierarchy between the wake effect reduction and power losses minimization, in fact one of the scope of the proposed control approach is to investigate in which conditions it is better to prioritize the wind speed increasing with respect to the power losses reduction.

5.3 Case Study

Two different cases study are presented. First, the results obtained by solving the optimization problem in (5.12) are discussed. Then, considering only the power reserve

Table 5.1: Simulation set-up.

Parameter	Value
Separation	630 m
Sampling time	$T_s = 0.1$ s
Prediction Horizon	$H_p = 4$ s
Constant time	$\eta = 0.125$ s
Free-stream wind	11 m/s
Turbulence Intensity	TI = 0
Voltage	$V_{n,i} = 33$ kV
Cable Parameters	
Section [mm^2]	Resistence [Ω]
95	0.248
240	0.098
500	0.0456

maximization as objective for regulating the wind turbine generation, the advantages of the participation of wind farm in frequency support is investigated.

5.3.1 Part I: Electrical Cable Losses Minimization

A wind farm layout of 12 wind turbines laid in 3 rows and 4 columns is considered to test the proposed control strategy. The 5-MW NREL benchmark turbines are used and spaced $5D$ (i.e., 630 m) in both the x and y directions. The inter-array cables considered for this study are 3-phase XLPE-Cu, operating at 33 kV and are connected as shown in Figure 5.3. In Table 5.1 the cable parameters are presented. The AEOLUS SimWindFarm (SWF) Simulink toolbox [72] has been used for simulating the wind speed at wind farm grid points in two dimensions. Wake effects within the wind farm is modeled according to the dynamic wake meandering model [93] for given ambient turbulent intensity and wind speed direction. In order to have a clearer view of the power available and power losses changes produced applying the proposed strategy, a laminar flow is modeled using a grid size of 2500×2500 m^2 and the points are spaced 15 m. The reader is referred to Figure 3.2 that shows the steady-state wind field through the wind farm with wind direction of 0 degrees. In Table 5.1 the parameters for the simulation set-up are listed. In order to ensure the priority of the multi-objectives functions as presented in Section 3.2, the vector of weights in (5.12) is set equal to

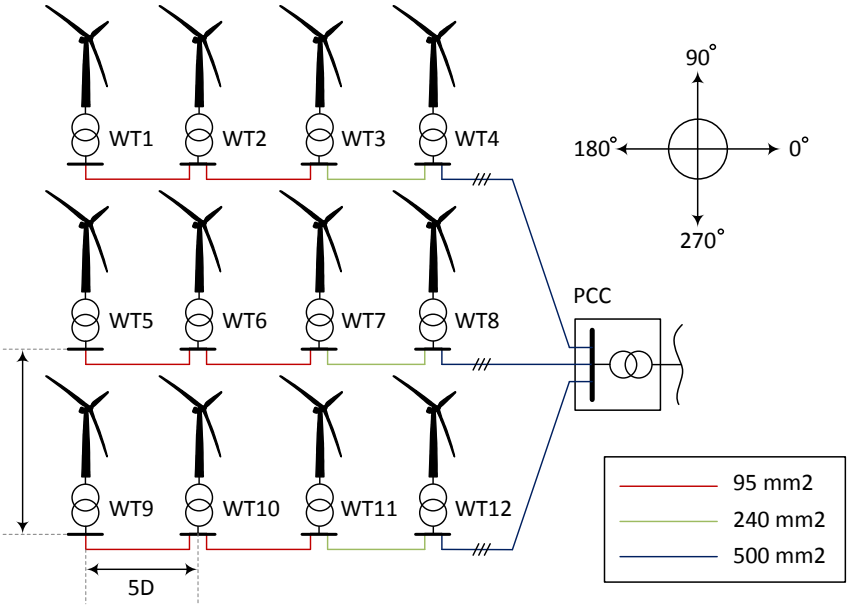

Figure 5.3: Wind farm layout.

$\mathbf{w} = [0.4, 0.1, 0.25, 0.25]$ such that higher priority is given at the tracking objective and equal importance at the electrical power losses and wake minimization.

Two scenarios are simulated as follows. The first scenario analyzes the system response of the wind farm controller when the power required by TSO changes dynamically during the simulation time. The second scenario shows the effects on the power reserve and the power losses when the proposed multi-objective optimization problem is solved by the wind farm controller.

Scenario 1: Power tracking

Figure 5.4 shows the power response of the system for a wind speed coming from 0 degrees. The wind farm works in derated operation, hence the available power (blue line) is higher than the power demand profile (red line). The proposed control strategy ensures that the total power generated by the farm (grey-dashed line) tracks the fast variations of the power demand ensuring that the tracking error is kept lower than 0.12% of the average power demand. In order to see how the controller optimizes the power set-points among the turbines, Figure 5.5 shows the available, generated and reference powers for

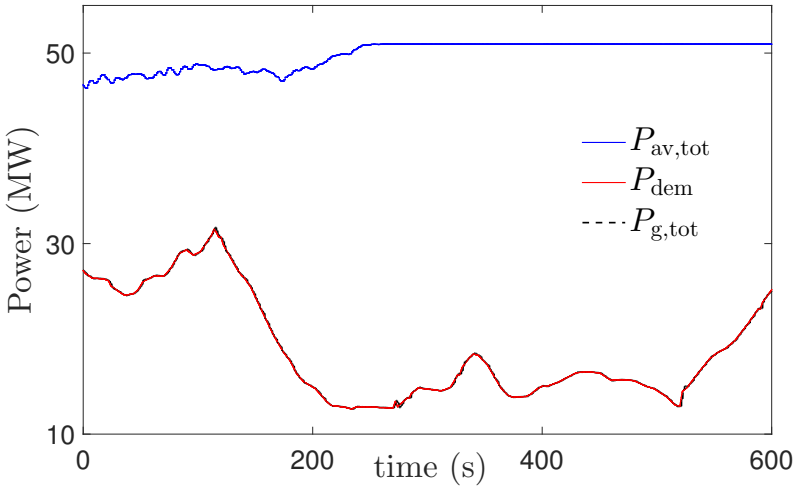

Figure 5.4: Scenario 1: Available $P_{\text{av,tot}}$, demanded P_{dem}, and generated $P_{\text{g,tot}}$ wind farm powers.

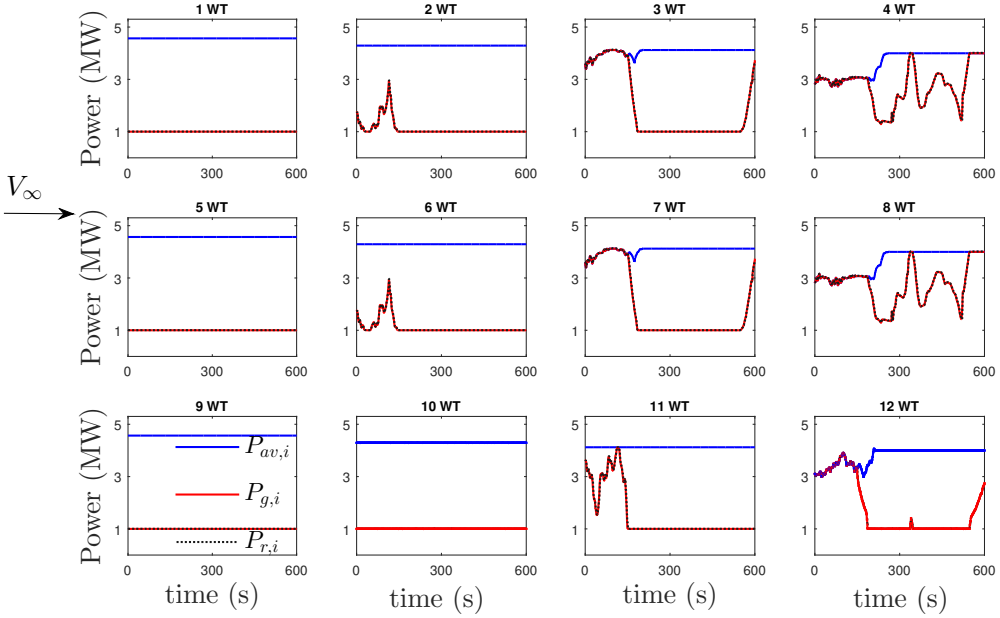

Figure 5.5: Scenario 1: Power generated $\text{P}_{\text{g},i}$, available $P_{\text{av,i}}$, and power set-points required by the controller $P_{r,i}$.

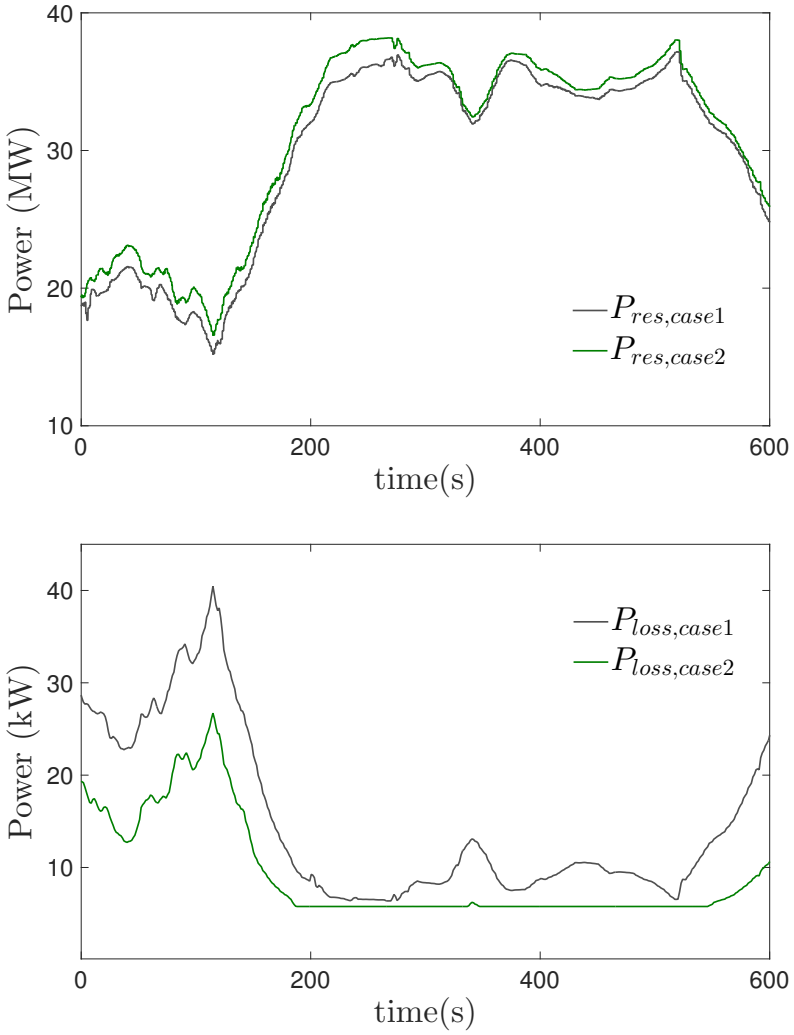

Figure 5.6: Scenario 1: Power reserve and power losses profiles.

each turbine. According to the cost functions J_3 and J_4 in (5.12) the power set-points for each turbine are found to improve the overall power reserve while decreasing the electrical cable losses. The latter is reduced by minimizing the powers generated by the turbines furthest from the PCC, see Figure 5.3. Meanwhile, the power reserve is improved reducing the wake effect through the wind farm, then improving the overall power available of the farm. As discussed in the previous Section 5.2. In order to reduce the wake effect the power references are set such that the highest power contribution is required to the most downstream turbines while the power generation of the other turbines is reduced until to have the minimum power generated from the most downstream turbines. Until time $0 \leq t \leq 150$ s, in order to track the power demand, the power generated by the wind turbines (3-7-11-4-8-12 WTs) produces exactly the available power, while the upstream turbines (1-5-9 WTs) generate the minimum power 1 MW, which avoids the shutdown. At time $t \geq 150$ s, when the power demand decreases, only the most downstream turbines (4-8-12 WTs) are required to produce more power. The effect of the aforementioned optimal power distribution in overall power reserve and electrical power losses are shown in Figure 5.6. Here, two cases are compared: Case 1 (grey line) is obtained when the MPC is stated to minimize only the first two objectives J_1 and J_2, that is only tracking is achieved. Case 2 (green line) all the full multi-objective optimization problem in (5.12) is solved. The power reserve improves while the power losses decrease.

Scenario 2: Power regulation for different wind directions

For a more comprehensive evaluation of the proposed control strategy towards power reserve maximization and power losses minimization, the system model is simulated for $t < t_1$ to ensure only tracking. Therefore, the global cost function in the general problem formulation (5.12) includes only the first and second objective functions f_1 and f_2. Then, for $t > t_1$ the complete multi-objective problem is solved. In this scenario, in order to have a clearer evaluation of the power distribution, the power demand is kept constant at $P_{\text{dem}} = 30$ MW. Figure 5.7 shows the power set-points (dashed grey line), the power generation (red line) and the power available (blue line) for each wind turbine. Initially, the tracking is ensured by requiring the same contribution for each turbine, which is equal to 2.5 MW. Then, for $t > t_1$ the power distribution changes. The controller seeks

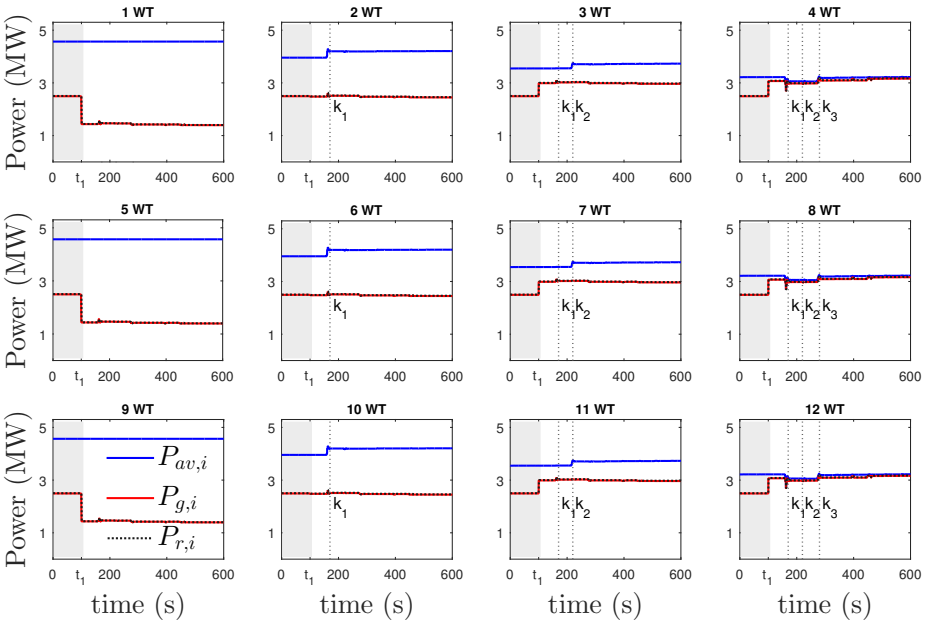

Figure 5.7: Scenario 2: Power generated $P_{\mathrm{g},i}$, available $P_{\mathrm{av},i}$ and power set-points required by the controller $P_{\mathrm{r},i}$).

to find the optimal power references for the turbines that ensure minimization of both wake effects and power losses. Here, the power generation of the first column is reduced to 2.8 MW, while the powers produced by the third and the last columns are respectively increased to 3 MW and to the maximum available power. Meanwhile, the generation for the second column is kept constant at 2.5 MW. The reduction of the power contribution of the turbines in the first column increases their induction factors such that also the wind speed deficits in (3.7) are decreased and the powers available improved. However, the effects in the variations of the power set-points can be seen only after certain periods denoted by k_i, which depend on the travel time required by the wakes to cross the wind farm. In Figure 5.8 are shown the power reserve and electrical power losses for several wind directions.

The minimization of power losses is obtained for each direction by reducing the power generation of the turbines closer to the PCC. Meanwhile, the decreasing of the wind deficits is achieved by generating more power with the downstream turbines, which change according to the direction of the wind. Therefore, the best balance between the

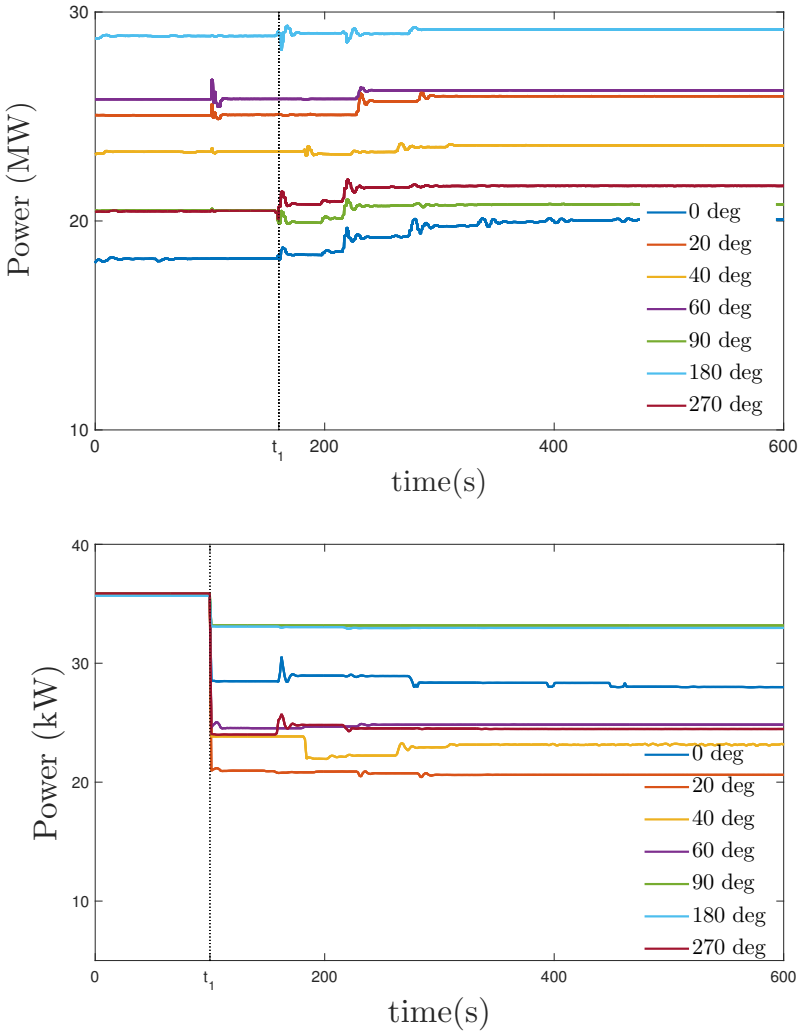

Figure 5.8: Scenario 2: Power reserve and power loss for several wind direction.

two objectives is obtained for a wind direction of 0 degrees.

5.3.2 Part II: Frequency Support Evaluation

The backward power distribution has resulted to be a reliable approach to indirectly change the induction factors of the turbines such that the wind deficits on the outflow field could be reduced. For the sake of completeness, this section is dedicated to compare the latter distribution method with two other approaches commonly applied to regulate the power set-points among the turbines [169]. For doing so, the MPC controller as stated in (5.12) is employed. Being out of the scope of this case study, the electrical power minimization expressed by the control objective J_4 is not included, hence $w_4 = 0$. Therefore, the multi-objective control problem becomes

$$\begin{aligned}
&\underset{\hat{\mathbf{u}}(k)}{\text{minimize}} \quad w_1(Q\mathbf{x}_k)'(Q\mathbf{x}_k) + w_2(S\Delta\mathbf{u}_k)'(S\Delta\mathbf{u}_k) + w_3\mathbf{1}_{n_t}(\Omega\mathbf{x}_k) \\
&\text{subject to} \\
&\quad \mathbf{x}_{(k+j+1|k)} = \mathbf{A}_d\mathbf{x}_{(k+j|k)} + \mathbf{B}_d\mathbf{u}_{(k+j|k)} + \mathbf{B}_l P_{dem} \qquad j \in [0, H_p - 1] \cap \mathbb{Z}_{\geq 0} \\
&\quad P_{\min} \leq \mathbf{u}_{(k+j|k)} \leq \mathbf{P}_{\text{av}}(k)
\end{aligned} \tag{5.14}$$

Here, the elements of the block-diagonal matrix $\mathbf{\Omega} = \text{diag}(\omega_1, \ldots, \omega_{n_t})$ are set differently to provide three different distribution modes:

1. **Equal distribution:** the power demand is equally distributed among the turbines, such that $P_{\text{g},i} = \frac{P_{\text{dem}}}{n_t}$. Hence, $\omega_1 = \omega_2 = \cdots = \omega_{n_t}$.
2. **Proportional distribution:** the power demand is distributed proportionally to the available power as formulated in (3.10). Hence, $\omega_i = \frac{P_{\text{av},i}}{P_N}$ with $i = 1, \ldots, n_t$.
3. **Backward distribution:** the elements ω_i are defined as formulated in (5.9).

In order to test the performance in terms of increasing of power reserve for the three distribution approaches, different operational and atmospheric conditions have been simulated using SimWindFarm toolbox [72] as simulator for a wind farm composed by three rows of five turbines as shown in Figure 5.9. Notice that this type of layout, where the turbines placed on two consecutive rows are not totally aligned, is preferred since it helps to reduce the impact of the wake effects on the downstream turbines.

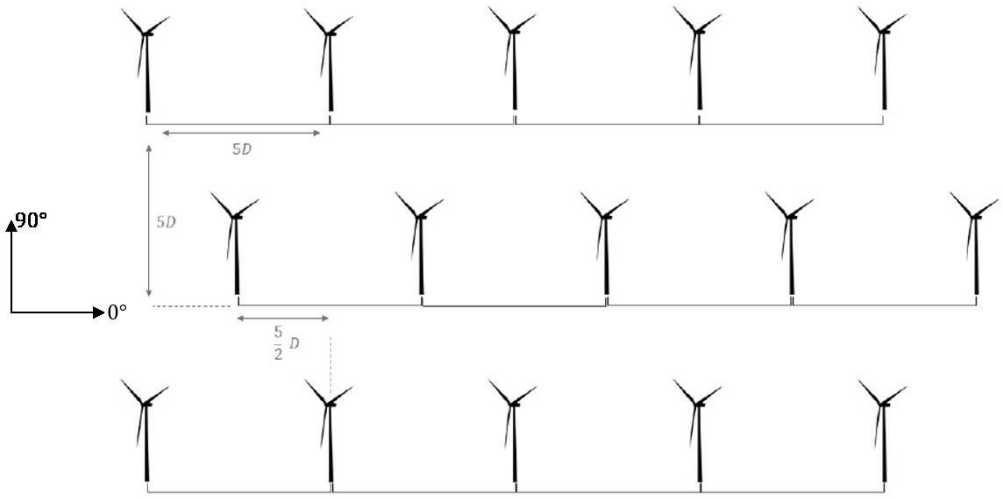

Figure 5.9: Wind farm layout.

Power reserve: a sensitivity analysis

To evaluate the sensibility of the investigated power regulation approaches on power demand, several de-loading conditions have been simulated going from 55% up to 95% of the maximum steady-state power $P_{\text{av}}^{\text{ss}}$. Moreover, the sensitivity of the distribution approaches with respect to the variation of the main wind speed direction was investigated. Figure 5.10 shows the values of power reserve at steady-state conditions for different values of power demand and different wind directions. The backward distribution provides a better performance for all the wind speed directions except for 0 degrees. In fact, for the latter case, when the power demand is higher than 85% of $P_{\text{av}}^{\text{ss}}$ it can be noticed that the highest power reserve is provided by the equal distribution. To better understand this result, the power contribution of a row of turbines (the bottom row in Figure 5.9) is shown in Figure 5.11 for both backward and equal distributions. Nevertheless, for high power demand, in the case of backward distribution only the upstream turbine is deloaded producing a significant wake reduction on the second turbine but also involves a greater power generated by the second and third turbines which implies an augmentation of the wakes faced by the downstream turbines. On the other hand, when the turbines provide the same power, only the last turbine produces power close to the available one while the other turbines are deloaded, thus the wind deficit experienced by the downstream turbines is less significant than the backward distribution case and

therefore the power reserve is higher. Notice that, this behavior has resulted only for 0 degrees since in this circumstance the impact of wake on power generation is more significant being the rotors turbines totally waked. For the same reason, at 0 degrees the differences in power reserve for the three distributions are more evident than the other wind directions. Finally, it can be observed that the proportional distribution provides the lower values in terms of power reserve. However, it is worth to mention that this strategy is typically used to provide the power demand while considering fatigue loads minimization. Therefore, a further investigation considering also loads minimization could be interesting for defining the best power distribution strategy able to find a balance between minimization of wake losses and fatigue loads.

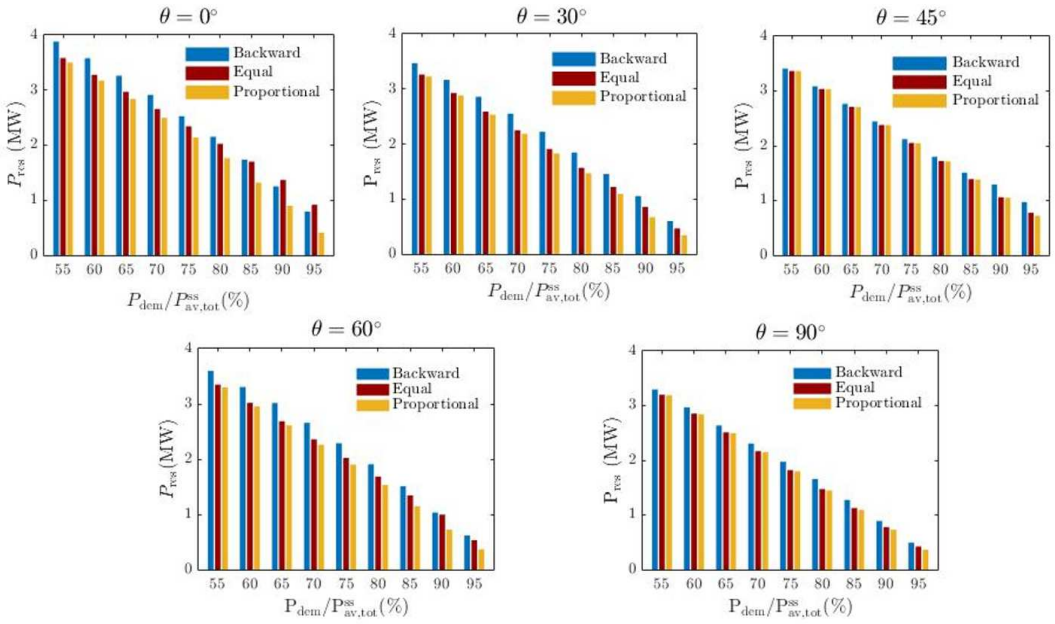

Figure 5.10: Power reserve values for different deloading operations and main wind speed direction.

Effect on frequency response

When the amount of wind generation into the interconnected electrical system is high, wind farms can be asked to provide frequency support. Hence, the regulation of the wind turbines can be set to improve primary frequency response of the system and provide

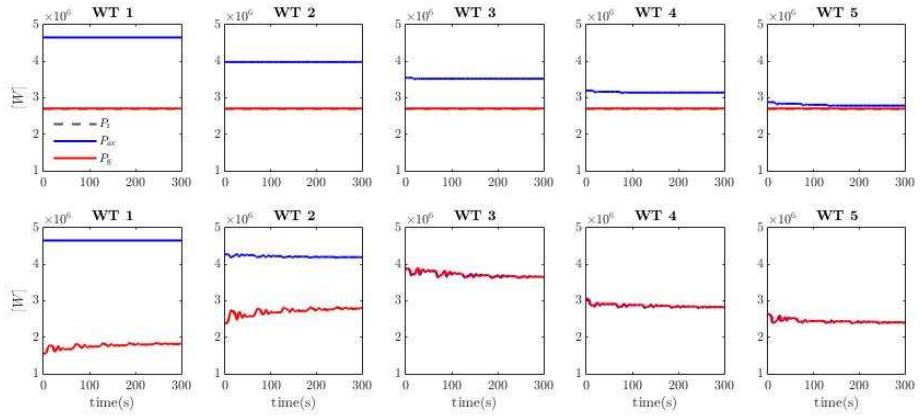

Figure 5.11: Distribution of the generated power among a row of wind turbines. Top plot: equal distribution strategy. Bottom plot: backward distribution strategy

additional source of flexibility for power system operators. To this end, through this dissertation, one of the major objectives considered for designing the wind farm control strategies has been to improve the capacity of the wind farm to help in primary frequency support by improving the power reserve. In order to assess the impact on frequency regulation of the three different power regulations under investigation, the frequency response after a frequency droop in the interconnected grid is investigated in this case study. In order to ensure that the wind farm can provide the power reserve, an initial deloading is set to provide a power demand equal to $40\%P_{\text{av}}^{\text{ss}}$ then at time $t > 5$ s the wind farm power generation increases to inject the amount of power reserve into the grid, as shown in Figure 5.12. During this period all the turbines produce the maximum power, however only for a short time span of about 3 s the wind farm can deliver a power equal to $P_{\text{av}}^{\text{ss}}$, within this time all the power stored in the rotor inertia is delivered. Then, the high generation of the wake decreases the overall available power thus only the $90\%P_{\text{av}}^{\text{ss}}$ can be delivered into the grid. Figure 5.13 shows the frequency response, the droop occurs at time $t = 5$ s (point A), it follows a deep frequency decline which can be arrested by providing inertia support, i.e., delivering the stored kinetic energy in the rotating mass, as discussed in Section 2.2. After this initial droop has been arrested, i.e., the frequency nadir is reached (point B), at almost $t = 6.5 - 7$ s, the wind farm continues to help in primary frequency support releasing the power reserve to stabilize the frequency to a steady-state value (point C or C'). It can be seen that with the backward regulation the frequency at the steady-state is qual to $f_C = 49.77$ Hz higher than the one reached by

the equal and proportional distributions, almost $f_{C'} = 49.68$ Hz. However, the frequency nadir is a bit lower when the backward distribution is followed due to the different pitch dynamics among the turbines. Pitch responses for each turbines, in both the backward and equal distribution cases, are shown in Figure 5.14 for the bottom row of turbines. It can be seen that while the pitch angle response in the case of equal distribution (bottom plot) is almost equal among the turbines, going from about 7 degrees to 0 degrees, for the backward distribution (top plot) the pitch dynamics are different. According to the turbine power generation, the pitch changes faster for the downstream turbines (WT5 and WT4), while the rate of change is low for the most upstream turbines that are generating pitched at 10 degrees to generate the minimum power. Therefore, the latter affects the overall dynamic response by decreasing the point of frequency nadir. For instance, in order to avoid such a drawback for the backward distribution, it can be considered to include in the formulation of the multi-objective control problem presented in (5.12) an additional objective to combine inertia and primary frequency supports, and so reducing the frequency nadir.

5.4 Summary

In order to improve the participation of wind energy in the electricity balancing market, wind farms should be able to provide ancillary services, for instance frequency regulation. Typically, wind farm should operate in curtailed mode to provide enough power reserve to be delivered into the grid for ensuring primary frequency control. In this condition, the wind turbine generation can be optimally regulated to provide different objectives. Therefore, a multi-objective optimization problem that is solved with the predictive control model technique has been presented in this chapter. Using a surrogate model of the wind turbine power response, it has been possible to predict within the prediction horizon of the MPC and optimize the power set-points for each turbines. Doing this, the effect of the wake on the overall available power and the electrical cable losses within the inter-array collection grid could be minimized. It has been shown that a backward power regulation among the turbines can improve the available power but, in some cases this regulation generates a drawback for the minimization of electrical losses. Therefore, a trade-off between electrical power and wake minimization has been found to provide both the objectives by properly assigning specific weights at each objective. The results

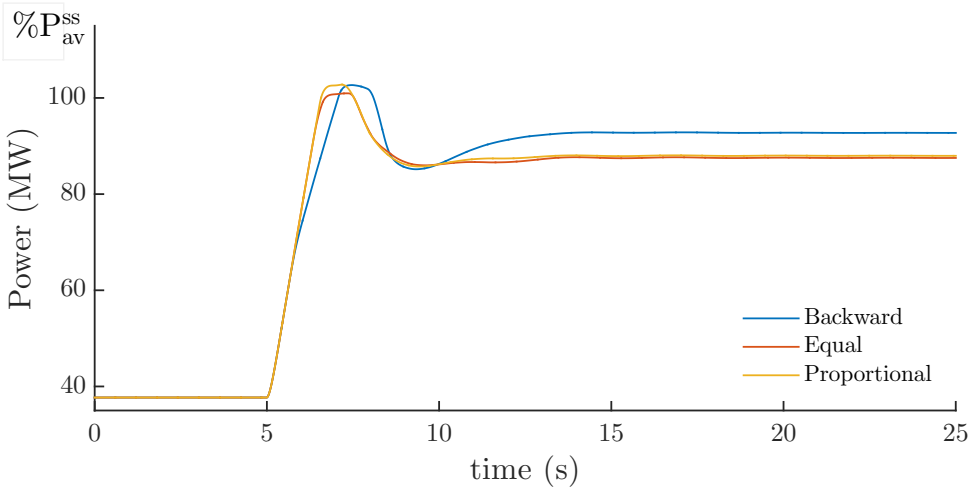

Figure 5.12: Power generated by the wind farm to provide frequency support before, $t < 5$ s, and after the frequency event.

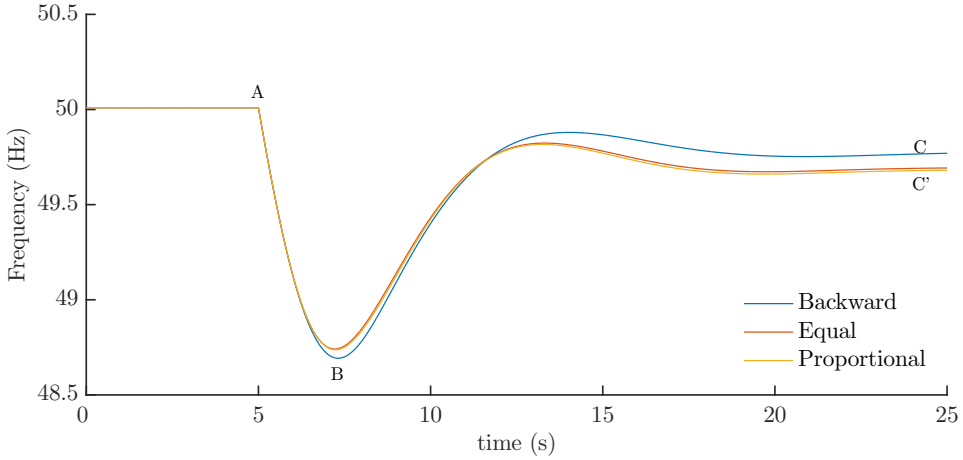

Figure 5.13: Frequency response of the electrical grid including a wind farm of 25 MW.

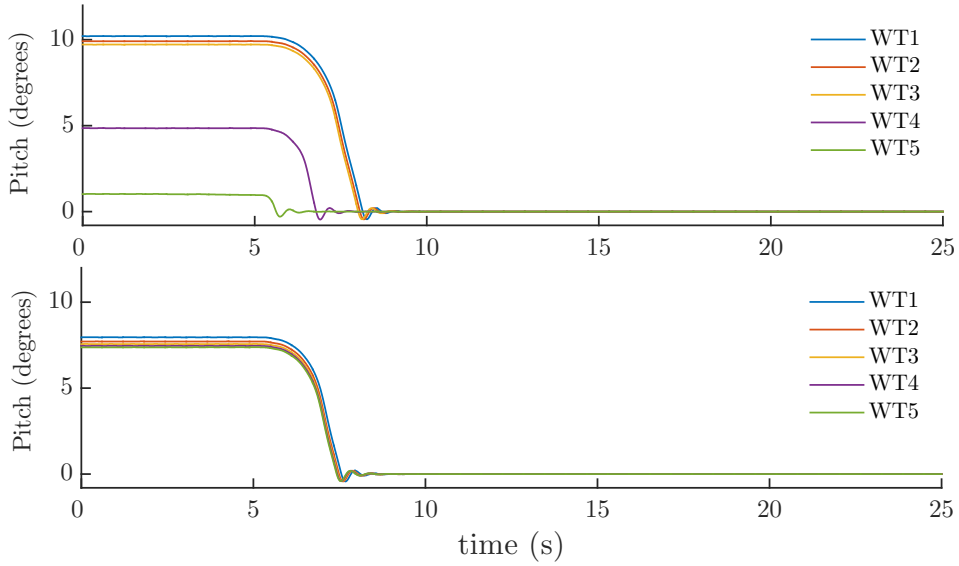

Figure 5.14: Pitch response for one row of turbines. Top plot: equal power regulation. Bottom plot: backward regulation.

have shown that the proposed control is able to track the power demand by the TSO during normal operation while minimizing the power losses and increasing the power reserve for all the simulation cases, in particular the highest improvement is achieved when the turbines are extremely affected by the wakes (i.e., at 0 degrees).

To see the effect of the proposed control approach when the wind farm provides primary frequency support, a frequency droop in the interconnection grid has been simulated. The results show that the backward distribution helps to restore the frequency at the steady-state point within 13 s after the initial droop. Additional simulation case studies were also presented that shown the proposed controller can deal with several atmospheric conditions and power generations. Moreover, a comparison with other commonly used power regulations has been presented in order to see the benefits of the proposed control approach in terms of frequency support. As a result, it is possible to conclude that the proposed approach provides a fast controller able to ensure the power demanded by the TSO while maximizing the power reserve and, guaranteeing to release quickly the latter power into the grid to restore the frequency at the nominal value after an event occurred.

Part III

Decentralized Control for improving energy production

Overview

With the aim of reducing costs, modern wind farms consist of a large number of turbines located close to each other. In this arrangement, turbines upstream produce wakes that affect the power generation of the other turbines. As a result, the power production of each turbine is highly coupled to the operating conditions of the other turbines, which decrease the wind speed faced by the turbines. Such negative impact can be reduced with suitable control strategies that send power commands to each turbine considering couplings. In this circumstance, centralized control approaches may demand large information sharing between turbines and the central controller. Complex communications and large information exchange result difficult to process over times suitable to satisfy the current power generation requirements (typically about seconds [63]) and the high communication dependency make the system exposed to failures. To overcome this problem, this part of the thesis proposes a possible solution to mitigate the aforementioned issues by designing a non-centralized wind farm control scheme based on splitting the wind farm into almost uncoupled groups by solving a novel mixed-integer partitioning problem. The control architecture corresponds to a hierarchical structure where a supervisory controller coordinates the generation of each group to satisfy the power demanded by the grid operator and additional grid requirements. The controller at the turbine level seeks to optimize the distribution of the power set-points among turbines such that the impact of the power losses due to the wake effect is reduced. The effectiveness of the proposed scheme in terms of reduction of computational costs and power regulation is evaluated by simulations for a wind farm of 42 turbines. With the proposed control approach the computation time is consistently reduced compared to the centralized control strategy meanwhile the performance on optimal power distribution is slightly affected.

Chapter 6

Non-centralized predictive control: a wake-based partitioning approach

6.1 Introduction

Driven by economy scale costs and the need of replacing conventional power systems with wind farms of similar capacity, the number of turbines in the recently installed wind farms is even more increasing. Related wind farm models used to design the control strategies become more complex and difficult to control with centralized design concepts. Moreover, the ambitious targets arising from the new grid codes require to control larger number of state information, increasing the computational burden and so the reliability of ensuring real-time control with a centralized scheme. Typically, at the wind farm level, a dedicated supervisory computer coordinates the operation of each turbine in order to generate the power demanded by the TSO [**?**]. This supervisory device needs to gather information from a large number of sensors, compute a large set of commands and send them to each turbine. With larger number of turbines, a centralized control approach requires expensive communication networks, high computation power, and reduces the overall system resiliency, being too sensitive to the status of the communication link [**?**].

An alternative to mitigate the aforementioned issues consists in dividing the wind farm into smaller groups of turbines, denoted as *partitions*. Each partition is equipped with

a controller that communicates only with the turbines in the subset and the supervisor. Thus, communication links and computational costs can be significantly reduced. This idea has been applied to several large-scale systems, e.g., traffic systems, energy systems, smart grids and water systems [17, 71, 118]. The application of partitioning techniques for controlling wind farms in a decentralized manner has been started only recently [9, 64, 146], mainly it consists on determining the partitions by considering the dynamical couplings due to the wake effects. One pioneering work in this regard was proposed in [146], in which by exploiting the problem structure a combination of online and offline computations are used to reduce the solving time.

Among modern non-centralized control algorithms, alternating direction method of multipliers (ADMM), dual-decomposition and consensus-based control algorithms have attracted more attention for wind farm control [10, 14, 21, 171]. In [171], fast gradient methods via dual-decomposition are used for power regulation and load alleviation, in which most of the computational tasks are shared by local distributed predictive controllers at wind turbine level and reducing the computational cost of the central unit. ADMM was also used in [9] to solve iteratively a clustering-based distributed optimization problem in order to improve yaw misalignment issues of turbines within wind farms and the total power production. Other limited-communication methodologies use consensus algorithms to maximize the power generation and stored kinetic energy [55, 170]. These consensus algorithms have been successfully used for optimal power-sharing between wind farms and energy storage devices [14, 172]. Non-centralized control approaches have also been used in wind farms to mitigate negative wake effects in the power production by computing axial induction factors or yaw misalignment [21, 64]. As these approaches rely on complex wake models and complex non-convex optimization problems, the online implementation might be difficult.

In [143], a hierarchical control scheme based on artificial partitioning of a large-scale wind farm was proposed. The work presented in this chapter extends this result improving the partitioning procedure and using a hierarchical non-centralized MPC scheme. Firstly, partitioning of the wind farm is cast as a mixed-integer linear optimization problem taking into account the coupling among turbines caused by wakes. Once the wind farm is split into a few almost uncoupled subsets, a three-level MPC scheme is designed with

the aim of ensuring the power regulation at the levels imposed by the TSO and seeking to maximize the power reserve available for ancillary service provision.

6.2 Wind Farm Partitioning

The partitioning problem for large-scale systems constitutes a relevant alternative in the design of non-centralized controllers, allowing the identification of multiple sub-systems in an appropriate manner as it has been presented in Section 2.3.4. As the first step towards optimally designing a non-centralized control strategy, the wind farm is partitioned into several almost uncoupled subsets of turbines. Typically, the partitioning can be addressed in two different ways. The first alternative consists in determining a partitioning based on the dynamical coupling of the whole system, whereas the other possible approach considers information coupling considering not only the dynamical representation of the system, but also all the coupled constraints involved in the control design. In this thesis, the partitions are designed organizing the wind turbines in subsets according to the coupling level associated with the wake effect. Among the different approaches proposed for partitioning large-scale systems [10, 15, 118], here the partitioning approach proposed in [143] is considered and improved in order to provide a more robust partitioning algorithm.

In large wind farms, couplings among turbines caused by wakes are significant and lead to substantial power losses. However, these couplings only affect a certain number of turbines according to the turbulence intensity and the wind speed characteristics in the surrounding area. As a possible strategy to better control the wind farm to mitigate the overall wake effect, the wind turbines can be separated in subsets such that the turbines affected by the same wake are in one subset. In order to do this, the coupling dynamics should be modeled with relatively simple model to be included in the partitioning problem formulation. As discussed in Chapter 2, by properly modeling the wake interactions high fidelity code involving differential equations are required. However, the high computational burden associated with these models are impractical for updating the partitions in real-time. In Chapter 4, the *Park's model* was used to simulate the wind across a wind farm, the wind speed deficit was given as a function of the distance among the turbines, the wind speed direction and the number of wakes

affecting the downstream turbines. Based on this geometrical-based formulation of the wake impact, in this thesis the strengths of the coupling among the turbines can be computed as

$$\epsilon_{ij} = \left| \frac{R}{r_{ij}(x_{ij})} \right| \frac{A^s_{ij}(x_{ij})}{A_0}, \tag{6.1}$$

if turbine T_i is placed downstream of turbine T_j (i.e., the wind speed faced by the i-th turbine is affected by the wake caused by j-th turbine); otherwise, $\epsilon_{ij} = 0$. Notice that a similar formulation for defining wind turbines subsets was presented in [10]. From (6.1) it follows that the strength of the wake decreases with the separation among the turbines $r_{ij}(x_{ij})$ and is proportional to the portion of the rotor shadowed by the upstream wake, defined as A^s_{ij}. The latter, function of the wind speed direction ϕ, is computed as

$$A_{s,i}(\phi) = r_i(x_{ij})^2 \cos^{-1}\left(\frac{L_{ij}}{r_i(x_{ij})}\right) + r_0 \cos^{-1}\left(\frac{d_{ij} - L_{ij}}{r_i(x_{ij})}\right) + d_{ij} z_{ij}, \tag{6.2}$$

being L_{ij} the distance between the centres of the wake area and the shadow area, d_{ij} the distance between the centres of the wake area and the rotor area and z_{ij} the distance between the intersection points of the wake and rotor area.

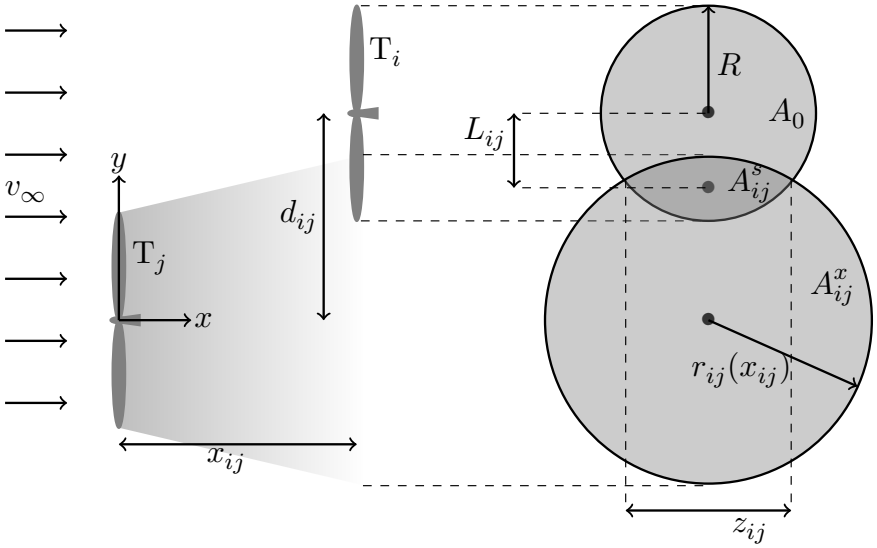

Figure 6.1: Wake expansion.

The proposed partitioning approach provide a clever way to organize the turbines such that the The wake generated by an upstream turbine can affect the incoming wind

speed of different downstream turbines in accordance with the turbulence intensity of the surrounding area, the intensity and the main direction of the freestream wind speed.

6.2.1 Partitioning Problem

With the aim of considering wake effects, the interactions due to the wake propagations are represented as a weighted directed graph $\mathcal{G} = (\mathcal{V}, \mathcal{E})$, where $\mathcal{V} = \{1, 2, \ldots, n\}$ is the set of vertices, where each vertex corresponds to a wind turbine and $\mathcal{E} = \{(i, j) : i, j \in \mathcal{V}\}$ is the set of edges with weights ϵ_{ij} in (6.1).

Then, according to the wind farm layout and the predominant free-stream wind speed direction ϕ, the wind farm can be sorted in m subsets and the number of turbines within each subset can be found by solving the following optimization problem:

$$\underset{\delta_{il}}{\text{minimize}} \quad \sum_{q=1}^{3} w_q f_q(\delta_{il}), \tag{6.3a}$$

$$\text{subject to} \quad \sum_{i \in \mathcal{V}} \delta_{il} \geq 1, \quad \forall\, l \in \mathcal{K}, \tag{6.3b}$$

$$\sum_{l \in \mathcal{K}} \delta_{il} = 1, \quad \forall\, i \in \mathcal{V}, \tag{6.3c}$$

with $\delta_{il} \in \{0, 1\}$ a Boolean decision variable such that $\delta_{il} = 1$ if turbine T_i belongs to subset l, with $l \in \mathcal{K} = \{1, 2, \ldots, m\}$, and 0 otherwise. The non-empty constraint (6.3b) and the exclusive constraint (6.3c) ensure that the subsets cannot be empty and turbine T_i can only belong to one subset l.

The objective function (6.3a) consists of three terms weighted by $w_q > 0$ $(q = 1, 2, 3)$:

1. The first term f_1 in the objective function (6.3a) is stated as the sum of the edge weights at each partition $l \in \mathcal{K}$, i.e.,

$$f_1 \triangleq -\sum_{l \in \mathcal{K}} \sum_{i \in \mathcal{V}} \sum_{j \in \mathcal{V} \setminus \{i\}} (\epsilon_{ij} + \epsilon_{ji}) \delta_{il} \delta_{jl}. \tag{6.4}$$

   Depending on farm layout and the v_∞ direction, only a number of downstream turbines is affected by the wake caused by an upstream turbine. The aim of this term is to ensure that turbines coupled by the same wake belong to the same subset.

2. The second term is added to (6.3a) in order to minimize the distance d_{ij} between turbines belonging to the same subsets, i.e.,

$$f_2 \triangleq \sum_{l\in\mathcal{K}} \sum_{i\in\mathcal{V}} \sum_{j\in\mathcal{V}\setminus\{i\}} d_{ij}\delta_{il}\delta_{jl}. \tag{6.5}$$

   There might be cases where there is no coupling among turbines, i.e., $\sum_{i\in\mathcal{V}}\sum_{j\in\mathcal{V}\setminus\{i\}}(\epsilon_{ij}+\epsilon_{ji})=0$, e.g., when wind turbines are located in a row (or a column) and the freestream wind direction is such that the wakes generated by the upstream turbines do not affect any other turbine. In such a case, to guarantee a unique solution, turbines can be arranged according to their geographical distance.

3. Finally, in order to balance the number of turbines in each subset, an extra term is added to minimize the difference between the number of turbines among all subsets, i.e.,

$$f_3 \triangleq \sum_{l=1}^{m-1} \sum_{l'=l+1}^{m} |\sum_{i\in\mathcal{V}} \delta_{il} - \sum_{j\in\mathcal{V}} \delta_{jl'}|. \tag{6.6}$$

Setting the weights w_q, the aforementioned objectives are hierarchically prioritized to find the optimal partition $\mathcal{P}^* = \{\mathcal{P}_1, \ldots, \mathcal{P}_m\}$.

The optimization problem (6.3) is nonlinear; however it can be recast as a mixed-integer linear programming problem as follows. The procedure to transform products of logical variables, in terms of linear inequalities was presented in [22], which however requires the introduction of auxiliary Boolean variable δ_{ijl} such that $\delta_{ijl} \triangleq \delta_{il}\delta_{jl}$. Notice that $\delta_{ijl}=1$ if and only if $\delta_{il}=1$ and $\delta_{jl}=1$, and therefore

$$\delta_{ijl} = \begin{cases} -\delta_{il} + \delta_{ijl} \leq 0, \\ -\delta_{jl} + \delta_{ijl} \leq 0, \\ \delta_{il} + \delta_{jl} - \delta_{ijl} \leq 1. \end{cases}$$

Let also define a dummy variable $\varrho_{ll'} \in \mathbb{R}$ such that $\varrho_{ll'} \geq |\sum_{i\in\mathcal{V}} \delta_{il} - \sum_{i\in\mathcal{V}} \delta_{jl'}|$, then (6.6) can be replaced by

$$f_3 = \sum_{l=1}^{m-1} \sum_{l'=l+1}^{m} \varrho_{ll'}. \tag{6.7}$$

Therefore, the optimization problem (6.3) becomes

$$\underset{\delta_{ijl},\, \varrho_{ll'}.}{\text{minimize}} \quad \sum_{q=1}^{3} w_q f_q(\delta_{ijl}, \varrho_{ll'}), \tag{6.8a}$$

$$\text{subject to} \quad \sum_{i\in\mathcal{V}} \sum_{j\in\mathcal{V}\setminus\{i\}} \delta_{ijl} \geq 1, \quad \forall\, l \in \mathcal{K}, \tag{6.8b}$$

$$\sum_{l\in\mathcal{K}} \delta_{ijl} = 1, \quad \forall\, i,j \in \mathcal{V}, \tag{6.8c}$$

$$-\delta_{il} + \delta_{ijl} \leq 0, \quad \forall\, i,j \in \mathcal{V},\ \forall\, l \in \mathcal{K}, \tag{6.8d}$$

$$-\delta_{jl} + \delta_{ijl} \leq 0, \quad \forall\, i,j \in \mathcal{V},\ \forall\, l \in \mathcal{K}, \tag{6.8e}$$

$$\delta_{il} + \delta_{jl} - \delta_{ijl} \leq 1, \quad \forall\, i,j \in \mathcal{V},\ \forall\, l \in \mathcal{K}, \tag{6.8f}$$

$$\sum_{i\in\mathcal{V}} \delta_{il} - \sum_{j\in\mathcal{V}} \delta_{jl'} \leq \varrho_{ll'}, \quad 1 \leq l \leq m-1, \tag{6.8g}$$

$$\sum_{i\in\mathcal{V}} \delta_{il} - \sum_{j\in\mathcal{V}} \delta_{jl'} \geq -\varrho_{ll'}, \quad 1 \leq l \leq m-1, \tag{6.8h}$$

where $l' = l + 1$ and f_q $(q = 1, 2, 3)$ are given in (6.4), (6.5), (6.7). As a consequence of using the auxiliary Boolean variable δ_{ijl}, constraints (6.8d), (6.8e), (6.8f) must be added to the original problem (6.3), [22] and the original no-empty and exclusive constraints in (6.3b), (6.3c) must be rewritten as (6.8b), (6.8c), respectively. Additional constraints (6.8g), (6.8h) are needed to be able to use the dummy variable $\varrho_{ll'}$ and hence using (6.7) instead of (6.6).

6.2.2 Number of Subsets

In order to solve the m-partitioning problem (6.8), it is necessary to provide the number of subsets m. A detailed strategy to determine this number for a drinking water network is proposed in [15]. In the current work, a similar approach is presented assuming that the air flow within a wind farm can be modeled as a simplified flow-based distribution network. Many engineering systems have been modeled as flow-based distribution systems [15, 71], which consist of several elements of diverse nature, e.g., storage, actuator, joint, sink, source and flow. Unlike other energy sources, wind cannot be stored, and hence the wind flow in a farm can be obtained identifying only the following elements:

1. *Source:* element generating the resource. It is equivalent to the turbine facing the free-stream wind condition v_∞ and generating the wake in the outflow field. The set of these elements is denoted by $\bar{\mathcal{V}}_{\text{so}}$.

2. *Actuator:* element that receives and provides the resources. The set of actuator elements is denoted by $\bar{\mathcal{V}}_{\text{ac}}$ and corresponds to the set of turbines increasing the wake effect generated by the upstream turbines $j \in \bar{\mathcal{V}}_{\text{so}}$ proportionally to the operational conditions and, in turn, affected by the wakes generated by the upstream turbines.

3. *Sink:* element that receives the resource from either the source and/or the actuator. It is equivalent to the turbine only receiving wakes, e.g., the most downstream turbine. The set of sinks is denoted by $\bar{\mathcal{V}}_{\text{si}}$.

4. *Link:* directed link (i, j) allowing resource flow from an element i to j. For a wind farm, this link corresponds to the wake generated by the turbine $i \in \bar{\mathcal{V}}_{\text{so}} \cup \bar{\mathcal{V}}_{\text{ac}}$ and moving through a turbine $j \in \bar{\mathcal{V}}_{\text{ac}} \cup \bar{\mathcal{V}}_{\text{si}}$. The set of link elements is denoted by $\bar{\mathcal{E}} \subset \{(i, j) : i, j \in \bar{\mathcal{V}}\}$, with $\bar{\mathcal{V}} = \bar{\mathcal{V}}_{\text{so}} \cup \bar{\mathcal{V}}_{\text{si}} \cup \bar{\mathcal{V}}_{\text{ac}}$.

Therefore, the flow-based distribution system can be identified as a directed graph $\bar{\mathcal{G}} = (\bar{\mathcal{V}}, \bar{\mathcal{E}})$ where each element $i \in \bar{\mathcal{V}}$ has a direct relationship with the turbines in the graph $\mathcal{G}$. The introduced elements for a flow-based distribution system and the representation of the system by a directed graph allow finding the number of subsets as proposed in [15], where three further indicators are defined:

1. *Network resource-feeding index*, denoted by τ_i with $i \in \bar{\mathcal{V}} \setminus \bar{\mathcal{V}}_{\text{so}}$, gives information about the number of sources or actuator elements that provide the wakes for the element $i \in \bar{\mathcal{V}} \setminus \bar{\mathcal{V}}_{\text{so}}$. Assuming the graph $\bar{\mathcal{G}}$ is split into m subsets, it is possible to identify the subsets of sinks $\bar{\mathcal{V}}_{\text{si},l}$ and sources $\bar{\mathcal{V}}_{\text{so},l}$ for each partition $l \in \bar{\mathcal{K}}, \bar{\mathcal{K}} = \{1, \ldots, m\}$, while the maximum resource-feeding index per partition is defined by $\tau_l^* = \max_{i \in \bar{\mathcal{V}}_{\text{si},l}} \tau_i$.

2. *Sink co-relation index*: The proportion of sinks in each subset $l \in \bar{\mathcal{K}}$ with respect the total number of sinks in the flow-based graph $\bar{\mathcal{G}}$, i.e., $\sigma_l = \sum_{i \in \bar{\mathcal{V}}_{\text{so},l}} \tau_i / \sum_{i \in \bar{\mathcal{V}}_l} \tau_i$ with $\bar{\mathcal{V}}_l = \bar{\mathcal{V}}_{\text{so},l} \cup \bar{\mathcal{V}}_{\text{si},l} \cup \bar{\mathcal{V}}_{\text{ac},l}$ the set of flow elements in the subset l.

3. *Resource-feeding co-relation index*: The availability of sources in the subset $l \in \mathcal{K}$ feeding the sink element $i \in \bar{\mathcal{V}}_{\text{si},l}$ for which $\tau_i = \tau_l^*$. It is assessed with respect to the total number of sources $j \in \bar{\mathcal{V}}_{\text{so}}$ feeding the element i, i.e., $\beta_l = \sum_{j \in \bar{\mathcal{V}}_{\text{so},l}} \alpha_{ij} / \sum_{j \in \bar{\mathcal{V}}_{\text{so}}} \alpha_{ij}$, where $\alpha_{ij} = 1$ if the flow element $\epsilon_{ij} = 1$ with $\epsilon_{ij} \in \bar{\mathcal{E}}$, and 0 otherwise.

The number of subsets is assessed by setting both a desired *maximum sink co-relation index* and a *minimum resource-feeding co-relation index*, hence the subsets should satisfy $\sigma_l \leq \sigma^*$ and $\beta_l \geq \beta^*$. The parameter σ^* is set to ensure that the number of sink elements is balanced among the subsets such that there are not subsets without sinks. Furthermore, identifying for each subset the maximum resource-feeding index τ_l^* and their respective sources, it is desired that each subset includes a minimum number of these sources indicated by β^*.

6.2.3 Algorithm and Implementation Aspects

Figure 6.2 summarizes the partitioning approach proposed in this chapter. Assuming an initial number of subsets m, the partitioning problem for the information sharing graph $\mathcal{G}$ is first solved and the optimal partition set $\mathcal{P}^*$ is found. Then, the analogy with the flow-based distribution graph $\bar{\mathcal{G}}$ is used to check whether or not the criteria for the proper number of subsets are fulfilled. An iterative loop is repeated increasing the initial number of subsets $m = m + 1$ until the aforementioned criteria for defining the number of subsets are satisfied.

The partition obtained with the previous procedure $\mathcal{P}^*$ depends on the distances x_{ij} and the wind turbine arrangement within the farms (i.e., the set of downstream and upstream turbines), which in turn depends on the predominant free-stream wind speed direction ϕ. Furthermore, the computational burden to solve the proposed partitioning problem for large wind farms can be high and inconsistent with the time scale related to the variation of wind direction within a range and the sampling time used into the wind farm controller. Nevertheless, the subset can be determined offline and one can keep a look-up table to update the subset whenever the predominant free-stream wind speed direction changes.

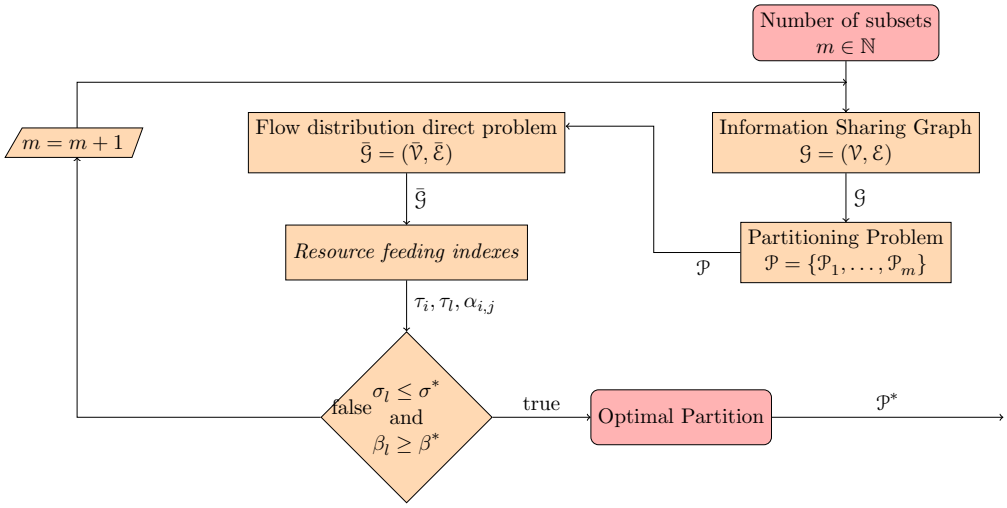

Figure 6.2: Optimal partitioning algorithm flowchart.

As the wind speed direction is sensitive to turbulence and other atmospheric and geographical conditions such as eventual obstacles surroundings, a predominant wind speed direction can be used to select the corresponding subset. This can be obtained by time averaging of data gathered from sensors and for wind farms located in non-highly turbulent sites and the predominant wind speed can be considered constant for about 10 minutes [58]. Therefore, during this time interval the subsets are kept constant to provide robustness to the proposed control approach.

6.3 Wind Farm Control Strategy

Once the system is partitioned as indicated in the previous section for a set of predominant free-stream wind speed directions

$$\Phi = \{\phi_1, \ldots, \phi_w\},$$

there is a set $\mathcal{P}^*$ of optimal partition sets for each angle $\phi \in \Phi$. Then, for a given direction ϕ and the corresponding partition set

$$\mathcal{P}^* = \{\mathcal{P}_1, \ldots, \mathcal{P}_m\},$$

the proposed non-centralized hierarchical control approach is structured as indicated in Figure 6.3, where $\mathcal{P}_l$ is a set of n_l indexes corresponding to the wind turbines in the subset $l \in \mathcal{K} = \{1, \ldots, m\}$.

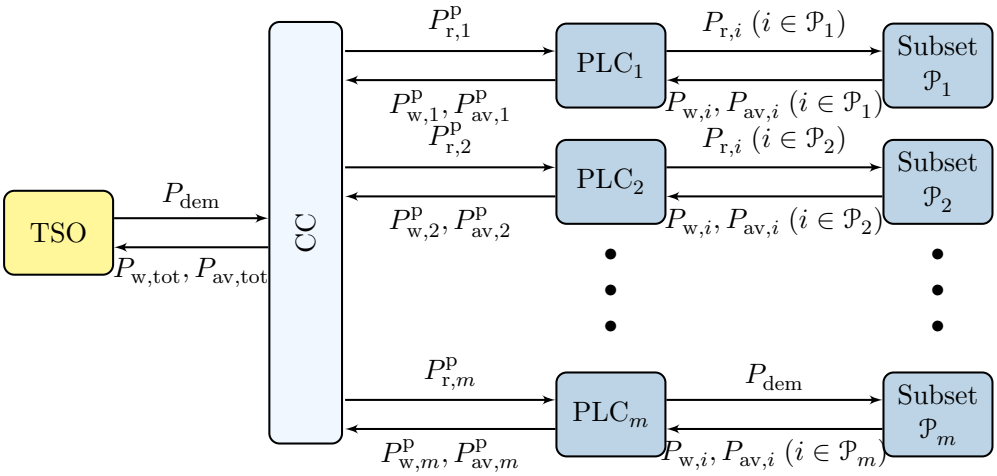

Figure 6.3: Scheme of the proposed wind farm non-centralized control strategy for a given ϕ and the corresponding partition set $\mathcal{P}^*$ with m elements.

At the highest level, the Central Controller (CC) collects information regarding the generated power $P^{\text{p}}_{\text{w},l}$ and the available power $P^{\text{p}}_{\text{av},l}$ in each subset and then sends the corresponding commands $P^{\text{p}}_{\text{r},l}$. This controller aims to ensure that the total power delivered at the Point of Common Coupling (PCC) by the wind farm $P_{\text{w,tot}}$ matches the TSO's power demand P_{dem}. In a lower level, the Partition Level Controllers (PLC) use the measure of the generated power $P_{\text{w},i}$ and the available power $P_{\text{av},i}$ at each turbine in the corresponding subset to impose a reference $P_{\text{r},i}$ to each turbine. Finally, at the lowest level, the wind turbine control guarantees that the generated power satisfies the set-point $P_{\text{r},i}$.

6.3.1 Wind turbine Controller

Each wind turbine is equipped with a power controller that allows working in derated mode if necessary [23, 72]. Thus, the power generated by the i-th wind turbine is given by

$$\dot{P}_{\text{w},i} = -\frac{1}{\eta}(P_{\text{w},i} - \min(P_{\text{av},i}, P_{\text{r},i})), \tag{6.9}$$

where η is a time constant, $P_{\text{r},i}$ is the reference sent by the PLC, and

$$P_{\text{av},i} = \min\left(\frac{\rho\pi R^2}{2} C_{\text{p,max}} v_i^3, P_{\text{rated}}\right) \tag{6.10}$$

is the wind turbine available power, with $C_{\mathrm{p,max}} = \max_{a_i} C_{\mathrm{p}}(a_i)$ and P_{rated} the wind turbine rated power.

6.3.2 Partition Level Controllers (PLCs)

The PLCs aim to ensure the total power generated in each partition matches the power demanded by the CC. In addition, these controllers seek to distribute the power contribution of each turbine in order to maximize the total available power, which in turn maximizes the power reserve of the entire farm available for ancillary services. The power reserve is defined as $P_{\mathrm{res}} = P_{\mathrm{av,tot}} - P_{\mathrm{w,tot}}$.

For a given partition $\mathcal{P}_l$, with $l \in \mathcal{K}$ and n_l turbines, the corresponding PLC relies on an MPC strategy based on the following optimization problem:

$$\underset{\mathbf{u}_l(k)}{\text{minimize}} \quad \sum_{q=1}^{3} \sum_{k=1}^{H_p-1} \gamma_q J_q(\mathbf{x}_l(k), \mathbf{u}_l(k)) \tag{6.11a}$$

$$\text{subject to} \quad \mathbf{x}_l(k+j+1|k) = \mathbf{A}_{d,l}\mathbf{x}_l(k+j|k) + \mathbf{B}_{d,l}\mathbf{u}_l(k+j|k), \tag{6.11b}$$

$$P_{\min} \leq u_{l,i}(k+j) \leq P_{\mathrm{av},i}, \ \forall\, i \in \mathcal{P}_l \tag{6.11c}$$

where $\gamma_q > 0$ are prioritization weights such that $\sum_{q=1}^{3} \gamma_q = 1$, $\mathbf{x}_l \in \mathbb{R}^{n_l}$ is the state vector and $\mathbf{u}_l \in \mathbb{R}^{n_l}$ is the vector of manipulated variables, with elements $x_{l,i} = P_{\mathrm{w},i}$ and $u_{l,i} = P_{\mathrm{r},i}$ $(i \in \mathcal{P}_l)$, respectively. The time indexes $k \in \mathbb{N}$, $j \in \{0, \ldots, H-1\}$ and the prediction horizon H are defined such that $\mathbf{x}_l(k+j|k)$ denotes the vector of measured generated power at the instant k corresponding to the control input $\mathbf{u}_l(k+j|k)$.

The solution of problem (6.11) is the optimal control input $\hat{\mathbf{u}}_l \triangleq \hat{\mathbf{u}}_l(k|k)$ corresponding to the set-points for each the turbine $i \in \mathcal{P}_l$. Notice that the first constraint (6.11b) corresponds to the discretized version of (6.9), used to predict the power response of the wind turbines in the partition $\mathcal{P}_l$, where $\mathbf{A}_{d,l}$ and $\mathbf{B}_{d,l}$ are the discretized versions of the matrices

$$\mathbf{A}_l = -(1/\eta)\,\mathbf{I}_{n_l}, \qquad \mathbf{B}_l = (1/\eta)\,\mathbf{I}_{n_l}.$$

Finally, in the last constraint (6.11b), $P_{\min}$ denotes the minimum power used as a lower bound to avoid solutions implying the shutting-down of some turbines.

The cost function (6.11a) covers three objectives:

1. Minimizing the tracking error, i.e., $J_1(\mathbf{x}_l(k), P^{\mathrm{p}}_{\mathrm{r},l}(k)) \triangleq \|P^{\mathrm{p}}_{\mathrm{r},l}(k) - \sum_{i=1}^{n_l} x_{l,i}(k)\|_2$, where $P^{\mathrm{p}}_{\mathrm{r},l}$ is the set-point imposed by the CC.

2. Maximizing the available power, i.e., $J_2(\mathbf{u}_l(k)) \triangleq \|\mathbf{R}\ \mathbf{u}_l(k)\|_2$, where the elements of the matrix $\mathbf{R}$ are defined as

$$[\mathbf{R}]_{ij} = \begin{cases} (\tau_i + \kappa)^{-\mu}, & \text{if } i = j,\ \mu = \max(0, (P^{\mathrm{p}}_{\mathrm{av},l} - P^{\mathrm{p}}_{\mathrm{r},l})/P^{\mathrm{p}}_{\mathrm{av},l}), \\ 0, & \text{if } i \neq j. \end{cases}$$

   Here τ_i is the network resource-feeding index introduced in Section 6.2, $P^{\mathrm{p}}_{\mathrm{av},l}$ is the total available power in the subset $\mathcal{P}_l$ and $\kappa > 0$ is a small constant to avoid singularity when the turbines are not affected by wakes.
   When $P^{\mathrm{p}}_{\mathrm{r},l}$ is lower than the total available power, $J_1 = 0$ can be achieved with different power contributions from each turbine. This degree-of-freedom can be used to maximize the available power and thus the power reserve. Inspired by the backward scheme presented in [140], here a simpler approach is proposed based on penalizing the contributions of the most upstream turbines. The idea consists in reducing the contribution of the upstream turbines to reduce the wind speed deficits faced by the downstream turbine.
   As the power demand $P^{\mathrm{p}}_{\mathrm{r},l}$ is close to the available power, the backward distribution may not be effective. In order to mitigate this issue, the exponent μ ($0 \leq \mu \leq 1$), defined as the ratio between the power reserve and the available power, is reduced. Thus, in circumstance of high power demands, all turbines contribute with the same power, whereas, for higher derating operations, the backward distribution is used.

3. Limiting fast variations of the control inputs to smooth the operation and avoid possible damage on the turbine, $J_3(\mathbf{u}_l(k)) \triangleq \|\mathbf{u}_l(k) - \mathbf{u}_l(k-1)\|_2$.

6.3.3 Central Controller (CC)

The aim of the CC is to ensure the entire wind farm delivers the power P_{dem} required by the TSO. To this end, the CC receives, from each PLC, information about the total generated power $P^{\mathrm{p}}_{\mathrm{w},l}$ and the total available power $P^{\mathrm{p}}_{\mathrm{av},l}$ corresponding to the partition, and then produces a set of power references for each subset $P^{\mathrm{p}}_{\mathrm{r},l}$.

As a consequence of the partitioning procedure, all turbine subsets can be considered uncoupled. Moreover, in order to keep the controller simple, the dynamic response of each partition can be described by a first-order system representing an aggregated wind turbine as follows:

$$\dot{P}^{\mathrm{p}}_{\mathrm{w},l} = -\frac{1}{\eta_l}(P^{\mathrm{p}}_{\mathrm{w},l} - P^{\mathrm{p}}_{\mathrm{r},l}),$$

where η_l is a time constant that depends on the number of turbines in $\mathcal{P}_l$ and the PLC. The CC relies on an MPC strategy based on the following optimization problem:

$$\underset{\mathbf{u}_{\mathrm{p}}(k)}{\text{minimize}} \quad \sum_{k=1}^{H_p-1} \|\mathbf{Q}\,\mathbf{x}_{\mathrm{p}}(k)\|_2 + \|\mathbf{S}\,(\mathbf{u}_{\mathrm{p}}(k) - \mathbf{u}_{\mathrm{p}}(k-1))\|_2 \tag{6.12a}$$

$$\text{subject to} \quad \mathbf{x}_{\mathrm{p}}(k+j+1|k) = \mathbf{E}_d\mathbf{x}_{\mathrm{p}}(k+j|k) + \mathbf{F}_d\mathbf{u}_{\mathrm{p}}(k+j|k) + \mathbf{G}_d P_{\mathrm{dem}}(k+j|k), \tag{6.12b}$$

$$\mathbf{P}^{\mathrm{p}}_{\mathrm{min}} \leq \mathbf{u}_{\mathrm{p}}(k+j) \leq \mathbf{P}^{\mathrm{p}}_{\mathrm{av}}, \tag{6.12c}$$

with $k \in \mathbb{N}$, $j \in \{0, \ldots, H_{\mathrm{p}}-1\}$, and H_{p} the prediction horizon. As for the PLC, (6.12b) corresponds to the discrete version of the following approximated dynamic model of the entire wind farm:

$$\dot{\mathbf{x}}_{\mathrm{p}}(t) = \mathbf{E}\,\mathbf{x}_{\mathrm{p}}(t) + \mathbf{F}\,\mathbf{u}_{\mathrm{p}}(t) + \mathbf{G}\,P_{\mathrm{dem}}(t), \tag{6.13}$$

where

$$\mathbf{x}_{\mathrm{p}} = \begin{bmatrix} P^{\mathrm{p}}_{\mathrm{w},1} & \ldots & P^{\mathrm{p}}_{\mathrm{w},m}, & \xi \end{bmatrix}^T,$$

$$\xi = (P_{\mathrm{dem}} - \sum_{i=1}^{m} P^{\mathrm{p}}_{\mathrm{w},i}),$$

$$\mathbf{u}_{\mathrm{p}} = \begin{bmatrix} P^{\mathrm{p}}_{\mathrm{r},1} & \ldots & P^{\mathrm{p}}_{\mathrm{r},m} \end{bmatrix}^T,$$

$$\mathbf{E} = \begin{bmatrix} -1/\eta_1 & 0 & \ldots & 0 \\ 0 & \ddots & \vdots & \vdots \\ \vdots & & -1/\eta_m & \vdots \\ -1 & \ldots & -1 & 0 \end{bmatrix}, \qquad \mathbf{F} = \begin{bmatrix} 1/\eta_1 & 0 & \ldots \\ 0 & \ddots & \vdots \\ \vdots & & 1/\eta_m \\ 0 & \ldots & 0 \end{bmatrix}, \qquad \mathbf{G} = \begin{bmatrix} 0 \\ \vdots \\ 0 \\ 1 \end{bmatrix}.$$

Constraint (6.12c) ensures the power references remain within the operating limits given by the minimum power

$$\mathbf{P}^{\mathrm{p}}_{\mathrm{min}} = \begin{bmatrix} n_1 P_{\mathrm{min}} & \ldots & n_m P_{\mathrm{min}} \end{bmatrix}^T$$

to avoid shutting-down partitions and the available power defined as

$$\mathbf{P}_{\text{av}}^{\text{p}} = \begin{bmatrix} P_{\text{av},1}^{\text{p}} & \cdots & P_{\text{av},m}^{\text{p}} \end{bmatrix}^T,$$

where $P_{\text{av},l}^{\text{p}} = \sum_{i \in \mathcal{P}_l} P_{\text{av},i}$.

In the cost function (6.12a) is the sum of two objectives, the first is included to minimize the error in the tracking of the power demand. Therefore, the matrix $\mathbf{Q} = \text{diag}(0, \ldots, 0, Q_\xi)$ penalizes only the integral of tracking error. The second objectives is related to the smooth operation and, the matrix $\mathbf{S}$ penalizes the rate of variation of the power references.

6.4 Case Study

The proposed partitioning approach and control strategy were tested for a wind farm of 210 MW rated power with 42 benchmark NREL-5MW wind turbines spaced 630 m (i.e., 5 rotor diameters) and placed as shown in Figure 6.4. The wind field and wake effect have been simulated for the free-stream wind speed of $v_\infty = 11$ m/s using SimWindFarm [72], a MATLAB/Simulink toolbox for wind farm simulation and control. The MPC controllers were implemented with YALMIP [94] and CPLEX.

Wind farm partitioning

As mentioned in Section 6.2, the proposed partitioning approach depends on the predominant wind speed direction ϕ and is time-consuming for wind farm layout as the analyzed in this section. Therefore, the partitions were computed offline for the set of angles

$$\Phi = \{\phi = (30 \cdot i)^\circ, \quad i = 0, 1, \ldots, 11\}.$$

A justification of this selection can be found in Section 6.4.2. The partition obtained using the procedure in Section 6.2 for a wind speed direction of $\phi = 30^\circ$ is illustrated in Figure 6.4. The flow-based distribution graph $\bar{\mathcal{G}} = (\bar{\mathcal{V}}, \bar{\mathcal{E}})$ is obtained by relating each turbine in the information sharing graph $\mathcal{G}$ to an element of the flow based distribution system. The network resource feeding indices for each sink and the respective sources are given in Table 6.1.

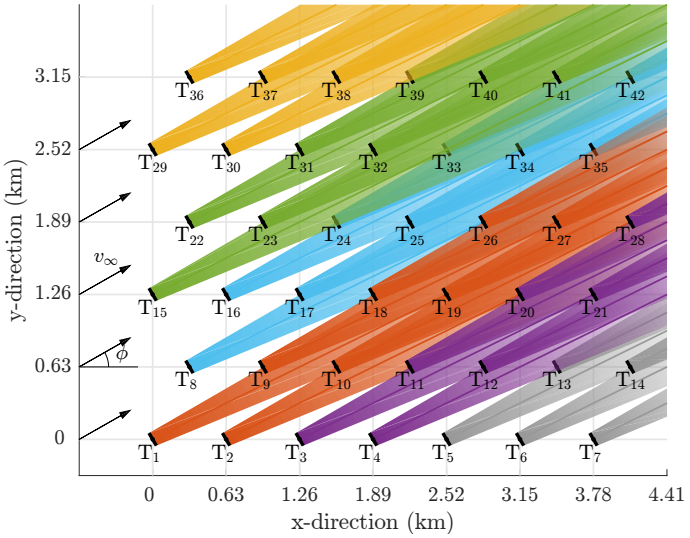

Figure 6.4: Wind farm layout and optimal partitioning for a wind speed direction of $\phi = 30^\circ$: light blue $\mathcal{P}_1$, red $\mathcal{P}_2$, green $\mathcal{P}_3$, yellow $\mathcal{P}_4$, gray $\mathcal{P}_5$, and purple $\mathcal{P}_6$.

Table 6.1: Sinks, resource feeding indexes and sources in the directed graph $\bar{\mathcal{G}}$ and their connection with the turbines in the information sharing graph $\mathcal{G}$.

T_i Sink, $i \in \mathcal{V}_{\text{si}}$	τ_i, $i \in \mathcal{V}$si	T_j Source, $j \in \mathcal{V}_{\text{so}}$
T_{37}	1	T_{29}
$T_{38}, T_{39}, T_{10}, T_{13}, T_{14}$	2	$T_{(29,30)}, T_{(22,30)}, T_{(15,22)}, T_{(4,5)}, T_{(6,7)}$
$T_{41}, T_{42}, T_{35}, T_{27}, T_{28}, T_{21}$	3	$T_{(15,16,22)}, T_{(8,15,16)}, T_{(1,8,16)}, T_{(1,2,8)}, T_{(1,2,3)}, T_{(2,3,4)}$

The result of the multi-objective optimal partitioning problem in (6.3) was determined by setting the maximum sink co-relation index $\sigma^* = 0.3$, i.e., on each subset the number of sink elements should be lower than the 30% of the total amount of sink elements. Moreover, the minimum resource feeding co-relation index β^* per subset was set at 0.5, i.e., the source elements feeding the most affected sink in each subset are at least equal to the 50% of the total sources feeding the element. In this case, the minimum number of subsets ensuring the desired values of σ^* and β^* is $m = 6$, i.e., $\mathcal{K} = \{1, \ldots, 6\}$. Thus, the maximum resource-feeding index for each subset τ_l^*, with $l \in \mathcal{K}$, along with the corresponding turbine $i \in \mathcal{V}_l$ for which $\tau_i = \tau_l^*$ is: $\tau_1^* = 3$ for $\text{T}_{(42,35)}$, $\tau_2^* = 3$ for $\text{T}_{(27)}$, $\tau_3^* = 2$ for $\text{T}_{(41,42)}$, $\tau_4^* = 2$ for T_{38}, $\tau_5^* = 2$ for $\text{T}_{(13,14)}$ and $\tau_6^* = 3$ for $\text{T}_{(21,28)}$.

The weights in (6.3a) have been set as $w_1 = 0.7$, $w_2 = 0.1$ and $w_3 = 0.2$, i.e., the highest

Table 6.2: Time constants η_l and the number of turbines in each subset $\mathcal{P}_l$ for different wind speed directions.

Wind speed direction	Partitions											
	$\mathcal{P}_1$		$\mathcal{P}_2$		$\mathcal{P}_3$		$\mathcal{P}_4$		$\mathcal{P}_5$		$\mathcal{P}_6$	
ϕ	n_1	η_1 (s)	n_2	η_2 (s)	n_3	η_3 (s)	n_4	η_4 (s)	n_5	η_5 (s)	n_6	η_6 (s)
0°	7	0.28	7	0.28	7	0.28	7	0.28	7	0.28	7	0.28
30°	9	0.30	8	0.28	8	0.26	5	0.21	5	0.18	7	0.25
60°	12	0.16	6	0.15	6	0.15	6	0.15	6	0.15	6	0.15
90°	9	0.3	9	0.3	6	0.18	6	0.18	6	0.18	6	0.18

priority is given at coupling among turbines due to the wake effect. Meanwhile, the lower priority is set for the second objective f_2 since it ensures a unique solution when there is no wake interaction among the turbines. The balance of the number of turbines at each partition is only ensured by the third objective function f_3 minimizing the difference of the number of turbines belonging to different partitions. It is worthwhile to note that increasing the value of w_3 at the expense of the weight w_1 might yield a different result since the difference among the numbers of turbines in the subset gets close to zero.

Control design

In order to design the MPC strategies, the time constant in (6.9) was set to $\eta = 0.125$ s. For the PLC, the sampling time used to discretize the partition model in (6.9) was set to 0.05 s, the prediction horizon to $H = 3$, and the weights in (6.11a) to $\gamma_1 = 0.5$, $\gamma_2 = 0.4$ and $\gamma_3 = 0.1$. For the CC in (6.12), the sampling time was set to 0.1 s, the prediction horizon at $H_mathcalp = 3$, and the weights to $Q_\xi = 0.8$ and $\mathbf{S} = 0.2 \cdot \mathbf{I}_6$. The time constants η_l for each partition $l \in \mathcal{K}$ are given in Table 6.2. As the number of turbines in each subsets is different, the time constants η_l needed to approximate the dynamics of each subset are also different.

In order to highlight the effect of redistributing the power contribution of each wind turbine in the partition, in all simulations, for all $t < t_0 = 50$ s the weight on the control input in (6.11) is selected as $\mathbf{R} = \mathbf{I}_{n_l}$, i.e., equal contribution is required for every turbine, whereas, for all $t \geq t_0$ the contribution are distributed as discussed in Section 6.3.

6.4.1 Test 1: Power Regulation

First, the proposed control strategy was evaluated in the case of a predominant wind speed direction of $\phi = 30^{\circ}$ and a power demanded by the TSO of $P_{\text{dem}} = 60$ MW. Hence, the wind farm operates in derated mode. The total available power $P_{\text{av,tot}}$ is higher (about 53%) . The partitioning in this case results in the following subsets:

$$\mathcal{P}_1 = \{8, 16, 17, 24, 25, 33, 34, 35, 42\},$$
$$\mathcal{P}_2 = \{1, 2, 9, 10, 18, 19, 26, 27\},$$
$$\mathcal{P}_3 = \{15, 22, 23, 31, 32, 39, 40, 41\},$$
$$\mathcal{P}_4 = \{29, 30, 36, 37, 38\},$$
$$\mathcal{P}_5 = \{5, 6, 7, 13, 14\},$$
$$\mathcal{P}_6 = \{3, 4, 11, 12, 20, 21, 28\}.$$

Figure 6.4 illustrates the partitioning and the wake effect.

Figure 6.5a shows the total power generated $P_{\text{w,tot}}$ (black line), the set-point P_{dem} (gray line) and the total available power $P_{\text{av,tot}}$ (blue line). The redistribution of the power contribution starts to affect the available power only after $t = t_0 + t$, where $t \approx 60$ s is the time the wind takes to travel from one turbine to the next downstream one [31]. Comparing the initial and final values of $P_{\text{av,tot}}$, it can be observed that the power contributions imposed by each PLC are capable of increasing the power reserve with about 2.7% (from 167.5 MW at $t = t_0$ to 172 MW at $t = 600$ s) without affecting the power demand tracking.

Figure 6.5b and Figure 6.5c show the available and generated powers, $P^{\text{p}}_{\text{av},l}$ and $P^{\text{p}}_{\text{w},l}$ respectively, for each subset. It can be observed that Subsets $\mathcal{P}_4$ and $\mathcal{P}_5$ make the higher contributions ($P^{\text{p}}_{\text{w},5} = 12.4$ MW, $P^{\text{p}}_{\text{w},4} = 11$ MW), whereas the lowest ones are observed in case of Subsets $\mathcal{P}_1$ and $\mathcal{P}_2$ ($P^{\text{p}}_{\text{w},1} = 8.5$ MW, $P^{\text{p}}_{\text{w},2} = 8.8$ MW). The remaining subsets produce $P^{\text{p}}_{\text{w},3} = P^{\text{p}}_{\text{w},6} = 9.6$ MW. In Figure 6.5b, the available power $P^{\text{p}}_{\text{av},l}$ increases in all subsets compared with the initial values, except for Subsets $\mathcal{P}_3$ showing a small reduction (close to 1.5%).

Figure 6.6 shows the power generated by each turbine in each partition. It can be observed the backward distribution of the power contribution of each turbine imposed by the PLCs in each partition. The largest contribution is done by the most downstream

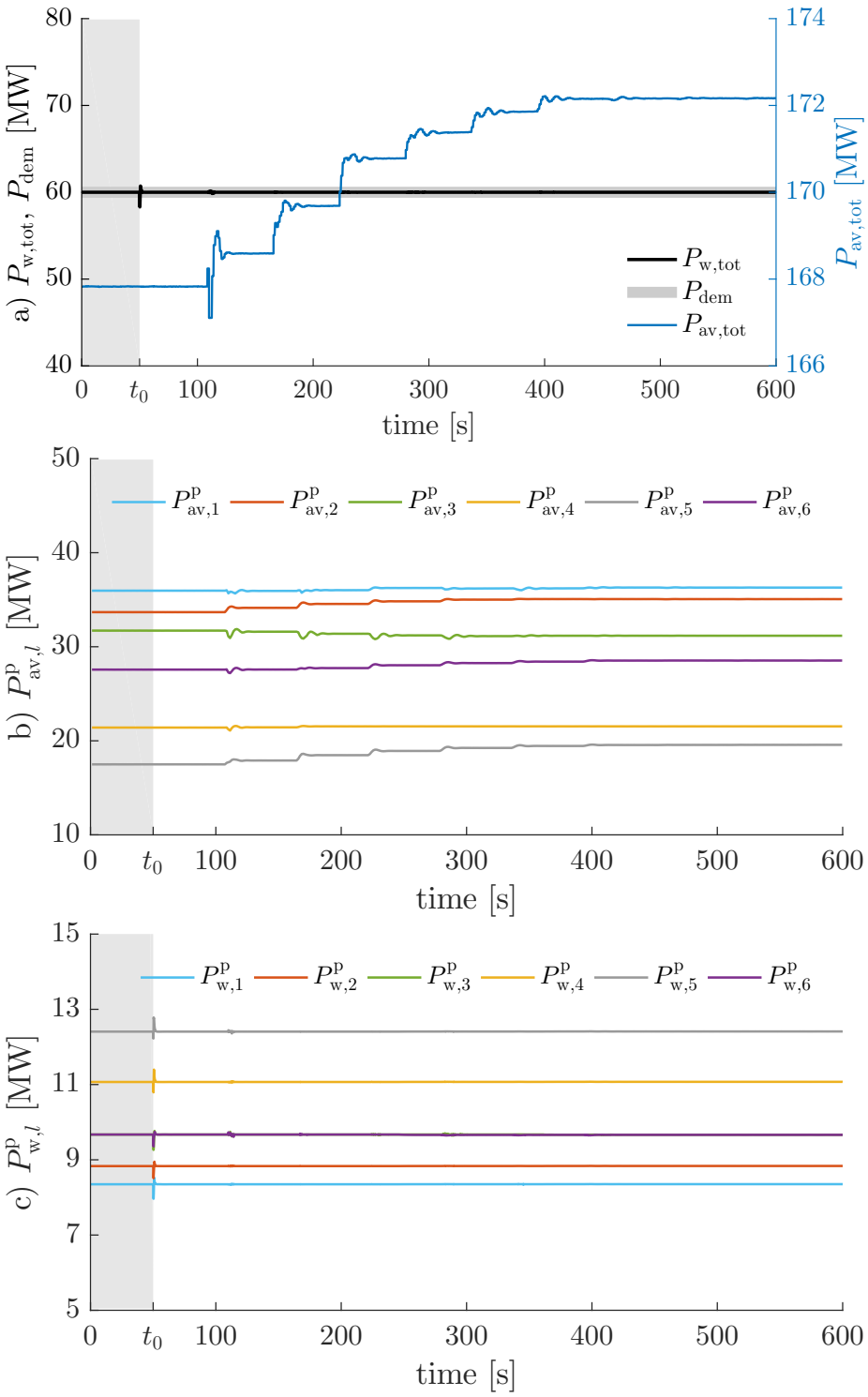

Figure 6.5: Test 1: Closed-loop response for $P_{\mathrm{dem}} = 60$ MW, $\phi = 30^{\circ}$, and $v_{\infty} = 11$ m/s. a) Total generated and available power, b) Available power for each partition, c) Generated power for each partition.

turbines whereas the most upstream ones tend to reduce the power generation. In this scheme, the power generation of some of the upstream turbines reaches the minimum value P_{min}.

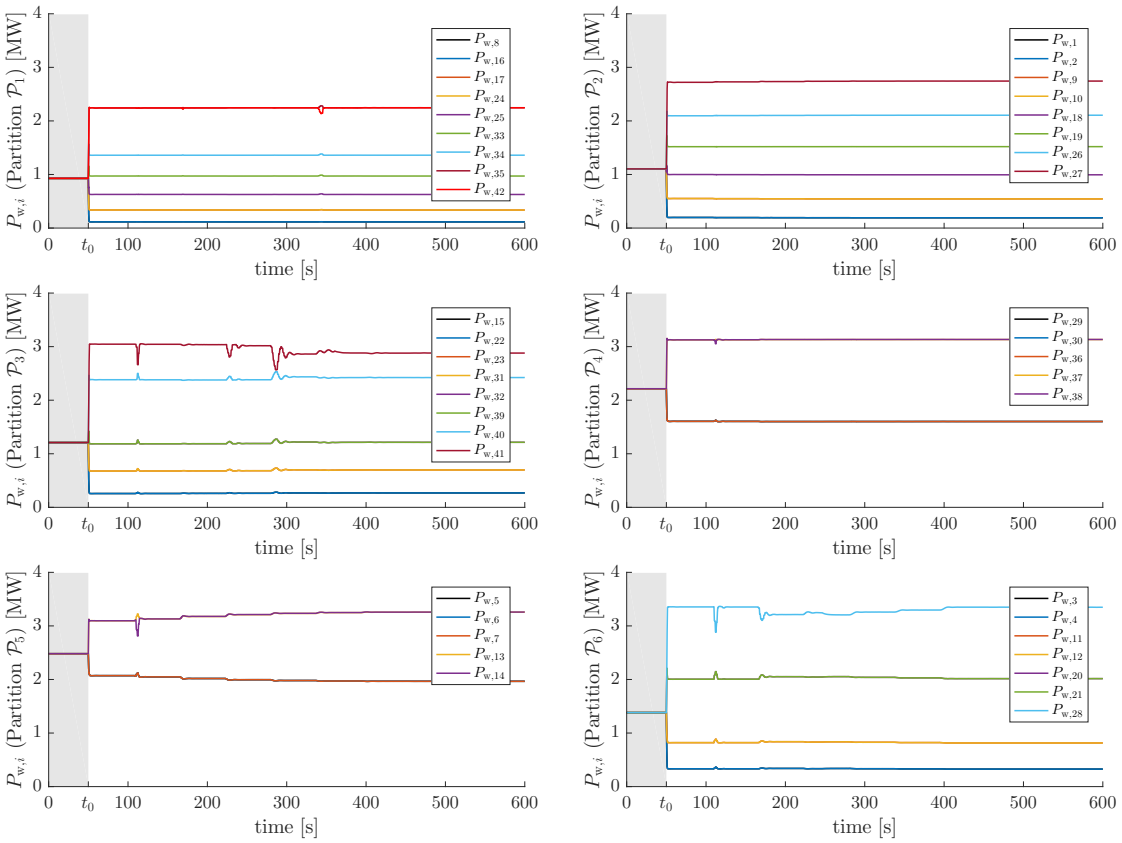

Figure 6.6: Test 1: Closed loop response for $P_{\text{dem}} = 60$ MW, $\phi = 30^{\circ}$, and $v_{\infty} = 11$ m/s. Generated power by every turbine in each partition.

Figure 6.7(a) shows the total available power for different values of power demand: $P_{\text{dem}} = 60$MW (blue line), 70MW (red line), 80MW (yellow line) and 100MW (purple line). It can be observed that, in cases of high derating operations ($P_{\text{dem}} < 80$ MW), the total available power increases compared to the values obtained with the uniform power contribution scheme ($t < t_0$). In these circumstances, the coefficient μ used in the weight $\mathbf{R}$ in (6.11a) results to be 0.64 and 0.5, respectively, and the power contribution of each turbine at each subset is determined according to the backward distribution. On the other hand, when the power demand is close to $P_{\text{av,tot}}$, μ is close to zero and the matrices $\mathbf{R}$ tend to $\mathbf{I}_{n_l}$. As a result, the set-points $P_{\text{r},i}$ are similar and every turbine in the partition

is required to contribute approximately the same power level. The motivation for using this scheme is due to the fact that when P_{dem} is high, turbines reach their maximum power limits, especially the most downstream ones, and the backward distribution stops being effective. In order to see this, Figure 6.7(b) shows the wind farm available power for different values of power demand, given as percentage of P_{greedy}, when the power among the turbines is regulated on the basis of the backward distribution. Two wind speed directions at 0 and 30 degrees are investigated. At low power demand, the backward distribution improves the available power with a better performance when the wind turbines are totally in the wakes of the upstream turbines, i.e., the wind speed is coming from 0 degrees. In fact, in this case the wake reduction has more effect on the overall wind farm power losses. However, above 82% of P_{greedy} the benefit of following the backward distribution is not significant. Going further to increase the power demand, this distribution might not be the best solution and the equal contribution from all the turbines can provide a better performance. Finally, in the case the wind farm is asked to generate more power than P_{greedy} for short time period, the distribution of the power among the turbines has not effect on the overall performance.

6.4.2 Test 2: Sensitivity to Wind Speed Directions

In this test, the proposed non-centralized control strategy is evaluated when the partitioning does not correspond to the exact predominant wind speed direction. As previously mentioned, the subset is computed off-line for a set of directions and selected from a table with an estimated wind speed direction. The aim of this test is to analyze the effect of this approximation.

Figure 6.8 presents both the total available and the total generated power for the actual predominant wind directions $\phi_{\text{real}} \in \{15^\circ, 20^\circ, 30^\circ, 40^\circ, 50^\circ\}$ while the MPC controller is designed for $\phi = 30^\circ$. It can be observed that in all cases, the controller is able to deliver the power demanded by the TSO, $P_{\text{dem}} = 60$ MW. Moreover, the backward power distribution is also capable of increasing the total available power. Nevertheless, when the direction ϕ used for the design does not correspond to the real predominant wind speed direction ϕ_{real}, some deterioration in the system response can be observed. The available power profiles in Figure 6.8b indicate that the largest increase regarding the initial values ($t < t_0$), when the backward distribution is not active, is observed in

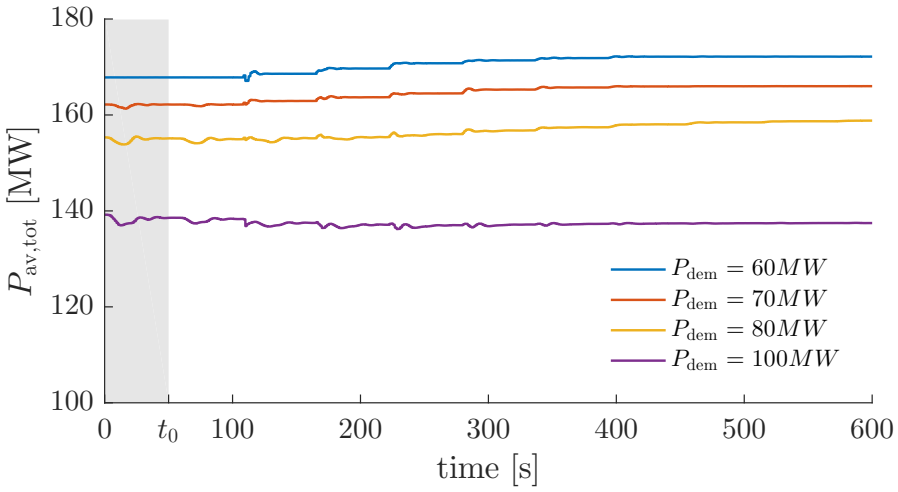

(a)

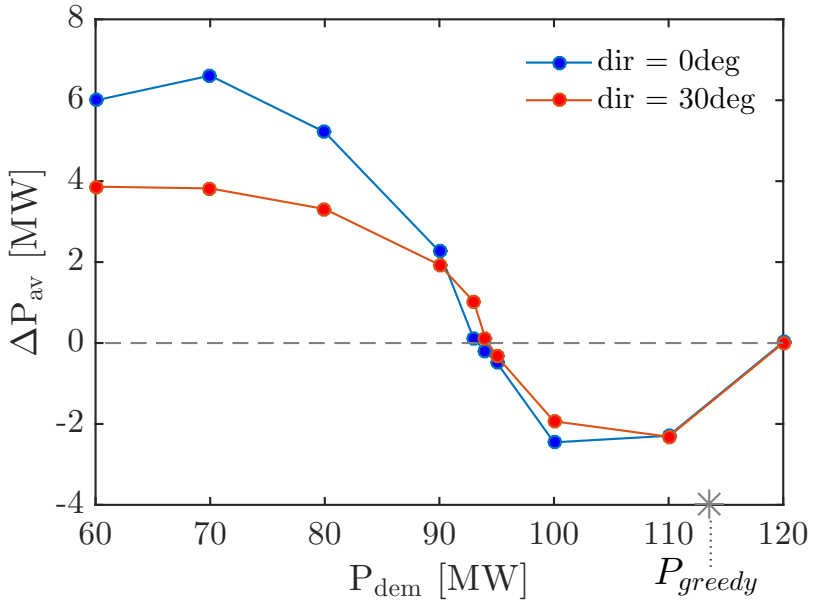

(b)

Figure 6.7: Test 1:Total available for several set-points of P_{dem}. Figure(a): Time response. Figure(b): Power improvements obtained with the backward distribution with respect to the equal distribution.

the case where the ϕ used in the controller design coincides with ϕ_{real}. Notice that the initial values are different for each ϕ_{real} as wind speed deficit depends on this angle. The increase in the available power can be compared using the expression

$$\Delta P_{\text{av}} = \frac{P_{\text{av,tot}}(t = 600\,\text{s}) - P_{\text{av,tot}}(t_0)}{P_{\text{av,tot}}(t_0)} \cdot 100\%, \tag{6.14}$$

with $P_{\text{av,tot}}(t = 600\,\text{s})$ and $P_{\text{av,tot}}(t_0)$ respectively the available power at the steady-state when the backward distribution is followed and the available power when the turbines provide the same power. Figure 6.8c shows the values of ΔP_{av} corresponding to the aforementioned cases.

The previous analysis can be repeated to cover the entire 360° range and to propose a set of sectors in which a controller designed for a given direction will work properly also for different wind direction belonging to the same sector. This approximation avoids the problem of changing the controllers for any change of wind speed direction and provides a more robust control strategy. Table 6.3 lists the directions used to compute the subsets and the sectors in which the corresponding controllers are valid. Here, the entire 360° range was divided in equal sectors. If a wind speed history of the farm site is available, the identification of the sectors in Table 6.3 can be defined using the corresponding wind rose information. In fact, if the specific distribution of the wind speed direction is known, then the partitions (and the size of each angle sector) can be updated according to the frequency of the wind direction.

6.4.3 Test 3: Comparison between Non-centralized and Centralized Control Approaches

One of the aims of proposing a non-centralized control approach is to reduce the computation time. In order to evaluate this point, in this section, the proposed scheme is compared with a centralized control scheme. The simulations were performed for a predominant wind speed direction of 30° and for three different partition schemes: $m = 4, 5, 6$. The centralized control scheme corresponds to the PLC with one partition. The total generated and the total available power for all cases can be seen in Figure 6.9. Clearly, the best performance is achieved with the centralized scheme, which has more information but also requires more computation time. Nevertheless, it can be observed that the non-centralized schemes are able to achieve values of total available power close

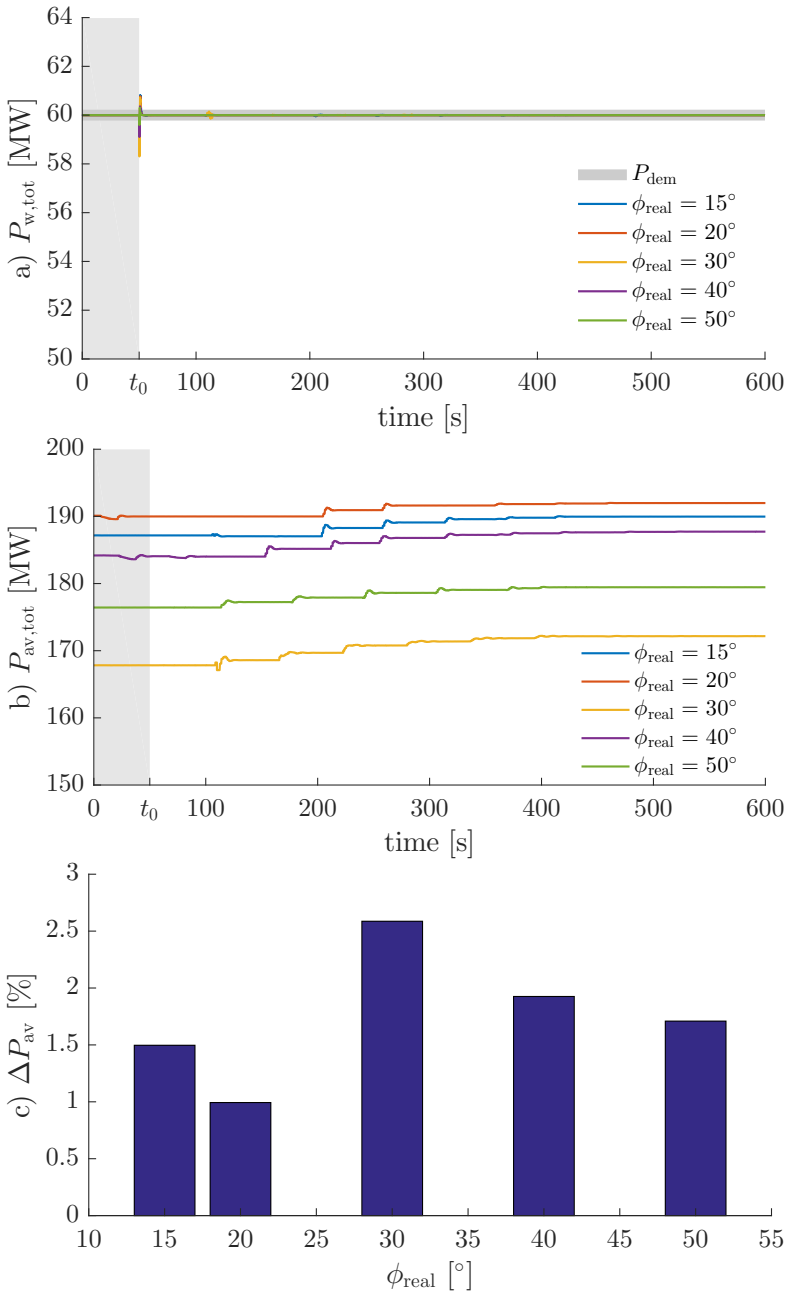

Figure 6.8: Test 2: Closed-loop response when the controller is based on a wind speed direction of 30° but the real direction is ϕ_{real}. a) Total generated power, b) Total available power. c) Total available power increment (6.14).

Table 6.3: Test 2: Angle ϕ used in partitioning and the sectors in which the controller performs properly.

Design angle ϕ [°]	Validity sector [°]
0	$-10 \leq \phi \leq 10$
30	$15 \leq \phi \leq 50$
60	$55 \leq \phi \leq 80$
90	$85 \leq \phi \leq 100$
120	$105 \leq \phi \leq 140$
150	$145 \leq \phi \leq 170$
180	$175 \leq \phi \leq 190$
210	$195 \leq \phi \leq 230$
240	$235 \leq \phi \leq 260$
270	$265 \leq \phi \leq 280$
300	$285 \leq \phi \leq 320$
330	$325 \leq \phi \leq 350$

to the centralized option. The increase in the available power ΔP_{av} (6.14) results in 0.6% for the case $m = 4$ (blue line) and in 2.6% for the case $m = 6$ (yellow line), which is close to the centralized values.

With the aim of comparison, Table 6.4 lists computation times, total available power and the increase in the power reserve. The computation times were determined using a computer with an Intel i7 processor, 8 GB of RAM running Windows 10. The first and second rows in Table 6.4 present the time the solver needs to find the solution of the optimization problems (6.12), (6.8). Notice that in the non-centralized cases, the solver times for local controllers correspond to the worst case (partitions with the highest number of turbines). As the CC and each PLC run in parallel (on different computers), the estimation of the total solver time must be taken as the largest time value, which is indicated as $t_{s,\text{tot}} = \max\left(\max\left(t_s(\text{PLC})_i\right), t_s(\text{CC})\right)$, with $i \in \mathcal{K}$ and $t_s(\text{CC})$ the solver time for the central controller. The computation improvement between the centralized case and the case of 6 partitions can be evaluated as

$$\Delta t_s = \frac{t_s(\text{CMPC}) - t_{s,\text{tot}}}{t_s(\text{CMPC})} \cdot 100\%. \tag{6.15}$$

Therefore, the proposed scheme achieves an improvement of almost 70% of the computation time, with a similar response for the total available power.

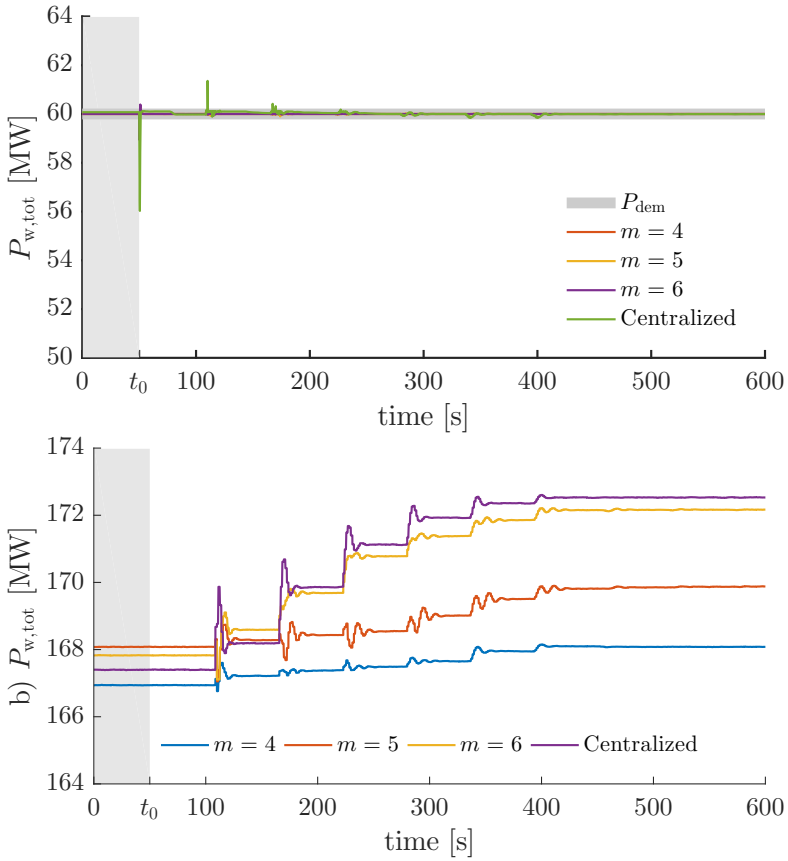

Figure 6.9: Test 3: Comparison among non-centralized schemes with several numbers of partitions m and a centralized approach. a) Total generated power. b) Total available power.

Table 6.4: Solver time for the centralized and non-centralized MPC approaches (PLC and CC) together with the percentage of improvement with respect to the centralized case and total available power at steady state.

	Centralized (CMPC)		Decentralized		
		m	4	5	6
Solver time [s]	0.1081	t_s(PLC):	0.009	0.0079	0.0046
		t_s(CC):	0.0898	0.0401	0.0328
Computational improvement (Δt_s)	0		0.18	0.63	0.7
$\Delta P_{\text{av,tot}}$ [%]	3.06		0.68	1.07	2.59

6.5 Summary

This chapter has presented a novel active power control strategy for wind farms based on non-centralized predictive control with a wake-based partitioning approach. Such novel control strategy aims to reduce the high communication and computational burden that can be an issue for guaranteeing online control of large wind farms. To this end, a partitioning algorithm, stated as a mixed-integer multi-objective problem, has been designed to divide the wind farm into smaller subsets of turbines such that the amount of information shared with the central control could be reduced and the overall system resiliency is improved. The subsets are identified such that the couplings due to the wake effects among the turbines within different partitions are minimized. Therefore, each partition is considered as an independent unit controlled by a local predictive controller defined to solve a multi-objective optimal control problem in order to provide the power profile set by the central controller and optimally regulate the power set-points among the turbines such that the overall available power is improved.

The results show that the non-centralized approach reduces consistently the computational costs with respect to a fully centralized strategy, allowing the proposed controller to be suitable for real-time applications. Moreover, the drawback due to the reduction of the information sharing only slightly affects the overall performance of the wind farm generation. In fact, the results show that the decreasing of the available power is lower than 1% respect to the centralized case and, increasing the number of partitions, the available power converges to the centralized case.

Part IV

General Conclusion and Remarks

Chapter 7

Conclusions

In this doctoral thesis, novel advanced control strategies for the design of optimization-based wind farm controllers have been presented. In the first part of this dissertation, an identification of the expectations and the major issues nowadays related to wind farm operation, as well as new opportunities to improve wind generation and participation in electrical grid support were discussed. Then, as *first contribution* of this thesis, these main challenges have been translated into control objectives to be addressed by wind farm and wind turbine controllers to improve the existing control systems while optimizing the wind farm operation whenever possible. The second part of this thesis was devoted to design the aforementioned wind farm controllers in a centralized manner considering wind farms with relatively low number of turbines to validate the proposed control approaches. As *second contribution* of this dissertation, model-based control strategies formulated according to the receding horizon idea have been stated to solve multi-objectives optimization problems to basically optimize the automatic generation of the wind farm while considering operational limits and constraints. Specifically, in order to ensure the priority among the objective functions such that the main objective of following a power profile imposed by the electrical grid treated as the most important one, the lexicographic minimizers procedure was proposed in Chapter 4. The resulting optimal regulation of the power set-points among the turbines was used to set the elements of a weighting vector used to ensure the minimization of the overall wake effect when designing a multi-objective MPC as presented in Chapter 5. In that chapter, also the electrical cable losses in the inter-array collection grid have been considered in the minimization problem. Therefore, a trade-off between electrical power and wake mini-

mizations has been found to provide both the objectives by properly assigning specific weights at each objective. As *third contribution* of this thesis, a new power distribution algorithm has been presented in order to exploit the degree-of-freedom for distributing the power among the turbines in the case of de-loading operation modes, such that the capability of wind farm to provide frequency support was improved. The latter approach has been compared with other commonly used regulation approaches to highlight its benefits in terms of power reserve maximization. In order to cope with the limitations of centralized control that requires full-information exchange among the turbines, Part III was devoted to present a novel non-centralized control approach. The main issue that has been addressed in this part of the thesis is the high computational burden caused by the large number of turbines that nowadays are placed in a wind farm, which affects the reliability and robustness of the centralized control architecture. As *fourth contribution* of this thesis, a partitioning approach considering the dynamic variation of the couplings among the turbines due to the wake effect is presented to divide the turbines in subsets. These were identified such that the couplings due to the wake effects among the turbines within different partitions were minimized. Each subset was, therefore, considered as an independent unit controlled by local controllers in a decentralized manner as presented in Chapter 6. It has been shown that the non-centralized approach has reduced consistently the computational costs, allowing the proposed controller to be suitable for real-time applications.

7.1 Answering the Research Questions

The main conclusions of the arguments addressed through this thesis can be summarized by answering at the research questions presented in Chapter 2.

Q1: Which kind of wind farm controllers can be designed to provide grid support?

Closed-loop wind farm controllers are nowadays the best solution to provide a robust control that can adapt the control actions according to the changing of wind farm operation, atmospheric conditions and fast variation of grid requirements. Finding a trade-off between robustness and performance was the main criterion followed to design wind

farm controllers able to enhance the participation of wind farms in grid support. In this thesis, the proposed controllers were based on simplified models describing the wind turbine and wind farm dynamics, however accurate enough to guarantee proper control performance while keeping the computational time within the time-span (approximately 10 ms - 2 s) for ensuring grid support. The results have shown that for all the proposed control strategies, it has been possible to follow the fast variation of the power demanded by the grid while, whenever possible, ensuring other control objectives to improve the power reserve. In particular, for the case of full-waked conditions an improvement of about 8% resulted with respect to the case where no maximization of capacity reserve is considered.

Q2: How the operation of a wind turbine can influence the power delivered by a wind farm?

Aerodynamics interactions among the wind turbines in a wind farm affect the maximum power that a wind turbine can generate. Hence, considering them when optimizing the wind farm production is crucial. In this circumstance, greedy control that extracts the maximum power from each turbine (MPPT operation), no longer guarantees the maximization of power generation at the farm level. Therefore, advanced control strategies have been proposed in this thesis to properly regulate the power set-points for the turbines, they must be regulated by a higher control level that ensures the wind farm provides the aforementioned grid requirements. In particular, when a wind turbine is required to track a deloaded power reference to sustain the grid, e.g., for frequency support purposes or power curtailment constraints, the linear programming problem presented in Chapter 3 to optimally regulate the power among the turbines has resulted to improve the overall power reserve with respect to the more common proportional distribution and equal distribution [76]. It seeks to distribute the power contribution of each turbine in order to reduce the wind speed deficits caused by wake effects by prioritizing the power contribution of the most downstream turbines and thus attenuating the wake disturbances. As a result, with this approach the frequency, dropped from the nominal value for some imbalances in the grid, can be driven back to an higher steady-state value.

Q3: Which wind farm dynamics are needed to be considered when designing a wind farm model such that a control strategy can be used in an online closed-loop framework?

Modeling assumptions are necessary to make the wind farm controller suitable for on-line control. In Chapter 4 it has been shown that in order to design a predictive controller, a surrogate steady-state model of the wind farm dynamics is required. To keep the computational costs and the complexity of the optimal control problem formulation low, a first-order system has been used to describe the power response of a wind turbine. With the aim of ensuring power reference tracking, the dynamics of the wind farm power generation could be described as the sum over the power generated by the turbines. In fact, since the automatic generation control requires to follow the fast variation of power demand (about within 1-2 seconds), the slower and highly non-linear dynamics of the wake effects could be neglected by avoiding the need of including a full wake model in the MPC formulation. It can be concluded that, if for this application there was not need of a wake model, it could be indispensable in other cases, for instance, when the yaw control settings is included in the optimal formulation. However, this latter case has been only partially treated during this doctoral study and partial results are presented in Appendix B.

Q4: Which control objective should be stated in an optimization-based control for wind farm to provide frequency support?

Over this thesis, three main objectives besides following the power reference imposed by the grid have been considered:

1. Maximization of power reserve.
2. Minimization of wind speed deficits due to the wake effect.
3. Minimization of electrical cable-losses within the wind farm.

When solving a multi-objective optimization problem, different regulations of the control signals among the turbines could be found according to the priority associated with each objective. In Chapter 4, the strict priority between the minimization of tracking error and maximization of power reserve has been ensured by solving the problem with

the lexicographic programming method. Therefore, the optimization problem has been stated as a set of optimization problems, such that the two objectives are considered separately, thus treating the non-convex nature of the overall cost function. In Chapter 5, also the minimization of cable-losses have been included in the MPC formulation. However, the priority among the latter objective and the minimization of wake effect is influenced by dynamic external factors, such as atmospheric conditions and the level of the power demanded by the grid. Therefore, the prioritization among the objectives has been dynamically adapted by properly tuning the weighting terms in the MPC formulation.

Q5: How the computational burden can be reduced while ensuring the reliability of the controller when the number of turbines in the wind farm becomes larger?

Once the wind farm operations have been concerned according to the answer to key research question Q4, then in Chapter 6 the constrained optimization problem has been solved in a non-centralized manner. The main reason of doing so has been to provide a wind farm control strategy able to provide real-time control when the large number of turbines made difficult to control with the centralized approach presented over this thesis. It resulted that the reduction of information sharing among the turbines in the non-centralized approach has decreased the overall performance with respect to the centralized scheme but also has decreased the computational time for more than 70%. Nevertheless, it can be observed that the non-centralized scheme has been able to achieve values of total available power close to the centralized counterpart.

Q6: How can optimally distributed the wind controllers? Is a centralized approach the best solution?

In this thesis, for dividing the wind farm into smaller subsets a partitioning algorithm, which could lead to better control the wind farm in order to mitigate the overall wake effect, has been presented. A mixed-integer multi-objective problem has been designed such that the couplings among the turbines due to the wake effects within different partitions were minimized. Therefore, the communication links among the turbines belonging from different subsets were weak, thus each partition could be treated as an independent unit. In order to keep the time convergence of the partitioning problem low, the dynamic

variations of the couplings with the wake propagation have been estimated in the partitioning formulation based on the *Jensen's wake model*. Moreover, an heuristic strategy to determine the optimal number of subsets presented for a drinking water network in [15] has been adapted to wind farms such that the performance of the controller could be maintained as close as possible to the centralized case.

Q7: How the non-centralized control approach influences the overall performance of controlling a wind farm with respect the centralized approach?

In the hierarchical non-centralized architecture, two control levels have been identified: 1) the PLC, each partition has been considered as an independent unit controlled by a local MPC; 2) the CC, designed to ensure the grid requirements. Therefore, each subset at the CC level has been treated as an aggregated wind turbine drastically reducing the information to be shared with the central controller. Proportionally to the increasing of the number of subsets, i.e., the number of aggregated turbines to optimally regulate, the performance of the non-centralized approach has been increased. Driven by a trade-off between computational time and performance (measured as the capability to improve the overall available power), the non-centralized controller showed a reduction of the performance for almost 1% with respect to the centralized case but, increasing the number of partitions, the performance converges to the centralized case.

7.2 Directions for Future Research

There are still many aspects and open problems regarding the closed-loop dynamical wind farm control that need to be investigated. This thesis has made efforts to show novel approaches in the design of on-line optimization-based wind farm controllers, either formulating the well known MPC approach or fully designing novel control algorithms for the wind farm control purposes. In the following, some suggested ideas for future directions are given:

- The MPC strategy presented in Chapter 4 could be improved developing a wind speed estimator that can predict the effect of the optimal wind turbine power set-points on the available power some steps ahead, required by the wake to reach the

downstream turbine. Predicting the wake effect could improve the performance on maximizing the overall power reserve, however the practical implementation of such wind estimator is not trivial. Linearized wake models have resulted to not work properly [21], thus the use of non-linear models should be considered. Moreover, the issue of designing an MPC strategy managing two different time scales should be considered, since it has to predict the fast dynamics of the wind turbine response as well as the slow dynamics of the wake propagation.

- The use of Kalman filters or similar methodologies to help addressing some of model error or external disturbance could be considered in the closed-loop control.

- Eventually, some of the presented control tools could be employed to address another important issue in wind farm control: the fatigue reduction. Both wind turbine and wind farm controllers could be adapted in order to integrate the system mechanical stress reduction.

- The partitions used for designing the non-centralized MPC in Chapter 6 have been obtained considering that the wind speed direction can be considered constant within 10 min. It is still an open problem to proof the on-line feasibility of the proposed control approach when considering more realistic environments and operations. In the case of quicker variation of the wind speed direction, faster updating of the sub-sets should be ensured. Therefore, further work should be done to synchronize the partitioning problem with the time horizon within the new set of optimal control actions is provided, for instance the use of a look-up table could neglect such a problem.

- Distributed controllers can be designed for controlling wind farms, in this case the main issue is how treating the problem constraints. The wind turbines need to share information with the drawback of increasing in the number of required direct communications among them. The partitioning algorithm in 6.8 could be used to reduce the number of coupled constraints, therefore the computational burden, in the same way as done in the presented non-centralized approach when system constraints are not active. For the distributed case, the grid requirements should be directly sent to each subsets by neglecting the need of a central unit. This

will increase the system resiliency, however a detailed estimation of the performance should be done with respect to the centralized and non-centralized control approaches.

- As the var capacity of a wind turbine converter, i.e., the capability of providing reactive power, depends on active power generated by the turbines, the MPC could be stated to solve an active and reactive power optimization problems. Beyond tracking and power reserve maximization, adding an extra cost function at the multi-objective MPC in Chapter 5, the wind farm controller could also provide minimization of voltage variation at the PCC such as suddenly manage a fault event. Preliminary results have been already obtained during the last part of this doctoral program, but further work is required on this topic.

- Another interesting aspect is to explore the economic profits due to the participation of wind farms in balancing market. It is clear that in the case the wind generation is not high, the best economic compensation is obtained by maximizing the generation of the wind farm. However, for those countries where RE generation is significant, the participation in primary market is, or will be, mandatory. An additional cost function taking into account the economic benefits to optimally regulate the wind farm power generation could be included into the MPC formulation.

Appendix A

PALM Simulation Model

The true wind farm is replaced by the high-fidelity "PArallelized Large-eddy simulation Model (PALM)" [99], this is programmed in FORTRAN, while almost all academic wind farm control algorithms are implemented in MATLAB or Python. One of the contributions of this thesis is the development of the PALM Supervisory Controller, which provides a communication interface between PALM and wind farm controllers implemented in MATLAB. This allows the straight-forward evaluation of such control algorithms in a high-fidelity simulation environment. The PArallelized large-eddy simulation model PALM is a meteorological model for atmospheric and oceanic boundary-layer flows. It has been developed as a turbulence resolving large-eddy simulation (LES) model and is open source, available in the public domain [75]. In the LES approach, only the large eddies are simulated due to spatially filtering the Navier-Stokes equations. The dynamic influence of the small turbulent scales are consequently not resolved, but their influence is accounted for with a so called subgrid model. PALM is based on the unsteady, filtered, incompressible Navier-Stokes equations and the subgrid-scale turbulent kinetic energy (SGS-TKE) model [39]. PALM can simulate the effect of the Coriolis forces and if non-cyclic boundary conditions are imposed, it can generate time dependent turbulent inflow data by using a turbulence recycling method. Two different turbine models are available in PALM. The ADM model and the rotating actuator disk model [23]. Both these turbine models can be utilized with the PALM Supervisory Controller that is a MATLAB/FORTRAN interface allowing for communicating with a wind farm controller implemented in MATLAB. This communication infrastructure is used for evaluating the

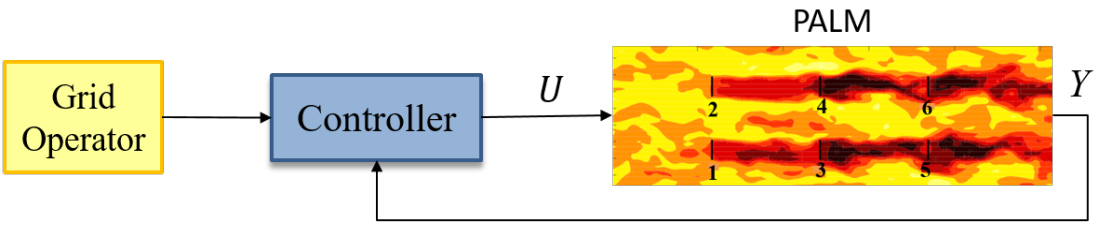

Figure A.1: Block scheme of the control strategy for yaw γ and thrust coefficient C'_T optimization.

set of control signals $\mathcal{U}$ by using measurements from PALM $\mathcal{Y}$. According to the turbine model used, the control signals are

- PALM+ADM
  - $\mathcal{Y}$: wind speed v_i, power generated $P_{\mathrm{g},i}$, axial force $F_{t,i}$
  - $\mathcal{U}$: thrust coefficient C'_{T_i}, yaw angle γ_i^*
- PALM+ADM-R
  - $\mathcal{Y}$: wind speed v_i, power generated $P_{\mathrm{g},i}$, axial force $F_{t,i}$, generator speed $\omega_{g,i}$
  - $\mathcal{U}$: generator torque $T_{g,i}$, yaw angle γ_i^*, pitch angle β_i^*

For the present work the PALM-ADM option is employed.

Appendix B

A Constrained Wind Farm Controller: Yaw Angle Optimization

As part of this doctoral thesis a collaborative work was carried out at the Delft Center for Systems and Control. Here, starting from the original idea of providing power tracking at the farm level, the author has contributed to design an MPC controller to provide: 1) minimization of the dynamical loading on a farm level by optimal regulating the power reference among the turbines for de-loading operation, and 2) optimize the yaw angle settings to maximize the possible power that can be harvested by the farm for ensuring tracking also when the power demand exceeds the available for non-yawed operation. In the literature, to the best of the author knowledge, yaw control is almost employed to maximize the power generation at the farm level [52], [21], [64], but considering time-varying yaw actuation to provide power tracking is a novelty of this work. For this reason, this appendix is devoted to summarize part of the results obtained by the collaboration with Sjoerd Boersma, Bart M. Doekemeijer and Jan-Willem van Wingerden as presented in [25]. Figure B.1 shows a block scheme of the proposed control approach. As presented in chapter chapter 4, when using PALM the dynamics of the turbines are described by the first-order response of the thrust coefficient $C'_{T,i}$, which corresponds also to the variable manipulated by the MPC controller, see 4.20. Basically, the description of the controller design is very similar to the one presented in the previous chapter Chapter 4, however an additional state vector corresponding to the vector of axial forces acting on the rotor

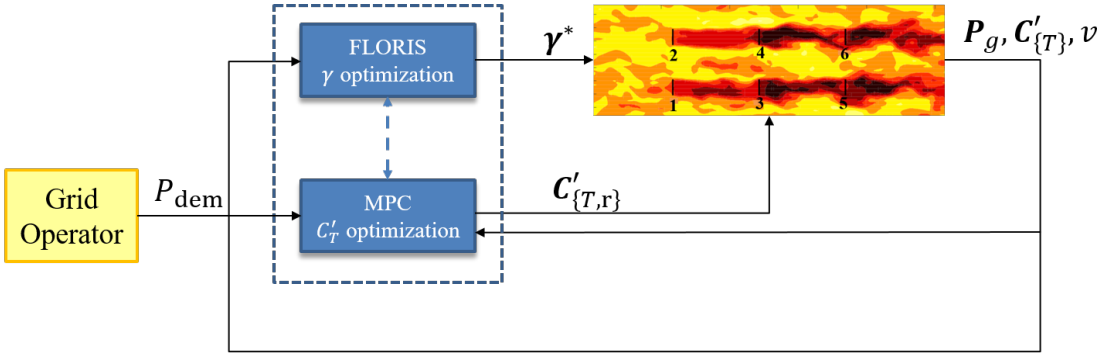

Figure B.1: Block scheme of the control strategy for yaw γ and thrust coefficient C'_T optimization. Figure adapted from [25].

turbines $\mathbf{F}_t$ is added in this work. Being,

$$F_{\text{t},i} = \frac{\pi R^2}{2} \left(v_i \cos[\gamma_i]\right)^2 C'_{T,i}. \tag{B.1}$$

According to the PALM block scheme in appendix A, the sets of measurements and control signals are respectively, $\mathcal{Y} = \{F_{\text{t},i}, P_{\text{g},i}, v_i\}$ and $\mathcal{U} = \{C'_{T,\text{r}_i}, \gamma_i^*\}$. In order to find optimal yaw settings, the FLOw Redirection and Induction in Steady-state (FLORIS) optimization tool [60] is employed, which uses the steady-state surrogate wake model presented in [**?**]. Under the assumption that the power reference is known for the upcoming 15-minutes, the optimal yaw angles are kept constant within this time-span. Nevertheless, the turbines are aligned with the mean wind direction, i.e., the yaw is kept at zero, every-time the power demand is estimated to be ensured operating in de-loading operation. Under this circumstance, the available power can be maximized by properly setting the induction factors as proposed in part II and consequently reducing the additional loading due to the yaw actuation [33]. Therefore, yaw angles different from zero are only set when the power available is below the demand to guarantee the tracking objective; in this circumstances, the optimal yaw angles γ_i^* are obtained as minimizing

$$J = -\sum_{i=1}^{n_t} P_{\text{g},i}^{ss}(\gamma_i^{ss}), \qquad \text{s.t.} \quad -25^\circ \leq \gamma_i^{ss} \leq 25^\circ, \tag{B.2}$$

being the yaw limited to avoid high loads generation and $P_{\text{g},i}^{ss}$ the power generated in steady-state conditions.

The MPC controller solves a multi-objective optimization-based problem on seconds-scale with the aim of tracking the power reference and minimizing the axial loads. That is,

$$\begin{aligned}
&\underset{\tilde{\mathbf{C}}'_{\mathbf{T},\mathrm{r}}(k)}{\text{minimize}} \quad (P_{\mathrm{dem}} - \sum_{i=1}^{n_t} P_{\mathrm{g},i})' Q (P_{\mathrm{dem}} - \sum_{i=1}^{n_t} P_{\mathrm{g},i}) + (\mathbf{F}_{\mathrm{k}} - \mathbf{F}_{\mathrm{k}-1})' S (\mathbf{F}_{\mathrm{k}} - \mathbf{F}_{\mathrm{k}-1}) \\
&\text{subject to} \\
&\quad \mathbf{x}_{(k+j+1|k)} = \mathbf{A}_d \mathbf{x}_{(k+j|k)} + \mathbf{B}_d(\gamma_0, v_0)\mathbf{C}'_{\mathbf{T},\mathrm{r}(k+j|k)} + \mathbf{B}_l P_{dem} \\
&\quad \mathbf{P}_{\mathrm{g}(k+j|k)} \leq \mathbf{P}_{\mathrm{av,k}} \\
&\quad C'_{T,\min} \leq C'_{T,\min_{(k+j|k)}} \leq C'_{T,\max}
\end{aligned} \tag{B.3}$$

with $j \in [0, H_p - 1] \cap \mathbb{Z}_{\geq 0}$, $C'_{T,\min} = 0.1$ and $C'_{T,\max} = 2$. The parameter used to set-up the PALM simulator are referred to Table 4.1. For a more detailed statement of the control approach, the reader is referred to the paper [25].

Results

The value of the weighting matrixes $Q = q \in \mathbb{R}$ and $S = s\mathbf{I}_{n_t \times n_t}$ in B.3 were found with a proper tuning process. Figure B.2 shows, for different values of $s \in \mathbb{R}$, the values of the performance index used to estimate the effect of axial force minimization for each turbine, $\Delta F_i = (F_{i,\mathrm{k}} - F_{i,\mathrm{k}-1})^2$ and $\Delta F_{\mathrm{tot}} = \sum_{i=1}^{n_t} \Delta F_i$. It can be seen that the latter, i.e., the overall axial force, decreases when the minimization of the loads is included in the objective function. However, only small improvements on this reduction can be obtained by changing the weights s. Furthermore, the increasing of s has major effect on the upstream turbines, e.g., $T1$, $T2$, $T3$, for which the dynamical loads decreases. Meanwhile, for the downstream turbines the effect of adding the loads minimization is not observed, this could be related with the highly waked wind flow faced by these turbines.

Finally, Figure B.3 shows the improvements in power tracking performance when the yaw control is activated. In this case study, the power reference signal, computed as formulated in 4.21 for $p = 0.9$, is high enough to overcome the greedy power for certain period. Under this circumstance, the optimal yaw settings were found equal to $\gamma_i^* = [-24.3\,, -24.3\,, -16.2\,, -16.2\,, 0\,, 0]$ degrees. Hence, the downstream turbines are kept non-yawed to avoid additional dynamical loads on the rotor. Top plot in Figure B.3

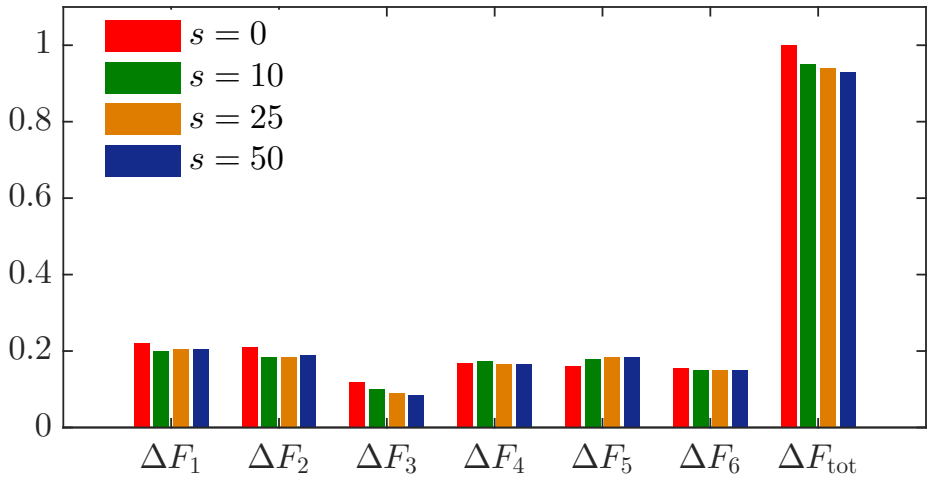

Figure B.2: Performance valued of dynamical loads variation for each turbine and for the overall wind farm. Figure adapted from [25].

shows the power demand (red dashed line), the power generated (blue line) and the power greedy (black dashed line) at the farm level for no yawed turbines case. From time $t = 300$ s to $t = 450$ s, the power reference signal cannot be ensured being below the wind farm available power. However, when the yaw control is activated (bottom plot) the power generated by the farm improves to follow the power demand.

Conclusions

In this Appendix it has been briefly described the feedback control loop extensively investigated in [25] with the aim of showing the possibility to use the additional degree-of-freedom available in the case of deloading wind farm operation to minimize the dynamical loads acting on the wind turbines. Furthermore, the possibility of improving the available power for high power generation conditions by properly setting the yaw angles of the turbines was also discussed. The proposed control strategy tested with the high fidelity simulation-environment PALM was able to ensure the fast variation of the power demanded by the grid with a MPC controller operating on a sample time of 1 s. In the case of deloading operations, it has been shown that the dynamical loads could be reduced by smoothing the backward distribution among the turbines, i.e., the controller tends to regulate the power such that the turbines are derated proportionally to their

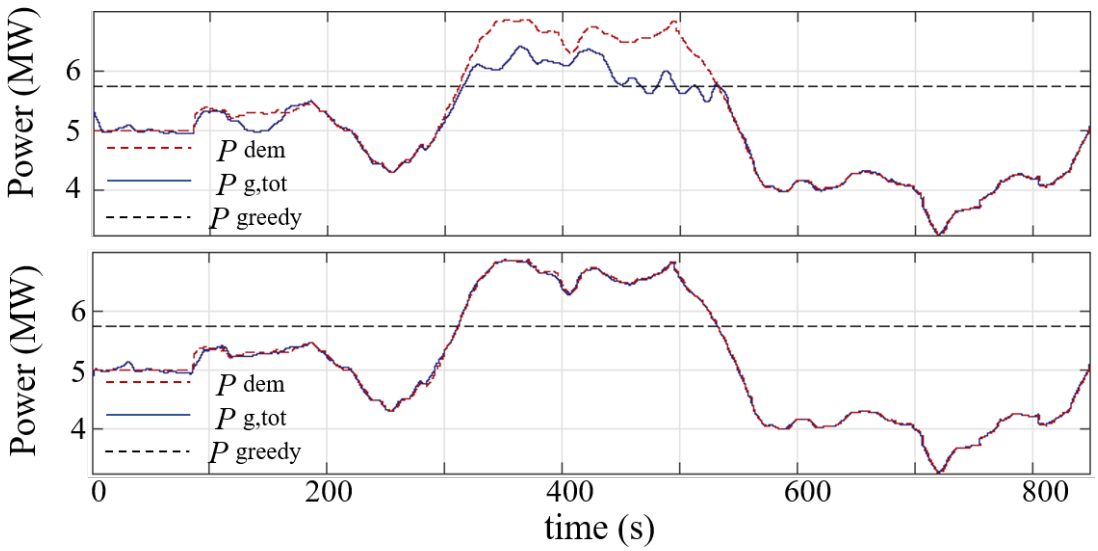

Figure B.3: Power tracking response for no-yawed $\gamma = 0$, top plot, and yawed $\gamma = \gamma^*$ conditions. Figure adapted from [25].

available power. Finally, the yaw control has shown to really be useful for improving the power tracking performance, however the assumption of knowing the power demanded by the grid 15-minute in advance could represent a critical point for such a control strategy.

References

[1] Eduardo Jose Adam and Jacinto L Marchetti. Designing and tuning robust feedforward controllers. *Computers & Chemical Engineering*, 28(9):1899–1911, 2004. [Cited on page 47]

[2] International Energy Agency. World energy outlook. 2008. [Cited on page 3]

[3] Ahmad Shabir Ahmadyar and Gregor Verbič. Control strategy for optimal participation of wind farms in primary frequency control. In *PowerTech, IEEE Eindhoven*, pages 1–6, 2015. [Cited on page 42]

[4] Ahmad Shabir Ahmadyar and Gregor Verbič. Coordinated operation strategy of wind farms for frequency control by exploring wake interaction. *IEEE Transactions on Sustainable Energy*, 8(1):230–238, 2017. [Cited on page 42]

[5] Jacob Aho, Paul Fleming, and Lucy Y Pao. Active power control of wind turbines for ancillary services: A comparison of pitch and torque control methodologies. In *American Control Conference (ACC), 2016*, pages 1407–1412. IEEE, 2016. [Cited on page 93]

[6] J Alejandro, Alicia Arce, and Carlos Bordons. Combined environmental and economic dispatch of smart grids using distributed model predictive control. *International Journal of Electrical Power & Energy Systems*, 54:65–76, 2014. [Cited on page 48]

[7] A. Ameri, A. Ounissa, C. Nichita, and A. Djamal. Power loss analysis for wind power grid integration based on weibull distribution. *Energies*, 10(4):1–16, 2017. [Cited on page 104]

[8] O. Anaya-Lara. *Wind Energy Generation: Modelling and Control*. John Wiley & Sons Ltd, 2009. [Cited on page 16]

[9] J. Annoni, C. Bay, K. Johnson, E. Dall'Anese, E. Quon, T. Kemper, and P. Fleming. A framework for autonomous wind farms: Wind direction consensus. *Wind Energy Science Discussions*, 2018:1–17, 2018. [Cited on page 128]

[10] Jennifer Annoni, Christopher Bay, Timothy Taylor, Lucy Pao, Paul Fleming, and Kathryn Johnson. Efficient optimization of large wind farms for real-time control. In *Annual American Control Conference (ACC)*, pages 6200–6205. IEEE, 2018. [Cited on pages 51, 52, 128, 129, and 130]

[11] Jennifer Annoni, Pieter MO Gebraad, Andrew K Scholbrock, Paul A Fleming, and Jan-Willem van Wingerden. Analysis of axial-induction-based wind plant control using an engineering and a high-order wind plant model. *Wind Energy*, 19(6):1135–1150, 2016. [Cited on page 36]

[12] Jennifer Annoni, Andrew Scholbrock, Matthew Churchfield, and Paul Fleming. Evaluating tilt for wind farms (i). In *American Control Conference (ACC), 2017*, 2017. [Cited on page 57]

[13] Kyriaki E Antoniadou-Plytaria, Iasonas N Kouveliotis-Lysikatos, Pavlos S Georgilakis, and Nikos D Hatziargyriou. Distributed and decentralized voltage control of smart distribution networks: Models, methods, and future research. *IEEE Transactions on smart grid*, 8(6):2999–3008, 2017. [Cited on page 50]

[14] Stefanos Baros and Marija D Ilić. Distributed torque control of deloaded wind DFIGs for wind farm power output regulation. *IEEE Transactions on Power Systems*, 32(6):4590–4599, 2017. [Cited on page 128]

[15] Julian Barreiro-Gomez. Partitioning for large-scale systems: Sequential dmpc design. In *The Role of Population Games in the Design of Optimization-Based Controllers*, pages 163–178. Springer, 2019. [Cited on pages 47, 49, 80, 108, 129, 133, 134, and 162]

[16] Julian Barreiro-Gomez, Carlos Ocampo-Martinez, Fernando D. Bianchi, and Nicanor Quijano. Data-driven decentralized algorithm for wind farm control with population-games assistance. *Energies*, 12(6), 2019. [Cited on page 39]

[17] Julian Barreiro-Gomez, Carlos Ocampo-Martinez, and Nicanor Quijano. Time-varying partitioning for predictive control design: Density-games approach. *Journal of Process Control*, 75:1 – 14, 2019. [Cited on pages 50 and 128]

[18] Rebecca Jane Barthelmie, K Hansen, Sten Tronæs Frandsen, Ole Rathmann, and Schepers. Modelling and measuring flow and wind turbine wakes in large wind farms offshore. *Wind Energy*, 12(5):431–444, 2009. [Cited on pages 59 and 84]

[19] Lakshmi Dhevi Baskar, Bart De Schutter, and Hans Hellendoorn. Traffic management for automated highway systems using model-based predictive control. *IEEE Transactions on Intelligent Transportation Systems*, 13(2):838–847, 2012. [Cited on page 48]

[20] Majid Bastankhah and Fernando Porté-Agel. A new analytical model for wind-turbine wakes. *Renewable Energy*, 70:9938–, 01 2014. [Cited on pages 34 and 37]

[21] Christopher J Bay, Jennifer Annoni, Timothy Taylor, Lucy Pao, and Kathryn Johnson. Active power control for wind farms using distributed model predictive control and nearest neighbor communication. In *Annual American Control Conference (ACC)*, pages 682–687. IEEE, 2018. [Cited on pages 37, 51, 52, 57, 128, 163, and 167]

[22] Alberto Bemporad and Manfred Morari. Control of systems integrating logic, dynamics, and constraints. *Automatica*, 35(3):407–427, 1999. [Cited on pages 132 and 133]

[23] Fernando D Bianchi, Hernan De Battista, and Ricardo J Mantz. *Wind turbine control systems: principles, modelling and gain scheduling design*. Springer Science & Business Media, 2006. [Cited on pages 16, 17, 19, 22, 27, 74, 137, and 165]

[24] Eilyan Bitar and Pete Seiler. Coordinated control of a wind turbine array for power maximization. In *American Control Conference (ACC), 2013*, pages 2898–2904. IEEE, 2013. [Cited on page 60]

[25] S Boersma, BM Doekemeijer, S Siniscalchi-Minna, and JW van Wingerden. A constrained wind farm controller providing secondary frequency regulation: An

les study. *Renewable Energy*, 134:639–652, 2019. [Cited on pages xvi, xviii, 51, 90, 92, 167, 168, 169, 170, and 171]

[26] Carlo L. Bottasso and J. Schreiber. Online model updating by a wake detector for wind farm control. *2018 Annual American Control Conference (ACC)*, pages 676–681, 2018. [Cited on page 34]

[27] CARLO LUIGI Bottasso, Alessandro Croce, and Barbara Savini. Performance comparison of control schemes for variable-speed wind turbines. In *Journal of physics: Conference series*, volume 75, page 012079. IOP Publishing, 2007. [Cited on page 50]

[28] CAISO. Pay for performance regulation draft final proposal. technical report, california independent system operator corp. *CAISO. , Folsom, CA, 2012*, 2012. [Cited on page 93]

[29] Filippo Campagnolo, Vlaho Petrović, Carlo L Bottasso, and Alessandro Croce. Wind tunnel testing of wake control strategies. In *2016 American Control Conference (ACC)*, pages 513–518. IEEE, 2016. [Cited on pages 36 and 37]

[30] Matthew J Churchfield, Sang Lee, John Michalakes, and Patrick J Moriarty. A numerical study of the effects of atmospheric and wake turbulence on wind turbine dynamics. *Journal of turbulence*, (13):N14, 2012. [Cited on page 34]

[31] Umberto Ciri, Mario A Rotea, and Stefano Leonardi. Model-free control of wind farms: A comparative study between individual and coordinated extremum seeking. *Renewable Energy*, 113:1033–1045, 2017. [Cited on pages 35, 39, 61, 84, and 144]

[32] Antonio Colmenar-Santos, Severo Campíez-Romero, Lorenzo Enríquez-Garcia, and Clara Pérez-Molina. Simplified analysis of the electric power losses for on-shore wind farms considering weibull distribution parameters. *Energies*, 7(11):6856–6885, 2014. [Cited on page 101]

[33] Rick Damiani, Scott Dana, Jennifer Annoni, Paul Fleming, Jason Roadman, Jeroen van Dam, and Katherine Dykes. Assessment of wind turbine component loads under yaw-offset conditions. *Wind Energy Science*, 3(1):173–189, 2018. [Cited on page 168]

[34] DQ Dang, S Wu, Y Wang, and W Cai. Model predictive control for maximum power capture of variable speed wind turbines. In *2010 Conference Proceedings IPEC*, pages 274–279. IEEE, 2010. [Cited on page 50]

[35] Iñigo Martinez de Alegría, Jon Andreu, José Luis Martín, Pedro Ibanez, José Luis Villate, and Haritza Camblong. Connection requirements for wind farms: A survey on technical requierements and regulation. *Renewable and Sustainable Energy Reviews*, 11(8):1858–1872, 2007. [Cited on page 6]

[36] Rogério G De Almeida and JA Peças Lopes. Participation of doubly fed induction wind generators in system frequency regulation. *IEEE Transactions on Power Systems*, 22(3):944–950, 2007. [Cited on pages 29 and 31]

[37] Antonio De Paola, David Angeli, and Goran Strbac. Scheduling of wind farms for optimal frequency response and energy recovery. *IEEE Transactions on Control Systems Technology*, 24(5):1764–1778, 2016. [Cited on page 42]

[38] Simon De Rijcke, Johan Driesen, and Johan Meyers. Power smoothing in large wind farms using optimal control of rotating kinetic energy reserves. *Wind Energy*, 18(10):1777–1791, 2015. [Cited on page 42]

[39] James W Deardorff. Stratocumulus-capped mixed layers derived from a three-dimensional model. *Boundary-Layer Meteorology*, 18(4):495–527, 1980. [Cited on page 165]

[40] Gauthier Delille, Justine Yuan, and Laurent Capely. Taking advantage of load voltage sensitivity to stabilize power system frequency. In *2013 IEEE Grenoble Conference*, pages 1–6. IEEE, 2013. [Cited on page 48]

[41] Stefano Di Cairano and Alberto Bemporad. Model predictive control tuning by controller matching. *IEEE Transactions on Automatic Control*, 55(1):185–190, 2009. [Cited on page 47]

[42] Stefano Di Cairano and Alberto Bemporad. Model predictive control tuning by controller matching. *IEEE Transactions on Automatic Control*, 55(1):185–190, 2009. [Cited on page 73]

[43] Bart M Doekemeijer, Sjoerd Boersma, Lucy Y Pao, Torben Knudsen, and Jan-Willem van Wingerden. Online model calibration for a simplified les model in pursuit of real-time closed-loop wind farm control. 2018. [Cited on page 40]

[44] Bart M. Doekemeijer, Paul Fleming, and Jan-Willem van Wingerden. A tutorial on the synthesis and validation of a closed-loop wind farmcontroller using a steady-state surrogate model. In *Annual American Control Conference (ACC)*. IEEE, 2019. [Cited on pages 34, 35, and 37]

[45] BM Doekemeijer, Sjoerd Boersma, Lucy Y Pao, and Jan-Willem van Wingerden. Ensemble kalman filtering for wind field estimation in wind farms. In *2017 American Control Conference (ACC)*, pages 19–24. IEEE, 2017. [Cited on page 44]

[46] Janaka Ekanayake and Nick Jenkins. Comparison of the response of doubly fed and fixed-speed induction generator wind turbines to changes in network frequency. *IEEE Transactions on Energy conversion*, 19(4):800–802, 2004. [Cited on page 29]

[47] ESCAEU. [Cited on pages xvi and 102]

[48] M. Fischetti and D. Pisinger. Optimizing wind farm cable routing considering power losses. *European Journal of Operational Research*, 2017. [Cited on page 104]

[49] Martina Fischetti and David Pisinger. Optimizing wind farm cable routing considering power losses. *European Journal of Operational Research*, 270(3):917–930, 2018. [Cited on page 102]

[50] Paul Fleming, Jake Aho, Pieter Gebraad, Lucy Pao, and Yingchen Zhang. Computational fluid dynamics simulation study of active power control in wind plants. In *American Control Conference (ACC)*, pages 1413–1420, 2016. [Cited on pages 34, 60, and 63]

[51] Paul Fleming, Jennifer Annoni, Jigar J Shah, Linpeng Wang, Shreyas Ananthan, Zhijun Zhang, Kyle Hutchings, Peng Wang, Weiguo Chen, and Lin Chen. Field test of wake steering at an offshore wind farm. *Wind Energy Science*, 2(1):229–239, 2017. [Cited on page 37]

[52] Paul A Fleming, Pieter MO Gebraad, Sang Lee, Jan-Willem van Wingerden, Kathryn Johnson, Matt Churchfield, John Michalakes, Philippe Spalart, and Patrick Moriarty. Evaluating techniques for redirecting turbine wakes using sowfa. *Renewable Energy*, 70:211–218, 2014. [Cited on pages 36 and 167]

[53] Sten Frandsen, Rebecca Barthelmie, Sara Pryor, Ole Rathmann, Søren Larsen, Jørgen Højstrup, and Morten Thøgersen. Analytical modelling of wind speed deficit in large offshore wind farms. *Wind Energy*, 9(1-2):39–53, 2006. [Cited on page 57]

[54] Sten Tronæs Frandsen. *Turbulence and turbulence-generated structural loading in wind turbine clusters*. 2007. [Cited on page 16]

[55] Xiaodan Gao, Ke Meng, Zhao Yang Dong, Dongxiao Wang, Mohamed Shawky El Moursi, and Kit Po Wong. Cooperation-driven distributed control scheme for large-scale wind farm active power regulation. *IEEE Transactions on Energy Conversion*, 32(3):1240–1250, 2017. [Cited on page 128]

[56] Carlos E Garcia and Manfred Morari. Internal model control. a unifying review and some new results. *Industrial & Engineering Chemistry Process Design and Development*, 21(2):308–323, 1982. [Cited on page 47]

[57] Jorge L. Garriga and Masoud Soroush. Model predictive control tuning methods: A review. *Industrial & Engineering Chemistry Research*, 49(8):3505–3515, 2010. [Cited on page 46]

[58] M Gaumond, P-E Réthoré, Søren Ott, Alfredo Pena, Andreas Bechmann, and Kurt Schaldemose Hansen. Evaluation of the wind direction uncertainty and its impact on wake modeling at the horns rev offshore wind farm. *Wind Energy*, 17(8):1169–1178, 2014. [Cited on page 136]

[59] Durga Gautam, Lalit Goel, Raja Ayyanar, Vijay Vittal, and Terry Harbour. Control strategy to mitigate the impact of reduced inertia due to doubly fed induction generators on large power systems. *IEEE Transactions on Power Systems*, 26(1):214–224, 2010. [Cited on page 29]

[60] Pieter MO Gebraad, Paul A Fleming, and Jan-Willem van Wingerden. Wind turbine wake estimation and control using floridyn, a control-oriented dynamic wind plant model. In *American Control Conference (ACC), 2015*, pages 1702–1708. IEEE, 2015. [Cited on page 168]

[61] Pieter MO Gebraad and Jan-Willem van Wingerden. Maximum power-point tracking control for wind farms. *Wind Energy*, 18(3):429–447, 2015. [Cited on page 39]

[62] PMO Gebraad, FW Teeuwisse, JW Wingerden, Paul A Fleming, SD Ruben, JR Marden, and LY Pao. Wind plant power optimization through yaw control using a parametric model for wake effects a CFD simulation study. *Wind Energy*, 19(1):95–114, 2016. [Cited on pages 34, 37, and 57]

[63] Vahan Gevorgian, Yingchen Zhang, and Erik Ela. Investigating the impacts of wind generation participation in interconnection frequency response. *IEEE Transactions on Sustainable Energy*, 6(3):1004–1012, 2015. [Cited on page 125]

[64] Nicolò Gionfra, Guillaume Sandou, Houria Siguerdidjane, Damien Faille, and Philippe Loevenbruck. Wind farm distributed pso-based control for constrained power generation maximization. *Renewable Energy*, 133:103–117, 2019. [Cited on pages 37, 57, 128, and 167]

[65] Nicolo Gionfra, Houria Siguerdidjane, Guillaume Sandou, and Damien Faille. Hierarchical control of a wind farm for wake interaction minimization. *IFAC-PapersOnLine*, 49(27):330–335, 2016. [Cited on page 52]

[66] Tuhfe Göçmen, Paul Van der Laan, Pierre-Elouan Réthoré, Alfredo Peña Diaz, Gunner Chr Larsen, and Søren Ott. Wind turbine wake models developed at the technical university of denmark: A review. *Renewable and Sustainable Energy Reviews*, 60:752–769, 2016. [Cited on page 40]

[67] Jay P. Goit, Wim Munters, and Johan Meyers. Optimal coordinated control of power extraction in les of a wind farm with entrance effects. *Energies*, 9(1), 2016. [Cited on page 51]

[68] Jay P. Goit and Johan Meyers. Optimal control of energy extraction in wind-farm boundary layers. *Journal of Fluid Mechanics*, 768:5–50, 2015. [Cited on page 51]

[69] Javier Serrano González, Manuel Burgos Payán, Jesús Manuel Riquelme Santos, and Francisco González-Longatt. A review and recent developments in the optimal wind-turbine micro-siting problem. *Renewable and Sustainable Energy Reviews*, 30:133–144, 2014. [Cited on page 102]

[70] Juan M Grosso, Carlos Ocampo-Martínez, and Vicenç Puig. Learning-based tuning of supervisory model predictive control for drinking water networks. *Engineering Applications of Artificial Intelligence*, 26(7):1741–1750, 2013. [Cited on page 80]

[71] Juan M Grosso, Carlos Ocampo-Martinez, and Vicenç Puig. A distributed predictive control approach for periodic flow-based networks: application to drinking water systems. *International Journal of Systems Science*, 48(14):3106–3117, 2017. [Cited on pages 48, 128, and 133]

[72] Jacob Deleuran Grunnet, Mohsen Soltani, Torben Knudsen, Martin Nygaard Kragelund, and Thomas Bak. Aeolus toolbox for dynamics wind farm model, simulation and control. In *The European Wind Energy Conference & Exhibition, EWEC*, 2010. [Cited on pages 63, 75, 82, 109, 116, 137, and 141]

[73] GWEC. General wind energy council, Feb. 2019. [Cited on pages xiii and 6]

[74] KM Hangos and Zs Tuza. Optimal control structure selection for process systems. *Computers & Chemical Engineering*, 25(11-12):1521–1536, 2001. [Cited on page 50]

[75] Leibniz Universität Hannover, 2018. [Cited on pages 90 and 165]

[76] Anca D Hansen, Müfit Altin, Ioannis D Margaris, Florin Iov, and Germán C Tarnowski. Analysis of the short-term overproduction capability of variable speed wind turbines. *Renewable Energy*, 68:326–336, 2014. [Cited on page 159]

[77] Anca D Hansen, Poul Sørensen, Florin Iov, and Frede Blaabjerg. Centralised power control of wind farm with doubly fed induction generators. *Renewable Energy*, 31(7):935–951, 2006. [Cited on pages xiv, 37, 39, 41, and 60]

[78] Anca Daniela Hansen and Ioannis D Margaris. Type iv wind turbine model. 2014. [Cited on page 25]

[79] Kurt Schaldemose Hansen, Gunner Chr Larsen, Robert Menke, Nikola Vasiljevic, Nikolas Angelou, Ju Feng, Wei Jun Zhu, Andrea Vignaroli, C Xu, Wen Zhong Shen, et al. Wind turbine wake measurement in complex terrain. In *Journal of Physics: Conference Series*, volume 753, page 032013. IOP Publishing, 2016. [Cited on page 16]

[80] Martin OL Hansen. *Aerodynamics of wind turbines*. Routledge, 2015. [Cited on page 16]

[81] L Holdsworth, Janaka Bandara Ekanayake, and Nicholas Jenkins. Power system frequency response from fixed speed and doubly fed induction generator-based wind turbines. *Wind Energy*, 7(1):21–35, 2004. [Cited on pages 59 and 63]

[82] IRENA. Renewable capacity highlights, Mar. 2019. [Cited on pages xiii, 4, and 5]

[83] Nicholas Jenkins, A Burton, D Sharpe, and E Bossanyi. *Wind Energy Handbook*. John Wiley & Sons Ltd, United Kingdom, 2001. [Cited on page 17]

[84] N. O. Jensen. A note on wind generator interaction. Technical report, Roskilde, Denmark, 1983. [Cited on pages 34 and 60]

[85] Jason Jonkman, Sandy Butterfield, Walter Musial, and George Scott. Definition of a 5-mw reference wind turbine for offshore system development. *National Renewable Energy Laboratory, Golden, CO, Technical Report No. NREL/TP-500-38060*, 2009. [Cited on pages 22 and 82]

[86] I. Katic, Hojstrup, and N. O. Jensen. A simple model for cluster efficiency. In *European Wind Energy Association Conference and Exhibition*, pages 407–410, 1986. [Cited on pages 34 and 83]

[87] Eric C Kerrigan and Jon M Maciejowski. Designing model predictive controllers with prioritised constraints and objectives. In *Proceedings. IEEE International Symposium on Computer Aided Control System Design*, pages 33–38. IEEE, 2002. [Cited on pages 73 and 79]

[88] Ali C. Kheirabadi and Ryozo Nagamune. A quantitative review of wind farm control with the objective of wind farm power maximization. *Journal of Wind*

Engineering and Industrial Aerodynamics, 192:45 – 73, 2019. [Cited on pages 35 and 39]

[89] Brendan Kirby, Michael Milligan, and Erik Ela. Providing minute-to-minute regulation from wind plants. Technical report, National Renewable Energy Lab.(NREL), Golden, CO (United States), 2010. [Cited on page 6]

[90] Torben Knudsen, Thomas Bak, and Mikael Svenstrup. Survey of wind farm control—power and fatigue optimization. *Wind Energy*, 18(8):1333–1351, 2015. [Cited on pages 37 and 39]

[91] Arne Koerber and Rudibert King. Combined feedback–feedforward control of wind turbines using state-constrained model predictive control. *IEEE Transactions on Control Systems Technology*, 21(4):1117–1128, 2013. [Cited on page 50]

[92] Ratul Lahkar and William H Sandholm. The projection dynamic and the geometry of population games. *Games and Economic Behavior*, 64(2):565–590, 2008. [Cited on page 50]

[93] Gunner Chr Larsen, Helge Madsen Aagaard, Ferhat Bingöl, Jakob Mann, Sørensen Jens N Okulov Valery Troldborg Niels Nielsen Niels Morten Ott, Søren, Kenneth Thomsen, et al. Dynamic wake meandering modeling. Technical report, Risø National Laboratory, 2007. [Cited on pages 35, 58, and 109]

[94] Johan Lofberg. Yalmip: A toolbox for modeling and optimization in MATLAB. In *Proc. IEEE International Symposium on Computer Aided Control Systems Design*, pages 284–289, 2005. [Cited on pages 84 and 141]

[95] Jan Marian Maciejowski. *Predictive control: with constraints*. Pearson education, 2002. [Cited on pages 44 and 45]

[96] José M Maestre, Rudy R Negenborn, et al. *Distributed model predictive control made easy*, volume 69. Springer. [Cited on page 48]

[97] James F Manwell, Jon G McGowan, and Anthony L Rogers. *Wind energy explained: theory, design and application*. John Wiley & Sons, 2010. [Cited on page 58]

[98] Jason R Marden, Shalom D Ruben, and Lucy Y Pao. A model-free approach to wind farm control using game theoretic methods. *IEEE Transactions on Control Systems Technology*, 21(4):1207–1214, 2013. [Cited on page 39]

[99] Björn Maronga, Micha Gryschka, Rieke Heinze, Fabian Hoffmann, Farah Kanani-Sühring, Marius Keck, K Ketelsen, Marcus Oliver Letzel, Matthias Sühring, and Siegfried Raasch. The parallelized large-eddy simulation model (palm) version 4.0 for atmospheric and oceanic flows: model formulation, recent developments, and future perspectives. *Geoscientific Model Development Discussions 8 (2015), Nr. 2, S. 1539-1637*, 2015. [Cited on pages 90 and 165]

[100] Luis A Martínez-Tossas, Matthew J Churchfield, and Stefano Leonardi. Large eddy simulations of the flow past wind turbines: actuator line and disk modeling. *Wind Energy*, 18(6):1047–1060, 2015. [Cited on page 34]

[101] Paul R Maurath, Alan J Laub, Dale E Seborg, and Duncan A Mellichamp. Predictive controller design by principal components analysis. *Industrial & engineering chemistry research*, 27(7):1204–1212, 1988. [Cited on page 47]

[102] Juan Manuel Mauricio, Alejandro Marano, Antonio Gómez-Expósito, and José Luis Martínez Ramos. Frequency regulation contribution through variable-speed wind energy conversion systems. *IEEE Transactions on Power Systems*, 24(1):173–180, 2009. [Cited on pages 7 and 29]

[103] T. A. Meadowcroft, G. Stephanopoulos, and C. Brosilow. The modular multivariable controller: I: Steady-state properties. *AIChE Journal*, 38(8):1254–1278, 1992. [Cited on page 81]

[104] Ömer Göksu. Deliverable 3-2: Specifications of the control strategies and the simulation the test cases. Technical report, DTU, 2017. [Cited on page 43]

[105] Johan Meyers and Charles Meneveau. Large eddy simulations of large wind-turbine arrays in the atmospheric boundary layer. In *48th AIAA aerospace sciences meeting including the new horizons forum and aerospace exposition*, page 827. [Cited on pages 34 and 90]

[106] Kaisa Miettinen. *Nonlinear multiobjective optimization*, volume 12. Springer Science & Business Media, 2012. [Cited on pages 73 and 81]

[107] TH Mohamed, H Bevrani, AA Hassan, and T Hiyama. Decentralized model predictive based load frequency control in an interconnected power system. *Energy Conversion and Management*, 52(2):1208–1214, 2011. [Cited on page 48]

[108] Manfred Morari and Jay H Lee. Model predictive control: past, present and future. *Computers & Chemical Engineering*, 23(4-5):667–682, 1999. [Cited on pages 47 and 80]

[109] Johan Morren, Sjoerd WH De Haan, Wil L Kling, and JA Ferreira. Wind turbines emulating inertia and supporting primary frequency control. *IEEE Transactions on power systems*, 21(1):433–434, 2006. [Cited on page 29]

[110] Eduard Muljadi and Charles P Butterfield. Pitch-controlled variable-speed wind turbine generation. *IEEE transactions on Industry Applications*, 37(1):240–246, 2001. [Cited on page 27]

[111] W. Munters and J. Meyers. Towards practical dynamic induction control of wind farms: analysis of optimally controlled wind-farm boundary layers and sinusoidal induction control of first-row turbines. *Wind Energy Science*, 3(1):409–425, 2018. [Cited on page 51]

[112] Wim Munters and Johan Meyers. An optimal control framework for dynamic induction control of wind farms and their interaction with the atmospheric boundary layer. *Philosophical Transactions of the Royal Society A: Mathematical, Physical and Engineering Sciences*, 375(2091):20160100, 2017. [Cited on page 37]

[113] Wim Munters and Johan Meyers. Dynamic strategies for yaw and induction control of wind farms based on large-eddy simulation and optimization. *Energies*, 11(1):177, 2018. [Cited on page 37]

[114] Alfredo Núñez, Carlos Ocampo-Martinez, José María Maestre, and Bart De Schutter. Time-varying scheme for noncentralized model predictive control of large-scale systems. *Mathematical Problems in Engineering*, 2015, 2015. [Cited on page 50]

[115] Elis Nycander and Lennart Söder. Review of european grid codes for wind farms and their implications for wind power curtailments. In *17th International Wind Integration Workshop Stockholm, Sweden — 17 – 19 October 2018 :*, 2018. QC 20181023. [Cited on page 7]

[116] Carlos Ocampo-Martinez. *Model predictive control of wastewater systems*. Springer Science & Business Media, 2010. [Cited on page 44]

[117] Carlos Ocampo-Martinez. *Model predictive control of wastewater systems*. Springer Science & Business Media, 2010. [Cited on page 48]

[118] Carlos Ocampo-Martinez, Samuele Bovo, and Vicenç Puig. Partitioning approach oriented to the decentralised predictive control of large-scale systems. *Journal of Process Control*, 21(5):775–786, 2011. [Cited on pages 50, 128, and 129]

[119] Carlos Ocampo-Martinez, Ari Ingimundarson, Vicenç Puig, and Joseba Quevedo. Objective Prioritization Using Lexicographic Minimizers for MPC of Sewer Networks. *IEEE Transactions on Control Systems Technology*, 16(1):113–121, 2008. [Cited on pages 74 and 81]

[120] A Papadopoulos, S Rodrigues, E Kontos, T Todorcevic, P Bauer, and R Teixeira Pinto. Collection and transmission losses of offshore wind farms for optimization purposes. In *2015 IEEE Energy Conversion Congress and Exposition (ECCE)*, pages 6724–6732. IEEE, 2015. [Cited on page 103]

[121] Jinkyoo Park and Kincho H Law. Layout optimization for maximizing wind farm power production using sequential convex programming. *Applied Energy*, 151:320–334, 2015. [Cited on page 57]

[122] Ruben Pena, JC Clare, and GM Asher. Doubly fed induction generator using back-to-back pwm converters and its application to variable-speed wind-energy generation. *IEE Proceedings-Electric Power Applications*, 143(3):231–241, 1996. [Cited on page 24]

[123] C. Pilong. Pjm manual 12: Balancing operations. *Technical Report, PJM*, 2015. [Cited on page 92]

[124] Xavier Prats, Vicenç Puig, Joseba Quevedo, and Fatiha Nejjari. Lexicographic optimisation for optimal departure aircraft trajectories. *Aerospace Science and Technology*, 14(1):26 – 37, 2010. [Cited on page 73]

[125] David M Prett and Carlos E García. *Fundamental process control: Butterworths series in chemical engineering*. Butterworth-Heinemann, 2013. [Cited on page 80]

[126] Wei Qi, Yong Liang, and Zuo-Jun Max Shen. Joint planning of energy storage and transmission for wind energy generation. *Operations Research*, 63(6):1280–1293, 2015. [Cited on page 102]

[127] Wei Qiao, Ganesh Kumar Venayagamoorthy, and Ronald G Harley. Real-time implementation of a statcom on a wind farm equipped with doubly fed induction generators. *IEEE transactions on industry applications*, 45(1):98–107, 2009. [Cited on page 43]

[128] Steffen Raach, Sjoerd Boersma, Jan-Willem van Wingerden, David Schlipf, and Po Wen Cheng. Robust lidar-based closed-loop wake redirection for wind farm control. *IFAC-PapersOnLine*, 50(1):4498–4503, 2017. [Cited on pages 40 and 50]

[129] Steffen Raach, Jan-Willem van Wingerden, Sjoerd Boersma, David Schlipf, and Po-Wen Cheng. $_{\infty}$ controller design for closed-loop wake redirection. *2017 American Control Conference (ACC)*, pages 703–708, 2017. [Cited on page 50]

[130] G Ramtharan, Nick Jenkins, and JB Ekanayake. Frequency support from doubly fed induction generator wind turbines. *IET Renewable Power Generation*, 1(1):3–9, 2007. [Cited on page 42]

[131] J. B. Rawlings and D. Q. Mayne. *Model predictive control: theory and design*. Nob Hill Publishing, 2009. [Cited on page 44]

[132] Gilberto Reynoso-Meza, Sergio Garcia-Nieto, Javier Sanchis, and F Xavier Blasco. Controller tuning by means of multi-objective optimization algorithms: A global tuning framework. *IEEE Transactions on Control Systems Technology*, 21(2):445–458, 2012. [Cited on page 47]

[133] Moumita Sarkar, Müfit Altin, Poul E. Sørensen, and Anca D. Hansen. Reactive power capability model of wind power plant using aggregated wind power collection system. *Energies*, 12(9), 2019. [Cited on pages xvi, 102, and 103]

[134] Riccardo Scattolini. Architectures for distributed and hierarchical model predictive control–a review. *Journal of process control*, 19(5):723–731, 2009. [Cited on page 48]

[135] Mesut E Sezer and DD Šiljak. Nested ε-decompositions and clustering of complex systems. *Automatica*, 22(3):321–331, 1986. [Cited on page 50]

[136] Rabia Shakoor, Mohammad Yusri Hassan, Abdur Raheem, and Yuan-Kang Wu. Wake effect modeling: A review of wind farm layout optimization using jensen's model. *Renewable and Sustainable Energy Reviews*, 58:1048–1059, 2016. [Cited on page 33]

[137] Carl R Shapiro, Johan Meyers, Charles Meneveau, and Dennice F Gayme. Wind farms providing secondary frequency regulation: evaluating the performance of model-based receding horizon control. *Wind Energy Science*, 3(1):11–24, 2018. [Cited on pages 35, 57, and 74]

[138] C.R. Shapiro, P Bauweraerts, J Meyers, C Meneveau, and D F Gayme. Model-based receding horizon control of wind farms for secondary frequency regulation. *Wind Energy*, 20:1261–1275. [Cited on pages 40 and 51]

[139] Sara Siniscalchi-Minna, Fernando Bianchi, Mikel De Prada Gil, and Carlos Ocampo-Martinez. A wind farm control strategy for power reserve maximization. *Renewable Energy*, under review. [Cited on pages 39 and 58]

[140] Sara Siniscalchi-Minna, Fernando D Bianchi, Mikel De-Prada-Gil, and Carlos Ocampo-Martinez. A wind farm control strategy for power reserve maximization. *Renewable Energy*, 131:37–44, 2019. [Cited on pages 36 and 139]

[141] Sara Siniscalchi-Minna, Fernando D Bianchi, and Carlos Ocampo-Martinez. Predictive control of wind farms based on lexicographic minimizers for power reserve maximization. In *Annual American Control Conference (ACC)*, pages 701–706. IEEE, 2018. [Cited on pages 42 and 73]

[142] Sara Siniscalchi-Minna, Mikel De-Prada-Gil, Fernando Daniel Bianchi, Carlos Ocampo-Martínez, and Bart De Schutter. A multi-objective predictive control strategy for enhancing primary frequency support with wind farms. In *Journal of Physics: Conference Series*, volume 1037, page 032034. IOP Publishing, 2018. [Cited on page 101]

[143] Sara Siniscalchi-Minna, Carlos Ocampo-Martinez, Fernando D Bianchi, Mikel De-Prada-Gil, and Bart De-Schutter. Partitioning approach for large wind farms: Active power control for optimizing power reserve. In *IEEE Conference on Decision and Control (CDC)*, pages 3183–3188. IEEE, 2018. [Cited on pages 128 and 129]

[144] Maryam Soleimanzadeh and Rafael Wisniewski. Wind speed dynamical model in a wind farm. In *IEEE ICCA 2010*, pages 2246–2250. IEEE, 2010. [Cited on page 35]

[145] Maryam Soleimanzadeh, Rafael Wisniewski, and Kathryn Johnson. A distributed optimization framework for wind farms. *Journal of Wind Engineering and Industrial Aerodynamics*, 123:88–98, 2013. [Cited on pages 40 and 50]

[146] Vedrana Spudic and Mato Baotic. Fast coordinated model predictive control of large-scale distributed systems with single coupling constraint. In *European Control Conference (ECC),*, pages 2783–2788. IEEE, 2013. [Cited on pages 98 and 128]

[147] Vedrana Spudic, M Jelavic, M Baotic, and Nedjeljko Peric. Hierarchical wind farm control for power/load optimization. *The science of making torque from wind (Torque2010)*, 2010. [Cited on pages 51 and 98]

[148] Rodrigo Toro, Carlos Ocampo-Martínez, Filip Logist, Jan Van Impe, and Vicenç Puig. Tuning of predictive controllers for drinking water networked systems. *IFAC Proceedings Volumes*, 44(1):14507–14512, 2011. [Cited on page 80]

[149] L Tyler, Manfred Morari, and F Kraus. Propositional logic in control and monitoring problems. *IFAC Proceedings Volumes*, 30(11):1169–1174, 1997. [Cited on page 80]

[150] Akie Uehara, Alok Pratap, Tomonori Goya, Tomonobu Senjyu, Atsushi Yona, Naomitsu Urasaki, and Toshihisa Funabashi. A coordinated control method to

smooth wind power fluctuations of a pmsg-based wecs. *IEEE Transactions on energy conversion*, 26(2):550–558, 2011. [Cited on page 29]

[151] Nayeem Rahmat Ullah, Torbjörn Thiringer, and Daniel Karlsson. Temporary primary frequency control support by variable speed wind turbines—potential and applications. *IEEE Transactions on Power Systems*, 23(2):601–612, 2008. [Cited on page 29]

[152] M Vali, JW van Wingerden, S Boersma, V Petrović, and M Kühn. A predictive control framework for optimal energy extraction of wind farms. In *Journal of Physics: Conference Series*, volume 753. IOP Publishing, 2016. [Cited on page 57]

[153] Mehdi Vali, Vlaho Petrović, Sjoerd Boersma, Jan-Willem van Wingerden, Lucy Y. Pao, and Martin Kühn. Adjoint-based model predictive control for optimal energy extraction in waked wind farms. *Control Engineering Practice*, 84:48 – 62, 2019. [Cited on page 51]

[154] Mattia Vallerio, Jan Van Impe, and Filip Logist. Tuning of nmpc controllers via multi-objective optimisation. *Computers & Chemical Engineering*, 61:38–50, 2014. [Cited on page 47]

[155] Ton van den Boom and Bart De Schutter. Mpc for max-plus-linear systems: Closed-loop behavior and tuning. In *Proceedings of the 2001 American Control Conference.(Cat. No. 01CH37148)*, volume 1, pages 325–330. IEEE, 2001. [Cited on page 47]

[156] JH Van der Lee, WY Svrcek, and BR Young. A tuning algorithm for model predictive controllers based on genetic algorithms and fuzzy decision making. *ISA transactions*, 47(1):53–59, 2008. [Cited on page 47]

[157] Dirk Van Hertem and Oriol Gomis-Bellmunt. *HVDC grids*. Wiley Online Library, 2016. [Cited on page 102]

[158] Jan-Willem van Wingerden, Lucy Pao, Jacob Aho, and Paul Fleming. Active power control of waked wind farms. *IFAC-PapersOnLine*, 50(1):4484–4491, 2017. [Cited on pages xix, 50, 74, and 93]

[159] Aswin N Venkat, Ian A Hiskens, James B Rawlings, and Stephen J Wright. Distributed mpc strategies with application to power system automatic generation control. *IEEE transactions on control systems technology*, 16(6):1192–1206, 2008. [Cited on page 48]

[160] Shuo Wang, Jiabing Hu, Xiaoming Yuan, and Li Sun. On inertial dynamics of virtual-synchronous-controlled dfig-based wind turbines. *IEEE Transactions on Energy Conversion*, 30(4):1691–1702, 2015. [Cited on page 29]

[161] H. Waschl, J. B. Jogensen, J. K. Huusom, and L. del Re. A tuning approach for offset-free MPC with conditional reference adaptation. In *Proceedings of the 19th World Congress*, pages 24–29, Cape Town, South Africa, 2014. [Cited on page 73]

[162] Harald Waschl, Daniel Alberer, and Luigi del Re. Automatic tuning methods for mpc environments. In *International Conference on Computer Aided Systems Theory*, pages 41–48. Springer, 2011. [Cited on page 47]

[163] WindEurope. Wind energy in europe, scenarios for 2030, Sep. 2017. [Cited on pages xiii and 5]

[164] WindEurope. Financing and investment trends., Sep. 2018. [Cited on page 4]

[165] Willy Wojsznis, John Gudaz, Terry Blevins, and Ashish Mehta. Practical approach to tuning mpc. *ISA transactions*, 42(1):149–162, 2003. [Cited on page 47]

[166] Qiuwei Wu and Yuanzhang Sun. *Modeling and Modern Control of Wind Power*. IEEE Press WILEY, 2019. [Cited on page 22]

[167] Ziping WU, Wenzhong GAO, Tianqi GAO, Weihang YAN, Huaguang ZHANG, Shijie YAN, and Xiao WANG. State-of-the-art review on frequency response of wind power plants in power systems. *Journal of Modern Power Systems and Clean Energy*, 6(1):1–16, Jan 2018. [Cited on page 29]

[168] Xibo Yuan and Yongdong Li. Control of variable pitch and variable speed direct-drive wind turbines in weak grid systems with active power balance. *IET Renewable Power Generation*, 8(2):119–131, 2013. [Cited on page 29]

[169] Andraž Zertek, Gregor Verbic, and Miloš Pantos. A novel strategy for variable-speed wind turbines' participation in primary frequency control. *IEEE Transactions on Sustainable Energy*, 3(4):791–799, 2012. [Cited on pages 31, 42, 59, and 116]

[170] Baohua Zhang, Mohsen Soltani, Weihao Hu, Peng Hou, Qi Huang, and Zhe Chen. Optimized power dispatch in wind farms for power maximizing considering fatigue loads. *IEEE Transactions on Sustainable Energy*, 9(2):862–871, 2017. [Cited on page 128]

[171] Haoran Zhao, Qiuwei Wu, Qinglai Guo, Hongbin Sun, and Yusheng Xue. Distributed model predictive control of a wind farm for optimal active power control part II: Implementation with clustering-based piece-wise affine wind turbine model. *IEEE Transactions on Sustainable Energy*, 6(3):840–849, 2015. [Cited on pages 37, 44, 60, and 128]

[172] Haoran Zhao, Qiuwei Wu, Qinglai Guo, Hongbin Sun, and Yusheng Xue. Optimal active power control of a wind farm equipped with energy storage system based on distributed model predictive control. *IET Generation, Transmission & Distribution*, 10(3):669–677, 2016. [Cited on pages 51 and 128]

[173] Haoran Zhao, Qiuwei Wu, Jianhui Wang, Zhaoxi Liu, Mohammad Shahidehpour, and Yusheng Xue. Combined active and reactive power control of wind farms based on model predictive control. *IEEE Transactions on Energy Conversion*, 32(3):1177–1187, 2017. [Cited on pages 43, 51, and 103]

[174] Shan Zhong and Xiaodong Wang. Decentralized model-free wind farm control via discrete adaptive filtering methods. *IEEE Transactions on Smart Grid*, 9(4):2529–2540, 2016. [Cited on page 39]